UNTANGLING CELLULAR AND MOLECULAR MECHANISMS OF FIBROTIC DISEASE

RAFAEL JOHANNES THOMAS KRAMANN

ISBN: 7104388905162
Layout: Egied Simons
Cover: Egied Simons
Printing: Simons Productions

UNTANGLING CELLULAR AND MOLECULAR MECHANISMS OF FIBROTIC DISEASE

ONTRAFELEN VAN CELLULAIRE EN MOLECULAIRE MECHANISMEN VAN FIBROTISCHE ZIEKTEN

Thesis

to obtain the degree of Doctor from the
Erasmus University Rotterdam
by command of the
rector magnificus

Prof.dr. H.A.P. Pols

and in accordance with the decision of the Doctorate Board.
The public defence shall be held on

Wednesday, 8 May 2019 at 14.30 hrs

by

RAFAEL JOHANNES THOMAS KRAMANN

born in Euskirchen, Germany

Erasmus University Rotterdam

DOCTORAL COMMITTEE

Promotors: Prof.dr. R. Zietse
Prof. dr. E. Hoorn

Other members: Prof.dr. J. Gribnau
Prof.dr. R. Goldschmeding
Prof.dr. D.J.G.M. Duncker

CONTENTS

I. INTRODUCTION

1. ORGAN FIBROSIS

1.1 Introduction to fibrosis

Tissue fibrosis, or scar formation, is the common final pathway of virtually all chronic diseases and affects nearly every organ, including kidney, heart, lung, bone marrow and liver, among others. Fibrotic disease represents a large and growing health care burden. However, despite contributing to as much as 45% of deaths in the developed world, fibrotic disease has been largely overlooked for many years resulting in a dire innovation gap in this disease space. One reason for this is that the cellular source of myofibroblasts, the cells that cause fibrosis, was very controversial and partly unclear for many years. Furthermore, the ultmative proof that specific ablation of fibrosis improves and or stabilizes organ function was still lacking.

Interstitial fibrosis and Myofibroblasts: Fibrosis is accompanied by substantial changes in tissue structure, notably within the interstitial compartment. Interstitium consists primarily of endothelium, pericytes (vascular supportive cells) and macrophages. Structural changes in the interstitium correlate well with loss of organ function, in many cases, highlighting the functional importance of this compartment . During chronic injury, the interstitium becomes expanded with increased myofibroblasts. Myofibroblasts are matrix producing interstitial cells that cause fibrosis. They are reactive cells that occur after acute or chronic injury or in pathologic conditions such as cancer. These cells are highly synthetically active and characterized by dense rough endoplasmic reticulum and collagen secretion granules . Myofibroblasts are contractile and express alpha-smooth muscle actin (α-SMA), which forms bundles of myofilaments, called stress fibers, promoting strong contractile force generation. In addition to α-SMA, plasma membrane fibronectin and vimentin are also myofibroblast markers. In kidney, myofibroblasts are defined by Collagen-1α1 expression, consistent with the matrix-secretory function of these cells .

The cellular origin of myofibroblast and controversy: There is intense interest in understanding exactly where myofibroblasts derive, because this knowledge will guide attempts to ablate these cells and forms the logical basis for antifibrotic therapeutic strategies. The hypothesis is that eradication of pathological myofibroblasts will not only halt scar secretion directly, but will also prevent loss of microvasculature, reducing hypoxia and promoting parenchymal health. Various cellular origins of myofibroblasts have been discussed, such as epithelial cells via a process called epithelial to mesenchymal transition (EMT), endothelial cells by endothelial mesenchymal transition (EndMT), circulating bone marrow derived cells such as

mesenchymal stem cells (MSCs) and hematopoetic cells, resident fibroblasts and pericytes (extensively discussed below and in my following reviews).

The Hedgehog signaling pathway: The Hedgehog (Hh) pathway regulates mesenchyme cell fate during development and growing evidence implicates a critical role of Hh in solid organ fibrosis and cancer. Three Hh ligands, sonic hedgehog (Shh), indian hedgehog (Ihh) and desert hedgehog (Dhh) are found in mammals and humans. These secreted proteins can act at short or long distances by binding to the membrance receptor Patched1 (Ptch1), thereby releasing tonic inhibition by Ptch1 on the transmembrane protein smoothened (Smo). Derepressed Smoothened translocates to the primary cilium promoting preservation of the full length activator forms of Gli2 (and Gli3) and their transportation to the nucleus, which induces transcription of the Hh target genes including Gli1 and Ptch1. Studies in mouse mutants suggest that Gli2 is principially important for the activator function in response to Hh while Gli3 is the major repressor; Gli1 seems to have only a role in amplifying the transcriptional response. In mammals Gli1 is not required for Hh signaling and Gli1-knockout mice develop normally, unless one copy of Gli2 is defective, whereas Gli2, knockout mice die at birth with severe skeletal and neural defects. Strong evidence indicates a role of Hh signaling in fibrotic disease as outlined in the review below.

1

ORIGIN, ACTIVATION AND REGULATION OF MATRIX-PRODUCING MYOFIBROBLASTS IN FIBROTIC DISEASE

Rafael Kramann[1,2,3,*], MD; Derek P. DiRocco[1,2,*], PhD; Benjamin D. Humphreys MD, PhD[1,2,4]

[1]Brigham and Women's Hospital, Boston, Massachusetts
[2] Harvard Medical School, Boston, Massachusetts
[3] RWTH Aachen University, Division of Nephrology, Aachen, Germany
[4]Harvard Stem Cell Institute, Cambridge, Massachusetts

Keywords: Pericyte, myofibroblast, fibrosis, interstitium,
Address reprint requests to:
Benjamin D. Humphreys MD, PhD
Harvard Institutes of Medicine Room 550
4 Blackfan Circle
Boston, Massachusetts 02115
Phone: 617-525-5971
Fax: 617-525-5965
Email: bhumphreys@partners.org

[*]R.K. and D.P.D. contributed equally

J Pathol. 2013 Nov;231(3):273-89.

ABSTRACT

Fibrosis or scar tissue formation results from chronic progressive injury in virtually every tissue and organ and affects a growing number of people in the developed world. Myofibroblasts drive fibrosis and recent work has demonstrated that mesenchymal cells including pericytes and perivascular fibroblasts are their main progenitors. Understanding the cellular mechanisms of pericyte/fibroblast to myofibroblast transition, myofibroblast proliferation and the key signaling pathways that regulate these processes will be essential to develop novel targeted therapeutics for the growing patient population suffering from solid organ fibrosis. In this review, we summarize the current knowledge about different progenitor cells of myofibroblasts, discuss major pathways that regulate their transdifferentiation and summarize the status of novel targeted anti-fibrotic therapeutics in development.

INTRODUCTION

Tissue fibrosis, or scar formation, is the common final pathway of virtually all chronic and progressive diseases and damages nearly every organ including kidney, heart, lung and liver as well as other tissues such as vasculature, skin, skeletal muscle and bone marrow. Scar tissue can form after an acute insult, or more slowly as a result of chronic injury from an underlying condition. Fibrotic matrix may initially aid in the tissue repair process, and even become resorbed after mild injury as functional tissue regenerates. However, during chronic injury fibrotic matrix deposition goes unchecked, slowly disrupting organ architecture, choking off blood supply and disrupting organ function. This process also reduces the capacity for tissue repair and ultimately culminates in organ failure. Fibrosis destroys the kidneys of diabetic patients [3, 4], the liver of hepatitis C patients , the heart of patients with hypertension, aortic stenosis and chronic kidney disease [5] and the lungs of patients with idiopathic pulmonary fibrosis [7].

Fibrotic disease represents a large and growing burden especially in the developed world with aging populations and growing numbers of patients suffering from diabetes, hypertension, and chronic kidney disease. Remarkably, there is currently no approved drug in the US to treat fibrosis. While pharmaceutical company interest in this field has recently picked up, there is still a dire innovation gap in this disease space. Understanding the pathophysiologic processes that drive myofibroblast recruitment and expansion will help to close this innovation gap.

Across different fields and disciplines researchers agree that myofibroblasts are the cells responsible for scar tissue formation and fibrosis [8]. However the source of these mesenchymal cells is not completely understood and remains an active area of research. Uncovering the origin of the cells that drive fibrosis, identifying mechanisms of recruitment, and understanding key regulatory pathways driving their transdifferentiation and expansion is essential to guide the development of novel targeted therapeutics in human fibrotic disease.

Origin of Interstitial Myofibroblasts in Fibrotic Disease

It has been accepted by scientists across disciplines that myofibroblasts are the matrix producing interstitial cells that cause fibrosis. Myofibroblasts are reactive cells that occur after acute or chronic injury or in pathologic conditions such as cancer [9, 10]. These cells are highly synthetically active and are characterized by dense rough endoplasmic reticulum and collagen secretion granules . Myofibroblasts are highly contractile and express alpha-smooth muscle actin (α-SMA, Acta2, Figure 1A), which forms bundles of myofilaments, called stress fibers, promoting strong contractile force generation [11]. In kidney, myofibroblasts are defined by Collagen-1a1 expression, consistent with the matrix-secretory function of these cells [13]

The cellular origin of myofibroblasts is an ongoing field of investigation and remains controversial. Evidence from research of the last few decades implicates several different cellular sources including circulating cells from bone marrow, hematopoietic precusors, epithelial and endothelial cells, local fibroblast pools, smooth muscle cell myofibroblast progenitors and pericytes (Figure 2).

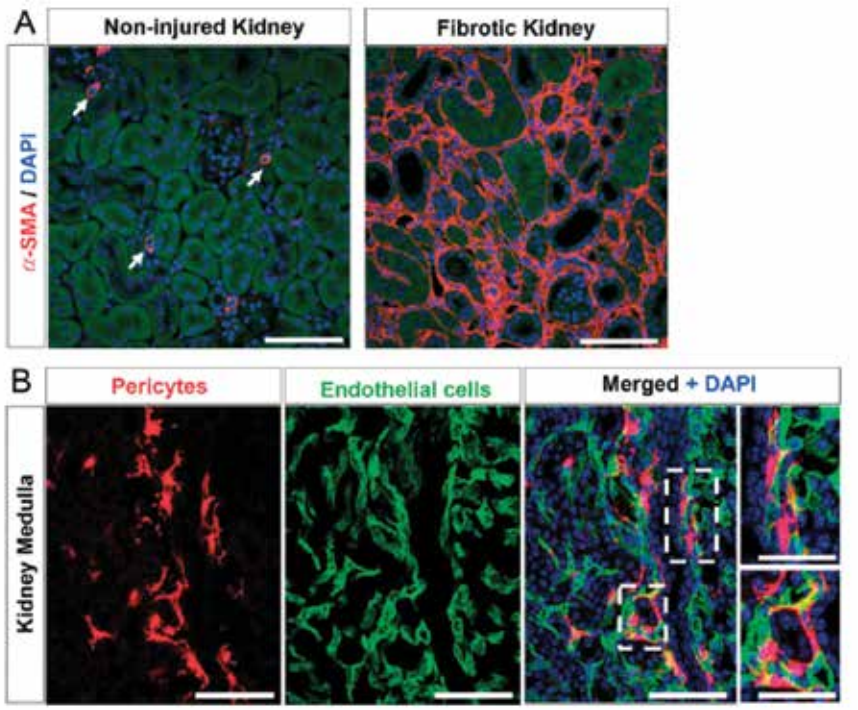

Figure 1. Expansion of myofibroblasts in kidney fibrosis and medullary pericytes. (A) **α**-Smooth muscle actin (**α**SMA; red) is almost absent in the interstitium of an uninjured healthy kidney and only expressed by vascular smooth muscle cells (arrow). However, after injury (unilateral ureteral obstruction) the fibrosis-driving myofibroblasts emerge and gain expression of **α**SMA. (**B**) Pericytes (red) surrounding capillaries (endothelial cells, green) in the medulla of a mouse kidney; it is thought that they are important cells for the stabilization of capillaries. Scale bars = 50 μm (25 μm in inserts).

Epithelial or endothelial origin of myofibroblasts Epithelial to mesenchymal transition (EMT) is an important process especially in development and cancer biology describing the reversible transition of terminally differentiated epithelial cells into mesenchymal cells with increased migratory potential and profound changes in their gene-expression profile [14]. In the last decade many publications suggest that epithelial cells, via EMT, might be a major source of myofibroblasts in solid organ fibrosis [15-18]. Early evidence for EMT was gathered in cell-culture studies showing that terminally differentiated epithelial cells can be stimulated to undergo a transition towards a spindle shaped phenotype with expression of α-SMA, vimentin and FSP1. However, *in vitro* cell culture is limited as a model for EMT because

various terminally-differentiated cell-types can be stimulated to gain the above mentioned markers by a process of de-differentiation which may not reflect the in vivo situation. Many publications reported EMT as a source of myofibroblasts in fibrogenesis of lung [21-23], liver and kidney using immunostaining for co-localization of epithelial and mesenchymal markers or lineage tracing techniques. However, most recent publications provide strong evidence against EMT as a source of myofibroblasts in liver [25], kidney [26] and lung [27]. More studies are needed using up-to date fate tracing technologies to conclusively answer the question if epithelial cells cross the basement membrane and contribute to the pool of myofibroblasts.

In the heart and the kidney endothelial cells (EndoMT) have been reported as source of myofibroblasts during myocardial fibrosis [28] [29, 30]. It has even been reported that terminally differentiated vascular endothelial cells can differentiate into mesenchymal-stem cell like cells with a tri-lineage differentiation capacity (chondrogen, osteogen and adipogen). This is a quite interesting although unexpected finding, however the authors used a Tie2-Cre driver line for their lineage tracing experiments and Tie2 is known to be expressed in myeloid lineage cells, in addition to endothelial cells. [29]. De Palma et al. reported that mesenchymal Tie2 expressing cells might be precusors of vascular pericytes in mammary tumors [32, 33]. Also STRO-1 one of the markers the authors use as a MSC marker has been reported to be an antigen of endothelial cells . Regarding their *in vitro* experiments with primary endothelial cells it has been noted for many years that primary endothelial cell cultures are contaminated with pericytes [34-36]. Although the authors demonstrate via flow cytometry that their endothelial cells are not expressing the pericyte marker NG2, experiments with a sorted pure CD31+ cell-population would have been more convincing. Thus, more studies are needed to elucidate whether terminally differentiated endothelial cells have the plasticity of MSC.

Circulating myofibroblast progenitors

Bone-marrow derived circulating cells from a stromal precusor population or hematopoetic progenitors have also been reported as a source of matrix-producing cells in fibrogenesis. It has been reported that bone-marrow precursors give rise to a significant proportion of myofibroblasts in fibrosis of the liver (reviewed in), the lung , the kidney [42-45] and the heart . However, other reports using bone-marrow transplantation of collagen-1α1 or -1α2 driven GFP suggest that only a very small fraction of myofibroblasts in liver fibrosis is originated by the bone marrow [11]. The same controversy exists in the kidney, where reports of experiments with bone-marrow chimerism of Collagen-1α1 [41] or Collagen-1α2 [49] came to the conclusion that there is no significant contribution of circulating bone-marrow derived cells to renal myofibroblasts. However, Lebleu et al. recently reported, after performing bone-marrow transplantation experiments with αSMA-RFP mice, that 35% of renal myofibroblasts after unilateral ureteral obstruction were bone marrow derived [49].

Among the candidates of bone-marrow derived circulating progenitors of myofibroblasts are mesenchymal stromal cells (MSC) and fibrocytes (CD45+, CD34+). Reich et al. reported recently that bone marrow derived collagenI+CD11b+ fibrocytes are very distinct from monocytes and were recruited to injured kidneys after UUO [50]. Depletion of CD11+ fibrocytes using the human diphtheria toxin receptor resulted in reduced renal collagen I deposition [51]. Given this controversy, further studies are needed to understand the contribution of bone-marrow progenitors to the myofibroblast pool in solid organ fibrosis and to elucidate which bone-marrow cell-type gives rise to myofibroblasts.

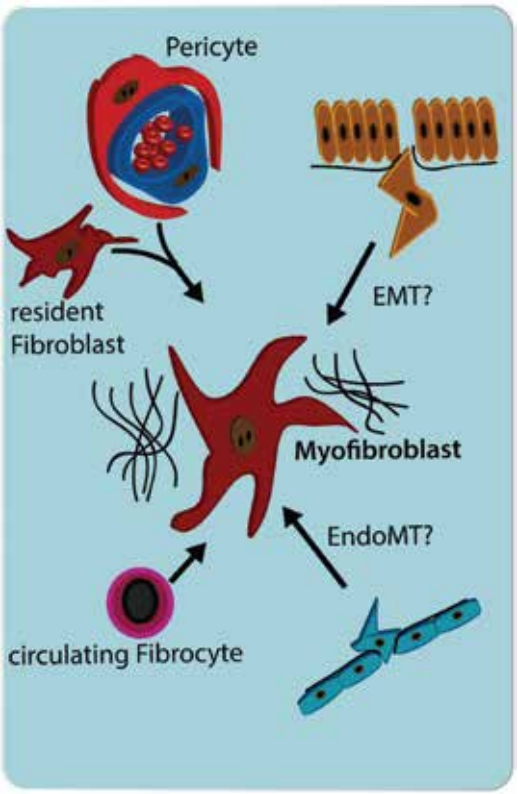

Figure 2. Concepts of myofibroblast recruitment in tissue fibrosis. Myofibroblast recruitment: the recent literature favours the theory that myofibroblasts are predominantly derived from local mesenchymal cells as pericytes and resident fibroblasts. Epithelial–mesenchymal transition (EMT) is still controversially discussed as one source of myofibroblasts. It is known that epithelial cells undergo transdifferentiation and acquire a mesenchymal phenotype; however, there are not many strong data suggesting that epithelial cells traverse the basement embrane. In the heart it has been reported that endothelial cells contribute to the pool of myofibroblasts via endothelial–mesenchymal transition (EndoMT). Bone marrow derived cells as fibrocytes or mesenchymal stem/ stromal cells (MSC), might also contribute to the recruitment of myofibroblasts.

Resident Mesenchymal Cells

The traditional view holds that myofibroblasts derive from resident fibroblasts which are thought to be quiescent in every tissue and become activated after injury, proliferate, gain α-SMA and start to produce extracellular matrix [11, 52, 53]. In the liver, portal fibroblasts and hepatic stelatae cells (HSCs), both distinct resident mesenchymal cells are able to gain α-SMA and contribute to myofibroblasts in fibrogenesis (reviewed in). HSCs, resident fibroblasts, portal fibroblasts and adventitial fibroblasts are all resident mesenchymal cells contributing to the myofibroblast population in fibrosis. In the last decade, indirect evidence has implicated another resident mesenchymal cell as a myofibroblast progenitor -the pericyte, which is abundant throughout the body . Our genetic lineage analysis provides strong evidence for the pericyte as the primary myofibroblast progenitor in the kidney. In a first experiment we genetically traced epithelial cells in kidney fibrosis and found no evidence that EMT contributes to myofibroblasts . Second, we performed lineage tracing using an inducible CreERt2 driven by the *FoxD1* to genetically tag interstitial pericytes. During nephrogenesis FoxD1 is expressed in the stroma surrounding cap mesenchyme, FoxD1+ cells give rise to pericytes and perivascular fibroblasts but also vascular smooth muscle cells and mesangial cells but no epithelial cells [15, 56]. We demonstrated, that in kidney fibrosis these genetically labeled pericytes/perivascuar fibroblasts expand, acquire α-SMA expression and contribute to the pool of myofibroblasts [25]. Our studies did not suggest that other cell-types besides pericytes contribute to myofibroblasts, however this is a difficult point to prove and more lineage tracing studies are required to confirm that pericytes are the major source of kidney fibroblasts. It also remains unclear whether all FoxD1-labeled cells are pericytes, or rather a mixture of pericytes and resident fibroblasts.

There are currently no studies showing pericytes contribute to fibrogenesis in the heart. Rock et al., recently reported that resident lung pericytes are a major source of activated myofibroblasts in bleomycin induces pulmonary fibrosis [57]. HSCs, the resident pericytes of the liver, have been thought for many years to be the major source of myofibroblasts [58]. In spinal cord scarring, Glast expressing pericytes (referred to as Type A pericytes in the spinal cord) in response to injury leave the vascular wall, gain α-SMA and fibronectin expression and contribute significantly to extracellular matrix remodeling and scar tissue formation [59]. Dulauroy and colleagues recently demonstrated that the majority of myofibroblasts developing after acute injury of muscle and dermis are generated from mesenchymal PDGFRα^{+}, ADAM12^{+} perivascular cells [60]. The functional role of pericytes is not completely understood, they seem to have various important roles including vessel stabilization (Figure 1B), regulation of the capillary diameter, angiogenesis, and regulation of endothelial cells, (reviewed in [60]). Crisan et al. reported in human tissue that some, if not all, pericytes express the typical surface marker pattern of mesenchymal stem/stromal cells and have a tri-lineage-capacity [41]. Furthermore, sorted human pericytes were able to differentiate into skeletal muscle cells when injected into the injured muscle of SCID-NOD

mice [41]. In a recent publication, Lebleu et al. reported that in renal fibrogenesis 50% of myofibroblasts arise from resident fibroblasts whereas 35% are recruited from the bone-marrow and 10% occur through EndoMT and 5% through EMT [41]. The authors reported fate tracing experiments in NG2-YFP and PDGFRβ-RFP mice showing a significant expansion of NG2+ or PDGFRβ+ cells after UUO. They generated mice where the viral thymidine kinase in expressed under the control of the NG2 or the PDGFRβ promoter in order to ablate proliferating cells that express NG2 or PDGFRβ using ganciclovir injections. Despite a 55% reduction of NG2+ cells and a 80% reduction of PDGFRβ+ cells by ganciclovir treatment authors reported that the severity of fibrosis after UUO remained unchanged, concluding that pericytes do not contribute to renal fibrosis [11, 15, 61, 62]. Furthermore, the authors reported that only a minority of 3% of NG2+ and 6% of PDGFRβ+ expressing cells co-label for α-SMA concluding that pericytes do not become myofibroblasts. However when we look at their representative pictures (their supplementary figure 6) showing staining of PDGFRβ -Cre+,YFPf/f and NG2-Cre+, YFPf/f mice for aSMA it seems like the authors underestimate the amount of co-stained cells (yellow). This study contradicts various studies showing that PDGFRβ+ cells contribute to the renal myofibroblast pool and produce extracellular matrix . PDGFRβ and NG2 are unspecific pericyte markers and expressed in various other cell-types [64]. Some groups even see PDGFRβ as a marker for interstitial fibroblasts [63], and PDGFRβ expression has been reported in the rat kidney-fibroblast cell line NRK49F[41] Our own experiments indicate that the majority if not all of α-SMA expressing cells co-label with PDGFRβ after unilateral ureteral obstruction (Figure 3). Asada et al. reported recently that the majority of erythropoietin producing kidney fibroblasts arise from myelin protein zero-cre (P0-Cre) extrarenal cells and are able to produce erytropoietin. He demonstrated using P0-Cre/R26ECFP mice a dramatic expansion of these cells after UUO and that almost all of the ECFP+ cells co-label with aSMA and PDGFRβ [65-67]. All these findings are raising the question about efficiency in the reported thymidine kinase ablation experiments of Lebleu et al., which might be caused by mosaic expression of the thymidine kinase transgene .

Given this controversy in the field, further studies are needed to understand the cellular source of myofibroblasts in fibrotic disease and the role of pericytes in injury, repair, regeneration and fibrogenesis of major organs like kidney, heart, lung and liver.

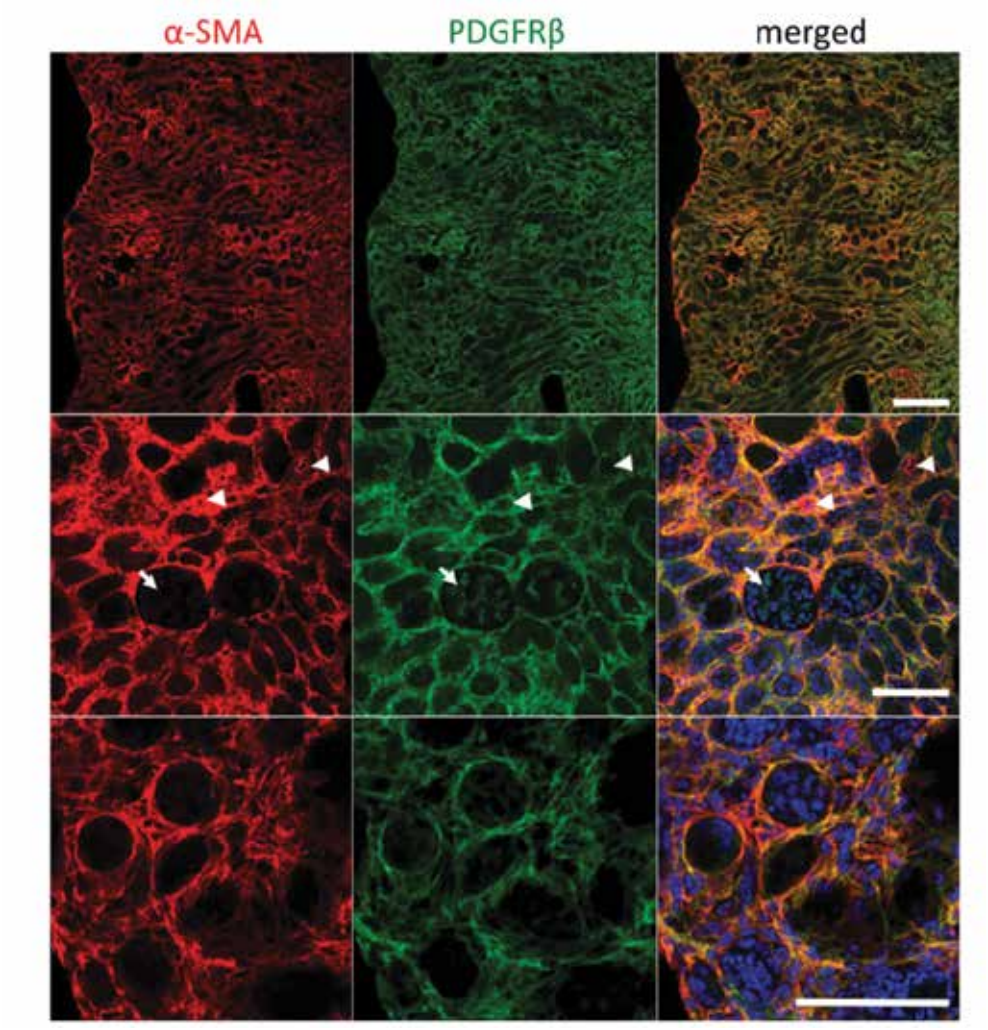

Figure 3 Most kidney myofibroblasts co-express αSMA and PDGFRβ. Co-staining of a fibrotic kidney (10 days after unilateral ureteral obstruction) for **α**-smooth muscle actin (**α**SMA; red, Cy3) and platelet-derived growth factor-**β** (PDGFR**β**; green, Cy5), indicating that the vast majority, if not all, **α**SMA+ myofibroblasts express PDGFR**β**. Note that mesangial cells in the glomerulus express PDGFR**β** but not **α**SMA (arrows) and vascular smooth muscle cells of the small arteries express very high levels of **α**SMA but stain only faintly for PDGFR**β** (arrowheads). Scale bars=200 **μ**m (upper panel); 40 **μ**m (all others).

Epithelial Injury Promotes Fibrosis

A key cellular event preceding development of fibrosis across different organs is injury to local epithelium. Chemical induction of epithelial injury is common to various rodent models of tissue fibrosis. For example, cisplatin-induced injury of renal tubular cells results in tubulo-interstital fibrosis, bleomycin infusion leads to alveolar epithelial cell death and pulmonary fibrosis, and systemic carbon tetrachloride exposure leads to hepatocyte necrosis and apoptosis in addition to severe liver fibrosis .

While exposure of epithelial cells to toxin exposure can result in the development of tissue fibrosis, there are examples of epithelial cell damage through genetic strategies that highlight the causative nature of epithelial damage and also demonstrate the importance of epithelial to stromal cell signaling in promotion of fibrosis. For example, in the kidney, Grgic et al. showed that targeted expression of the diphtheria toxin receptor in tubule cells allowed for potent induction of epithelial injury following diphtheria toxin exposure. This selective tubule epithelial cell injury then led to the development of interstitial fibrosis, capillary rarefaction, and mild glomerulosclerosis [70]. Interstitial pathology is also observed with targeted amplification of epithelial to interstitial cytokine signaling in the absence of epithelial insult. Kriz and colleagues overexpressed TGF-β1 in renal tubule cells, resulting in diffuse interstitial fibrosis prior to any epithelial cell damage. Subsequently, severe tubular damage developed, which was accompanied by massive tissue fibrosis [71].

Overall, it is becoming clear that a major initiating factor in scar tissue formation is exposure of epithelial cells to deleterious levels of genetic or chemical toxins, trauma, and inflammatory agents. This damage results in the enhanced production of secreted fibrogenic cytokines including TGF-β1, CTGF, PDGF, EGF and FGF, that signal from epithelial cells to the interstitial space that promote tissue inflammation, immune system response, and the activation, transformation and proliferation of pathogenic myofibroblasts [72-76].

Immune system activation promotes fibrosis

Chronic tissue injury results in the activation of the innate and adaptive immune response. Inflammation and the subsequent immune response is almost certainly a prerequisite for fibrosis in all settings as outlined in the thorough review of the immunological response in fibrosis by Wick et al. . During the initial stages of fibrosis there is prominent activation and recruitment of various mature lymphoid (natural killer/natural killer T-cells) and myeloid (eosinophils, neutrophils, mast cells, macrophages) lineage descendants into the injured tissue. Proinflammatory immunologic drivers of fibrosis include TNF-α, IL-1β, and the NALP3/ASC inflammasome as they are expressed in various tissues under fibrotic conditions.

Chronic inflammatory response persists when the CD4+ T helper type 17 (Th17) cell type dominates over the presence of T regulatory (Tregs) cells . The Th17 cytokine profile includes IL-17A, IL-22, and IL-23, however IL-17A appears to be a primary initiator of inflammation/ fibrosis as it has been implicated in pulmonary fibrosis, myocardial fibrosis, and hepatic

fibrosis . IL-17A is thought to be induced by IL-1β and in some cases TGF-β may induce its production [82, 83]. However, conflicting data suggests that IL-17A does not have pro-fibrotic effects and may only play a role in early inflammatory stages of tissue injury [84].

Profibrotic cytokine production is also characterized by an increase in the presence T helper type 2 (Th2) cells versus the T helper type 1 (Th1) cells. The Th2 cytokine profile is characterized by the increased production of IL-4, IL-5, IL-10, and IL-13 . Tissue samples with an imbalance in the Th1/Th2 profile in favor of Th2 resulted in impaired tissue repair and promotion of the migration, proliferation and activation of myofibroblasts . The Th1 profile is characterized by interferon gamma and IL-12 and appears to promote resolution of tissue inflammation and inhibition of fibrosis . Of the Th2 cytokines, IL-13 appears to be the main fibrotic effector in various models, including fluorescein isothiocyanate-induced pulmonary fibrosis, systemic sclerosis, radiation induced fibrosis, Crohns-disease induced fibrosis, and liver fibrosis . Profibrotic IL-13 signaling is primarily mediated through IL-13Rα1 .

Tissue damage and injury also results in the recruitment and infiltration of monocyte-derived cells, such as macrophages and dendritic cells. These immune cells have been shown to play a direct role in modulating the initiation and progression of inflammation and fibrosis. Either repression of macrophage activation or genetically targeted macrophage ablation alleviates progression of fibrosis . Macrophages can directly remodel extracellular matrix and can also signal to myofibroblasts, which can exacerbate tissue scarring. These deleterious macrophages have been identified in different subsets known as M1 or inflammatory macrophages, and M2a or profibrotic macrophages . M2a macrophages secrete a panel of cytokines, including TGF-β1, PDGF, FGF2, CCL18 and galectin-3, that can directly activate myofibroblasts and can serve as biomarkers that correlate with progression of fibrotic disease . M1 macrophages produce a proinflammatory effect on local tissue through release of various cytokines including IL-1, IL-6, TNF-α, and MCP-1 [105].

In addition to the M1 and M2a macrophage subtypes, it has recently been appreciated that a subset of macrophages called regulatory macrophages (M_{reg}M2c) can result in resolution of tissue fibrosis . These non-fibrotic macrophages are defined by secretion of IL-10 and their presence correlates with reduced fibrosis and inflammation in various organs [108]. Overall, the balance of these different macrophage populations within injured tissue plays a critical role in influencing the outcome towards either injury resolution or chronic inflammation and fibrosis.

Signaling pathways that promote fibrosis

A variety of pathways have been reported to regulate the transition of mesenchymal progenitors to myofibroblasts. We will focus on recent developments in seven signaling pathways (Figure 4): hedgehog-(Hh) Gli, platelet derived growth factor (PDGF), connective tissue growth factor (CTGF), epidermal growth factor (EGF). transforming growth factor β (TGFβ), Wnt and Notch signaling.

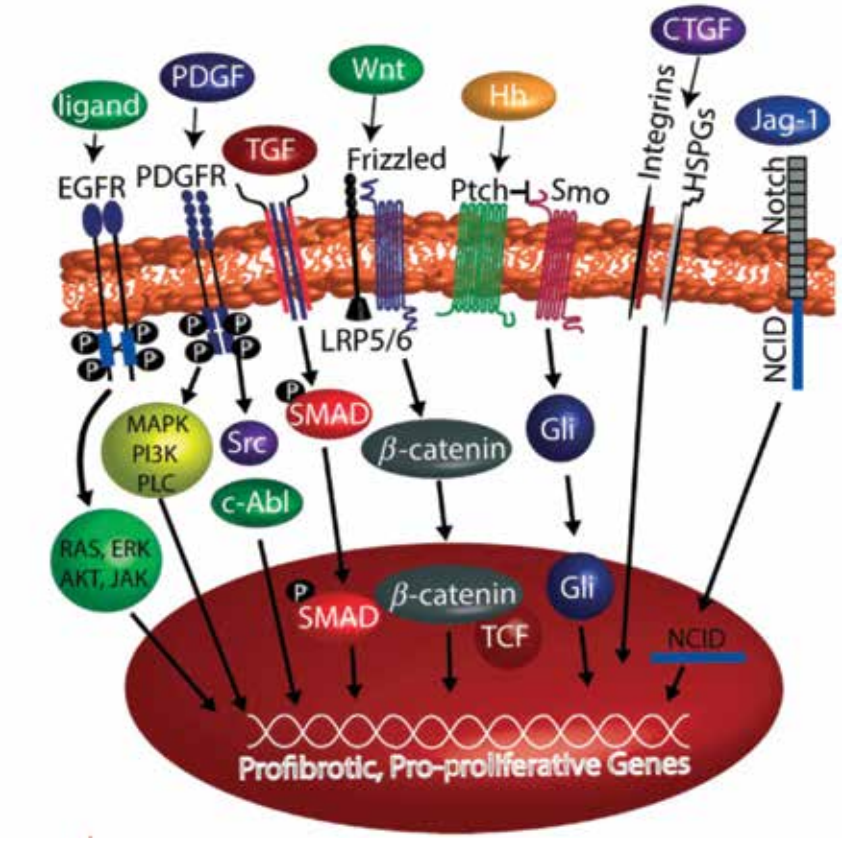

Figure 4. Key regulatory pathways driving transdifferentiation and expansion; growth factor signalling pathways important in fibrogenesis discussed in this review. Schematic illustration of platelet-derived growth factor (PDGF), transforming growth factor-β (TGFβ), Wnt, Hedgehog (Hh), connective tissue growth factor (CTGF), Notch and epidermal growth factor receptor (EGFR) signalling pathways.

HEDGEHOG-GLI SIGNALING

Members of Hh family of signaling proteins play important roles in determining cell fate, proliferation, embryonic patterning and morphogenesis [109]. The three Hh family members include sonic hedgehog (Shh), Indian hedgehog (Ihh) and desert hedgehog (Dhh). Prior to secretion, Hh ligands undergo intramolecular cleavage and lipid modification, and both events are required for signaling activities. Hh proteins act by binding to their membrane receptor Patched (Ptc), thereby releasing a tonic inhibition of Ptc on the transmembrane protein Smoothened (Smo). The activation of smoothened results in its translocation into the primary cilium with an accumulation of Supressor-of-fused (SUFU), Gli2 and Gli3 followed by the dissociation of the Gli2-SUFU complex within the cilium and the transport of the full-length activated Gli2 and Gli3 proteins to the nucleus which induce transcription

of hedgehog target genes, including Gli1 and Ptch1 [109]. The family of Gli proteins are the primary effectors of Hh signaling, all Gli proteins (Gli1, Gli2 and Gli3) have a DNA binding domain with five tandem C2H2 zing-fingers [110]. All Gli proteins contain an activator domain at their c-terminus, whereas only Gli2 and Gli3 also have an N-terminal repressor domain [111]. Hh signaling has multiple, context-dependent downstream effects such as controlling expression of patterning genes like Pax2 and Sall1 or regulating cell cycle by activating Cyclin D1 and N-Myc [112].

Emerging evidence implicates a critical role of the Hh pathway in fibrogenesis. In solid organ injury models and cancer, Hh ligands Shh and Ihh are secreted by epithelial-cells and transmit signals to the surrounding mesenchymal cells. In carcinogenesis, for example, Hh ligands from cancer cells act on adjacent stroma to promote the tumor micro environment [113]. Shin and colleagues recently reported that epithelial derived Shh after murine bladder injury induces Wnt expression in surrounding stromal cells leading to an increased epithelial and stromal proliferation in a paracrine fashion [113]. There is emerging evidence for Hh signaling in liver fibrogenesis (reviewed in [114]). The current concept of Hh signaling in liver fibrosis is that injury induces hepatocytes and cholangiocytes to produce the Hh ligands whereas sinusoidal lining cells reduce the expression of the Hh inhibitor Hhip upon injury. Hh responsive HSCs undergo transdifferentiation to a myofibroblastic phenotype and enter the cell-cycle [115]. Michelotti et al. recently reported that conditional knockout of smoothened in α-SMA expressing cells protected against liver fibrosis [116, 117].

In injury of the lung, Shh is upregulated in epithelial cells, and Ptch1 expression is increased in the pulmonary interstitium during fibrosis . We and others have shown that in kidney injury the Hh ligands Ihh and Shh are produced and secreted by epithelial cells and that interstitial pericytes/ fibroblasts respond to Hh [118]. Several Hh antagonistis are in clinical trials already [119], raising the prospect that these agents might be used to treat human kidney fibrosis. However in our hands targeting the Hh receptor Ptch1 with the cyclopamine derivate IPI-926, which has improved half-life and increased potency when compared to cyclopamine had no effect on the severity of kidney fibrosis despite complete inhibition of Gli1 expression. However Ding et al. reported that targeting Ptch1 with cyclopamine treatment as well as knockout of Gli1 was able to ameliorate kidney fibrosis [120]. The reasons for this discrepancy remain unclear and await further experimentation.

In our opinion, targeting the downstream Gli effectors of Hh signaling directly via small molecule compounds such as GANT61 may be superior to a therapeutic regime that acts upstream in the pathway. The cancer literature documents emerging evidence for non-canonical activation of Gli via TGFβ, PDGF and EGF signaling [121]. As these pathways play major roles in fibrosis there might exist a non-canonical activation of Gli effectors during fibrogenesis which would explain why inhibition of the Hh receptor had no effect. Clearly further studies are needed to elucidate the role of both canonical and non-canonical Hh signaling in fibrosis.

PLATELET-DERIVED GROWTH FACTOR

The PDGF family consists of four ligand isoforms (PDGF-A, -B, -C and –D). The biologically active PDGF protein forms disulfide-bonded homo-dimers PDGF-AA, BB, CC, DD and one heterodimer PDGF-AB. PDGF ligands induce homo- or hetero-dimerization of two tyrosine kinase receptors PDGFR-α and PDGFR–β. PDGF signaling plays a major role in wound healing, fibrosis, atherosclerosis and cancer [122]. PDGF stimulates the formation of granulation tissue and increases the proliferation and migration of neutrophils, macrophages, fibroblasts and smooth muscle cells [123]. The PDGFR–β inhibitor imatinib has been reported to inhibit proliferation of fibroblasts and recruitment of pericytes in dermal fibrogenesis [61]. In the kidney PDGFs are produced by endothelial cells, epithelial cells and macrophages upon injury and PDGFR-α and –β expressing interstitial fibroblasts / pericytes respond to the ligands and undergo transdifferentiation to myofibroblasts [124]. The PDGF system is upregulated in various models of kidney fibrosis, including unilateral ureteral obstruction, Thy 1.1 glomerulonephritis, lupus and ischemia-reperfusion injury. Chen et al. reported recently that all four PDGF isoforms are induced throughout kidney in fibrosis, with expression of both receptors in pericytes and myofibroblasts. Inhibition of PDGF signaling, either by imatinib, or neutralizing PDGFR antibodies amelioreated fibrosis [125].

In cardiac scarring after myocardial infarction all isoforms of PDGF and both receptors are upregulated [126, 127]. Lia et al. demonstrated that treatment with a neutralizing antibody against PDGFR-α attenuated atrial fibrosis in pressure overloaded mouse hearts . In human lung fibroblasts PDGF induces the production of Collagen I and fibronectin [128]. All PDGF ligands are upregulated in liver fibrosis induced by biliary duct ligation [128]. Interestingly, while treatment with a PDGF-C neutralizing antibody or knockout of PDGF-C ameliorates kidney fibrosis in mice, the extent of liver fibrosis remained unchanged [129-133]. While kidney fibroblasts show an increased proliferation in response to PDGF-C treatment, in liver myofibroblasts and HSCs PDGF-B and D might play the predominant role . These studies provide encouragement that the fibroblast/pericyte PDGF system represents a promising therapeutic target in fibrotic disease.

TRANSFORMING GROWTH FACTOR-β SIGNALING

The TGFβ cytokines (TGF-β1, TGF-β2, and TGF-β3) are ubiquitously expressed and play an active role in organism development, immune system regulation, and fibrotic disease. The TGFβ signaling pathway is a well-known and critical driver of fibrotic disease in a number of settings and tissue types, including diabetic nephropathy, rheumatoid arthritis, myocardial fibrosis, and idiopathic pulmonary fibrosis, among others . TGFβ ligands are synthesized by the majority of cell types of various mammalian organs and are first presented in a latent form as a pro-TGFβ multi-molecular construct that is tethered to the extracellular matrix (ECM) [136]. The N-terminal fragment is a disulfide bond linked homodimer called the latency associated peptide (LAP) and is non-covalently linked to a homodimer of the active

C-terminal fragment of the cytokine [135, 137, 138]. The LAP is associated with members of the latent TGF-β binding proteins (LTBPs) through disulfide bonds . The LTBPs are then bound to several ECM proteins through a transglutaminase linkage and remain in these latent complex reservoirs throughout various organs and tissues. Release of active TGFβ is accomplished through proteolytic cleavage and release of the active portion of TGFβ from the non-covalent interaction with the LAP.

In injured tissue, multiple signals are upregulated to accomplish the release of active TGFβ. This is achieved by physical interaction of LAP with matrix metalloproteinases (MMPs), integrins (particulary $\alpha_v\beta_6$) and thrombospondins, all of which are upregulated during fibrosis . Once the active form of TGFβ is released it binds to TGFβRII, which subsequently phosphorylates ALK-1 or ALK-5, two TGFβR1 members involved in TGFβ singaling. The RSmads Smad2/3 are then phosphorylated and bind to the co-Smad known as Smad4, which translocates the smad complex into the nucleus [134]. Once in the nucleus the complex binds to transcriptional coactivators including p300 and Creb-binding protein (CBP) or different transcriptional repressors including SkiL or TGIF to modify the transcription of various target genes [131, 140]. TGFβ can also signal through non-canonical pathways and has been shown to activate ERK, Pi3K, p38, JNK and ROCK .

In rheumatoid arthritis, signaling components of the TGFβ pathway are increased in synovial fibroblasts, neutralization of TGFβ can reverse experimental models of arthritis and overexpression of TGFβ in rabbit knees increased arthritic response [141-144]. In all animal models of diabetic nephropathy TGFβ is markedly increased and TGFβ signaling is upregulated in human biopsies of diabetic nephropathy. Genetic overexpression of TGFβ or exogenous TGFβ administration has been shown to drive renal fibrosis. Conversely, inhibiting TGFβ or its receptor with neutralizing antibodes, as well as genetic deletion of Smad3 has been shown to reduce renal fibrosis, including models of diabetic nephropathy .

Therapeutic inhibition of TGFβ remains a challenge due to its widespread expression and role in normal homeostatic procecess. For example, the neutralizing antibody CAT-192 was administered to patients with systemic sclerosis and did not provide any improvement while causing more serious adverse events than the placebo patients [146]. Strategies are currently being developed to selectively inhibit overactivation of TGFβ in fibrotic tissues, including testing of a monoclonal antibody that acts to inhibit integrin $\alpha_v\beta_{6,}$ in order to prevent cleavage of the LAP. This integrin is expressed in low levels in healthy tissues, while being strongly upregulated in fibrotic tissue and may result in fewer side effects as compared to general TGFβ inhibition [147].

EPIDERMAL GROWTH FACTOR RECEPTOR SIGNALING

Signaling through the receptor tyrosine kinase (RTK) epidermal growth factor receptor (EGFR), has been shown to promote fibrosis in different tissues. EGFR is a member of the ErbB family of RTKs and is also known as Her1/ErbB1. This family also includes Her2 (Neu/

ErbB2), Her3 (ErbB3), and Her4 (ErbB4). In addition to EGF, ligands for ErbB receptors include, transforming growth factor-α (TGF-α), heparin-binding EGF-like growth factor (HB-EGF), amphiregulin, neuregulin1-4, betacullulin, epiregulin and epigen [148]. ErbB1,3, and 4 exist in an inactive conformation that prevents homodimerization or heterodimerization with other ErbB receptors. ErbB2, on the other hand, is constitutively in an 'open' conformation, is constantly available for dimerization and, thus, is the preferred binding partner for the other receptors once they are activated. ErbB1,3 and 4 can be differentially activated through ligand binding to their extracellular domain, however there is no known ligand for ErbB2. Each ErbB family member can also be activated by ligand-independent mechanisms. (Reviewed in [149] and [150]). Dimerization results in transactivation of the receptor through autphosphorylation of the partner intracellular kinase domains and this subsequently allows for recruitment of binding partners from downstream cell signaling pathways such as the ERK-MAPK pathway, the PI3K pathway and the STAT3 pathway [151].

The involvement of the EGF signaling pathway in fibrosis has primarily been reported in the kidney and lung with anecdotal reports of EGFR signaling driving pancreatic fibrosis [152]. In the kidney, EGFR ligands including TGF-α and HB-EGF are released from renal epithelial cells after injury [153]. These ligands may then activate EGFR expressed on renal epithelial cells or on interstitial fibroblasts. Previous work has shown that targeted expression of a dominant-negative EGFR in renal proximal tubule cells could reduce tubulo-interstitial fibrosis in the subtotal nephrectomy and prolonged renal ischemia injury models [154]. Zhuang and colleagues utilized the Waved-2 mice, which express a defective EGFR with compromised activity, to show reduced renal fibrosis following induction of the unilateral ureteral obstruction model (UUO) in mice. They also showed that pharmacological blockade of EGFR with gefitinib could reduce renal fibrosis following UUO and that this outcome may be due to reduced production of inflammatory profibrotic cytokines from injured renal epithelium [155]. Sustained EGFR activation was also shown to play a role in the development of fibrosis for as long as 28 days after acute kidney injury and genetic suppression of EGFR activity could ameliorate this pathology [146]. An interaction between EGFR signaling and the TGFβ signaling pathway was shown by Chen et al., as TGFβ mediated fibrosis was shown to be dependent on EGFR activity in renal proximal tubules [156, 157].

In the lung, overexpression of the EGF pathway has been shown to promote lung fibrosis, and blockade of EGFR signaling can protect against pulmonary fibrosis . EGF ligands have been shown to be upregulated in models of lung injury as TGF-α is increased in rats that have been exposed to asbestos, and in the bleomycin model of idiopathic pulmonary fibrosis IPF [158]. Conditional overexpression of TGF-α in adult mouse lung has been shown to promote pulmonary fibrosis . Ishii et al. and Hardie et al, have both shown that EGFR blocking drugs can reduce lung fibrosis in the bleomycin and TGF-α overexpressing models, respectively [161]. On the contrary, there are reports indicating that blocking EGFR signaling can potentially play a role in worsening or exacerbating lung fibrosis. For example, the EGFR

inhibitor ZD1839 contributed to enhanced fibrosis in the bleomycin model of IPF [163]. Additionally, the EGFR ligand amphiregulin was shown to reduce fibrosis in the bleomycin model [164]. Overall, EGF signaling exerts a clear influence in the development of fibrosis in the kidney, however the role of this signaling pathway in lung fibrosis pathophysiology appears to be context-sensitive.

CONNECTIVE TISSUE GROWTH FACTOR

Connective tissue growth factor (CTGF), also called CCN2, belongs to the CCN family of matricellular proteins (reviewed in [163]). CTGF promotes angiogenesis, cell adhesion and is upregulated in fibrotic disease [165]. CTGF binds to extracellular matrix components as integrin β173 and heparin sulfated proteoglycans to promote adhesion as well as fibrogenesis [166]. CTGF has been reported to act as a co-factor for TGF-β induced expression of Collagen I and α-SMA [121]. Mice treated with a neutralizing antibody or siRNA against CTGF showed reduced lung fibrosis in response to bleomycin induced injury [167]. CTGF is strongly upregulated in fibrotic heart and might play a role in myocardial fibrosis [123]. In liver fibrosis CTGF is potently upregulated and promotes migration, proliferation and matrix production in activated HSCs [168]. In the kidney CTGF is highly produced by pericytes and podocytes [169, 170]. Pericytes stimulated with PDGF aquire a myofibroblastic phenotype. The first trials testing anti-CTGF antibodies to treat interstitial pulmonary fibrosis and liver fibrosis are underway.

WNT SIGNALING

The evolutionarily conserved Wnt family of secreted lipoglycoproteins regulate diverse morphogenic events during development. Wnt signaling has also been shown to play an essential role in stem cell renewal, tissue homeostasis, tissue regeneration and organogenesis [171, 172]. Numerous recent studies have implicated altered Wnt signaling in the progression of fibrotic disease in various organs. Canonical Wnt signaling, which results in stabilization and cytoplasmic accumulation of β-catenin followed by translocation into the nucleus and increased transcriptional activation, has been implicated in the fibroproliferative response. Wnt signaling has been shown to be active in wound healing responses and constitutively active β-catenin supports wound hyperplasia with excessive collagen synthesis [173, 174]. Distler and colleagues have reported on the important role of Wnt signaling in dermal and systemic sclerosis in a number of recent publications. They have shown that genetic stabilization or depletion of β-catenin can promote or ameliorate fibrosis, respectively [175]. They have also shown that canonical Wnt signaling is necessary for the TGF-β1 pathway to promote fibrosis . Wnt signaling activation has also been implicated in muscle fibrosis, pulmonary fibrosis and renal fibrosis among others .

A direct role for Wnt/β-catenin signaling in renal fibrosis was shown by Liu and colleagues, as targeted blockade of the pathway ablated progression of interstitial fibrosis.

The Wnt ligand Wnt4 had been suspected to play a role in kidney fibrosis, as it is strongly upregulated in interstitial myofibroblasts in a number of kidney fibrosis models [182]. We have recently shown that Wnt4 is expressed in medullary kidney myofibroblasts, however a targeted, cell specific genetic knockout of Wnt4 did not modulate the development or progression of fibrotic disease. While Wnt4 was knocked out other Wnt lignads were upregulated and supported continued activation of the β-catenin signaling pathway. This indicated compensation from the remaining Wnts and a possibility that β-catenin activation continued to drive fibrosis. Interestingly, genetic stabilization of β-catenin in interstitial cells contributed to spontaneous increases in α-SMA in uninjured mice [183]. A recent article by Duffield and colleagues highlights the importance of Wnt signaling pathway components in driving myofibroblast activation and proliferation, however they conclude that these effects are largely independent of β-catenin activity [183]. They show that Wnt ligands and the LRP-6 co-receptor act in concert with the PDGFRβ, TGFβR1 and CTGF signaling pathways in myofibroblasts and myofibroblast precursors and inhibition of these pathways can be achieved with Dickkopf-related protein 1 (DKK-1), a well known ligand for Wnt coreceptors LRP5/6 and inhibitor of the Wnt pathway. DKK-1 blockade of PDGF, TGFβ and CTGF signaling resulted in attenuation of myofibroblast transformation and activity. Clearly more research is needed to parse the contribution of β-catenin activity in the activation of myofibroblasts and the progression of fibrotic diseases.

NOTCH SIGNALING

The Notch family consists of four transmembrane receptors (Notch 1-4) activated by members of two ligand families, Jagged and Delta-like [184]. Binding of Notch ligands leads to cleaving of the transmembrane domain of Notch, allowing the release of the active Notch intracellular domain (NICD) [185]. Nuclear translocation of NICD results in transcription of the Notch target genes [186]. Various publications over the last decade indicate that the Notch signaling pathway might be involved in fibrogenesis. In renal fibrosis the ligand Jag-1 is upregulated in a TGF-beta dependent manner [187], tubulo-epithelial overexpression of NICD triggers interstitial fibrogenesis [188] and knockout of the receptor Notch 3 ameliorates kidney fibrosis after unilateral ureteral obstruction [189]. Dees et al. reported that NICD expression is upregualted in skin lesions of patients with systemic sclerosis and skin fibroblasts treated with recombinant human Jag-1 undergo transdifferentiation into myofibroblasts [190]. Notch signaling has also been linked to lung fibrosis as in murine lung fibroblasts Jag-1 overexpression was able to induce a transdifferentiation into myofibroblasts and Notch deficient mice (FX-KO) showed an decreased fibrotic response after intratracheal bleomycin instillation [191]. In human primary biliary cirrhosis increased levels of Jag-1 and Notch1/NICD have been reported [191]. It has recently been reported that Jag-1 and Notch-1 are upregulated in mouse myofibroblasts after biliary duct ligation *in vivo* [145]. A crosstalk between Hedgehog and Notch signaling might be required for HSC derived myofibroblasts

as blocking either pathway resulted in decreased expression of fibrotic readouts α-SMA and collagen I *in vitro* and conditional knockout of canonical Hh signaling in myofibroblasts resulted in decreased expression of Notch target genes *in vivo* [70].

Targeting the Notch signaling pathway might be a future strategy to treat fibrotic disease, however the involvement of Notch signaling in fibrosis in only partly understood and more studies are needed to elucidate it´s role in progression of fibrosis across different organs and tissues.

Therapeutic development for fibrotic disease

Fibrotic diseases represent a massive international public health and financial burden and the incidence of fibrotic disease is growing with the aging population demographic and the projected worldwide increase in the incidence of type II diabetes. Although this is a pressing medical issue it remains largely unaddressed, as there is currently only one approved drug in Europe and Asia indicated to treat IPF, called pirfenidone. Recently, biotech and pharmaceutical companies have given increased attention to fibrotic disease and there are a number of new therapies currently in clinical trials. Interestingly, the therapeutics in development reflect the broad array of signaling pathways and cell types that we have noted as being involved in the initiation and progression of fibrotic disease (Table 1).

The TGFβ pathway has been known to play a major role in fibrosis for over 20 years and multiple therapeutics have been developed to address this pathway. However, this pathway is also involved in regulating a variety of homeostatic functions including immune system control and tumor suppression. This has led to difficulty in creating systemic TGFβ pathway inhibitors as serious adverse events may arise during treatment of chronic fibrotic diseases. As mentioned previously, a TGF-β1 neutralizing antibody called CAT-192, or metelimumab, was tested in patients with systemic sclerosis and no conclusion could be made about efficacy, while patients receiving the drug experienced more adverse events, serious adverse events and deaths [6]. Despite safety concerns Sanofi/Genzyme is currently testing fresolimumab, a humanized antibody that blocks function of TGF-β1-3, in patients with FSGS (NCT01665391) and scleroderma (NCT01284322). Additionally, Eli Lilly and Company is testing a humanized monoclonal antibody against TGF-β1, named LY2382770, in diabetic kidney disease (NCT01113801). Biogen is targeting integrin $\alpha_v\beta_6$ with a humanized monoclonal antibody in order to prevent activation of LAP bound TGFβ from the ECM of inflamed and fibrotic tissue. A phase II clinical trial with this therapy, called STX-100, is currently recruiting patients with idiopathic pulmonary fibrosis (NCT01371305).

Anti-fibrotic therapeutics are also being developed to inhibit interleukins IL-4 and IL-13 that are commonly secreted by T helper type 2 cells. Novartis is developing an antibody to inhibit IL-13 known as QAX576 and is currently running trials in Crohn's disease and completed trials in patients with IPF, that unfortunately failed. Mediummune is developing an anti-IL-13 antibody called tralokinumab and is running a phase II trial in IPF (NCT01629667).

Finally, Sanofi is developing a bispecific-antibody (SAR156597) that inhibits both IL-4 and IL-13 and is currently recruiting IPF patients to test this compound in a phase I/II clinical trial (NCT01529853) [1].

Multiple signaling pathways downstream of receptor tyrosine kinases are active in driving fibrotic disease and therapeutics that inhibit these pathways are currently being tested. For example, BIBF-1120 (Vargatef) is an oral VEGFR, FGFR, and PDGFR inhibitor currently in phase III trials for treatment of IPF. The tyrosine kinase inhibitor Gleevec has been tested in trials to treat systemic sclerosis and IPF although it has appeared to fail both trials.

A variety of other pathways are being targeted by anti-fibrotic therapeutics. This includes a monoclonal antibody against CTGF (FG-3019) that is being developed by Fibrogen, Inc, to treat IPF and liver fibrosis (NCT01217632 & NCT00074698). An RNAi based approach is being developed by RXi Pharmaceuticals. Their compound, called RXI-109 is delivered by transdermal injection and is designed to inhibit the production of CTGF to block dermal fibrosis (NCT01640912). Other targets being addressed in fibrotic disease include the endothelin receptor (Bosentan, Ambrisentan, RE-021), LOXL2 (GS-6624), TNFα (entanercept), CCL2 (CNTO-888), and PTX-2 pathways (PRM-151) [2].

The wide range of targets being addressed by these compounds reflects uncertainty about which particular pathways are truly the driving force of fibrotic disease. The high rate of failure also highlights the difficulty in treating this disease and emphasizes the ambiguity in the underlying biology driving myofibroblast activation and persistence. The combination of clinical trials and basic research will ultimately reveal the essential core pathways of organ fibrosis and move this field closer to the identification of effective therapies for this widespread multi-organ chronic disease.

Conclusions

The source of the myofibroblast is still controversially discussed across different disciplines and organs. However, the recent literature points towards pericytes as a major source of fibrosis driving cells in multiple organs and tissues. Continued elucidation of markers specific to pericytes and genetic fate tracing experiments will be key in further establishing the pericyte as a major progenitor of myofibroblasts across different organs and tissues. Identifying the major cell-types involved in fibrosis and the pathways that drive their differentiation, expansion and proliferation is the first step towards novel targeted therapeutics to treat human fibrotic disease.

Acknowledgements

This work was supported by NIH DK088923 (to BDH), by an Established Investigator Award of the American Heart Association (to BDH) and by a fellowship of the Deutsche Forschungsgemeinschaft (to RK; KR4073/1-1) and by a research fellowship from the National Kidney Foundation to DPD (2011-D000691).

REFERENCES

Drug Name	Company	*Target/MOA*	Indication	Phase/Notes	Clinical Trials.gov identifier
pirfenidone	Intermune	*p38/TGFβ inhibitor*	IPF	Approved in Europe and Asia phase III In US - ongoing	NCT01366209
fresolimumab	Sanofi	*Anti-TGFβ monoclonal antibody*	Diffuse systemic sclerosis	phase I - recruiting	NCT01284322
			FSGS	Phase II - recruiting	NCT01665391
			IPF	Phase 1 - completed	NCT00125385
LY2382770	Lilly	*Anti-TGFβ monoclonal antibody*	Diabetic kidney disease- diabetic nephropathy, diabetic glomerulosclerosis	Phase II - recruiting	NCT01113801
STX-100	Biogen Idec	*Anti-$a_v b_6$ monoclonal antibody*	IPF	Phase II - recruiting	NCT01371305
macitentan	Actelion	*Endothelin receptor antagonist ET-A and ET-B*	IPF	Phase II - Fail	NCT00903331
bosentan	Actelion	*Endothelin receptor antagonist, ET-A and ET-B*	IPF	Phase III - Fail	NCT00631475
			Digital ulcers in SSc patients	Approved in EU	NCT00077584 NCT00319696
			Interstital lung disease with SSc	Phase II/III - did not improve outcomes vs. natural course	NCT00319033
ambrisentan	Gilead	*Endothelin receptor antagonist selective for ET-A*	IPF	Phase III - Fail	NCT00879229
RE-021	Retrophin	*Selective Endothelin type A receptor antagonist*	FSGS	Phase II – Not yet open	NCT01613118
FG-3019	Fibrogen	*Anti-CTGF*	Liver fibrosis due to HBV	phase II -ongoing	NCT01217632
			IPF	phase II - ongoing with promising preliminary results	NCT01262001

Drug Name	Company	*Target/MOA*	Indication	Phase/Notes	Clinical Trials.gov identifier
			Adolescents and adults with FSGS	Phase I - Terminated	NCT00782561
			Diabetic nephropathy	Phase II - Terminated	NCT00913393
			Locally advanced or metastatic pancreatic cancer	Phase I - ongoing	NCT01181245
PF-06473871	Pfizer	*Antisense CTGF*	Hypertrophic skin scarring	Phase II - recruiting	NCT01730339
RXI-109	RXi Pharmaceuticals	*CTGF RNAi*	Dermal scar prevention	Phase I - ongoing Phase I - recruiting	NCT01640912 NCT01780077
SAR156597	Sanofi	*Bi-specific IL-4/IL-13 mAB*	IPF	Phase I/II - recruiting	NCT01529853
tralokinumab	MedImmune	*IL13- inhibition*	IPF	Phase II - recruiting	NCT01629667
QAX576	Novartis	*IL13 - inhibition*	Pulmonary Fibrosis secondary to SSc	Phase II -Terminated due to SAE	NCT00581997
			IPF	Phase II - Terminated	NCT01266135
rilonacept	Regeneron	*IL-1 Trap*	SSc	Phase I/II - recruiting	NCT01538719
CNTO 888	Centocor	*MCP-1(CCL2) inhibition*	IPF	Phase II - completed	NCT00786201
etanercept	Pfizer/Amgen	*TNF-inhibition*	IPF	Phase II - Fail	NCT00063869
Actimmune	Intermune	*Human interferon gamma*	IPF	Phase III - Fail	NCT00075998
interferon-α *lozenge*	Amarillo Biosciences	*Oral IFN-α*	IPF	Phase II – Completed Phase II - Terminated	NCT01442779 NCT00690885
PRM-151	Promedior	*Recombinant pentraxin-2*	IPF	Phase I – completed improvements in FVC and 6MWT	NCT01254409
			Scarring in trabeculectomy	Phase II – completed	NCT01064817
belimumab	GlaxoSmithKline	*Anti-BAFF mAB*	Membranous glomerulnephritis	Phase II – recruiting	NCT01610492
pomalidomide	Celgene	*Multiple – anti angiogenic and immunomodulatory*	IPF	Phase II – Not yet recruiting	NCT01135199
			SSc	Phase II - Recruiting	NCT01559129
IW001	United Therapeutics	*Collagen V solution as immunomodulator*	IPF	Phase I - completed	NCT01199887
BMS-986020	Bristoly-Myers Squibb	*LPA1 receptor antagonist*	IPF	Phase II - recruiting	NCT01766817

SAR100842	sanofi	*LPA1/3 receptor antagonist*	Systemic sclerosis	Phase II - recruiting	NCT01651143
BIBF 1120	Boehringer Ingelheim	*VEGFR1-3, FGFR 1-3, PDGFRα/β inhibition*	IPF	Phase III - active, not recruiting Phase II showed positive trends in high dose	NCT01335464 NCT01335477
imatinib	Novartis	*BCR-ABL inhibitor / other tyrosine kinases*	SSc	Phase II - fail	NCT00613171
			IPF	Phase II/III - fail	NCT00131274
GSK2126458	GSK	*Pan-Pi3k/mTor inhibitor*	IPF	Phase I - recruiting	NCT01725139
CC-930	Celgene	*JNK inhibitor*	IPF	Phase II – Terminated poor benefit/risk	NCT01203943
bardoxolone methyl	Reata/Abbot	*Nrf2 pathway inducer*	Renal insufficiency, chronic type 2 diabetes	Phase III – Terminated per IDMC safety concerns	NCT01351675
GS-6624	Gilead	*LOXL2 inhibitor*	Pancreatic Cancer	Phase II - ongoing	NCT01472198
			Non-Alcoholic Steatohepatitis (NASH)	Phase II - recruiting	NCT01672879
			Liver Fibrosis with HIV, HCV or HIV/HCV	Phase II - recruiting	NCT01707472
			Grade 1-3 liver fibrosis	Phase II - active	NCT01452308
			myelofibrosis	Phase II - recruiting	NCT01369498
			IPF	Phase II - recruiting	NCT01769196
			PSC	Phase II - recruiting	NCT01672853

IPF – Idiopathic Pulmonary Fibrosis
SSc – Systemic Sclerosis
IL – Interleukin
TNF – Tumor Necrosis Factor
CTGF – Connective Tissue Growth Factor
HBV – Hepatitis B Virus
FSGS – Focal Segmental Glomerularsclerosis
LOXL2 – Lysyl Oxidase-Like-2
HIV – Human Immunodeficiency Virus
HCV – Hepatitis C Virus
VEGFR – Vascular Endothelial Growth Factor Receptor
FGFR – Fibroblast Growth Factor Receptor
PDGFR – Platelet Derived Growth Factor Receptor
MCP-1 – Monocyte Chemoattract Protein 1
LPA-1 – Lysophosphatidic Acid Receptor
BCR-ABL – Breakpoint Cluster Region-Ableson
Pi3k – Phosphoinositide 3-kinase
mTor – Mammalian Target of Rapamycin
TGFβ – Transforming Growth Factor Beta
Nrf2 – Nuclear Factor (erythroid-derived 2)-like 2
JNK – c-Jun N-terminal kinase
IFN – Interferon
BAFF – B-cell Activating Factor
PSC – Primary sclerosing cholangitis

Table 1: Therapeutics that are currently being tested or have been tested in fibrotic diseases (this list does not claim to be exhaustive).

1. Humphreys, B.D., *Targeting pericyte differentiation as a strategy to modulate kidney fibrosis in diabetic nephropathy.* Semin Nephrol, 2012. **32**(5): p. 463-70.
2. Ke, P.Y. and S.S. Chen, *Hepatitis C virus and cellular stress response: implications to molecular pathogenesis of liver diseases.* Viruses, 2012. **4**(10): p. 2251-90.
3. Weber, K.T., et al., *Myofibroblast-mediated mechanisms of pathological remodelling of the heart.* Nat Rev Cardiol, 2013. **10**(1): p. 15-26.
4. Kong, P., P. Christia, and N.G. Frangogiannis, *The pathogenesis of cardiac fibrosis.* Cell Mol Life Sci, 2013.
5. Wynn, T.A., *Integrating mechanisms of pulmonary fibrosis.* J Exp Med, 2011. **208**(7): p. 1339-50.
6. Duffield, J.S., et al., *Host responses in tissue repair and fibrosis.* Annu Rev Pathol, 2013. **8**: p. 241-76.
7. Otranto, M., et al., *The role of the myofibroblast in tumor stroma remodeling.* Cell Adh Migr, 2012. **6**(3): p. 203-19.
8. Eyden, B., *The myofibroblast: a study of normal, reactive and neoplastic tissues, with an emphasis on ultrastructure. part 2 - tumours and tumour-like lesions.* J Submicrosc Cytol Pathol, 2005. **37**(3-4): p. 231-96.
9. Hinz, B., *The myofibroblast: paradigm for a mechanically active cell.* J Biomech, 2010. **43**(1): p. 146-55.
10. Follonier Castella, L., et al., *Regulation of myofibroblast activities: calcium pulls some strings behind the scene.* Exp Cell Res, 2010. **316**(15): p. 2390-401.
11. Lin, S.L., et al., *Pericytes and perivascular fibroblasts are the primary source of collagen-producing cells in obstructive fibrosis of the kidney.* Am J Pathol, 2008. **173**(6): p. 1617-27.
12. Nakaya, Y. and G. Sheng, *EMT in developmental morphogenesis.* Cancer Lett, 2013.
13. Kalluri, R. and R.A. Weinberg, *The basics of epithelial-mesenchymal transition.* J Clin Invest, 2009. **119**(6): p. 1420-8.
14. Liu, Y., *Epithelial to mesenchymal transition in renal fibrogenesis: pathologic significance, molecular mechanism, and therapeutic intervention.* J Am Soc Nephrol, 2004. **15**(1): p. 1-12.
15. Humphreys, B.D., et al., *Fate tracing reveals the pericyte and not epithelial origin of myofibroblasts in kidney fibrosis.* Am J Pathol, 2010. **176**(1): p. 85-97.
16. Kida, Y. and J.S. Duffield, *Pivotal role of pericytes in kidney fibrosis.* Clin Exp Pharmacol Physiol, 2011. **38**(7): p. 467-73.
17. Le Hir, M., et al., *Characterization of renal interstitial fibroblast-specific protein 1/S100A4-positive cells in healthy and inflamed rodent kidneys.* Histochem Cell Biol, 2005. **123**(4-5): p. 335-46.
18. Mlodzik, K., et al., *Ecto-5'-nucleotidase is expressed by pericytes and fibroblasts in the rat heart.* Histochem Cell Biol, 1995. **103**(3): p. 227-36.
19. Kim, K.K., et al., *Alveolar epithelial cell mesenchymal transition develops in vivo during pulmonary fibrosis and is regulated by the extracellular matrix.* Proc Natl Acad Sci U S A, 2006. **103**(35): p. 13180-5.
20. Zeisberg, M., et al., *Fibroblasts derive from hepatocytes in liver fibrosis via epithelial to mesenchymal transition.* J Biol Chem, 2007. **282**(32): p. 23337-47.
21. Rastaldi, M.P., et al., *Epithelial-mesenchymal transition of tubular epithelial cells in human renal biopsies.* Kidney Int, 2002. **62**(1): p. 137-46.
22. Zeisberg, M., et al., *BMP-7 counteracts TGF-beta1-induced epithelial-to-mesenchymal transition and reverses chronic renal injury.* Nat Med, 2003. **9**(7): p. 964-8.
23. Iwano, M., et al., *Evidence that fibroblasts derive from epithelium during tissue fibrosis.* J Clin Invest, 2002. **110**(3): p. 341-50.
24. Chu, A.S., et al., *Lineage tracing demonstrates no evidence of cholangiocyte epithelial-to-mesenchymal transition in murine models of hepatic fibrosis.* Hepatology, 2011. **53**(5): p. 1685-95.

25. Rock, J.R., et al., *Multiple stromal populations contribute to pulmonary fibrosis without evidence for epithelial to mesenchymal transition.* Proc Natl Acad Sci U S A, 2011. **108**(52): p. E1475-83.
26. Zeisberg, E.M., et al., *Endothelial-to-mesenchymal transition contributes to cardiac fibrosis.* Nat Med, 2007. **13**(8): p. 952-61.
27. Phua, Y.L., et al., *Distinct sites of renal fibrosis in Crim1 mutant mice arise from multiple cellular origins.* J Pathol, 2013. **229**(5): p. 685-96.
28. Medici, D., et al., *Conversion of vascular endothelial cells into multipotent stem-like cells.* Nat Med, 2010. **16**(12): p. 1400-6.
29. De Palma, M., et al., *Tie2 identifies a hematopoietic lineage of proangiogenic monocytes required for tumor vessel formation and a mesenchymal population of pericyte progenitors.* Cancer Cell, 2005. **8**(3): p. 211-26.
30. De Palma, M., et al., *Targeting exogenous genes to tumor angiogenesis by transplantation of genetically modified hematopoietic stem cells.* Nat Med, 2003. **9**(6): p. 789-95.
31. Nin g, H., et al., *Mesenchymal stem cell marker Stro-1 is a 75 kd endothelial antigen.* Biochem Biophys Res Commun, 2011. **413**(2): p. 353-7.
32. Tigges, U., et al., *A novel and simple method for culturing pericytes from mouse brain.* Microvasc Res, 2012. **84**(1): p. 74-80.
33. Gitlin, J.D. and P.A. D'Amore, *Culture of retinal capillary cells using selective growth media.* Microvasc Res, 1983. **26**(1): p. 74-80.
34. Russo, F.P., et al., *The bone marrow functionally contributes to liver fibrosis.* Gastroenterology, 2006. **130**(6): p. 1807-21.
35. Forbes, S.J., et al., *A significant proportion of myofibroblasts are of bone marrow origin in human liver fibrosis.* Gastroenterology, 2004. **126**(4): p. 955-63.
36. Sch olten, D., et al., *Migration of fibrocytes in fibrogenic liver injury.* Am J Pathol, 2011. **179**(1): p. 189-98.
37. Kisseleva, T. and D.A. Brenner, *Anti-fibrogenic strategies and the regression of fibrosis.* Best Pract Res Clin Gastroenterol, 2011. **25**(2): p. 305-17.
38. Moore, B.B., et al., *CCR2-mediated recruitment of fibrocytes to the alveolar space after fibrotic injury.* Am J Pathol, 2005. **166**(3): p. 675-84.
39. Moore, B.B., et al., *The role of CCL12 in the recruitment of fibrocytes and lung fibrosis.* Am J Respir Cell Mol Biol, 2006. **35**(2): p. 175-81.
40. Phillips, R.J., et al., *Circulating fibrocytes traffic to the lungs in response to CXCL12 and mediate fibrosis.* J Clin Invest, 2004. **114**(3): p. 438-46.
41. LeBleu, V.S., et al., *Origin and function of myofibroblasts in kidney fibrosis.* Nat Med, 2013. **19**(8): p. 1047-53.
42. Falkenham, A., et al., *Early Fibroblast Progenitor Cell Migration to the AngII-Exposed Myocardium Is Not CXCL12 or CCL2 Dependent as Previously Thought.* Am J Pathol, 2013.
43. Frangogiannis, N.G., et al., *Critical role of monocyte chemoattractant protein-1/CC chemokine ligand 2 in the pathogenesis of ischemic cardiomyopathy.* Circulation, 2007. **115**(5): p. 584-92.
44. Haudek, S.B., et al., *Bone marrow-derived fibroblast precursors mediate ischemic cardiomyopathy in mice.* Proc Natl Acad Sci U S A, 2006. **103**(48): p. 18284-9.
45. Mollmann, H., et al., *Bone marrow-derived cells contribute to infarct remodelling.* Cardiovasc Res, 2006. **71**(4): p. 661-71.
46. Higashiyama, R., et al., *Negligible contribution of bone marrow-derived cells to collagen production during hepatic fibrogenesis in mice.* Gastroenterology, 2009. **137**(4): p. 1459-66 e1.
47. Kisseleva, T., et al., *Bone marrow-derived fibrocytes participate in pathogenesis of liver fibrosis.* J Hepatol, 2006. **45**(3): p. 429-38.

48. Roufosse, C., et al., *Bone marrow-derived cells do not contribute significantly to collagen I synthesis in a murine model of renal fibrosis.* J Am Soc Nephrol, 2006. **17**(3): p. 775-82.
49. Reich, B., et al., *Fibrocytes develop outside the kidney but contribute to renal fibrosis in a mouse model.* Kidney Int, 2013. **84**(1): p. 78-89.
50. Picard, N., et al., *Origin of renal myofibroblasts in the model of unilateral ureter obstruction in the rat.* Histochem Cell Biol, 2008. **130**(1): p. 141-55.
51. Iwaisako, K., D.A. Brenner, and T. Kisseleva, *What's new in liver fibrosis? The origin of myofibroblasts in liver fibrosis.* J Gastroenterol Hepatol, 2012. **27 Suppl 2**: p. 65-8.
52. Gabbiani, G., *The cellular derivation and the life span of the myofibroblast.* Pathol Res Pract, 1996. **192**(7): p. 708-11.
53. Rajkumar, V.S., et al., *Shared expression of phenotypic markers in systemic sclerosis indicates a convergence of pericytes and fibroblasts to a myofibroblast lineage in fibrosis.* Arthritis Res Ther, 2005. **7**(5): p. R1113-23.
54. Levinson, R.S., et al., *Foxd1-dependent signals control cellularity in the renal capsule, a structure required for normal renal development.* Development, 2005. **132**(3): p. 529-39.
55. Hatini, V., et al., *Essential role of stromal mesenchyme in kidney morphogenesis revealed by targeted disruption of Winged Helix transcription factor BF-2.* Genes Dev, 1996. **10**(12): p. 1467-78.
56. Grgic, I., J.S. Duffield, and B.D. Humphreys, *The origin of interstitial myofibroblasts in chronic kidney disease.* Pediatr Nephrol, 2012. **27**(2): p. 183-93.
57. Goritz, C., et al., *A pericyte origin of spinal cord scar tissue.* Science, 2011. **333**(6039): p. 238-42.
58. Dulauroy, S., et al., *Lineage tracing and genetic ablation of ADAM12(+) perivascular cells identify a major source of profibrotic cells during acute tissue injury.* Nat Med, 2012. **18**(8): p. 1262-70.
59. Armulik, A., G. Genove, and C. Betsholtz, *Pericytes: developmental, physiological, and pathological perspectives, problems, and promises.* Dev Cell, 2011. **21**(2): p. 193-215.
60. Crisan, M., et al., *Perivascular multipotent progenitor cells in human organs.* Ann N Y Acad Sci, 2009. **1176**: p. 118-23.
61. Chen, Y.T., et al., *Platelet-derived growth factor receptor signaling activates pericyte-myofibroblast transition in obstructive and post-ischemic kidney fibrosis.* Kidney Int, 2011. **80**(11): p. 1170-81.
62. Lin, S.L., et al., *Targeting endothelium-pericyte cross talk by inhibiting VEGF receptor signaling attenuates kidney microvascular rarefaction and fibrosis.* Am J Pathol, 2011. **178**(2): p. 911-23.
63. Asada, N., et al., *Dysfunction of fibroblasts of extrarenal origin underlies renal fibrosis and renal anemia in mice.* J Clin Invest, 2011. **121**(10): p. 3981-90.
64. Seikrit, C., et al., *Biological responses to PDGF-AA versus PDGF-CC in renal fibroblasts.* Nephrol Dial Transplant, 2013. **28**(4): p. 889-900.
65. Yamate, J., et al., *Immunohistochemical study of rat renal interstitial fibrosis induced by repeated injection of cisplatin, with special reference to the kinetics of macrophages and myofibroblasts.* Toxicol Pathol, 1996. **24**(2): p. 199-206.
66. Degryse, A.L., et al., *Repetitive intratracheal bleomycin models several features of idiopathic pulmonary fibrosis.* Am J Physiol Lung Cell Mol Physiol, 2010. **299**(4): p. L442-52.
67. Shi, J., et al., *Evidence of hepatocyte apoptosis in rat liver after the administration of carbon tetrachloride.* Am J Pathol, 1998. **153**(2): p. 515-25.
68. Grgic, I., et al., *Targeted proximal tubule injury triggers interstitial fibrosis and glomerulosclerosis.* Kidney Int, 2012. **82**(2): p. 172-83.
69. Koesters, R., et al., *Tubular overexpression of transforming growth factor-beta1 induces autophagy and fibrosis but not mesenchymal transition of renal epithelial cells.* Am J Pathol, 2010. **177**(2): p. 632-43.

70. Friedman, S.L., et al., *Therapy for fibrotic diseases: nearing the starting line.* Sci Transl Med, 2013. **5**(167): p. 167sr1.
71. Wick, G., et al., *The immunology of fibrosis.* Annu Rev Immunol, 2013. **31**: p. 107-35.
72. Zhang, Y., et al., *Enhanced IL-1 beta and tumor necrosis factor-alpha release and messenger RNA expression in macrophages from idiopathic pulmonary fibrosis or after asbestos exposure.* J Immunol, 1993. **150**(9): p. 4188-96.
73. Piguet, P.F., et al., *Tumor necrosis factor/cachectin plays a key role in bleomycin-induced pneumopathy and fibrosis.* J Exp Med, 1989. **170**(3): p. 655-63.
74. Tomita, K., et al., *Tumour necrosis factor alpha signalling through activation of Kupffer cells plays an essential role in liver fibrosis of non-alcoholic steatohepatitis in mice.* Gut, 2006. **55**(3): p. 415-24.
75. He, X., et al., *Inflammation and fibrosis during Chlamydia pneumoniae infection is regulated by IL-1 and the NLRP3/ASC inflammasome.* J Immunol, 2010. **184**(10): p. 5743-54.
76. Vilaysane, A., et al., *The NLRP3 inflammasome promotes renal inflammation and contributes to CKD.* J Am Soc Nephrol, 2010. **21**(10): p. 1732-44.
77. Wilson, M.S., et al., *Bleomycin and IL-1beta-mediated pulmonary fibrosis is IL-17A dependent.* J Exp Med, 2010. **207**(3): p. 535-52.
78. Feng, W., et al., *IL-17 induces myocardial fibrosis and enhances RANKL/OPG and MMP/TIMP signaling in isoproterenol-induced heart failure.* Exp Mol Pathol, 2009. **87**(3): p. 212-8.
79. Foster, R.G., et al., *Interleukin (IL)-17/IL-22-producing T cells enriched within the liver of patients with chronic hepatitis C viral (HCV) infection.* Dig Dis Sci, 2012. **57**(2): p. 381-9.
80. Rosenbloom, J., F.A. Mendoza, and S.A. Jimenez, *Strategies for anti-fibrotic therapies.* Biochim Biophys Acta, 2013. **1832**(7): p. 1088-103.
81. Gasse, P., et al., *IL-1 and IL-23 mediate early IL-17A production in pulmonary inflammation leading to late fibrosis.* PLoS One, 2011. **6**(8): p. e23185.
82. Nakashima, T., et al., *Impaired IL-17 signaling pathway contributes to the increased collagen expression in scleroderma fibroblasts.* J Immunol, 2012. **188**(8): p. 3573-83.
83. Lo Re, S., et al., *IL-17A-producing gammadelta T and Th17 lymphocytes mediate lung inflammation but not fibrosis in experimental silicosis.* J Immunol, 2010. **184**(11): p. 6367-77.
84. Wynn, T.A., *Fibrotic disease and the T(H)1/T(H)2 paradigm.* Nat Rev Immunol, 2004. **4**(8): p. 583-94.
85. Shi, Z., A.E. Wakil, and D.C. Rockey, *Strain-specific differences in mouse hepatic wound healing are mediated by divergent T helper cytokine responses.* Proc Natl Acad Sci U S A, 1997. **94**(20): p. 10663-8.
86. Furuie, H., et al., *Altered accessory cell function of alveolar macrophages: a possible mechanism for induction of Th2 secretory profile in idiopathic pulmonary fibrosis.* Eur Respir J, 1997. **10**(4): p. 787-94.
87. Mavalia, C., et al., *Type 2 helper T-cell predominance and high CD30 expression in systemic sclerosis.* Am J Pathol, 1997. **151**(6): p. 1751-8.
88. Yoshizaki, A., et al., *Cell adhesion molecules regulate fibrotic process via Th1/Th2/Th17 cell balance in a bleomycin-induced scleroderma model.* J Immunol, 2010. **185**(4): p. 2502-15.
89. Kolodsick, J.E., et al., *Protection from fluorescein isothiocyanate-induced fibrosis in IL-13-deficient, but not IL-4-deficient, mice results from impaired collagen synthesis by fibroblasts.* J Immunol, 2004. **172**(7): p. 4068-76.
90. Weng, H.L., et al., *The etiology of liver damage imparts cytokines transforming growth factor beta1 or interleukin-13 as driving forces in fibrogenesis.* Hepatology, 2009. **50**(1): p. 230-43.
91. Shimamura, T., et al., *Novel role of IL-13 in fibrosis induced by nonalcoholic steatohepatitis and its amelioration by IL-13R-directed cytotoxin in a rat model.* J Immunol, 2008. **181**(7): p. 4656-65.
92. Han, G., et al., *Th2-like immune response in radiation-induced lung fibrosis.* Oncol Rep, 2011. **26**(2): p. 383-8.

93. Chiaramonte, M.G., et al., *Regulation and function of the interleukin 13 receptor alpha 2 during a T helper cell type 2-dominant immune response.* J Exp Med, 2003. **197**(6): p. 687-701.
94. Duffield, J.S., et al., *Selective depletion of macrophages reveals distinct, opposing roles during liver injury and repair.* J Clin Invest, 2005. **115**(1): p. 56-65.
95. Duffield, J.S., et al., *Conditional ablation of macrophages halts progression of crescentic glomerulonephritis.* Am J Pathol, 2005. **167**(5): p. 1207-19.
96. Castano, A.P., et al., *Serum amyloid P inhibits fibrosis through Fc gamma R-dependent monocyte-macrophage regulation in vivo.* Sci Transl Med, 2009. **1**(5): p. 5ra13.
97. Mosser, D.M. and J.P. Edwards, *Exploring the full spectrum of macrophage activation.* Nat Rev Immunol, 2008. **8**(12): p. 958-69.
98. Wynn, T.A. and L. Barron, *Macrophages: master regulators of inflammation and fibrosis.* Semin Liver Dis, 2010. **30**(3): p. 245-57.
99. Wahl, S.M., et al., *Macrophage production of TGF-beta and regulation by TGF-beta.* Ann N Y Acad Sci, 1990. **593**: p. 188-96.
100. Henke, C., et al., *Macrophage production of basic fibroblast growth factor in the fibroproliferative disorder of alveolar fibrosis after lung injury.* Am J Pathol, 1993. **143**(4): p. 1189-99.
101. Martinet, Y., et al., *Exaggerated spontaneous release of platelet-derived growth factor by alveolar macrophages from patients with idiopathic pulmonary fibrosis.* N Engl J Med, 1987. **317**(4): p. 202-9.
102. Prasse, A., et al., *A vicious circle of alveolar macrophages and fibroblasts perpetuates pulmonary fibrosis via CCL18.* Am J Respir Crit Care Med, 2006. **173**(7): p. 781-92.
103. Chen, J.F., et al., *Pirfenidone inhibits macrophage infiltration in 5/6 nephrectomized rats.* Am J Physiol Renal Physiol, 2013. **304**(6): p. F676-85.
104. Spencer, M., et al., *Adipose tissue macrophages in insulin-resistant subjects are associated with collagen VI and fibrosis and demonstrate alternative activation.* Am J Physiol Endocrinol Metab, 2010. **299**(6): p. E1016-27.
105. Nishida, M., et al., *Adoptive transfer of macrophages ameliorates renal fibrosis in mice.* Biochem Biophys Res Commun, 2005. **332**(1): p. 11-6.
106. Murai, M., et al., *Interleukin 10 acts on regulatory T cells to maintain expression of the transcription factor Foxp3 and suppressive function in mice with colitis.* Nat Immunol, 2009. **10**(11): p. 1178-84.
107. van Strien, M.E., et al., *Anti-inflammatory effect by lentiviral-mediated overexpression of IL-10 or IL-1 receptor antagonist in rat glial cells and macrophages.* Gene Ther, 2010. **17**(5): p. 662-71.
108. Ingham, P.W., *Transducing Hedgehog: the story so far.* EMBO J, 1998. **17**(13): p. 3505-11.
109. Briscoe, J. and P.P. Therond, *The mechanisms of Hedgehog signalling and its roles in development and disease.* Nat Rev Mol Cell Biol, 2013. **14**(7): p. 416-29.
110. Hu, M.C., et al., *GLI3-dependent transcriptional repression of Gli1, Gli2 and kidney patterning genes disrupts renal morphogenesis.* Development, 2006. **133**(3): p. 569-78.
111. Yauch, R.L., et al., *A paracrine requirement for hedgehog signalling in cancer.* Nature, 2008. **455**(7211): p. 406-10.
112. Shin, K., et al., *Hedgehog/Wnt feedback supports regenerative proliferation of epithelial stem cells in bladder.* Nature, 2011. **472**(7341): p. 110-4.
113. Choi, S.S., et al., *The role of Hedgehog signaling in fibrogenic liver repair.* Int J Biochem Cell Biol, 2011. **43**(2): p. 238-44.
114. Michelotti, G.A., et al., *Smoothened is a master regulator of adult liver repair.* J Clin Invest, 2013. **123**(6): p. 2380-94.

115. Stewart, G.A., et al., *Expression of the developmental Sonic hedgehog (Shh) signalling pathway is up-regulated in chronic lung fibrosis and the Shh receptor patched 1 is present in circulating T lymphocytes.* J Pathol, 2003. **199**(4): p. 488-95.

116. Fabian, S.L., et al., *Hedgehog-Gli pathway activation during kidney fibrosis.* Am J Pathol, 2012. **180**(4): p. 1441-53.

117. Ding, H., et al., *Sonic hedgehog signaling mediates epithelial-mesenchymal communication and promotes renal fibrosis.* J Am Soc Nephrol, 2012. **23**(5): p. 801-13.

118. Sahebjam, S., L.L. Siu, and A.A. Razak, *The utility of hedgehog signaling pathway inhibition for cancer.* Oncologist, 2012. **17**(8): p. 1090-9.

119. Jenkins, D., *Hedgehog signalling: emerging evidence for non-canonical pathways.* Cell Signal, 2009. **21**(7): p. 1023-34.

120. Floege, J., F. Eitner, and C.E. Alpers, *A new look at platelet-derived growth factor in renal disease.* J Am Soc Nephrol, 2008. **19**(1): p. 12-23.

121. Leask, A., *Potential therapeutic targets for cardiac fibrosis: TGFbeta, angiotensin, endothelin, CCN2, and PDGF, partners in fibroblast activation.* Circ Res, 2010. **106**(11): p. 1675-80.

122. Rajkumar, V.S., et al., *Platelet-derived growth factor-beta receptor activation is essential for fibroblast and pericyte recruitment during cutaneous wound healing.* Am J Pathol, 2006. **169**(6): p. 2254-65.

123. Campanholle, G., et al., *Cellular mechanisms of tissue fibrosis. 3. Novel mechanisms of kidney fibrosis.* Am J Physiol Cell Physiol, 2013. **304**(7): p. C591-603.

124. Zymek, P., et al., *The role of platelet-derived growth factor signaling in healing myocardial infarcts.* J Am Coll Cardiol, 2006. **48**(11): p. 2315-23.

125. Liao, C.H., et al., *Cardiac mast cells cause atrial fibrillation through PDGF-A-mediated fibrosis in pressure-overloaded mouse hearts.* J Clin Invest, 2010. **120**(1): p. 242-53.

126. Lewis, C.C., et al., *Airway fibroblasts exhibit a synthetic phenotype in severe asthma.* J Allergy Clin Immunol, 2005. **115**(3): p. 534-40.

127. Mukherjee, S., et al., *Platelet derived growth factor-evoked Ca(2+) wave and matrix gene expression through phospholipase C in human pulmonary fibroblast.* Int J Biochem Cell Biol, 2013. **45**(7): p. 1516-24.

128. Martin, I.V., et al., *Platelet-derived growth factor (PDGF)-C neutralization reveals differential roles of PDGF receptors in liver and kidney fibrosis.* Am J Pathol, 2013. **182**(1): p. 107-17.

129. Huang, C., et al., *Blockade of KCa3.1 Ameliorates Renal Fibrosis Through the TGF-beta1/Smad Pathway in Diabetic Mice.* Diabetes, 2013.

130. Yamamoto, T., et al., *Expression of transforming growth factor beta is elevated in human and experimental diabetic nephropathy.* Proc Natl Acad Sci U S A, 1993. **90**(5): p. 1814-8.

131. Pohlers, D., et al., *Constitutive upregulation of the transforming growth factor-beta pathway in rheumatoid arthritis synovial fibroblasts.* Arthritis Res Ther, 2007. **9**(3): p. R59.

132. Bujak, M. and N.G. Frangogiannis, *The role of TGF-beta signaling in myocardial infarction and cardiac remo deling.* Cardiovasc Res, 2007. **74**(2): p. 184-95.

133. Daniels, C.E., et al., *Imatinib mesylate inhibits the profibrogenic activity of TGF-beta and prevents bleomycin-mediated lung fibrosis.* J Clin Invest, 2004. **114**(9): p. 1308-16.

134. Pohlers, D., et al., *TGF-beta and fibrosis in different organs - molecular pathway imprints.* Biochim Biophys Acta, 2009. **1792**(8): p. 746-56.

135. Wipff, P.J. and B. Hinz, *Integrins and the activation of latent transforming growth factor beta1 - an intimate relationship.* Eur J Cell Biol, 2008. **87**(8-9): p. 601-15.

136. Saharinen, J. and J. Keski-Oja, *Specific sequence motif of 8-Cys repeats of TGF-beta binding proteins, LTBPs, creates a hydrophobic interaction surface for binding of small latent TGF-beta.* Mol Biol Cell, 2000. **11**(8): p. 2691-704.

137. Yu, Q. and I. Stamenkovic, *Cell surface-localized matrix metalloproteinase-9 proteolytically activates TGF-beta and promotes tumor invasion and angiogenesis.* Genes Dev, 2000. **14**(2): p. 163-76.

138. Poczatek, M.H., et al., *Glucose stimulation of transforming growth factor-beta bioactivity in mesangial cells is mediated by thrombospondin-1.* Am J Pathol, 2000. **157**(4): p. 1353-63.

139. Massague, J., *How cells read TGF-beta signals.* Nat Rev Mol Cell Biol, 2000. **1**(3): p. 169-78.

140. Wahl, S.M., et al., *Reversal of acute and chronic synovial inflammation by anti-transforming growth factor beta.* J Exp Med, 1993. **177**(1): p. 225-30.

141. Ledbetter, S., et al., *Renal fibrosis in mice treated with human recombinant transforming growth factor-beta2.* Kidney Int, 2000. **58**(6): p. 2367-76.

142. Border, W.A., et al., *Suppression of experimental glomerulonephritis by antiserum against transforming growth factor beta 1.* Nature, 1990. **346**(6282): p. 371-4.

143. Sato, M., et al., *Targeted disruption of TGF-beta1/Smad3 signaling protects against renal tubulointerstitial fibrosis induced by unilateral ureteral obstruction.* J Clin Invest, 2003. **112**(10): p. 1486-94.

144. Inazaki, K., et al., *Smad3 deficiency attenuates renal fibrosis, inflammation,and apoptosis after unilateral ureteral obstruction.* Kidney Int, 2004. **66**(2): p. 597-604.

145. Denton, C.P., et al., *Recombinant human anti-transforming growth factor beta1 antibody therapy in systemic sclerosis: a multicenter, randomized, placebo-controlled phase I/II trial of CAT-192.* Arthritis Rheum, 2007. **56**(1): p. 323-33.

146. Beyer, C. and J.H. Distler, *Tyrosine kinase signaling in fibrotic disorders: Translation of basic research to human disease.* Biochim Biophys Acta, 2013. **1832**(7): p. 897-904.

147. Baselga, J. and S.M. Swain, *Novel anticancer targets: revisiting ERBB2 and discovering ERBB3.* Nat Rev Cancer, 2009. **9**(7): p. 463-75.

148. Yarden, Y. and M.X. Sliwkowski, *Untangling the ErbB signalling network.* Nat Rev Mol Cell Biol, 2001. **2**(2): p. 127-37.

149. Harris, R.C., E. Chung, and R.J. Coffey, *EGF receptor ligands.* Exp Cell Res, 2003. **284**(1): p. 2-13.

150. Blaine, S.A., et al., *Epidermal growth factor receptor regulates pancreatic fibrosis.* Am J Physiol Gastrointest Liver Physiol, 2009. **297**(3): p. G434-41.

151. Pang, M., et al., *A novel STAT3 inhibitor, S3I-201, attenuates renal interstitial fibroblast activation and interstitial fibrosis in obstructive nephropathy.* Kidney Int, 2010. **78**(3): p. 257-68.

152. Terzi, F., et al., *Targeted expression of a dominant-negative EGF-R in the kidney reduces tubulo-interstitial lesions after renal injury.* J Clin Invest, 2000. **106**(2): p. 225-34.

153. Liu, N., et al., *Genetic or pharmacologic blockade of EGFR inhibits renal fibrosis.* J Am Soc Nephrol, 2012. **23**(5): p. 854-67.

154. Tang, J., et al., *Sustained Activation of EGFR Triggers Renal Fibrogenesis after Acute Kidney Injury.* Am J Pathol, 2013. **183**(1): p. 160-72.

155. Chen, J., et al., *EGFR signaling promotes TGFbeta-dependent renal fibrosis.* J Am Soc Nephrol, 2012. **23**(2): p. 215-24.

156. Liu, J.Y., et al., *Up-regulated expression of transforming growth factor-alpha in the bronchiolar-alveolar duct regions of asbestos-exposed rats.* Am J Pathol, 1996. **149**(1): p. 205-17.

157. Madtes, D.K., et al., *Expression of transforming growth factor-alpha and epidermal growth factor receptor is increased following bleomycin-induced lung injury in rats.* Am J Respir Cell Mol Biol, 1994. **11**(5): p. 540-51.

158. Hardie, W.D., et al., *Conditional expression of transforming growth factor-alpha in adult mouse lung causes pulmonary fibrosis.* Am J Physiol Lung Cell Mol Physiol, 2004. **286**(4): p. L741-9.

159. Ishii, Y., S. Fujimoto, and T. Fukuda, *Gefitinib prevents bleomycin-induced lung fibrosis in mice.* Am J Respir Crit Care Med, 2006. **174**(5): p. 550-6.

160. Hardie, W.D., et al., *EGF receptor tyrosine kinase inhibitors diminish transforming growth factor-alpha-induced pulmonary fibrosis.* Am J Physiol Lung Cell Mol Physiol, 2008. **294**(6): p. L1217-25.

161. Suzuki, H., et al., *Epidermal growth factor receptor tyrosine kinase inhibition augments a murine model of pulmonary fibrosis.* Cancer Res, 2003. **63**(16): p. 5054-9.

162. Fukumoto, J., et al., *Amphiregulin attenuates bleomycin-induced pneumopathy in mice.* Am J Physiol Lung Cell Mol Physiol, 2010. **298**(2): p. L131-8.

163. Kular, L., et al., *The CCN family: a new class of inflammation modulators?* Biochimie, 2011. **93**(3): p. 377-88.

164. Hinz, B., et al., *Recent developments in myofibroblast biology: paradigms for connective tissue remodeling.* Am J Pathol, 2012. **180**(4): p. 1340-55.

165. Kennedy, L., et al., *CCN2 is necessary for the function of mouse embryonic fibroblasts.* Exp Cell Res, 2007. **313**(5): p. 952-64.

166. Ponticos, M., et al., *Pivotal role of connective tissue growth factor in lung fibrosis: MAPK-dependent transcriptional activation of type I collagen.* Arthritis Rheum, 2009. **60**(7): p. 2142-55.

167. Huang, G. and D.R. Brigstock, *Regulation of hepatic stellate cells by connective tissue growth factor.* Front Biosci, 2012. **17**: p. 2495-507.

168. Ren, S., et al., *LRP-6 is a coreceptor for multiple fibrogenic signaling pathways in pericytes and myofibroblasts that are inhibited by DKK-1.* Proc Natl Acad Sci U S A, 2013. **110**(4): p. 1440-5.

169. Angers, S. and R.T. Moon, *Proximal events in Wnt signal transduction.* Nat Rev Mol Cell Biol, 2009. **10**(7): p. 468-77.

170. Clevers, H., *Wnt/beta-catenin signaling in development and disease.* Cell, 2006. **127**(3): p. 469-80.

171. Cheon, S.S., et al., *beta-Catenin stabilization dysregulates mesenchymal cell proliferation, motility, and invasiveness and causes aggressive fibromatosis and hyperplastic cutaneous wounds.* Proc Natl Acad Sci U S A, 2002. **99**(10): p. 6973-8.

172. Lam, A.P. and C.J. Gottardi, *beta-catenin signaling: a novel mediator of fibrosis and potential therapeutic target.* Curr Opin Rheumatol, 2011. **23**(6): p. 562-7.

173. Beyer, C., et al., *beta-catenin is a central mediator of pro-fibrotic Wnt signaling in systemic sclerosis.* Ann Rheum Dis, 2012. **71**(5): p. 761-7.

174. Beyer, C., et al., *Blockade of canonical Wnt signalling ameliorates experimental dermal fibrosis.* Ann Rheum Dis, 2013. **72**(7): p. 1255-8.

175. Akhmetshina, A., et al., *Activation of canonical Wnt signalling is required for TGF-beta-mediated fibrosis.* Nat Commun, 2012. **3**: p. 735.

176. Brack, A.S., et al., *Increased Wnt signaling during aging alters muscle stem cell fate and increases fibrosis.* Science, 2007. **317**(5839): p. 807-10.

177. Lam, A.P., et al., *Nuclear beta-catenin is increased in systemic sclerosis pulmonary fibrosis and promotes lung fibroblast migration and proliferation.* Am J Respir Cell Mol Biol, 2011. **45**(5): p. 915-22.

178. Chilosi, M., et al., *Aberrant Wnt/beta-catenin pathway activation in idiopathic pulmonary fibrosis.* Am J Pathol, 2003. **162**(5): p. 1495-502.

179. Hao, S., et al., *Targeted inhibition of beta-catenin/CBP signaling ameliorates renal interstitial fibrosis.* J Am Soc Nephrol, 2011. **22**(9): p. 1642-53.

180. Surendran, K., S.P. McCaul, and T.C. Simon, *A role for Wnt-4 in renal fibrosis.* Am J Physiol Renal Physiol, 2002. **282**(3): p. F431-41.

181. Surendran, K., et al., *Matrilysin (MMP-7) expression in renal tubular damage: association with Wnt4.* Kidney Int, 2004. **65**(6): p. 2212-22.
182. Dirocco, D.P., et al., *Wnt4/beta-Catenin Signaling in Medullary Kidney Myofibroblasts.* J Am Soc Nephrol, 2013.
183. Fortini, M.E., *Notch signaling: the core pathway and its posttranslational regulation.* Dev Cell, 2009. **16**(5): p. 633-47.
184. Borggrefe, T. and R. Liefke, *Fine-tuning of the intracellular canonical Notch signaling pathway.* Cell Cycle, 2012. **11**(2): p. 264-76.
185. Morrissey, J., et al., *Transforming growth factor-beta induces renal epithelial jagged-1 expression in fibrotic disease.* J Am Soc Nephrol, 2002. **13**(6): p. 1499-508.
186. Bielesz, B., et al., *Epithelial Notch signaling regulates interstitial fibrosis development in the kidneys of mice and humans.* J Clin Invest, 2010. **120**(11): p. 4040-54.
187. Djudjaj, S., et al., *Notch-3 receptor activation drives inflammation and fibrosis following tubulointerstitial kidney injury.* J Pathol, 2012. **228**(3): p. 286-99.
188. Dees, C., et al., *Notch signalling regulates fibroblast activation and collagen release in systemic sclerosis.* Ann Rheum Dis, 2011. **70**(7): p. 1304-10.
189. Liu, T., et al., *Notch1 signaling in FIZZ1 induction of myofibroblast differentiation.* Am J Pathol, 2009. **174**(5): p. 1745-55.
190. Spee, B., et al., *Characterisation of the liver progenitor cell niche in liver diseases: potential involvement of Wnt and Notch signalling.* Gut, 2010. **59**(2): p. 247-57.
191. Xie, G., et al., *Cross-talk between notch and hedgehog regulates hepatic stellate cell fate.* Hepatology, 2013.

As extensively discussed above there are several key questions in fibrosis research:

1) What is the cellular origin of myofibroblasts?
2) Does inhibition of fibrosis improve or stabilize organ function?
3) How can myofibroblast be targeted to treat fibrotic disease?

In **chapter 2-3**, we describe the results of genetic fate tracing studies showing that resident perivascular Mesenchymal Stem Cells (MSCs) are a major source of myofibroblasts in kidney, heart, lung liver and bone marrow. Our data indicate that genetic ablation of these cells tremendously ameliorates kidney fibrosis, cardiac fibrosis and bone marrow fibrosis. Importantly, the reduced fibrosis severity following ablation of myofibroblasts resulted in stabilized cardiac function in a pressure overload induced heart failure model and also rescued bone marrow failure in murine myelofibrosis. In **chapter 3-4** we report that pharmacologically targeting Gli proteins is a promising therapeutic strategy to treat kidney and bone marrow fibrosis. In **chapter 5** we report parabiosis and single-cell RNA-Sequencing data indicating that circulating cells contribute a minor fraction to kidney myofibroblasts. While they do not produce large amounts of extracellular matrix the data indicate that they primarily act via proinflammatory signaling to resident pericytes and myofibroblasts.

2

PERIVASCULAR GLI1+ PROGENITORS ARE KEY CONTRIBUTORS TO INJURY-INDUCED ORGAN FIBROSIS

Rafael Kramann,[1,2,*] Rebekka K. Schneider,[3] Derek P. DiRocco,[1] Flavia Machado,[1] Susanne Fleig,[1] Philip A. Bondzie,[4] Joel M. Henderson,[4] Benjamin L. Ebert,[3,5] and Benjamin D. Humphreys[1,5,*]

[1]Renal Division, Brigham and Women's Hospital, Department of Medicine, Harvard Medical School, Boston, MA 02115, USA
[2]Division of Nephrology and Clinical Immunology and Medical Faculty, RWTH Aachen University, Pauwelsstrasse 30, 52074 Aachen,Germany
[3]Division of Hematology, Brigham and Women's Hospital, Department of Medicine, Harvard Medical School, Boston, MA 02115, USA
[4]Department of Pathology and Laboratory Medicine, Boston University School of Medicine, Boston, MA 02118, USA
[5]Harvard Stem Cell Institute, Cambridge, MA 02138, USA

Correspondence to:
*Benjamin D Humphreys, MD, PhD
Renal Division, Brigham and Women's Hospital, Department of Medicine,
Harvard Medical School, Boston, Massachusetts;
77 Avenue Louis Pasteur
02115, Boston, MA
Phone: 617-525-5971
Fax: 617-525-5965
E-mail: bhumphreys@partners.org

Or
*Rafael Kramann, MD
Renal Division, Brigham and Women's Hospital, Department of Medicine,
Harvard Medical School, Boston, Massachusetts;
77 Avenue Louis Pasteur
02115, Boston, MA
Phone: 857-210-5633
Fax: 617-525-5965
E-mail: rkramann@ukaachen.de

Running Title: Gli1+ progenitors contribute to fibrosis

SUMMARY

Mesenchymal stem cells (MSCs) reside in the perivascular niche of many organs, including kidney, lung, liver, and heart, although their roles in these tissues are poorly understood. Here, we demonstrate that Gli1 marks perivascular MSC-like cells that substantially contribute to organ fibrosis. In vitro, Gli1+ cells express typical MSC markers, exhibit tri-lineage differentiation capacity, and possess colony-forming capacity, despite constituting a small fraction of the platelet-derived growth factor-β (PDGFRβ)+ cell population. Genetic lineage tracing analysis demonstrate that tissue-resident, but not circulating, $Gli1^+$ cells proliferate following kidney, lung, liver, or heart injury to generate myofibroblasts. Genetic ablation of these cells substantially ameliorates kidney and heart fibrosis, and preserves ejection fraction in a model of induced heart failure. These findings implicate perivascular $Gli1^+$ MSC-like cells as a major cellular origin of organ fibrosis and demonstrate these cells may be a relevant therapeutic target to prevent solid organ dysfunction following injury.

INTRODUCTION

More than half a century ago it was noted that subcutaneously implanted bone marrow cells formed bone [3]. Once isolated, the cell type responsible for this effect was termed mesenchymal stem cells (MSC) in reference to multipotent cells within bone marrow capable of giving rise to mesenchymal tissues [4]. These MSC possess stem cell characteristics including self-renewal and clonogenic capacity [5]. In recent years MSC have been isolated from virtually all postnatal and fetal tissues including placenta, adipose tissue, muscle, umbilical cord, skin, dental pulp, tendon and characterized *in vitro* [4]. Vasculature represents the *in vivo* niche of MSC, helping to explain why MSC have such a broad tissue distribution [3]. However, our current knowledge about MSC is almost entirely based on *in vitro* observations of cultured MSC. The term MSC-like is used to refer to cells *in vivo* that are perivascular and give rise to typical cultured MSC, that possess trilineage differentiation potential, a defined surface marker expression pattern and a spindle-shaped appearance. MSC-like cells localize to the pericyte niche in microvasculature, where they make close contact to endothelial cells, and they also reside in the adventitia of larger vessels, where they do not contact endothelia [6].

Exogenously infused MSC modulate tissue injury and repair, largely through paracrine secretion of anti-apoptotic, anti-scarring, pro-angiogenic and immunomodulatory factors involved in tissue regeneration [6]. These properties have led to novel therapeutic strategies involving exogenous administration of MSC in various injury and disease settings. Almost 400 clinical trials involving exogenous MSC are ongoing or have been performed (www.FDA.gov). Despite the broad therapeutic potential of this cell type, the in vivo role of perivascular MSC-like cells remains undefined due to the absence of specific *in vivo* markers. Recently Zhao et al. demonstrated that Gli1 is just such a marker of perivascular MSC-like cells in the mouse incisor [6]. Gli1^{+} incisor cells express typical MSC surface markers in culture and possess trilineage differentiation capability. Using a Gli1-CreER^{t2} genetic fate tracing approach, the authors showed that following incisor injury newly formed dentin tubules derive from Gli1^{+} cells.

We demonstrate that, in mice, perivascular Gli1^{+} cells from bone-marrow, muscle, heart, lung, liver and kidney express a typical MSC marker pattern *in vivo*, are plastic adherent and possess trilineage differentiation capability towards chondrocytes, osteoblasts and adipocytes *in vitro*. Gli1^{+} cells form an extensive perivascular network and possess increased colony forming unit capability. Following organ injury these resident Gli1^{+} cells are committed to the myofibroblast lineage. Genetic ablation of Gli1^{+} cells ameliorates fibrosis and improves organ function, providing a proof-of-principle for therapeutic targeting of this cell type in fibrotic disease.

RESULTS

Gli1$^+$ cells form an extensive network around the vasculature, express a typical MSC marker pattern in vivo and possess trilineage differentiation capability ***in vitro***

While examining expression of Hedgehog (Hh) pathway constituents, we observed that Gli1 is specifically expressed in cells surrounding vasculature, from microvascular capillaries to large arteries (Figure S1A). The perivascular localization and low frequency of these cells suggested a possible MSC-like identity, similar to the recent report that Gli1 marks mouse incisor MSCs [7].

To comprehensively assess the distribution of these cells in solid organs and tissues, we crossed Gli1-CreER^{t2} driver mice to a tdTomato-reporter for inducible genetic labeling. Gli1-CreER^{t2}; R26tdTomato mice were pulsed with tamoxifen at 8 weeks and 48 hours later Gli1$^+$ cells were identified in the perivascular niche across all tissues tested (Figure 1A-C). Immunostaining for endogenous Gli1 protein and Gli1 mRNA expression of sorted cell populations validated this model (Figure S1B-C). Gli1$^+$ cells formed an extensive perivascular network (1) localized in the adventitia of large arteries (Figure 1A) and arterioles (Figure 1C arrows) distant from endothelial cells (adventitial niche) and (2) intimately associated with the microvasculature in direct contact to CD31$^+$ endothelial cells (Figure 1C, arrowheads). Immunogold staining and electron microscopy confirmed that Gli1$^+$ cells lie directly adjacent to endothelial cells (Figure 1B). Gli1$^+$ cells were also positioned around biliary ducts of the liver and around larger airways of the lung (Figure 1C, asterisk). Gli1$^+$ cells consistently expressed the mesenchymal marker PDGFR-β (Figure 1A,C). In contrast to mouse incisor where Gli1$^+$ cells are predominantly peri-arterial [8, 9], we found that many Gli1$^+$ cells also exist in a pericyte niche adjacent to endothelial cells of muscle, bone-marrow, lung, heart, kidney and liver. To better define the relationship of Gli1$^+$ cells relative to vasculature, we performed fluorescence microangiography (FMA), . This demonstrated very close apposition of Gli1$^+$ cells around capillaries in both heart and kidney, with tdTomato$^+$ cell processes wrapping around fluorescent microbead filled capillaries (Movies S1-S2).

Figure 1: Gli1 defines a perivascular MSC-like cell population residing as adventitial progenitors and in the pericyte niche

(A) Adult Gli1Cre-ER^{t2}; tdTomato mice 48h after tamoxifen administration. Aortic root with innominate artery (IA), left common carotid artery (LCCA) and left subclavian artery (LSCA). Gli1$^+$ cells reside in the adventitia (A) distant from CD31$^+$ endothelial cells of the intima (I) and media (M) and are PDGFR-β$^+$. Scale bars 20μm or as indicated.

(**B-C**) Gli1-tdTomato$^+$ cells also reside adjacent to CD31$^+$ endothelial cells across organs tested (EC in B and arrowheads in C). Transmission electron microscopy (TEM) picture of immunogold labeled (arrows in B) Gli1$^+$ interstitial kidney cell adjacent to an endothelial cell (EC, asterisk in B capillary lumen). Gli1$^+$ cells are PDGFR-β+ (small arrowheads in C). Gli1-tdTomato$^+$ are located around biliary ducts (asterisk liver) and pulmonary bronchi and bronchioles (asterisk lung). Scale bars: 0.2μm in B and 20μm in C.

(**D**) Sorted Gli1-tdTomato$^+$ cells possess *in vitro* trilineage differentiation capacity towards osteoblasts (alkaline phosphatase-AP + von Kossa-vKo staining), adipocytes (Oilred O staining) and chrondrocytes (Alcian Blue staining, experiments were repeated at least 3 times, Scale bars all 50μm, AP+vKo 100μm).

(**E**) Flow cytometry of whole organs demonstrates a typical MSC surface pattern of Gli1-tdTomato$^+$ cells. Data is presented as mean ± SEM, n=3, see also figure S1.

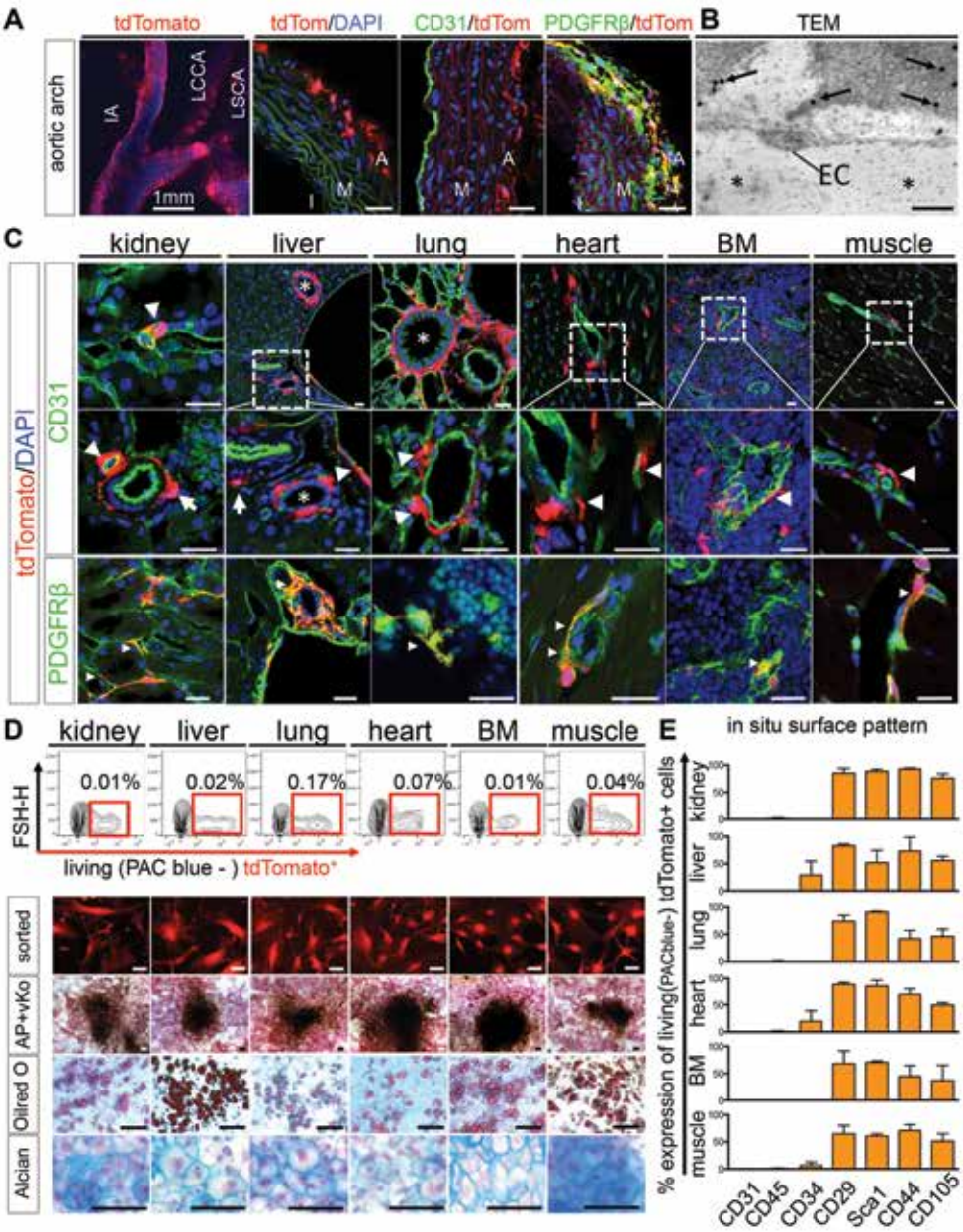
A
tdTomato
tdTom/DAPI
CD31/tdTom
PDGFRβ/tdTom
aortic arch
IA
LCCA
LSCA
1mm
A
M
I
B
TEM
EC
C
kidney
liver
lung
heart
BM
muscle
tdTomato/DAPI
CD31
PDGFRβ
D
FSH-H
0.01%
0.02%
0.17%
0.07%
0.01%
0.04%
living (PAC blue -) tdTomato+
sorted
AP+vKo
Oilred O
Alcian
E
in situ surface pattern
% expression of living(PACblue-) tdTomato+ cells
CD31
CD45
CD34
CD29
Sca1
CD44
CD105

We employed fluorescence-activated cell-sorting (FACS) of whole digested organs and tissues to define the overall frequency of Gli1$^+$ cells (Figure 1D). To characterize Gli1$^+$ cells by accepted criteria defined for MSC, we cultured sorted Gli1$^+$ cells and determined that they had trilineage differentiation capacity towards chondrocytes, adipocytes and osteoblasts regardless of their origin (Figure 1D). Further, we performed whole organ flow cytometry without pre-culture of the cells and confirmed the expression of a typical mouse MSC marker pattern [10] on Gli1$^+$ cells *in vivo* (Figure 1E). Importantly, Gli1$^+$ cells were negative for the endothelial cell marker CD31 and the hematopoietic lineage marker CD45 while we observed low levels of CD34 expression in some organs (Figure 1E). Furthermore, we assessed the expression of other markers that have been described for MSC and/or pericytes by immunostaining of tissues. We demonstrated that Gli1$^+$ cells do not express significant levels of NG2, CD73, CD146 and STRO1, while we observed expression of 3G5, Nestin and PDGFRα (Figure S1D). These experiments show that Gli1$^+$ cells express typical markers and are a source of MSC-like cells across all organs tested.

Gli1$^+$ cells line the endosteum and vascular sinusoids in the bone marrow and retain a typical MSC surface pattern in culture

In the bone marrow niche, MSC surround blood vessels and sinusoids but also line endosteum [3]. We observed Gli1$^+$ cells lining CD31$^+$ endothelial cells of bone marrow sinusoids as well as endosteum of the compact bone (Figure 2A), representing both the vascular and the endosteal niche. Since mouse bone marrow MSC in the endosteal niche cannot readily be isolated from the bone marrow, we applied an endosteal bone chip culture method. Interestingly, Gli1$^+$ cells migrated out of the bone fragments and proliferated in the culture dish (Figure 2B). Flow cytometric analysis of these cells indicated that ~32% had a Gli1$^+$ origin (Figure 2C). MSC isolated from bone chips (BM-MSC) as well as isolated from the myocardium (heart, H-MSC) maintained a typical MSC surface pattern with expression of CD44, CD29, CD105, Sca1 and absence of CD31, CD45, CD34 in culture (Figure 2C-D). Furthermore, Gli1$^+$ cells from bone, heart and kidney retained expression of 3G5, Nestin, PDGFRα and gained expression of CD146 and CD73, while we did not detect significant expression of NG2 or STRO1 in culture (Figure S2). These data suggest that Gli1$^+$ cells in culture are similar despite their origin from different organs.

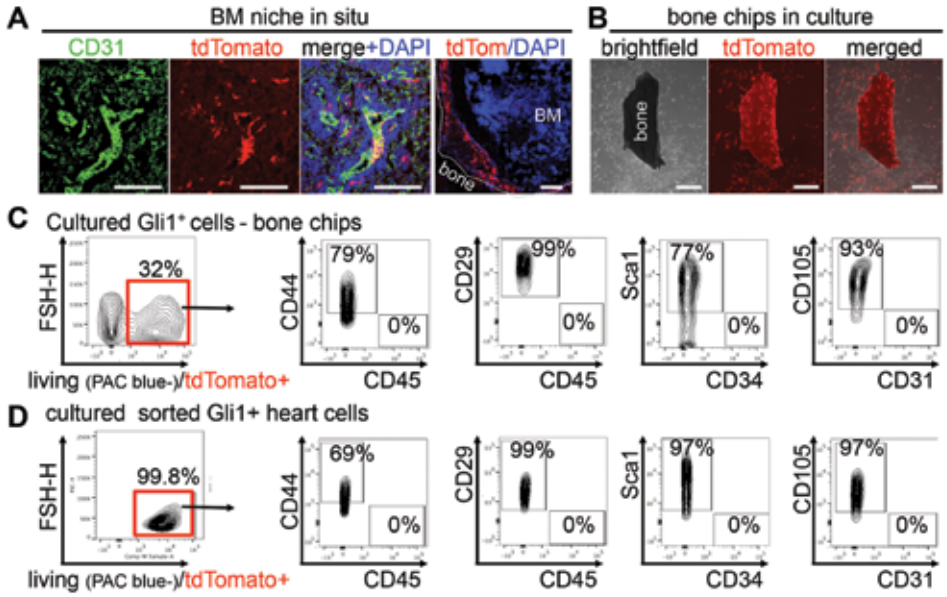

Figure 2: Gli1⁺ cells reside in a typical MSC niche of the bone-marrow and retain their typical MSC-like surface pattern in culture

(A) Gli1-tdTomato⁺ cells surrounding endothelial cells of bone marrow sinusoids and along the endosteum. Scale bars 100µm.

(B) Gli1⁺ cells migrating out of compact bone chips in vitro. Scale bars 200µm.

(C) Flow cytometry of BM-MSC isolated from compact bone chips of Gli1CreER^{t2}; tdTomato mice after 4 weeks of culture indicating that 32% of the cells are of Gli1⁺ origin (tdTomato⁺) and maintain a typical mouse MSC surface profile.

(D) Flow cytometry of cultured (4 weeks) Gli1⁺tdTomato⁺ cells from the myocardium with a similar surface profile. Data represents at least 3 independent experiments, see also figure S2.

Gli1⁺ cells represent only a small fraction of the PDGFR-β⁺ cell population with increased colony forming unit capability

Our results had indicated that Gli1 expression in adult mice defines PDGFRβ⁺ MSC-like perivascular cells. However, a critical question was whether there were any functional differences between Gli1⁺ cells and Gli1⁻, PDGFRβ⁺ cells. Flow cytometric analyses of whole organs indicated that all Gli1⁺ cells express PDGFRβ but they represent only a small fraction of the total PDGFR-β⁺ population (Figure 3A).

We next asked whether Gli1⁺ cells differ in their clonogenic potential from Gli1⁻PDGFRβ⁺ and PDGFRβ⁻Gli1⁻ cells. We sorted these populations from lung, heart, kidney and cultured bone chips and assessed colony formation after 2 weeks. Indeed, the clonogenic frequency of the Gli1⁺PDGFRβ⁺ fraction was significantly higher than that of the other populations across tissues tested (Figure 3B-C). Furthermore, colonies from the Gli1⁺, PDGFRβ⁺ fraction were substantially larger (Figures 3D, S3A). Gli1⁺ cells showed stable growth over many passages *in vitro* (cells were grown for >30 passages from bone chips, >10 passages from all other organs).

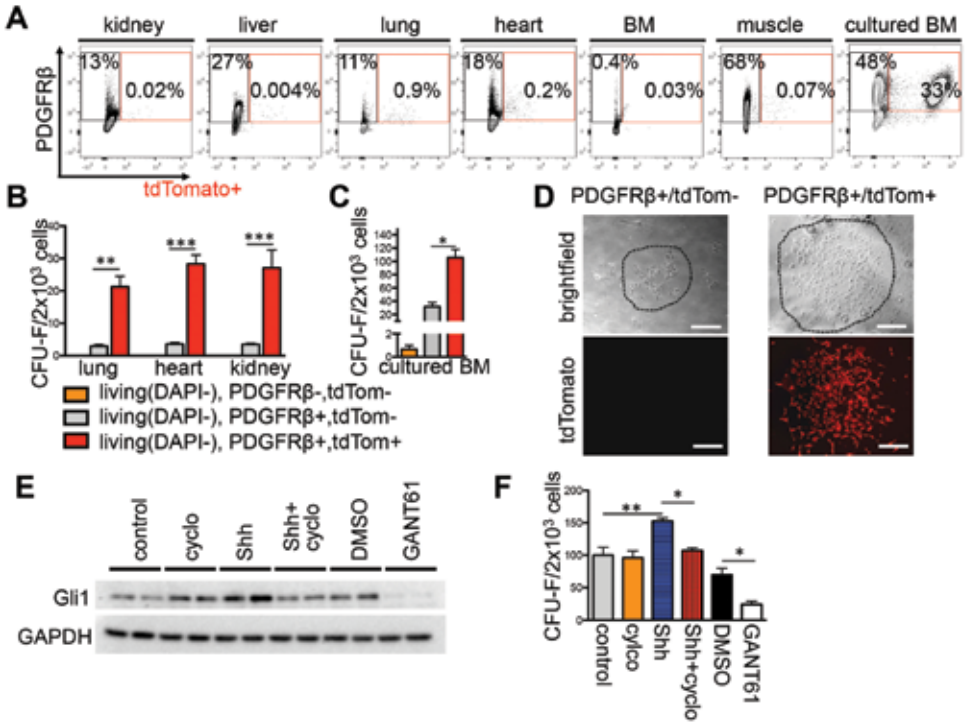

Figure 3: Gli1⁺ cells represent a small CFU-F enriched fraction of the PDGFRβ⁺ population while inhibition of Gli reduces their self-renewal (

(**A**) Gli1-tdTomato⁺ cells represent only a small fraction of the PDGFRβ⁺ kidney cell population.

(**B**) PDGFRβ⁺, Gli1tdTomato+ cells exhibit superior clonogenicity by CFU-F assay (>50cells/colony at 14 days, n = 3,*p < 0.05 by t-test, mean ± SEM).

(**C**) Gli1tdTomato⁺ cells from cultured bone chip also exhibit superior clonogenicity by CFU-F assay.

(**D**) Colonies cultured from whole hearts 7 days after sorting.

(**E**) Gli1 protein level is regulated by the hedgehog pathway in Gli1⁺ cells cultured from bone chips.

Gli1⁺ cells constitutively express Gli *in vitro* while pharmacologic inhibition of Gli reduces their colony forming unit capability

Gli1⁺ cells retain significant mRNA expression of most Hh pathway members *in vitro* including Gli1-3 (Figure S3B). Given reported roles for Hh signaling in cell proliferation, we next investigated whether inhibition or activation of Hh signaling affects the CFU-F capability of Gli1⁺ cells. Exogenous Shh increased Gli1 protein and colony number, and the smoothened inhibitor cyclopamine blocked this effect but cyclopamine alone had no effect arguing against autocrine Hh ligand secretion (Figure 3E-F). By contrast, targeting Gli directly with the small molecule antagonist GANT61 decreased Gli1 protein levels and also decreased CFU-F capacity (Figure 3E-F). These results suggest constitutive expression of Gli1 in MSC-like cells *in vitro*. That direct inhibition of Gli reduced clonogenic capacity also implicates Gli in the self-renewal of Gli1⁺ progenitor cells.

Perivascular Gli1+ cells expand and become myofibroblasts after injury of major organs

The MSC is most commonly defined as a cell with trilineage differentiation capability and CFU-F capacity *in vitro* [12]. Our results thus far suggested that Gli1+ cells in adult mice fulfill these criteria among organs tested and additionally express an MSC surface pattern *in vivo*. It has been proposed that MSC in the perivascular niche become activated upon organ injury and support tissue regeneration after injury [13]. This prompted us to perform fate-tracing and ablation studies of Gli1+ cells following injury to major organs including kidney (unilateral ureteral obstruction, UUO and severe bilateral ischemia reperfusion injury, IRI), heart (angiotensin-2, AT2-induced myocardial fibrosis, ascending aortic constriction, AAC), liver (carbon tetrachloride, CCL4 induced fibrosis) and lung (intratracheal bleomycin instillation). To track the fate of genetically labeled Gli1+ cells, we labeled them via tamoxifen administration and followed their fate in various organ injury models for up to 52 days. The injury was induced at least 10 days after tamoxifen administration to eliminate any possibility of recombination after injury [14].

In both models of kidney injury we observed a dramatic increase of Gli1+ cells in the medulla, the inner cortex and around arteries throughout the kidney and to a lower extent in the outer cortex (Figures 4A and S4A-C). The proliferative expansion and distribution of Gli1+ cells following kidney injury suggested that they may differentiate into myofibroblasts. One of the defining features of myofibroblasts is expression of alpha-smooth muscle actin (α-SMA), and indeed most Gli1+ cells acquired expression of α-SMA after injury (Figure 4A, S4A-C). Thus Gli1+ cells proliferate and differentiate into myofibroblasts in kidney fibrosis.

To exclude the possibility that 'leaky' recombination might label cells that activate Gli1 expression following injury, we performed UUO surgery in bigenic Gli1CreER^{t2}; tdTomato mice without tamoxifen injection. There was no significant recombination under these conditions (Figure S4D-F). We also excluded the possibility that residual tamoxifen might label Gli1+ cells following injury by extending the time between tamoxifen administration and UUO surgery from 10 days to 3 months. Importantly, the frequency of labeled cells following UUO was comparable to our original experiments, indicating that recombination was not occurring after surgery (Figure S4D-F). We also counterstained fibrotic kidneys following UUO and demonstrated that indeed all myofibroblasts (~96% of α-SMA+ cells) express PDGFRβ (Figure S4H-I), consistent with a recent report [15, 16],

Cardiac fibrosis in the AT2-induced hypertensive heart disease model primarily affects coronary arteries and arterioles with extensions of collagen from the perivascular space into the cardiac interstitium and this is what was observed in Gli1CreER^{t2}; tdTomato mice (Figure 4B). Fate tracing experiments revealed expansion of Gli1+ cells in the perivascular space where the vast majority of Gli1+ cells differentiated into α-SMA positive myofibroblasts (Figure 4B-D). We also used AAC surgery to induce pressure-overload heart failure as a second model with perivascular but also interstitial myocardial fibrosis. In this case we

observed both perivascular Gli1$^+$ expansion but also expansion of Gli1$^+$ cells in the cardiac interstitium distant from arteries and arterioles (Figure 4E-I) that also differentiated into α-SMA positive myofibroblasts (Figure 4G,I).

Large interstitial Collagen I-positive fibrotic areas were entirely full of Gli1$^+$ cells (Figure S4J), consistent with matrix secretion by Gli1$^+$ cells, prompting us to ask whether Gli1$^+$ cells mediate scarring following myocardial infarction. Indeed after coronary artery ligation the entire left ventricular scar area was full of α-SMA positive Gli1$^+$ cells (Figure S4K-M). We next quantitated the contribution of Gli1$^+$ cells to the myofibroblast pool in kidney and heart. This analysis revealed that ~45% of myofibroblasts in the kidney and ~60% of cardiac myofibroblasts derived from Gli1$^+$ progenitors (Figure S5A). Given the significant contribution of Gli1$^+$ cells to the myofibroblast pool in heart and kidney we then asked whether Gli1$^+$ cells also contribute to the myofibroblast pool following liver and lung injury. Indeed, we observed significant expansion and differentiation into α-SMA$^+$ cells following liver and lung injury (Figure 5A-F). Gli1$^+$ cells contributed to ~37% of α- SMA$^+$ interstitial cells following lung injury and ~39% of interstitial α-SMA$^+$ cells in liver fibrosis (Figure S6G).

Following injury of major organs Gli1$^+$ cells expanded through proliferation (S6A-F) and the majority of Gli1$^+$ cells acquired α-SMA expression (Figures 4-5), suggesting that perivascular Gli1$^+$ cells are committed to the myofibroblast lineage after injury. In line with these *in vivo* fate tracing studies, isolated FACS purified Gli1$^+$ cells from healthy bone marrow or heart did not express α-SMA 7 days after isolation. However, treatment with transforming growth factor beta (TGF-β) resulted in significant up-regulation of α-SMA mRNA and expression of α-SMA$^+$ stress fibers (Figure 5G-J).

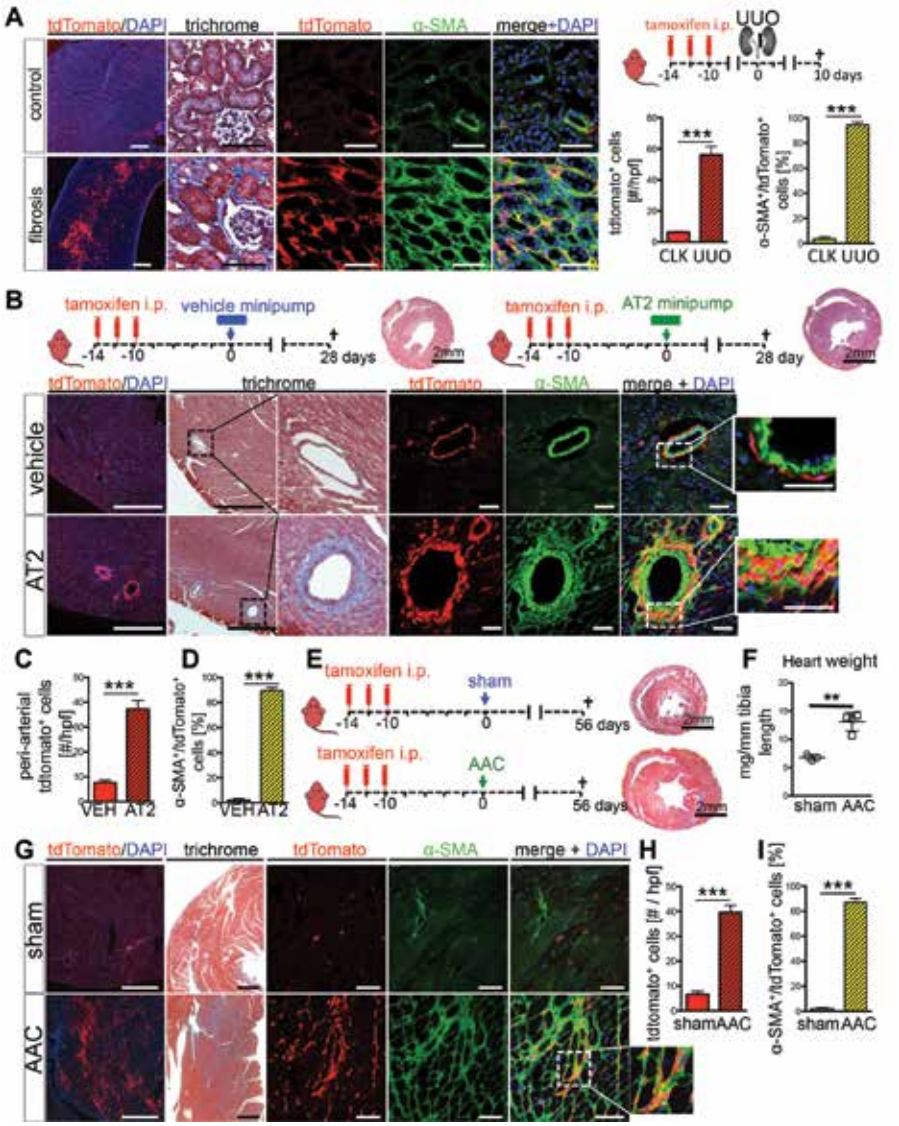

Figure 4: Following kidney or heart injury Gli1⁺ cells expand and differentiate into myofibroblasts

(**A**) Genetic lineage analysis of Gli1⁺ cells after unilateral ureteral obstruction (UUO, n=4). Gli1⁺ cells expand after UUO and acquire alpha smooth muscle actin (α-SMA) expression. tdTomato or α-SMA increase measured in 400x high power fields (hpf). Scale bars: left panel 500µm, all others 50µm; ***p<0.001 by t-test, mean ± SEM.

(**B**-**D**) Myocardial fibrosis induced by angiotensin 2 (AT2, n=4; PBS, n=3) causes hypertension induced, predominantly perivascular fibrosis around myocardial arteries where Gli1⁺ cells expand and differentiate into α-SMA⁺ myofibroblasts. Quantification by confocal micrographs in 400x hpf. Scale bars: left two panels 500µm, all others 50µm; ***p<0.001 by t-test, mean ± SEM.

(**E**-**I**) Ascending aortic constriction induces cardiac hypertrophy, fibrosis and chronic heart failure (AAC, n=4; sham n=3). Following AAC, Gli1⁺ cells expand dramatically in the myocardial interstitium and acquire α-SMA expression. Quantification by confocal micrographs in 400x hpf. For studying co-expression of tdTomato and α-SMA it is important to study the perinuclear region due to a converse α-SMA tdTomato expression pattern (see figure S4G). Scale bars: left two panels 500µm, all others 50µm; **p<0.05, ***p<0.001 by t-test, mean ± SEM, see also figures S4-5.

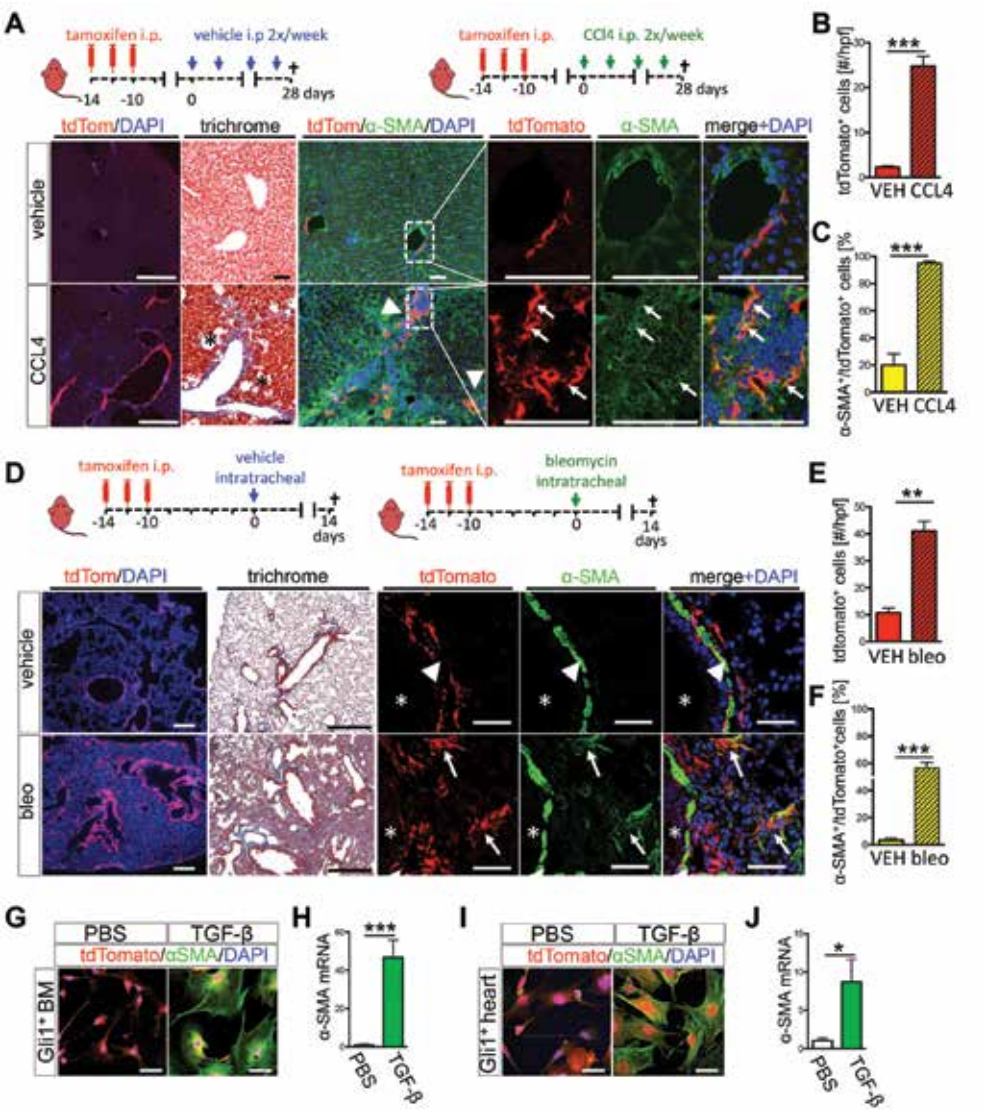

Figure 5: Fate tracing of Gli1⁺ cells in liver and lung injury

(A-C) Hepatic fibrosis was induced by carbon tetrachloride injections (CCL4, n=5; vehicle, n=3) twice per week and the fate of Gli1-labeled cells analyzed. Hepatocyte necrosis (asterisk) and fibrosis was visible, with expansion of Gli1⁺tdTomato⁺ cells in fibrotic areas (arrowheads). Gli1⁺ cells acquired α-SMA expression (arrows). Throughout figure, quantification was from confocal micrographs in 400x hpf, in this case from periportal and pericentral fields in B and C. Scale bars: left panel 500µm, all others 50µm, ***p<0.001 by t-test, mean ± SEM.

(D-F) Pulmonary fibrosis was induced by bleomycin (n=4) or vehicle (n=3). Low magnification (left panel) shows Gli1⁺ expansion (quantification in E) with severe pulmonary fibrosis (trichrome). Gli1⁺ cells line the peri-bronchial smooth muscle cell layer (arrowhead, bronchus-lumen = asterisk) of a healthy non-injured lung. In fibrosis Gli1⁺ cells expand into interstitium and acquire α-SMA expression (arrows, quantification in (F). Scale bars: left two panels 500µm, all others 20µm; **=p<0.01, ***=p<0.001 by t-test, mean±SEM

(G-J) Sorted Gli1⁺ cells compact bone or myocardium differentiate into α-SMA⁺ myofibroblasts after exposure (24h) to transforming growth factor beta (TGF-β) *in vitro* (n=3). Scale bars: 50µm; *p<0.05, ***p<0.001 by t-test, mean±SEM, see also figure S4-5.

Gli1+ cells do not express NG2 in homeostasis or fibrosis but acquire NG2 expression during angiogenesis

Although not all pericytes express NG2 [16], NG2 has been proposed as a marker of mature pericytes by some authors . With an important role in angiogenesis where it promotes endothelial cell migration and proliferation [19], NG2 expression may not be static but rather induced in pericytes during angiogenesis and microvascular remodelling [6]. By contrast, many pericytes might show reduced or no expression of NG2 during homeostasis. In tumors, it has been demonstrated that PDGFRβ+/NG2- perivascular cells can differentiate into mature NG2+ pericytes [17]. Moreover, recent work suggests that during injury and repair of the mouse incisor, Gli1+ progenitors differentiate into NG2+ mature pericytes. Interestingly, the authors also demonstrated that Gli1+ cells give rise to the entire MSC population from the mouse incisor, whereas NG2+ cells only contribute a minor subpopulation [20]. These data suggested that Gli1 expression may define immature perivascular cells, distinct from mature NG2+ pericytes, and constitute the major progenitor pool for MSC. We therefore asked whether Gli1+ cells could acquire expression of NG2 during fibrosis. Interestingly, we observed that only a small fraction of Gli1+ cells expressed NG2 (~5%) and this fraction actually decreased following UUO or AAC (Figure S5B). Of note, Gli1+ cells retained expression of other pericyte/MSC markers 3G5, PDGFRα, PDGFRβ and Nestin during fibrosis *in vivo* (Figure S5C).

Given a reported role for NG2 in angiogenesis [21], we next asked whether Gli1+ cells gain NG2 expression following myocardial infarction since angiogenesis is involved in the repair process of this model. Indeed, we observed Gli1+ cells expressing NG2 and CD146 assembling vascular like structures within the left-ventricular scar following coronary artery ligation (Figure S5D). Gli1+ cells from bone chips did not express NG2 in vitro (Figure S2). We then tested whether cultured cells acquire NG2 expression and contribute to neovascularization in an *in vivo* matrigel-plug angiogenesis assay. Four weeks after implantation of Gli1+ cells, we observed developing vessels with Gli1+ cells surrounding CD31+ endothelial cells (Figure S5E). Gli1+ cells adjacent to endothelial cells acquired expression of NG2 and CD146 (Figure S5E).

These experiments suggest that Gli1+ cells acquire expression of NG2 during angiogenesis. Because NG2 can directly bind to PDGF-AA [22], an essential autocrine regulator of VEGF expression and therefore angiogenesis [23], these results are also consistent with a pro-angiogenic role for NG2 expression in Gli1+ MSC-like cells.

Gli inhibition and myofibroblast differentiation reduces Gli1+ progenitor endothelial cell - tube association *in vitro*

Hh signaling plays a critical role in angiogenesis, while detachment of perivascular cells from capillaries has been proposed as an early event triggering capillary destabilization and hypoxia in fibrosis [24]. We therefore studied tube formation with Gli1+ cells and

endothelial cells (EC) in 3-dimensional collagen gels *in vitro*. Interestingly, Shh treatment increased the number of Gli1$^+$ cells in the gels and promoted their association with EC tubes. Inhibition of Gli1 by GANT61 dramatically reduced the fraction of Gli1$^+$ cells associated with EC-tubes (Figure S6H-K). Our previous data demonstrates that TGF-β treatment leads to myofibroblast differentiation of Gli1$^+$ cells. In the tube formation assays TGF-β significantly reduced the fraction of Gli1$^+$ cells adjacent to EC-tubes, whereas treatment with vascular endothelial growth factor (VEGF-165) resulted in a high fraction of Gli1$^+$ cells associated with EC-tubes. This data suggests that several pathways are important in Gli1$^+$ progenitor – EC-tube association and that myofibroblast differentiation reduces association of Gli1$^+$ cells with EC.

Resident but not circulating Gli1$^+$ progenitor cells contribute to fibrosis

It has been proposed that bone marrow-derived MSC circulate and home to injured kidney where they differentiate into α-SMA$^+$ myofibroblasts [25]. Since our results suggest that Gli1$^+$ cells are myofibroblast progenitors, are MSC-like and that they are located both within organs but also in the bone marrow, we therefore asked whether Gli1$^+$ cells circulate and home to injured organs. While bone marrow transplantation (BMTX) is a standard approach to trace the fate of circulating cells, irradiation injury may promote fibrosis, alter MSC properties and it is unclear whether MSC actually engraft following BMTX [6, 10]. We therefore utilized both BMTX and also parabiosis, where two mice are conjoined and share one blood circulation, to ask whether Gli1$^+$ cells circulate and home to injured tissue.

Ptprc^a-Pepc^b mice harboring the common leukocyte antigen variant CD45.1 were lethally irradiated and received whole bone marrow of bigenic Gli1CreER^{t2};tdTomato donors (CD45.2) that were injected with tamoxifen prior to sacrifice and BM harvest. Five weeks later, the mice underwent UUO or sham surgery (Figure 6A). Flow cytometric analysis using antibodies specific for the common leukocyte antigen variants demonstrated a successful engraftment of CD45.2$^+$ donor cells into recipient bone marrow (Figure 6B). These engrafted CD45.2$^+$ donor leukocytes migrated into the kidney following UUO surgery, as expected (Figure 6C). However, only a small number of Gli1$^+$ cells engrafted into bone marrow (Figure 6D-E), whereas many more Gli1$^+$ cells were trapped in the lung (Figure 6C-E), consistent with previous reports . The number of Gli1-tdTomato$^+$ cells between sham, contralateral (CLK) or UUO kidney did not differ significantly and importantly no interstitial tdTomato$^+$ cells were observed (Figure 6D, F). Some Gli1$^+$ cells were also trapped in kidney glomeruli (Figure 6F). Interestingly, Gli1$^+$ cells persisted in the lung at >6 weeks after transplantation, some even expressing α-SMA (Figure 6F). These results suggest that engrafted Gli1$^+$ donor cells do not circulate and home to the kidney nor contribute to the myofibroblast pool following injury (UUO). Since only a small fraction of Gli1$^+$ cells engrafted in bone marrow, however, we next turned to the parabiosis model to examine Gli1$^+$ cell circulation.

Bigenic Gli1CreER^{t2}; tdTomato mice received tamoxifen and were conjoined 10 days after the last tamoxifen injection (Figure 6G). Shared circulation was verified 4 weeks after parabiosis surgery (Figure 6H) and UUO surgery was performed in the Ptprc^{a}-Pepc^{b} CD45.1^{+} parabiont. Mice were sacrificed 10 days later. Flow cytometric analysis of PBS perfused spleens and kidneys showed a complete cross-circulation with CD45.1^{+} and CD45.2^{+} leukocytes in the tissue of both mice (Figure 6 I-K). There was a significant influx of CD45.2^{+} leukocytes from the Gli1CreER^{t2}; tdTomato parabiont in the UUO kidney of the CD45.1^{+} parabiont (≈17% of all kidney cells, Figure 6J,L), but few Gli1-tdTomato^{+} cells were detected in CLK or UUO kidney of the CD45.1^{+} parabiont (Figure 6J, M). Microscopic evaluation failed to detect any Gli1-tdTomato^{+} cells in the CD45.1^{+} parabiont despite robust fibrosis and α-SMA positive myofibroblast expansion (Figure 6N). This experiment provides clear evidence that neither circulating nor bone marrow-derived Gli1^{+} cells contribute to the myofibroblast pool in kidney fibrosis.

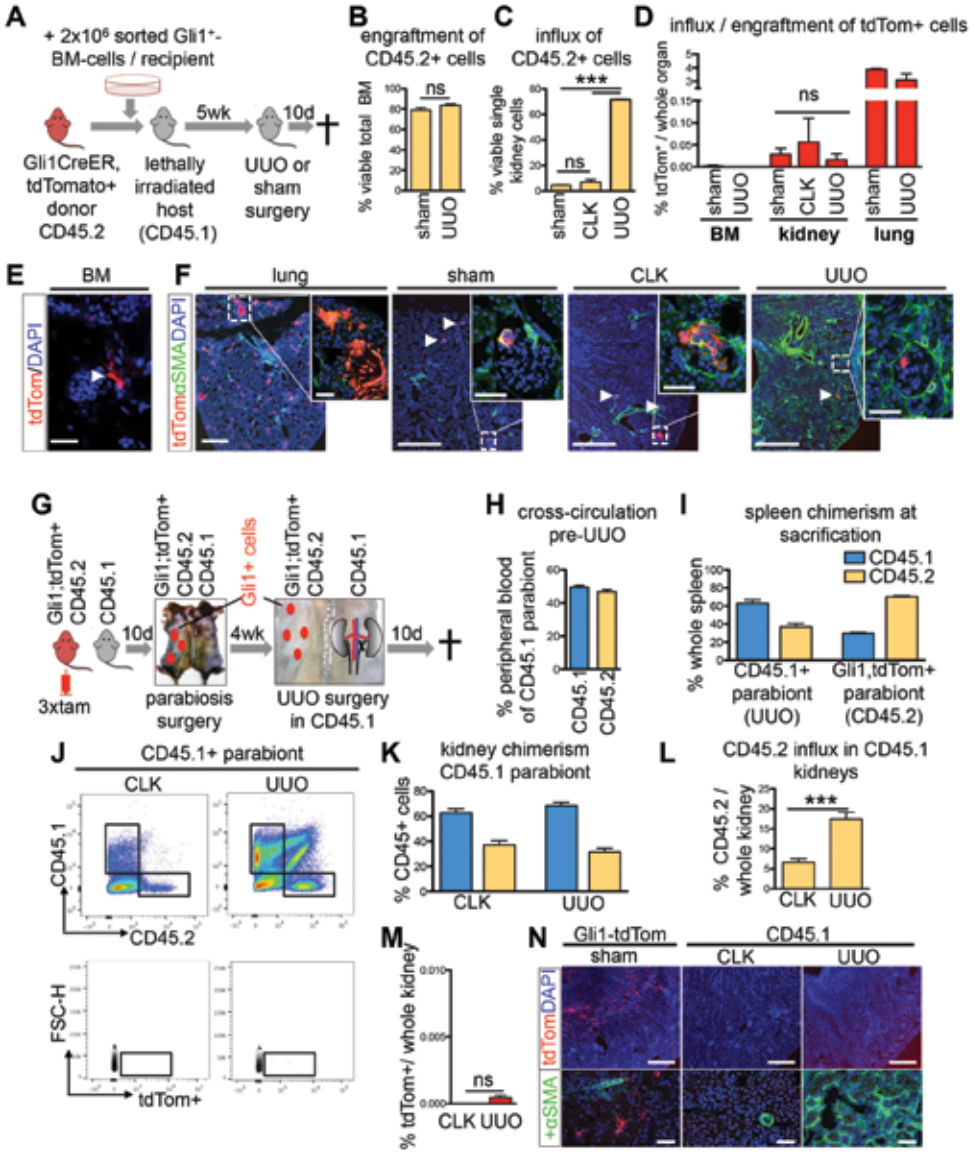

Figure 6: Circulating Gli1⁺ cells do not contribute to kidney fibrosis

(A) Bone marrow transplantation scheme. Marrow from genetically labeled Gli1CreER^{t2}, tdTomato donors was transplanted into lethally irradiated, unlabeled CD45.1 recipients. 2x10^6 sorted Gli1$^+$ cells from bone chips was added to the whole bone-marrow cell-solution to increase the number of transplanted Gli1$^+$ cells. After verifying engraftment, recipients underwent 5 UUO (n = 5) or sham (n = 3) surgery.

(B) Verification of engraftment of CD45.2$^+$ donor leukocytes into CD45.1 recipients.

(C) CD45.2$^+$ leukocytes from Gli1CreER^{t2}, tdTomato donor increase in UUO kidney of the CD45.1$^+$ recipient compared to the contralateral (CLK) or sham kidney. Data assessed by flow cytometry of whole digested kidneys. (n=3 sham, n=5 CLK, n=5 UUO). ***p<0.001 by one way ANOVA with posthoc Tukey.

(D) No increase in tdTomato$^+$ cells in recipients kidneys 10 days after UUO (n=3 sham, n=5 CLK, n=5 UUO). P = NS by one way ANOVA with posthoc Tukey.

(E-F) tdTomato+ cell distribution in bone marrow (BM), lung, sham-, contralateral- (CLK) and UUO kidneys of recipients. Scale bars 25μm left panel all others 500μm, inserts 50μm.
(G-H) Parabiosis experimental design. After tamoxifen, Gli1CreER^{t2}; tdTomato mice (CD45.2+) were conjoined with unlabeled (CD45.1+) mice. Shared circulation was verified by flow cytometric analysis of peripheral blood from the CD45.1+ parabiont (H, n=8). Thereafter UUO was performed in the CD45.1+ parabiont and analyzed 10 days after surgery.
(I) Spleen chimerism for the common leukocyte antigen variants assessed by flow cytometry (n=8 pairs, mean±SEM).
(J) Flow cytometric plots of whole digested CLK and UUO kidney from the CD45.1+ parabiont indicating influx of leukocytes from the Gli1-tdTomato parabiont with almost no detection of tdTomato+.
(K) Chimerism for CD45.1+ versus CD45.2+ leukocytes in CLK and UUO kidneys (n=8, mean±SEM).
(L) Influx of CD45.2+ leukocytes from the Gli1-tdTomato parabiont in CLK and UUO kidneys (n=8, ***p<0.001 by t-test, mean±SEM).
(M) Gli1-tdTomato cells do not circulate. Almost no tdTomato+ cells are detected in the kidneys of the CD45.1 (n=8; p = NS by t-teat, mean ± SEM).
(N) Gli1-tdTomato+ cells are seen in the uninjured kidneys of the CD45.2 parabiont, however no Gli1-tdTomato+ cells are observed in the CD45.1 parabiont despite robust fibrosis (aSMA staining). Scale bars: top panel 500μm, bottom 50μm.

Ablation of Gli1+ cells ameliorates kidney fibrosis

To assess the functional contribution of Gli1+ cells to fibrosis, we crossed mice with an inducible human diphtheria toxin receptor allele (iDTR) to Gli1CreER^{t2} mice (Figure 7A). After tamoxife-induced recombination of the transcriptional stop sequence, administration of DTX ablates Gli1+ cells in this model. Tamoxifen was given to bigenic mice before UUO or sham surgery. Following surgery, mice were injected with either DTX or vehicle (PBS) as indicated (Figure 7B). Successful ablation of Gli1+ cells following UUO was verified by quantitative PCR for DTR mRNA (Figure 7F). There was a striking reduction in kidney fibrosis readouts after DTX compared to vehicle, whereas ablation of the Gli1+ progenitor cell population in the sham group had no appreciable effect (Figures 7C-E, S7A-F). Despite the fact that Gli1+ cells represent only 0.2% of the total PDGFRβ+ kidney cell population, their ablation following injury reduced fibrosis dramatically by ~50% (Figure S7A), indicating that the Gli1+ population plays a critical role regulating fibrosis during chronic injury. To test whether our ablation approach is specific to the Gli1+ population, we generated triple transgenic mice (Gli1CreER^{t2}; iDTR; tdTomato) and repeated the UUO ablation experiment. DTX administration substantially decreased tdTomato+ cells, as expected (Figure S7M-O). We detected apoptotic tdTomato+ cells (TUNEL+) after DTX injection yet we did not observe increased apoptosis in other renal cell populations, providing strong evidence that DTX caused the specific ablation of Gli1+ cells and not other cell types (Figure S7P-Q).

Ablation of Gli1+ cells reduces heart fibrosis and rescues left ventricular function following aortic banding

We next asked whether ablation of Gli1+ cells might improve organ function during chronic disease and utilized the AAC model of heart fibrosis with noninvasive measurement of cardiac function via echocardiography. Gli1CreER^{t2}; iDTR mice were injected with high dose tamoxifen and subjected to AAC or sham surgery. Mice were randomized to receive DTX or vehicle based on their echocardiographically measured peak velocity at the aortic suture

site immediately after surgery (Figure S7H) and their left ventricular ejection fraction (EF) at 2 weeks after surgery. DTX or vehicle was given as indicated at 3 and 5 weeks after surgery (Figure 7G).

Ablation of Gli1$^+$ cells after AAC reduced cardiac hypertrophy, heart-weight and cardiomyocyte cross-sectional area (Figure 7G-I). Quantitative PCR confirmed reduction of iDTR mRNA expression by ~75%, indicating successful ablation of Gli1-iDTR$^+$ cells (Figure 7J). Quantification of fibrotic readouts demonstrated a remarkable reduction of interstitial myocardial fibrosis following Gli1$^+$ cell ablation indicating that the perivascular Gli1$^+$ cell-population is in fact an important driver of interstitial myocardial fibrosis (Figures 7K-P, S7I-K). Importantly, echocardiographic analysis of left ventricular function demonstrated that ablation of Gli1$^+$ cells rescued chronic heart failure after AAC by preserving left ventricular ejection fraction and thus, myocardial function (Figure 7Q-R). These results indicate that cardiac Gli1$^+$ cells not only drive fibrogenesis in pressure-overload heart failure, but that this process impairs myocardial function.

Figure 7: Ablation of Gli1$^+$ cells via the human diphtheria toxin receptor ameliorates kidney and heart fibrosis and rescues left ventricular function in heart failure.
(A) Experimental scheme. Gli1CreER^{t2}; iDTR bigenic mice were administered tamoxifen, leading to heritable expression of the human DTR in Gli1$^+$cells, allowing ablation of these cells via diphtheria toxin (DTX) injection.
(B) Gli1CreER^{t2}; iDTR mice were subjected to UUO or sham surgery, injected with vehicle (VEH=PBS) or DTX following surgery as indicated (n=5 sham + VEH, n=7 sham + DTX, n=7 UUO + VEH, n=8 UUO + DTX).
(C-E) Ablation of Gli1$^+$ cells by DTX reduced severity of kidney fibrosis following UUO as demonstrated by trichrome staining, immunostaining and western blotting for α-SMA and quantification of interstitial fibrosis. Scale bars: left two panels 500µm, others 50µm; ***p<0.001 by one way ANOVA with posthoc Tukey, mean ± SEM.
(F) iDTR mRNA increases in UUO kidneys reflecting the expansion of Gli1$^+$; iDTR$^+$-cells, whereas DTX injection significantly reduced iDTR expression in UUO kidneys indicating ablation of Gli1$^+$,iDTR$^+$ cells; ***p<0.001 by t-test, mean ± SEM.
(G) Gli1CreER^{t2}; iDTR mice underwent ascending aortic constriction (AAC) or sham surgery and were randomized to subsequently receive either diphtheria-toxin (DTX, n=9 AAC, n=5 sham) or vehicle (PBS, n=10 AAC, n=5 sham). Note decreased heart size in DTX-treated mice.
(H-I) Ablation of Gli1$^+$ cells ameliorated cardiac hypertrophy as indicated by reduced heart weight and cardiomyocyte (CM) cross-sectional area (*p<0.05 by t-test, mean±SEM).
(J) Confirmation of ablation by reduction in mRNA for DTR receptor (*p<0.05 by t-test, mean ± SEM).
(K-L) Reduced interstitial fibrosis by trichrome stain following DTX injection. Scale bars: 50µm, ***p<0.001 by t-test; mean ± SEM.
(M-O) Reduced fibronectin and collagen-1 expression and quantification following DTX injection. Scale bars: 500µm left panel, 50µm right panel; ***p<0.001 by t-test.
(P) Reduced α–SMA following DTX injection.
(Q-R) After AAC, vehicle injected mice developed progressive heart failure, as expected (representative echocardiographic M-mode pictures in Q) with significantly reduced left ventricular ejection fraction (EF) at 8 weeks. Ablation of Gli1+ cells by DTX treatment rescued this progressive heart failure. *p<0.05; **p<0.01 by t-test, mean ± SEM, see also figure S6.

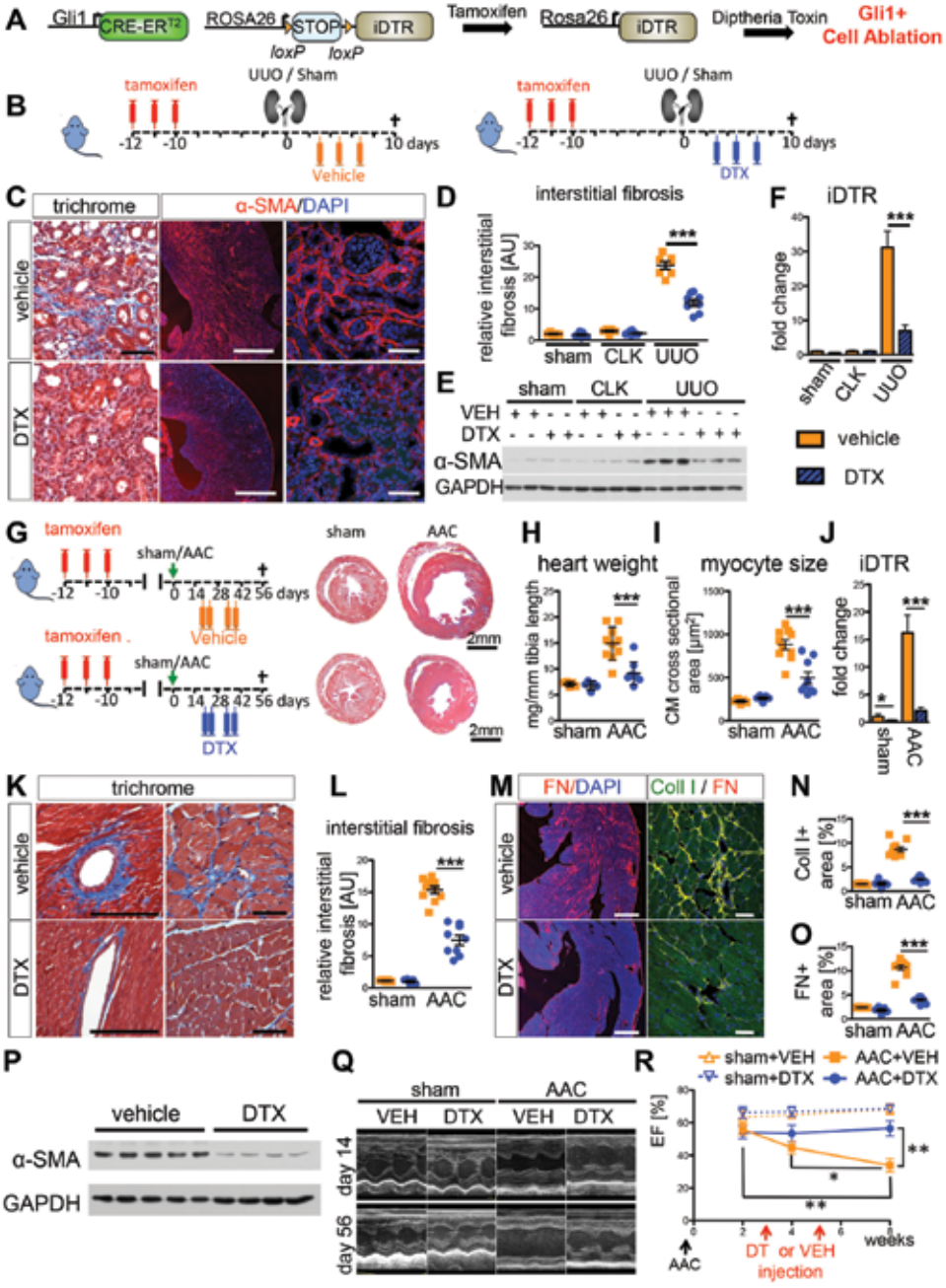
A
Gli1
CRE-ER T2
ROSA26
STOP
iDTR
loxP
loxP
Tamoxifen
Rosa26
iDTR
Diptheria Toxin
Gli1+
Cell Ablation
B
tamoxifen
UUO / Sham
-12
-10
0
10 days
Vehicle
tamoxifen
UUO / Sham
-12
-10
0
10 days
DTX
C
trichrome
α-SMA/DAPI
vehicle
DTX
D
interstitial fibrosis
relative interstitial fibrosis [AU]
***
sham
CLK
UUO
E
sham
CLK
UUO
VEH
DTX
α-SMA
GAPDH
F
iDTR
***
fold change
sham
CLK
UUO
vehicle
DTX
G
tamoxifen
sham/AAC
-12
-10
0 14 28 42 56 days
Vehicle
tamoxifen
sham/AAC
-12
-10
0 14 28 42 56 days
DTX
sham
AAC
2mm
2mm
H
heart weight
mg/mm tibia length
***
sham
AAC
I
myocyte size
CM cross sectional area [μm²]
***
sham
AAC
J
iDTR
fold change
*
***
sham
AAC
K
trichrome
vehicle
DTX
L
interstitial fibrosis
relative interstitial fibrosis [AU]
***
sham
AAC
M
FN/DAPI
Coll I / FN
vehicle
DTX
N
Coll I+ area [%]
***
sham
AAC
O
FN+ area [%]
***
sham
AAC
P
vehicle
DTX
α-SMA
GAPDH
Q
sham
AAC
VEH
DTX
VEH
DTX
day 14
day 56
R
sham+VEH
AAC+VEH
sham+DTX
AAC+DTX
EF [%]
**
*
**
weeks
AAC
DT or VEH injection

DISCUSSION

Knowledge concerning the *in vivo* function of MSC in specialized niches such as bone marrow and mouse incisor is growing rapidly [11]. Thus far however, little is known about the *in vivo* role of MSC in clinically important solid organs such as kidney, heart, lung and liver following injury and during repair. Here we demonstrate that Gli1 expression in adult mice marks a perivascular cell-population that forms an extensive network from the adventitia of large arteries to the pericyte niche in capillary beds of all major organs tested. These Gli1$^+$ cells express a typical mouse MSC surface profile *in vivo*, are enriched for CFU-F and possess a trilineage differentiation capability *in vitro,* therefore fulfilling the most commonly used definition of what has been termed an MSC [4]. Our data extends the recent finding that Gli1 labels MSC-like cells in the mouse incisor [26] and strongly suggests that Gli1 is a general *in vivo* marker for MSC-like cells during adult homeostasis. Indeed, it has become evident in recent years that the perivasculature comprising pericyte and adventitial locus might be the *in vivo* niche of MSC also explaining why MSC can be isolated from virtually all organs [27].

Our genetic fate tracing results indicate that resident perivascular Gli1$^+$ cells undergo proliferative expansion following injury and differentiate into myofibroblasts *in vivo.* Indeed, it was noted over a century ago that fibrosis emanates from blood vessels [28] and recent work implicates vascular pericytes as myofibroblast progenitors in the kidney [12], lung [29], spinal cord [23], dermis and skeletal muscle [13, 23, 27, 28, 30]. Despite this, the contribution of pericytes to kidney fibrosis has recently been questioned . To date, studies analyzing the role of pericytes in solid organ fibrosis has used broad stromal cell drivers that typically mediate recombination in several different cell types including vascular smooth muscle cells, mesangial cells, resident fibroblasts and pericytes . A particular strength of our work is that while PDGFRβ is expressed in a relatively large cell population across organs tested, Gli1 specifically labels a very small subset of this cell-population surrounding the ith fibroblasts and extracellular matrix has also been reported to facilitate cardiac hypertrophy . However, whether ablation of myofibroblasts can affect scaring, hypertrophy and left ventricular function has remained unclear. Our data clearly demonstrates that ablation of a myofibroblast progenitor population and descendants reduces fibrosis severity, cardiac hypertrophy and rescues systolic left ventricular function following injury. However, our data also suggests that Gli1$^+$ cells might gain markers of mature pericytes such as NG2 and participate in angiogenesis. Clearly, Gli1$^+$ cells are an intriguing and novel target for heart failure.

MSCs have recently been proposed as a source of scar forming myofibroblasts in heart fibrosis and myelofibrosis by others [3]. However, this hypothesis has remained speculative due to the absence of genetic fate tracing data. Our results support the idea that tissue resident perivascular MSC-like cells represent a major source of myofibroblasts. They further suggest that under conditions of chronic injury MSC-like cells are not beneficial but

actually promote organ fibrosis. This might contradict the hypothesis that MSC act beneficial as “medicinal MSC” that become activated and promote tissue regeneration following injury [13] or the fact that exogenous infused MSC promote regeneration or ameliorate progression in many diseases. While fibrotic scar is an adaptive response in certain acute injuries (in myocardial infarction, for example, fibrosis prevents left ventricular rupture), in chronic organ injury progressive myofibroblast expansion with scar deposition is pathologic and ultimately compromises organ function. Our results emphasize that MSC-like cells do not always act in a beneficial way.

Although ablation of Gli1$^+$ cells substantially ameliorated fibrosis in kidney and heart, we observed α-SMA$^+$ myofibroblasts that do not derive from Gli1$^+$ progenitors, suggesting a heterogeneous lineage for the myofibroblast pool. It is striking that Gli1$^+$ cells reflect a very small proportion of total organ cells and even PDGFRβ$^+$ cells, but their ablation reduces fibrosis by ~50% in kidney and heart. Combined with the enhanced clonogenic capacity of Gli1$^+$ cells compared to Gli1$^-$ interstitial cells, these results indicate that Gli1$^+$ MSC-like cells represent a functionally distinct interstitial sub-compartment. The similarity of these cells across organs also implies a conserved response to chronic injury culminating in fibrosis.

The precise identity of myofibroblasts in kidney fibrosis has been a subject of considerable controversy. In contrast with our results here, another recent study reported that neither PDGFRβ nor NG2 expressing cells contribute to the myofibroblast pool in kidney fibrosis [27, 30, 38]. However, early after this report another group demonstrated that PDGFRβ$^+$ cells do indeed contribute to the myofibroblast pool in kidney, lung and heart fibrosis . That myofibroblasts express PDGFRβ$^+$ has been known for many years . While the reasons for these discrepant results are unclear, mosaic transgene expression or expression patterns unfaithful to the endogenous allele, both known properties of random integration transgenics, is one possible explanation [38]. Our results here clearly indicate that all myofibroblasts express PDGFRβ and that Gli1$^+$ cells do not acquire significant NG2 expression in classical fibrosis models.

The contribution of circulating, bone marrow derived progenitor cells to the pool of myofibroblasts is also controversial and some evidence suggests that bone marrow-derived MSC enter the circulation and home to sites of injury. Our data from BMTX and parabiosis approaches provide conclusive evidence that Gli1$^+$ MSC-like cells are tissue resident cells that do not arise from the circulation. However, we cannot exclude a contribution from Gli1$^-$ circulating cells.

Most studies of Hh signaling during fibrosis suggest that Hh ligands Shh and Ihh drive myofibroblast proliferation and activation [43]. However, Hh signaling is also critical in angiogenesis and Shh gene transfer has been shown to reduce fibrosis and conserve left ventricular function following myocardial ischemia, possibly reflecting Shh driven pro-

angiogenic signaling in the heart . Consistent with this possibility, we found that both Shh and VEGF increased the number of Gli1^{+} cells associated with EC tubes. Shh also mediates pro-angiogenic signaling by upregulating VEGF expression [46] and VEGF can induce expression of the hedgehog transcriptional activator Gli1 [47], suggesting the possible existence of a positive feedback loop.

Our data suggest dual roles for Gli1^{+} cells in both fibrosis and angiogenesis. Gli1 is a transcriptional readout of Hh pathway activity indicating that Gli1^{+} MSC-like cells respond to Hh ligand. Consistent with this, nerve-derived Shh drives of Gli1 in mouse incisor MSC [48, 49] and a similar paradigm has been described for the hair follicle . Whether or not such a paracrine signaling loop exists for organ resident MSC-like cells is unclear. We analyzed bigenic ShhCreER^{t2+}, tdTomato^{+} mice for expression of Shh-positive cells in adult mice, and we did not observe any tdTomato^{+} cells in kidney or heart up to 2 weeks after tamoxifen injection or after injury (data not shown). The known roles for Gli1 in regulating cell proliferation and self-renewal of stem cells suggest similar roles in MSC-like cells [41]. Indeed, our data points toward constitutive expression of Gli1 in Gli1^{+} MSC-like cells *in vitro,* while inhibition of Gli by GANT61 reduces both self-renewal and association of Gli1^{+} cells with endothelial tubes. Whether steady state Gli expression might promote a quiescent state of perivascular Gli1^{+} cells will require further investigation.

EXPERIMENTAL PROCEDURES

METHODS

Animals

All mouse experiments were performed according to the animal experimental guidelines issued by the Animal Care and Use Committee at Harvard University. Gli1-nLacZ (i.e. Gli1^{tm2Alj}/J, JAX Stock 008211) Gli1CreER^{t2} (i.e. Gli1$^{tm3(re/ERT2)Alj}$/J, JAX Stock #007913), Rosa26tdTomato (i.e. B6-Cg-Gt(ROSA)26Sort$^{tm(CAG-tdTomato)Hze}$/J JAX Stock # 007909) iDTR mice (i.e. C57BL/6-Gt(ROSA)26Sor$^{tm1(HBEGF)Awai}$/J, JAX Stock # 007900), Ptprc^{a}-Pepc^{b} mice (B6.SJL-Ptprc^{a}-Pepc^{b}/Boy, JAX Stock # 002014) were purchased from Jackson Laboratories (Bar Harbor, ME). Offspring were genotyped by PCR according to the protocol from the Jackson laboratory. For lineage tracing studies 6-7 week old mice received 3 x 0.1mg/kg bodyweight tamoxifen in corn oil / 3% ethanol (Sigma) via intraperitoneal injection 10 days before surgery or disease induction. Unilateral ureteral obstruction (UUO) surgery was performed as previously described [51]. Briefly, after flank incision the left ureter was tied off at the level of the lower pole with two 4.0 silk ties. Mice were sacrificed at day 10 after surgery. For the unilateral ischemia re-perfusion injury (IRI), mice were anesthetized with pentobarbital

sodium (60 mg/kg body weight, intraperitoneally), the left kidney was exposed through flank incision and subjected to ischemia by clamping the renal pedicle with non-traumatic microaneurysm clamps (Roboz, Rockville, MD) for 35 min. Body temperatures were controlled at 36.5°C–37.5°C throughout the procedure. For the mouse model of angiotensin 2 induced myocardial fibrosis, we implanted osmotic minipumps (Alzet Model 2004) infusing angiotensin 2 (Sigma) dissolved in sterile normal saline (Baxter) at a rate of 1000ng/kg/min subcutaneously during a ketamine/xylazine (100/13 mg/kg bodyweight) anesthesia. Osmotic minipumps containing normal saline were implanted in control animals. Mice were euthanized at 28 days after surgery. Ascending aortic constriction (AAC) was performed in the Cardiovascular Facility of the Brigham and Women´s Hospital as previously described [52]. Briefly, mice were anesthetized with 3% isoflurane, intubated and ventilated on a Harvard rodent respirator (Type 845, Hugo Sachs Elektronik, March, Germany). An incision was made at the third intercostal space and ribs were gently spread with a microdissecting retractor (Biomedical Research Instruments). The ascending aorta was then isolated from the pulmonary artery approximately 3mm from the base of the heart and ligated around a blunted 27 gauge needle using 8-0 suture (Prolene, ETHICON). The ribs, chest musculature and skin was closed using 5-0 Dexon and 6-0 Prolene suture (ETHICON). Sham- operated mice underwent the same procedure without ligation of the ascending aorta. For the mouse model of myocardial infarction, mice underwent a similar procedure with sternotomy, the proximal left anterior descending artery was identified and ligated (8-0 suture, Prolene, ETHICON). For the model of bleomycin-induced lung fibrosis, mice were anesthetized with ketamine/xylazine (100/13 mg/kg bodyweight intraperitoneally) and the trachea was exposed by cervical incision. Bleomycin (Hospira) was dissolved in normal saline and intratracheally instilled via a 29 gauge needle at a dose of 2.5 U/kg bodyweight. Mice were euthanized at day 14 and lungs were perfused with Periodate Lysine-Paraformaldehyde (PLP) buffer and inflated to 25cm H2O trough the trachea. After ligation of the trachea (3-0 suture) the lungs were immersed in PLP for 2hours on ice, placed in 18% sucrose over night, and OCT embedded. Control mice underwent the same procedure but were instilled with normal saline. Liver injury and fibrosis was induced by intraperitoneal injection of carbon tetrachloride (CCL4, Sigma dissolved in mineral oil 1:3) at a dose of 1µl/g twice weekly for 4 weeks. Control mice received intraperitoneal injections of mineral oil (Sigma) alone. For all surgical procedures mice received buprenorphine (0.1mg/kg bodyweight subcutaneously) to achieve analgesia.

In vivo angiogenesis model

The *in vivo* matrigel plug angiogenesis model was performed as decribed previously [53, 54]. Briefly, Gli1+ cells were isolated according to the bone chip method and purified by fluorescence activated cell sorting. Matrigel (BD #354248) was thawed on ice. After trypsinization and centrifugation of the purified and cultured Gli1+ cells, the cell pellet was

dissolved in matrigel at a concentration of $8x10^6$ cells / ml. Wildtype C57BL6 mice (Charles river, n=6) were injected with 2 injections (200µl) at different locations in the abdominal subcutaneous adipose tissue. After 4 weeks the mice were sacrificed, the matrigel plugs were fixed in 4% paraformaldehyde (Electron Microscopy Sciences) and OCT frozen for cryosectioning and immunostaining.

Bone marrow transplantation experiments

For transplantation experiments of *Gli1-tdTomato* cells into CD45.1 wild type microenvironment, bigenic Gli1CreER^{t2}; tdTomato mice (CD45.2) received tamoxifen (3x 0.4mg/kg bodyweight p.o.) every other day until 3 days prior to euthanization, the bone marrow was harvested from leg bones and pelvis via crushing and $3x10^6$ freshly isolated whole bone marrow cells were injected into the tail-vein of lethally irradiated (1050 Rads) CD45.1 positive recipient mice (B6.SJL-Ptprc^a-Pepc^b/Boy, JAX Stock # 002014). To increase the number of Gli1$^+$ cells, $2x10^6$ FACS sorted Gli1-tdTomato+ cells isolated from bone chips of bigenic Gli1CreER^{t2}; tdTomato mice were added to the whole bone marrow cell suspension of each recipient prior to injection. Mice underwent UUO or sham surgery 5 weeks after cell injection and were euthanized 10 days later. Whole bone marrow was isolated via crushing of leg bones, kidney and lungs were digested and processed as described in the flow cytometry section and stained using common leukocyte variant specific antibodies (CD45.1 vs CD45.2) to verify engraftment of transplanted hematopoietic cells as described below.

Parabiosis

Bigenic Gli1CreER^{t2}; tdTomato mice (8 week old) received tamoxifen (3x0.4mg/kg bodyweight p.o) and were conjoined to wild-type CD45.1 mice (B6.SJL-Ptprc^a-Pepc^b/Boy, JAX Stock # 002014, 8 week old) at 10 days after the last tamoxifen injection. Parabiosis was performed as previously described [7]. Anesthesia was achieved by intraperitoneal injection of 100mg/kg bodyweight ketamine, 10mg/kg bodyweight xylazine and 3mg/kg bodyweight acepromacine. Buprenorphine (0.05-0.1mg/kg s.c.), meloxicam (1mg/kg s.c.) and local lidocaine (1%, s.c.) was given for analgesia. Blood chimerism was confirmed via flow cytometry of peripheral blood drawn from the retro-orbital plexus venosus of the CD45.1$^+$ parabiont (Ptprc^a-Pepc^b) 4 weeks after parabiosis surgery. After red blood cell lysis (BD Biosciences), leukocytes were stained for CD45.1 (APC-Cy7, ebioscience #25045382) and CD45.2 (FITC, ebioscience #110454) in PBS 10% FBS. After verification of cross-circulation in the peripheral blood a UUO surgery was performed at the right kidney of the CD45.1$^+$ parabiont unter 3% isoflurane (ISOTHESIA, Butler Schein) anesthesia and analgesia as described in the UUO surgery above. At 10 days after the UUO surgery the mice were euthanized. Kidneys (sham = Gli1; tdTomato-mouse, CLK = contralateral of the CD45.1 parabiont, UUO= unilateral ureteral obstruction of the CD45.1 parabiont) were digested and stained for CD45.1 and CD45.2 according to the protocol in the flow cytometry section.

Single-cell suspensions of spleen were prepared by pressing tissue through a cell strainer followed by red blood cell lysis.

Cell specific ablation experiments

For all ablation experiments, bigenic Gli1CreER^{t2}; iDTR mice received tamoxifen (3x 0.4mg/kg per oral gavage) 10 days before surgery and were then injected with diphtheria toxin dissolved in PBS (List Biological Laboratories) at a dose of 50ng/g bodyweight intraperitoneally as indicated (i.e. at day 3,5,7 following UUO and days 16, 18, 37, 39 following AAC surgery). Control mice received intraperitoneal injections of PBS.

In order to validate the cell-ablation, triple transgenic mice (Gli1CreER^{t2}; iDTR; tdTomato) were generated and injected with the above mentioned dose of tamoxifen. UUO surgery was performed 10 days after the last tamoxifen dose and DTX was administered in analogy to the other UUO ablation experiments. Mice were sacrificed 10 days after UUO surgery.

Tissue Preparation and Histology

Mice were anesthetized with isofluorane (Baxter) and perfused via the left ventricle with 4°C PBS for 1 minute. For histological analyses tissue sections were fixed in 10% formaldehyde for 1h, paraffin embedded and cut with a rotating microtome at 3µm thickness and stained according to routine histology protocols. For immunofluorescence studies, kidneys were fixed in 4% paraformaldehyde on ice for 1 hour, then incubated in 30% sucrose in PBS at 4°C overnight. OCT-embedded (Sakura Finetek) tissues were cryosectioned into 7 µm sections and mounted on Superfrost slides (Fisher Scientific). Sections were washed in 1X PBS, blocked in 10% normal goat serum (Vector Labs) and incubated with primary antibodies specific for Ki-67 (1:200, Vector Labs Cat. #VP-RM04), alpha SMA (1:200, Sigma, Cat No. A2547), alpha SMA-FITC (1:200, Sigma, # F3777), fibronectin (1:40, Abcam #ab23750), collagen1α1 (1:20, Southern Biotechnology #1310-01), DsRed (1:50, Clontech #632496), NG2 (1:50, Millipore #AB5320), CD146 (1:100 Abcam #ab75769), CD146-APC (1:100, Biolegend #134711), CD73 (1:5000, gift from Dr. Nicolas Picard, Institute of Anatomy University of Zurich), PDGFRα (1:50, R&D Systems #af1062), STRO1 (1:100, R&D Systems mab1038) and Nestin (1:100, Abcam #ab6142). Staining for the 3G5 antigen was performed by incubation of tissue sections with supernatant from the 3G5 hybridoma cell line (ATCC CRL-1814). Secondary antibodies were FITC-, Cy3, or Cy5-conjugated (Jackson ImmunoResearch). Sections were then stained with DAPI (4´,6´-´diamidino-2-phenylindole) and mounted in Prolong Gold (Life Technologies). Tunel staining was performed using the in situ cell death detection kit (Roche) according to the manufacturer instructions. Immunohistochemistry was performed using the primary antibody against Gli1 (1:500 R&D Systems #MAB3324) and a biotynilated secondary antibody (Jackson Immuno). Antigen retrieval was achieved by pressure cooker treatment and antigen unmasking solution (Vector). Staining was achieved using Avidin/Biotin Blocking kit, the ABC kit, the DAB kit and the DAB enhancing solution (all Vector laboratories) according to the manufacturer instructions.

For quantification of cell expansion, pictures (400x, n=5/organ) were taken as follows: in the kidney models random pictures of the inner cortex and outer medulla, in the angiotensin 2 model of myocardial fibrosis random pictures around arteries i.e. periarterial; in the AAC model random pictures of the interstitial myocardium (excluding arteries), in the liver-fibrosis model random pictures around central veins and the periportal field and in the bleomycin induced lung fibrosis model random pictures of interstitial lung (excluding large bronchi) were taken. Positive cells were counted manually using Image J (NIH). Quantification of α-SMA, collagen I and fibronectin positive surface area was performed by taking random pictures (400x, n=5 per organ) of each mouse using the number of stained pixels per total pixels in Adobe Photoshop CS5 (Adobe Systems, Inc., San Jose, CA). All images were obtained by confocal (Nikon C1 eclipse, Nikon, Melville, NY) or standard microscopy (Nikon eclipse 90i).

Fibrosis severity was scored at 400x magnification using a counting grid with 117 intersections (for the kidney 5 random pictures of the inner cortex, for the heart 6 pictures of different left ventricular regions i.e. anterior, anteroseptal, inferoseptal, inferior, inferolateral were used). The number of grid intersections overlying trichrome positive (blue) interstitial area was counted and expressed as a percentage of all grid intersections. For this calculation in the kidney, intersections that were in tubular lumen and glomeruli were subtracted from the total number of grid intersections. Cardiomyocyte cross sectional area was determined by measuring the cell surface area of 10 random cardiomyocytes in 400x pictures of the myocardium (3 trichrome stained pictures / heart) using Image J (NIH). To identify LacZ activity in kidney sections, PFA fixed frozen sections were incubated in standard 5-bromo-4-chloro-3-indolyl-β-d-galactoside (X-gal) for 48 hours counterstained with nuclear fast red and mounted. Fluorescence microangiography was performed as recently described [11].

Flow Cytometry and cell sorting

For flow cytometric analysis or fluorescence activated cell sorting (FACS) of whole organs and tissues, mice were euthanized exactly as described above and the organs of interest were placed in FACS Buffer (PBS, 10%FBS, 2% Penicillin Streptomycin, Life Technologies). After thoroughly mincing the tissue/organ using a sterile scalpel (Feather), the tissue/organ was placed in gentleMACS C Tubes (Miltenyi Biotec) containing 1.5ml DMEM (Life Technologies) with 0.1mg/ml Liberase TL (Roche). The tissue was then dissociated using the D program of the gentleMacs dissociator (Miltenyi Biotec) followed by 30 min incubation at 37°C. Following washing steps with FACS buffer and centrifugation (1500 rpm 5 min) the solution was filtered twice trough a 40µm cell strainer (BD Biosciences) and transferred to 5ml Polystyrene Round-Bottom FACS tubes (BD Biosciences). FACS sorting was performed using the FACSAria II cell sorter (BD Biosciences). For flow cytometric studies the samples were stained in 100-500µl FACS Buffer using the following fluorochrome conjugated antibodies: CD31-APC (Biolegend #102410), CD45-FITC (eBioscience #17-0291-82), CD34-

FITC (eBioscience #11-0341-85), CD29-APC (eBioscience #17-0291-82), Sca1-APC-Cy7 (Biolegend #108126), CD44-PE-Cy7 (eBioscience #25-0441-82), CD105-PE-Cy7 (Biolegend #120410), PDGFRβ (CD140b-APC Biolegend #136008), CD45.1 (APC-Cy7, ebioscience #25045382), CD45.2 (FITC, ebioscience #110454), CD146-APC (Biolegend # 134711), CD73-APC (Biolegend 127209) all 1:100 for 30 min, or the following primary non-conjugated antibodies NG2 (1:50, Millipore #AB5320), CD146 (1:100 Abcam #ab75769), PDGFRα (1:50, R&D Systems #af1062), STRO1 (1:100, R&D Systems mab1038), Nestin (1:100, Abcam #ab6142) for 30min. 3G5 staining was achieved by incubation of cells in supernatant of the 3G5 hybridoma cell line (ATCC #CRL-1814). The staining of the intracellular antigens Nestin was performed after fixation and permeabilization of the cells (Cytofix/Cytoperm solution, BD Biosciences). After incubation with directly conjugated antibodies, cells were PBS washed and subjected to flow cytometry. Following incubation with primary antibodies, cells were PBS washed and incubated with the appropriate AF647-conjugated antibody (Jackson Immuno). All flow cytometric analyses were performed at a LSR II Flow Cytometer (BD Biosciences). For all flow cytometric analyses and sorting DAPI (1mg/ml 1:1000) was added in order to exclude dead cells. Data were analyzed by using Flow Jo software (Version 9.6.2, Tree Star Inc).

Cell Culture Experiments

Gli1+ cells were grown in alpha MEM (GlutaMAX, Life Technologies) containing 20% MSC qualified FBS (Life Technologies), 2% Penicillin Streptomycin (Life Technologies), 1ng/ml murine basic fibroblast growth factor (Thermo Fisher Scientific) and 5ng/ml murine epidermal growth factor (Peprotech). Bone marrow MSC were isolated from compact bone chips of femur, tibia and pelvis according to the protocol by Zhu et al. [55]. For osteogenic or adipogenic differentiation flow-purified cells were plated in a 48 well, at a 60-70% or 90-100% confluence, the alpha MEM medium was exchanged with osteogenic or adipogenic differentiation medium, respectively (R&D Systems). After 21 days of cultivation, cells were stained according to routine protocols using Oilred O (Sigma). To achieve co-staining for alkaline phosphatase and von Kossa staining, cells were washed once with PBS, fixed with 10% neutral formalin buffer (VWR) for 10min, incubated for 15 min with distilled water followed by an incubation in an Naphthol-AS MX-PO4 (Sigma), Dimethylformamide (Fisher), Tris-HCL buffer with Red Violet LB salt (Sigma) for 45 min. After washing with distilled water cells were stained with 2.5% silver nitrate (Sigma) for 30 minutes.

For chondrogenic differentiation 2-10x10^4 cells were resuspended in 1ml chondrogenic differentiation medium (RnD Systems) in a 15ml conical tube (BD Biosciences) and centrifuged at 1500rpm for 5 min. The cell-pellets were cultivated upright in the 15 ml conical for 21 days. For detection of chondrogenic differentiation the cell-pellet was fixed in 4% paraformaldehyde. OCT-embedded (Sakura Finetek) cell-pellets were cryosectioned into 4 µm sections and mounted on Superfrost slides. After PBS washing the sections were

stained with Alcian blue (Santa Cruz Biotechnology) and counterstained with nuclear fast red (Sigma). For cell culture experiments, FACS sorted tdTomato+ cells from heart or kidney were cultured in 6 well plates, serum starved overnight (0.5% FBS) and treated with 10ng/ml TGF-β or vehicle for 24 hours. For α-SMA staining cells were grown on coverslips (Fisher) coated with collagen I (BD Biosciences) and treated with TGF-β for 72 hours. Sonic hedgehog conditioned media was produced from supernatant of confluent Cos7 cells stably transfected with pcDNA3-N-Shh or pcDNA3 control plasmid. In order to study Gli1 protein expression, FACS purified Gli1$^+$ cells from bone chips were serum starved for 24h (0.5% FBS) and cultured in MesenCult MSC medium (STEMCELL Technologies) containing 20% control supernatant with either PBS, 5μM cyclopamine (Sigma, 25mM stock in ethanol), 5μM GANT61 in DMSO (Cayman Chemical), DMSO (vehicle control for GANT61) or with 400μl of supernatant of Cos7 cells stably transfected with pcDNA3-N-Shh with our without addition of cyclopamine. Equivalent concentrations of ethanol (1:5000) were added to all conditions to control for the cyclopamine solvent. Medium was changed after 24h and cells were harvested for western blot after a total of 48h

CFU-F assay

Adult 8 week old bigenic Gli1CreER^{t2}; tdTomato mice received tamoxifen (3x0.4mg/kg BW, p.o.) every other day and were euthanized 3 days after the last tamoxifen injection. Whole organs were digested and stained for PDGFRβ (CD140b-APC, biolegend) as described above. PDGFRβ$^+$,tdTomato- or PDGFRβ+,tdTomato+ cells were sorted into 6 well plates using the FACSAria II cell sorter (BD Biosciences) in densities of 10^2 ~ 10^4 cells in MesenCult MSC medium (STEMCELL Technologies) for 14 days as previously described [56]. The presence of more than 50 cells in a cluster at 14 days after FACS was counted as a colony. For CFU-F assay and manipulation of the Hh pathway cells were sorted in 1.6ml MesenCult MSC medium in 6 wells containing Cos7 control supernatant (0.4ml) and addition of either PBS, 5μM cyclopamine (Sigma), 5μM GANT61 in DMSO (Cayman Chemical), DMSO (vehicle control for GANT61) or with 400μl of supernatant of Cos7 cells stably transfected with pcDNA3-N-Shh. Equivalent concentrations of ethanol (1:5000) were added to all conditions to control for the cyclopamine solvent. Medium was changed daily starting 48h after sort. Colonies were quantified at 14 days as mentioned above.

In vitro tube formation assay

Human umbilical cord endothelial cells (HUVECs, ATCC) were cultured in endothelial cell medium (EGM-2 Lonza) and propagated at 80% confluency. Gli1$^+$ cells were isolated from bone chips, purified via FACS and cultured as previously described. The tube formation assay was performed as follows: HUVECs (passage 5) were fluorescence labeled (CellTracker Green, Life Technologies) 1h prior to trypsinization according to the manufacturer's instructions. Labeled HUVECs and Gli1$^+$ cells (passage 4) were trypsinized and resuspended

at a concentration of 1x10^{7}cells/ml in 1xDMEM (Gibco). A collagen solution was prepared as previously described [57], 40µl of Gli1$^+$ cells and 200µl of HUVECs were added to the collagen solution. The cell collagen solution was then gently mixed and 28µl were plated in 96 half-area well TC-treated microplates (Corning). The plate was incubated for 15min at 37°C (5%CO^2) to allow for collagen polymerization. Afterwards 100µl EGM-2 medium (without VEGF) was added containing either 20% control supernatant of Cos7 cells or Shh supernatant. TGF-β (10ng/ml, Peprotech), GANT61 in DMSO (5µM), DMSO, or vascular endothelial growth factor (20ng/ml VEGF-165, Peprotech) was added, respectively. Medium was changed after 24h. The total number of EC tubes, and Gli1$^+$ cells and the number of Gli1$^+$ cells adjacent to EC tubes was quantified by counting in 10x pictures using inverted fluorescence microscopy at 72h.

Immunoelectron Microscopy

For immunoelectron microscopy, kidney tissue was fixed in Karnovsky's fixative and processed using standard electron microscopy procedures. After processing, ultrathin sections were obtained and antigen retrieval was performed in 0.05M Tris buffer (Tris, pH 10.0) for 24 hours at 65°C. Following antigen retrieval, grid-mounted tissue sections were immersed in a blocking solution (0.5% goat serum and 0.05% bovine serum albumin in 0.02M phosphate buffer), washed 3 times, then incubated with a primary antibody against tdTomato (1:10, Clontech #6324961) overnight at 4 degrees. This was followed by 3 washing steps and incubation with 20nm gold particle-labeled goat secondary antibody specific for rabbit IgG (1:10, GAR20; BBInternational, Cardiff, UK) at room temperature for 1 hour. Images were obtained using the JEOL JEM-1011 transmission electron microscope after staining the tissue with uranyl acetate and lead citrate

Real Time PCR Experiments

Tissue or cell-pellets were harvested and immediately snap frozen in liquid nitrogen. RNA from kidneys or cell-culture was extracted according to the manufacturer instructions using the RNeasy Mini Kit (Qiagen) and 600 ng of total RNA was reverse transcribed with iScript (BioRad). RNA from hearts (left ventricle) was isolated using Trizol Reagent (Life Technologies) according the manufacturer instructions. Following or during the RNA extraction DNA was removed by a DNAse digestion step (Life Technologies). Quantitative polymerase chain reactions were carried out with iQ-SYBR Green supermix (BioRad) and the BioRad CFX96 Real Time System with the C1000 Touch Thermal Cycler. Cycling conditions were 95°C for 3 minutes then 40 cycles of 95°C for 15 seconds and 60°C for 1 minute, followed by one cycle of 95°C for 10 seconds. Glyceraldehyde-3-phosphate dehydrogenase (GAPDH) was used as a housekeeping gene. Data was analyzed using the $2^{-\Delta\Delta ct}$ method. PCR products were electrophoresed on a 2% agarose gel in 1xTE and visualizes under UV light with ethidium bromide. Primers are listed in table S1.

Western Blot

Tissue was snap frozen in liquid nitrogen immediately after mice were euthanized and stored at -80°C. Kidney tissue samples were homogenized in lysis buffer containing 10mM HEPES, pH 7.4, 0.32M sucrose, 2mM EDTA, 1mM DTT, 1mM PMSF and 1 protease inhibitor tablet per 10ml of lysis buffer (Roche Cat. No. 11836153001). Protein from $Gli1^+$ cultured cells was isolated after PBS washing using a cell scratcher with the same buffer. Protein from heart tissue samples (left ventricles) was isolated via precipitation from the Trizol Reagent as bed elsewhere.[1]. The samples were sonicated and protein concentration was determined by the Bradford Assay using Bio-Rad Protein Assay Dye (Biorad). 10-20µg of protein from lysates was loaded on a 10% polyacrylamide gel and separated by SDS electrophoresis. Proteins were transferred to a Immobilion membrane (Millipore) blocked in 5% milk in PBST, probed overnight at 4°C with the primary antibodies: mouse anti-αSMA at 1:4000 (Sigma #A2547), rat anti-Gli1 at 1:1000 (R&D Systems #MAB3324, and rabbit anti-GAPDH at 1:4000 (Bethyl Laboratories, #A300-641A). Following incubation with primary antibody blots were washed probed with respective horseradish-peroxidase conjugated secondary antibodies at 1:4000 (Dako, Cat. No. P0447, P0448, P0450) for 1 hour at room temperature and then visualized using the Western Lightning ECL kit from PerkinElmer (#NEL100001EA).

Echocardiography

Echocardiography was performed in the AAC cell-ablation experiment immediately following sham or AAC surgery to determine the peak velocity at the ascending aorta or the constriction, 2 weeks after surgery before the randomization to DTX or Vehicle group and at 4 and 8 weeks after the surgery in low dose isoflurane anesthesia (1.5%) using a 28MHz linear array transducer connected to a digital ultrasound console (Vevo 2100 Visualsonics). Mice were gently restrained on a heated platform and pre-warmed ultrasound gel was used on their depilated chest. B-Mode loops were acquired from parasternal short and long-axis views and M-Mode images were recorded from parasternal short-axis view at the mid-papillary level. Peak velocity at the suture was determined by pulse waved (PW) Duplex sonography of the ascending aorta using color duplex sonography as a guide for detecting the area of strongest turbulence. Images and loops were stored and analyzed offline using the Vevo 2100 analysis software (1.6.0 Visualsonics). Left ventricular ejection fraction (EF) was calculated by identification of frames with the maximal and minimal cross-sectional area and width in the parasternal long axis view as described before [2].

Statistical Analysis

Data are presented as mean±SEM . Comparison of two groups was performed using unpaired t-test. Paired t-test was used for comparsion of repeated measured in the same group. For multiple group comparison analysis of variance with posthoc Tukey correction was applied. Statistical analyses were performed using GraphPad Prism 5.0c (GraphPad Software Inc., San Diego, CA). A p value of less than 0.05 was considered significant.

Primer pairs used for PCR

Gene	Sequence
GAPDH	Fw 5´-AGGTCGGTGTGAACGGATTTG -3´
	Rv 5`-TGTAGACCATGTAGTTGAGGTCA -3´
iDTR (HB-EGF)	Fw 5´-GGAGCACGGGAAAAGAAAG-3´
	Rv5´-GAGCCCGGAGCTCCTTCACA-3
Col1α1	Fw5´- TGACTGGAAGAGCGGAGAGT-3´
	Rv5´-GTTCGGGCTGATGTACCAGT -3´
fibronectin	Fw5´-ATCTGGACCCCTCCTGATAGT -3´
	Rv5´-GCCCAGTGATTTCAGCAAAGG-3´
α-SMA	Fw5´-CTGACAGAGGCACCACTGAA -3´
	Rv5´- CATCTCCAGAGTCCAGCACA-3´
Gli1	Fw5´- ATCACCTGTTGGGGATGCTGGAT-3´
	Rv5´- CGTGAATAGGACTTCCGACAG -3´
Gli2	Fw5´-GTTCCAAGGCCTACTCTCGCCTG -3´
	Rv5´- CTTGAGCAGTGGAGCACGGACAT-3´
Gli3	Fw5´-AGCAACCAGGAGCCTGAAGTCAT -3´
	Rv5´- GTCTTGAGTAGGCTTTTGTGCAA-3´
Ptc1	Fw5´- GCTGGAGGAGAACAAGCAAC-3´
	Rv5´- GAGCAAACATGTGCTCCAGA -3´
Smo	Fw5´- TGCCACCAGAAGAACAAGCCA-3´
	Rv5´-CCTCCATTAGGTTAGTGCGG -3´
Shh	Fw5´-TCACAAGAAACTCCGAACGATTT -3´
	Rv5´- GATGTCCACTGCTCGACCC-3´
Ihh	Fw5´-CTCTTGCCTACAAGCAGTTCA -3´
	Rv5´- CCGTGTTCTCCTCGTCCTT-3´
Dhh	Fw5´-GCCATCGCGGTGATGAACA -3´
	Rv5´-GCCTTCGTAGTGGAGTGAATCC -3´

Author contributions

R.K. designed and carried out experiments, analyzed results and wrote the manuscript, R.K.S., D.P.D. F.M., SF, P.B. and J.M.H. carried out experiments, analyzed the data and reviewed the manuscript, B.L.E. designed experiments and reviewed the manuscript, B.D.H. designed experiments, interpreted results and wrote the manuscript

Acknowledgements

This work was supported by NIH/NIDDK (DK088923 and DK103050), the NIDDK Diabetic Complications Consortium (DK076169), by the Harvard Stem Cell Institute and by an Established Investigator Award of the American Heart Association (all to BDH) and by a fellowship from the Deutsche Forschungsgemeinschaft (to RK Kr 40731-1 and RKS Schn 1188/3-1). We thank Sudeshna Fisch and Soeun Ngoy from the cardiovascular core of the Brigham and Women´s Hospital for technical support.

SUPPLEMENTARY FIGURES:

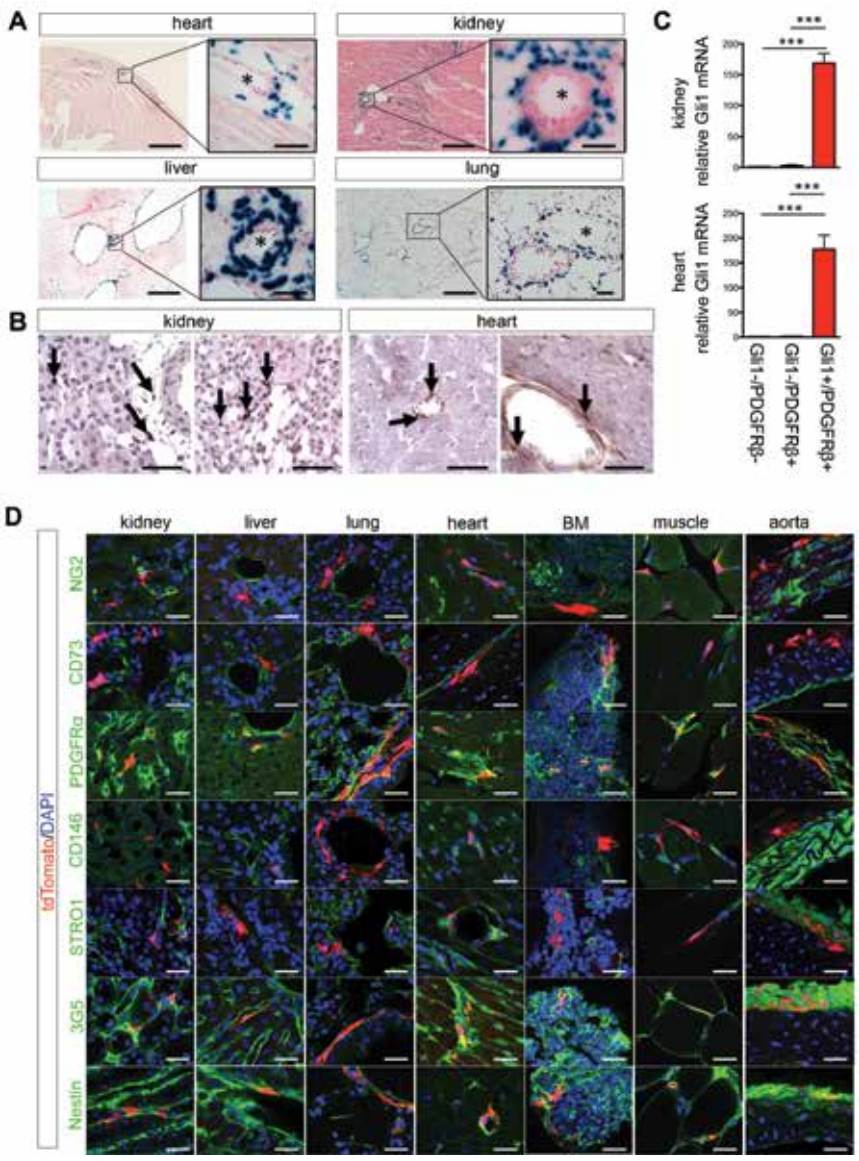

Figure S1: Related to figure 1. Perivascular cells express Gli1 and a typical MSC surface marker pattern.
(A) X-gal stained tissue sections from the Gli1-nLacZ mouse indicating Gli1 expressing cells are specifically located around the vasculature (* arteries). Scale bars: 500µm, inserts 50µm
(B) Immunohistochemical staining for endogenous Gli1 in mouse kidney and heart. Gli1+ cells (arrows) were located in the interstitium and adventitia of arteries. Scale bars 50µm
(C) Relative Gli1 mRNA expression of sorted cell populations of bigenic Gli1CreERt^2; tdTomato mice from kidney and heart. ***p<0.001 by one way ANOVA with posthoc Tukey
(D) Immunostaining for reported pericyte and MSC markers in healthy adult tissues. Scale bars: 25µm

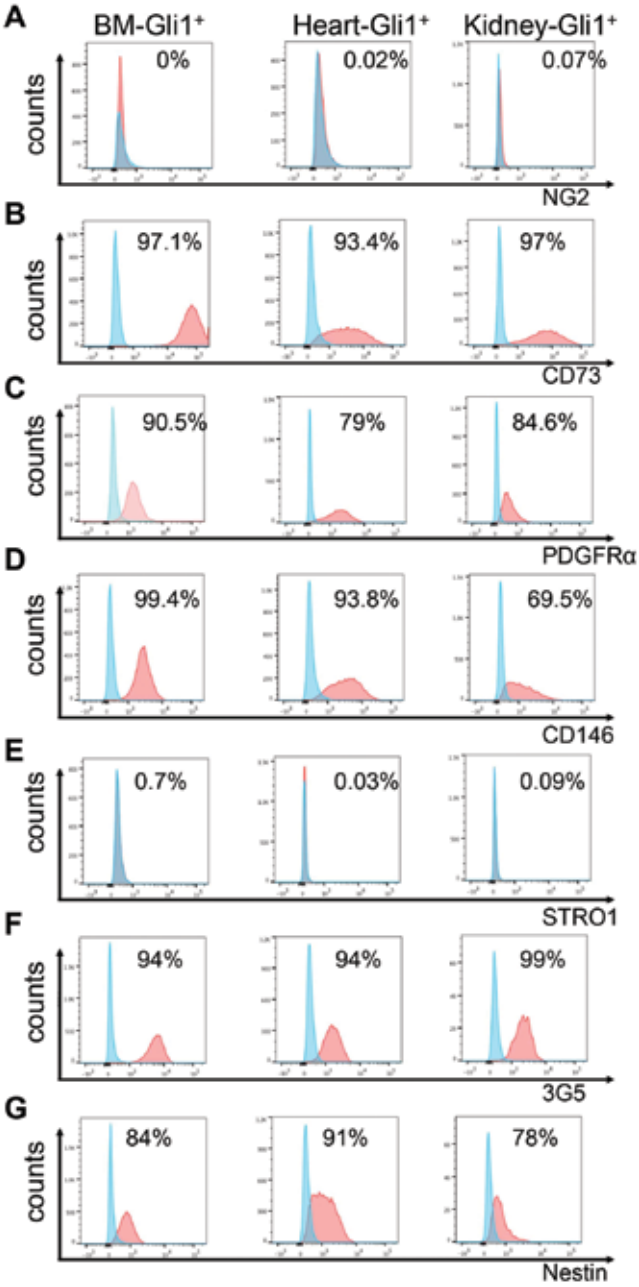

Figure S2: Related to figure 2. Representative flow cytometric plots of cultured Gli1$^+$ cells.
Cells were isolated from whole heart and kidney by digestion and from bone chips (BM), subsequently cultivatied, fluorescence activated cell sorted and additionally cultured for 8 weeks prior to flow cytometric characterization. Representative histograms for expression of: **(A)** NG2 **(B)** CD73 **(C)** PDGFRα **(D)** CD146 **(E)** STRO1 **(F)** 3G5 and **(G)** Nestin (negative control in blue, Gli1tdTomato$^+$ cells in red).

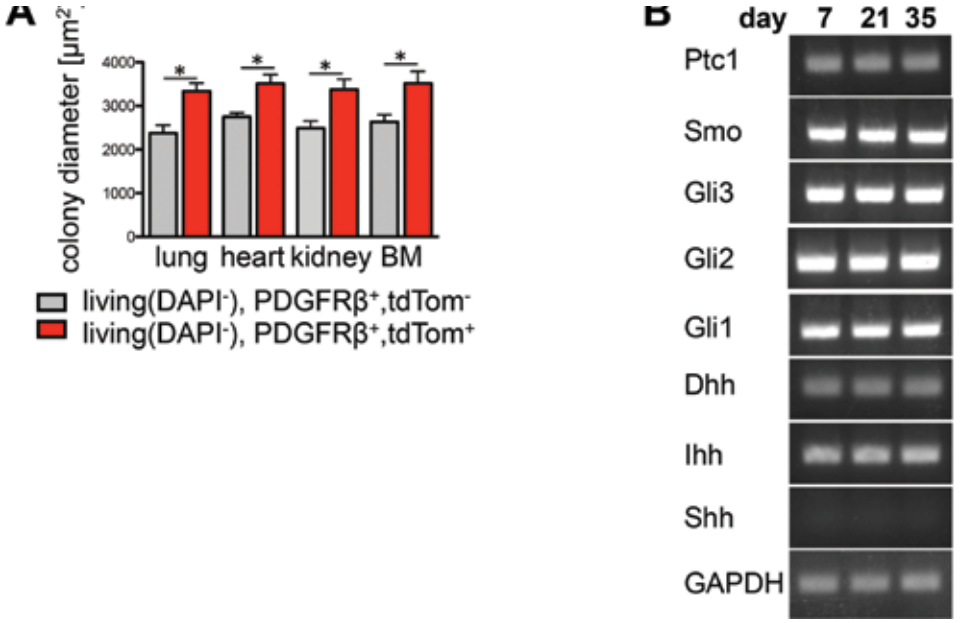

Figure S3: Related to figure 3. Colony size and mRNA expression of hedgehog pathway members in Gli1+ cells in vitro.

(**A**) The size of the formed colonies at 7 days was assessed by measurement of the colony diameter using inverted microscopy from fluorescence activated cell sorted, living (DAPI-), PDGFRβ+,tdTomato(tdTom)- and PDGFRβ+,tdTomato+ cells from whole digested lung, heart, kidney and bone marrow (bone chips isolation method) in 6 wells (n=3 biologic replicates each) *p<0.05 by t-test.

(**B**) Representative PCR bands of the hedgehog pathway members patched 1 (Ptc1), smoothened (Smo), Gli1-3, desert hedgehog (Dhh), Indian hedgehog (Ihh) and sonic hedgehog (Shh) after 7, 21 and 35 days of culture from fluorescence activated cell sorted Gli1+ cells liberated from bone chips.

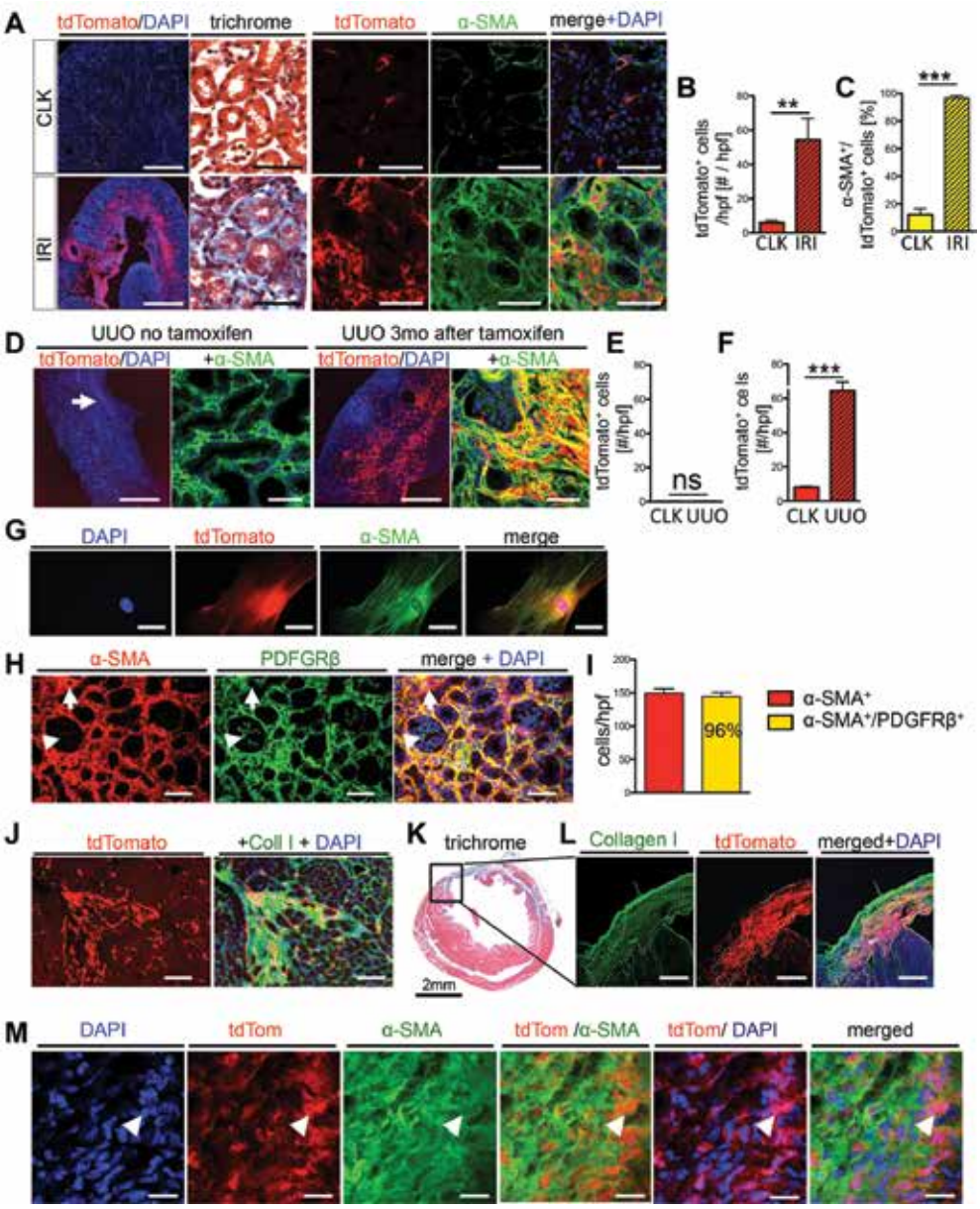
A
tdTomato/DAPI
trichrome
tdTomato
α-SMA
merge+DAPI
CLK
IRI
B
tdTomato+ cells /hpf [# / hpf]
**
CLK IRI
C
α-SMA+/ tdTomato+ cells [%]
***
CLK IRI
D
UUO no tamoxifen
UUO 3mo after tamoxifen
tdTomato/DAPI
+α-SMA
E
tdTomato+ cells [#/hpf]
ns
CLK UUO
F
***
CLK UUO
G
DAPI
tdTomato
α-SMA
merge
H
α-SMA
PDGFRβ
merge + DAPI
I
cells/hpf
96%
α-SMA+
α-SMA+/PDGFRβ+
J
tdTomato
+Coll I + DAPI
K
trichrome
2mm
L
Collagen I
tdTomato
merged+DAPI
M
DAPI
tdTom
α-SMA
tdTom /α-SMA
tdTom/ DAPI
merged

Figure S4: Related to figure 4. Fate tracing of Gli1+ cells in kidney and heart fibrosis *in vivo* and validation of the genetic mouse fate tracing approach.

(A-C) Bigenic Gli1,tdTomato+ mice were injected with tamoxifen, underwent unilateral ischemia reperfusion injury (IRI) of the kidney 10 days after the last injection of tamoxifen and were euthanized 4 weeks after the surgery (CLK contralateral non-injured kidney).

Following severe IRI, the Gli1-tdTomato+ cells dramatically expanded and acquired alpha smooth muscle actin (α-SMA) expression during progression of kidney fibrosis. Scale bars: left panel 500µm, all others 50µm, **p<0.01, ***p<0.001 by t-test, data is presented as mean±SEM, high power field (hpf) 400x

(D-F) To exclude leaky recombination in the absence of tamoxifen or residual tamoxifen in the system which might drive recombination of cells inducing Gli1+ expression following injury, we performed two mouse UUO experiments in bigenic Gli1CreER^{t2},tdTomato mice. A group of 3 bigenic mice underwent UUO surgery without tamoxifen treatment and sacrificed 10 days later, and another group of n=3 bigenic mice underwent UUO surgery 3 months after receiving tamoxifen, to exclude remaining tamoxifen in the mouse-system during injury. There was no significant recombination in the groupt that did not receive tamoxifen (arrow: one tdTomato+ cell) even during severe fibrosis following UUO with interstitial (α-SMA+) myofibroblasts. However, in the second group, where UUO surgery was performed late (3 months) after tamoxifen injection, we observed a significant expansion of tdTomato+ cells with a comparable fold change increase between contralateral (CLK) and UUO kidneys as in our initial experiments with only 10 days between tamoxifen administration and surgery. These results excluded the possibility that remaining tamoxifen would have resulted in recombination in cells that acquired Gli1 expression following injury or during disease progression. Scale bars 500µm left panels and 50µm right panels. ***p<0.001 by t-test

(G) Gli1-tdTomato+ sorted (FACS) cells from the heart treated with TGF-β for 24h and stained for α-SMA. tdTomato intensity is highest in the nucleus with a lower signal in the cytoplasm whereas for α-SMA a converse distribution can be observed, with no signal in the nucleus and α-SMA+ stress-fibers around the nucleus and in the cytoplasm. Therefore, to assess co-localization of tdTomato and α-SMA the perinuclear region has to be evaluated. Scale bars 50µm

(H-I) 10 day UUO kidneys co-stained for α-SMA and PDGFRβ indicating that the vast majority of kidney myofibroblasts (α-SMA+) expresses PDGFRβ (Quantification in n=3 wild-type mice with n=4 random high power fields-400x from inner cortex and outer medulla each). Scale bars 50µm

(J) Large interstitial myocardial scar 8 weeks after ascending aortic constriction (AAC) in bigenic Gli1,tdTomato+ mice. Scale bars: 100µm

(K-M) Bigenic Gli1,tdTomato+ mice received tamoxifen injection (3x0.1mg/kg bodyweight i.p.), underwent left coronary artery ligation surgery (left anterior descending, LAD) 10 days after the last tamoxifen injection and were sacrificed 28 days after surgery. Representative picture of a trichrome stained heart 4 weeks after coronary artery ligation (K) shows the infarction scar of the left ventricular wall. Collagen I immunostaining was used to delineate the scar area of the left ventricle (dashed line in L). Gli1+ cells expanded within the scar. Co-staining revealed that Gli1,tdTomato+ cells acquired perinuclear (arrowheads in M) alpha smooth muscle (α-SMA) expression. Scale bars 500µm in L and 20µm in M.

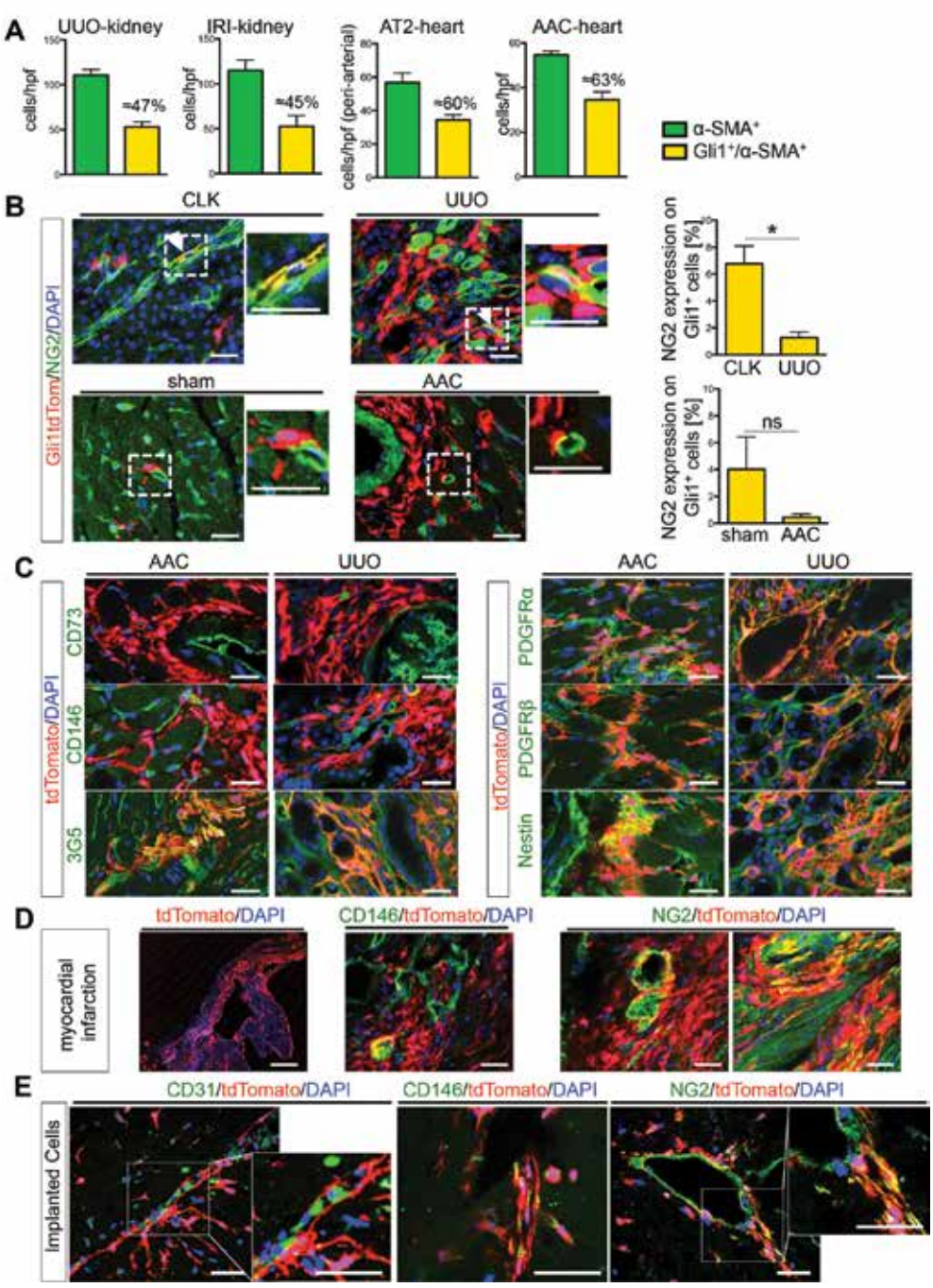
A
UUO-kidney
IRI-kidney
AT2-heart
AAC-heart
cells/hpf
cells/hpf (peri-arterial)
≈47%
≈45%
≈60%
≈63%
α-SMA+
Gli1+/α-SMA+
B
CLK
UUO
sham
AAC
Gli1tdTom/NG2/DAPI
NG2 expression on Gli1+ cells [%]
*
ns
CLK
UUO
sham
AAC
C
AAC
UUO
tdTomato/DAPI
CD73
CD146
3G5
PDGFRα
PDGFRβ
Nestin
D
myocardial infarction
tdTomato/DAPI
CD146/tdTomato/DAPI
NG2/tdTomato/DAPI
E
Implanted Cells
CD31/tdTomato/DAPI
CD146/tdTomato/DAPI
NG2/tdTomato/DAPI

Figure S5: Related to figure 4. Myofibroblast differentiation, pericyte and MSC marker expression of Gli1^{+} cells in kidney and heart fibrosis and fate tracing of Gli1^{+} cells angiogenesis in vivo.
(A) Quantification of all interstitial α-SMA^{+} cells and the number of α-SMA^{+} cells that co-label with tdTomato in kidney fibrosis (unilateral ureteral obstruction-UUO and ischemia reperfusion injury-IRI) and heart fibrosis (angiotensin 2 – AT2 and ascending aortic constriction-AAC). Quantification was performed by cell-counting in 5-high power fields (hpf 400x) from n=4 mice in UUO and n=5 mice in IRI, n=4 mice in AT2 vs n=3 mice with vehicle mini-pump, n=4 mice with AAC and n=3 sham AAC mice.
(B) NG2 expression by immunostaining in kidneys (CLK and UUO) and heart (sham versus ascending aortic constriction-AAC) from bigenic Gli1CreER^{t2},tdTomato mice (arrowheads indicate co-labeling). Quantification by cell counting in 3 high power fields-hpf 400x of n=4 mice in UUO and CLK, n=4 AAC and n=3 sham-AAC mice) *p<0.05 by t-test Scale bars 25μm
(C) Immunostained fibrotic heart (ascending aortic constriction-AAC) and kidneys (unilateral ureteral obstruction-UUO) for the pericyte and/or mesenchymal stem cell markers CD73, CD146, 3G5, PDGFRα, PDGFRβ and Nestin. Scale bars 25μm
(D) Left ventricular scar 4 weeks after coronary artery ligation in a bigenic Gli1CreER^{t2},tdTomato mouse, costaining with the pericyte markers CD146 or NG2. Scale bars left panel 500μm all others 25μm
(E) Matrigel plugs with Gli1^{+} cells, 4 weeks after implantation in the *in vivo* angiogenesis model. Co-staining for the endothelial cell marker CD31 indicates sprouting endothelial cells with Gli1^{+} cells associated in a pericyte-like distribution around CD31^{+} endothelial cells. NG2 and CD146 co-staining indicates that Gli1^{+} cells acquire expression of these mature pericyte markers during angiogenesis. Scale bars 50μm

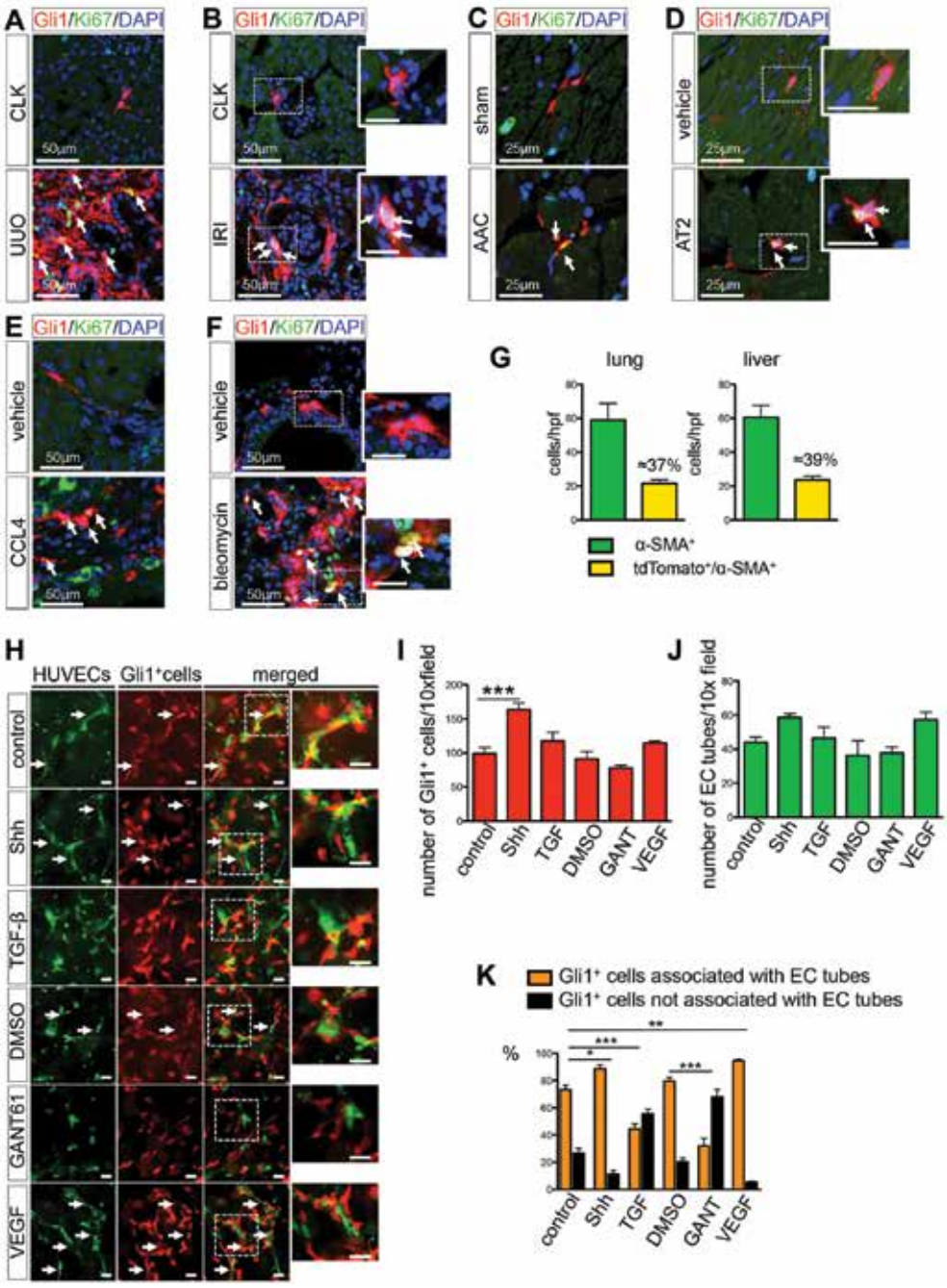
A
Gli1/Ki67/DAPI
CLK
UUO
50μm
B
Gli1/Ki67/DAPI
CLK
IRI
50μm
C
Gli1/Ki67/DAPI
sham
AAC
25μm
D
Gli1/Ki67/DAPI
vehicle
AT2
25μm
E
Gli1/Ki67/DAPI
vehicle
CCL4
50μm
F
Gli1/Ki67/DAPI
vehicle
bleomycin
50μm
G
lung
liver
cells/hpf
≈37%
≈39%
α-SMA+
tdTomato+/α-SMA+
H
HUVECs
Gli1+cells
merged
control
Shh
TGF-β
DMSO
GANT61
VEGF
I
number of Gli1+ cells/10xfield
***
control
Shh
TGF
DMSO
GANT
VEGF
J
number of EC tubes/10x field
control
Shh
TGF
DMSO
GANT
VEGF
K
Gli1+ cells associated with EC tubes
Gli1+ cells not associated with EC tubes
%
**
***
*
***
control
Shh
TGF
DMSO
GANT
VEGF

Figure S6: Related to figures 4-5. Proliferation, myofibroblast differentiation and tube formation of Gli1+ cells
(A-B) Representative images of proliferating (Ki67+, arrows) Gli1-tdTomato+ cells following injury of the kidney (UUO unilateral ureteral obstruction, IRI unilateral ischemia reperfusion injury, CLK non-injured contralateral kidney). Scale bars: as indicated, inserts 20µm. **(C-D)** Representative images of proliferating (Ki67+, arrows) Gli1-tdTomato+ cells following injury of heart (AAC, ascending aortic constriction; AT2 angiotensin minipump; vehicle, normal saline minipump). Scale bars: as indicated, inserts 20µm. **(E-F)** Representative images of proliferating (Ki67+, arrows) Gli1-tdTomato+ cells following injury of the liver and lung (CCL4, carbon tetrachloride; vehicle-liver: corn oil; vehicle lung: normal saline). Scale bars: as indicated, inserts 20µm. **(G)** Quantification of all interstitial α-SMA+ cells and the number of α-SMA+ cells that co-label with tdTomato in lung and liver fibrosis. Quantification was performed by cell-counting in 5-high power fields (hpf 400x) from n=4 mice that received bleomycin intratracheally vs. n=3 that received vehicle intratracheally and n=5 mice that received carbon tetrachloride for liver injury intraperitoneally versus n=3 that received vehicle. **(H-K)** Tube formation assay of human umbilical cord endothelial cells (HUVECs) labeled with a green cell tracer with Gli1+ cells (red tdTomato protein) isolated from bone chips in 3 dimensional collagen gels *in vitro*. Representative pictures and quantification of Gli1+ cell number (I), number of endothelial (EC) tubes, and Gli1+ cells associated with EC tubes (K) after treatment with phosphate bufferes saline (PBS, control), sonic hedgehog, transforming growth factor β (TGF- β), GANT61 (vehicle DMSO), and vascular endothelial growth factor A (VEGF). Scale bars 100µm *p<0.05, **p<0.01, ***p<0.001 by one way ANOVA.

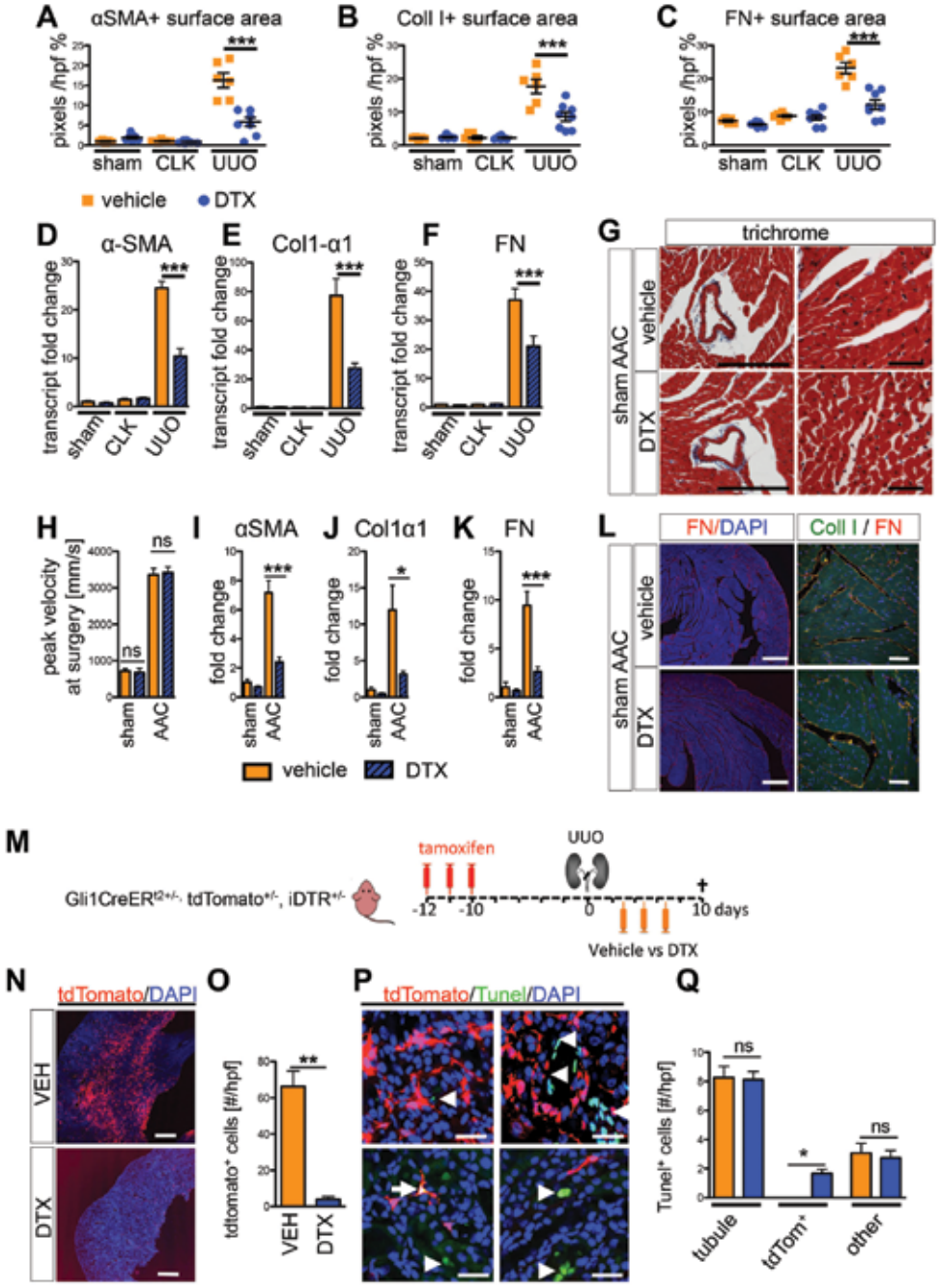
A
αSMA+ surface area
pixels /hpf %
***
sham
CLK
UUO
B
Coll I+ surface area
C
FN+ surface area
vehicle
DTX
D
α-SMA
transcript fold change
E
Col1-α1
F
FN
G
trichrome
sham AAC
vehicle
DTX
H
peak velocity at surgery [mm/s]
ns
AAC
I
αSMA
fold change
J
Col1α1
*
K
FN
L
FN/DAPI
Coll I / FN
M
Gli1CreER^t2+/-, tdTomato+/-, iDTR+/-
tamoxifen
UUO
-12
-10
0
10 days
Vehicle vs DTX
N
tdTomato/DAPI
VEH
DTX
O
tdtomato+ cells [#/hpf]
**
P
tdTomato/Tunel/DAPI
Q
Tunel+ cells [#/hpf]
tubule
tdTom+
other

Figure S7: Related to figure 7. Genetic ablation of Gli1+ cells in kidney and heart fibrosis.
(A-C) Ablation of Gli1+ cells in kidney fibrosis of bigenic Gli1CreER^{t2},iDTR mice (see Figure 7 B-E). Quantification of the immunostained (A) α-SMA+ surface area (B) collagen-I+ surface area and (C) fibronectin+ surface area (FN+) in sham, contralateral (CLK) and unilateral ureteral obstruction (UUO) kidneys after injection of vehicle or diphtheria-toxin (DTX). high power field (hpf); mean±SEM; ***p<0.001 one way ANOVA with posthoc Tukey.
(B-F) Quantitative realtime PCR for mRNA expression of (D) α-SMA, (E) collagen-IαI and (F) fibronectin (FN) from whole kidney lysates of sham, CLK and UUO kidneys after injection of vehicle or diphtheria-toxin (DTX). mean±SEM; ***p<0.001 one way ANOVA with posthoc Tukey
(G-L) Ablation of Gli1+ cells following ascending aortic constriction (AAC) surgery of bigenic Gli1CreER^{t2},iDTR mice (see Figure 7 G-R). (G) Representative trichrome pictures of the sham group after injection with diphtheria toxin (DTX) or vehicle. (H) Echocardiographically determined peak velocity at the suture site immediately after ascending aortic constriction (AAC) or sham surgery (AAC-vehicle n=10, AAC-DTX n=9, sham-vehicle n=5, sham-DTX n=5). (I-K) Quantitative realtime PCR for mRNA expression of (I) α-SMA, (J) collagenIαI and (K) fibronectin (FN) from whole kidney lysate of sham, CLK and UUO kidneys after injection of vehicle or diphtheria-toxin (DTX). (L) Representative pictures of heart sections from sham mice that received either vehicle or DTX stained for fibronectin (FN) and collagen I (Coll I). *p<0.05, ***p<0.001 one way ANOVA with posthoc Tukey.
(N-Q) To verify a significant cell ablation and exclude side effects on other non-Gli1+ cell populations, we generated triple transgenic mice that express bot the human diphtheria toxin receptor (iDTR) and tdTomato in Gli1+ cells. Mice received tamoxifen and were subjected to UUO surgery and sacrificed 10 days later. Representative pictures of UUO kidneys and quantification of tdTomato+ cells indicate a significant ablation of Gli1+ cells by DTX with only a small number of tdTomato+ cells remaining (N-O). Tunel staining was performed to quantify the number of apoptotic cells. Representative pictures of Tunel stained UUO kidneys (P) and quantification of tubular cells (tubule), Gli1-tdTomato+ cells and other renal cells indicate increased apoptosis in the Gli1+ cell population while we did not detect an effect on apoptosis in other cell populations. mean±SEM; *p<0.05, **p<0.01 by t-test

Movie S1: Related to figure 1. Fluorescence microangiography demonstrates the perivascular localization of Gli1+ MSC in the renal cortex. (online at http://www.cell.com/cell-stem-cell)

Movie S2: Related to figure 1. Fluorescence microangiography demonstrates the perivascular localization of Gli1+ MSC in the myocard. (online at http://www.cell.com/cell-stem-cell)

REFERENCES

1. Danis, A., *[Study of ossification in bone marrow grafts].* Acta Chir Belg, 1957. **56**(Suppl 3): p. 1-120.
2. Caplan, A.I., *Mesenchymal stem cells.* J Orthop Res, 1991. **9**(5): p. 641-50.
3. Caplan, A.I. and D. Correa, *The MSC: an injury drugstore.* Cell Stem Cell, 2011. **9**(1): p. 11-5.
4. Murray, I.R., et al., *Natural history of mesenchymal stem cells, from vessel walls to culture vessels.* Cell Mol Life Sci, 2014. **71**(8): p. 1353-74.
5. Crisan, M., et al., *A perivascular origin for mesenchymal stem cells in multiple human organs.* Cell Stem Cell, 2008. **3**(3): p. 301-13.
6. Zhao, H., et al., *Secretion of shh by a neurovascular bundle niche supports mesenchymal stem cell homeostasis in the adult mouse incisor.* Cell Stem Cell, 2014. **14**(2): p. 160-73.
7. Kramann, R., M. Tanaka, and B.D. Humphreys, *Fluorescence microangiography for quantitative assessment of peritubular capillary changes after AKI in mice.* J Am Soc Nephrol, 2014. **25**(9): p. 1924-31.
8. Boxall, S.A. and E. Jones, *Markers for characterization of bone marrow multipotential stromal cells.* Stem Cells Int, 2012. **2012**: p. 975871.
9. Pelekanos, R.A., et al., *Comprehensive transcriptome and immunophenotype analysis of renal and cardiac MSC-like populations supports strong congruence with bone marrow MSC despite maintenance of distinct identities.* Stem Cell Res, 2012. **8**(1): p. 58-73.
10. Morrison, S.J. and D.T. Scadden, *The bone marrow niche for haematopoietic stem cells.* Nature, 2014. **505**(7483): p. 327-34.
11. Park, D., et al., *Endogenous bone marrow MSCs are dynamic, fate-restricted participants in bone maintenance and regeneration.* Cell Stem Cell, 2012. **10**(3): p. 259-72.
12. Goritz, C., et al., *A pericyte origin of spinal cord scar tissue.* Science, 2011. **333**(6039): p. 238-42.
13. Henderson, N.C., et al., *Targeting of alphav integrin identifies a core molecular pathway that regulates fibrosis in several organs.* Nat Med, 2013. **19**(12): p. 1617-24.
14. Weber, K.T., et al., *Myocardial fibrosis in hypertensive heart disease: an overview of potential regulatory mechanisms.* Eur Heart J, 1995. **16 Suppl C**: p. 24-8.
15. Stark, K., et al., *Capillary and arteriolar pericytes attract innate leukocytes exiting through venules and 'instruct' them with pattern-recognition and motility programs.* Nat Immunol, 2013. **14**(1): p. 41-51.
16. Song, S., et al., *PDGFRbeta+ perivascular progenitor cells in tumours regulate pericyte differentiation and vascular survival.* Nat Cell Biol, 2005. **7**(9): p. 870-9.
17. Fukushi, J., I.T. Makagiansar, and W.B. Stallcup, *NG2 proteoglycan promotes endothelial cell motility and angiogenesis via engagement of galectin-3 and alpha3beta1 integrin.* Mol Biol Cell, 2004. **15**(8): p. 3580-90.
18. Stallcup, W.B., *The NG2 proteoglycan: past insights and future prospects.* J Neurocytol, 2002. **31**(6-7): p. 423-35.
19. Murfee, W.L., et al., *Perivascular cells along venules upregulate NG2 expression during microvascular remodeling.* Microcirculation, 2006. **13**(3): p. 261-73.
20. Goretzki, L., et al., *High-affinity binding of basic fibroblast growth factor and platelet-derived growth factor-AA to the core protein of the NG2 proteoglycan.* J Biol Chem, 1999. **274**(24): p. 16831-7.
21. Shikada, Y., et al., *Platelet-derived growth factor-AA is an essential and autocrine regulator of vascular endothelial growth factor expression in non-small cell lung carcinomas.* Cancer Res, 2005. **65**(16): p. 7241-8.
22. Schrimpf, C., et al., *The Role of Pericyte Detachment in Vascular Rarefaction.* J Vasc Res, 2014. **51**(4): p. 247-258.
23. LeBleu, V.S., et al., *Origin and function of myofibroblasts in kidney fibrosis.* Nat Med, 2013. **19**(8): p. 1047-53.

24. Cilloni, D., et al., *Limited engraftment capacity of bone marrow-derived mesenchymal cells following T-cell-depleted hematopoietic stem cell transplantation.* Blood, 2000. **96**(10): p. 3637-43.
25. Schrepfer, S., et al., *Stem cell transplantation: the lung barrier.* Transplant Proc, 2007. **39**(2): p. 573-6.
26. Atkins, R., *On Arterio-Capillary Fibrosis.* Br Med J, 1875. **1**(744): p. 444-6.
27. Humphreys, B.D., et al., *Fate tracing reveals the pericyte and not epithelial origin of myofibroblasts in kidney fibrosis.* Am J Pathol, 2010. **176**(1): p. 85-97.
28. Hung, C., et al., *Role of lung pericytes and resident fibroblasts in the pathogenesis of pulmonary fibrosis.* Am J Respir Crit Care Med, 2013. **188**(7): p. 820-30.
29. Dulauroy, S., et al., *Lineage tracing and genetic ablation of ADAM12(+) perivascular cells identify a major source of profibrotic cells during acute tissue injury.* Nat Med, 2012. **18**(8): p. 1262-70.
30. Asada, N., et al., *Dysfunction of fibroblasts of extrarenal origin underlies renal fibrosis and renal anemia in mice.* J Clin Invest, 2011. **121**(10): p. 3981-90.
31. Maccallum, J.B., *A Contribution to the Knowledge of the Pathology of Fragmentation and Segmentation, and Fibrosis of the Myocardium.* J Exp Med, 1899. **4**(3-4): p. 409-24.
32. Weber, K.T., et al., *Myofibroblast-mediated mechanisms of pathological remodelling of the heart.* Nat Rev Cardiol, 2013. **10**(1): p. 15-26.
33. Zeisberg, E.M., et al., *Endothelial-to-mesenchymal transition contributes to cardiac fibrosis.* Nat Med, 2007. **13**(8): p. 952-61.
34. Moore-Morris, T., et al., *Resident fibroblast lineages mediate pressure overload-induced cardiac fibrosis.* J Clin Invest, 2014. **124**(7): p. 2921-34.
35. Kakkar, R. and R.T. Lee, *Intramyocardial fibroblast myocyte communication.* Circ Res, 2010. **106**(1): p. 47-57.
36. Carlson, S., et al., *Cardiac mesenchymal stem cells contribute to scar formation after myocardial infarction.* Cardiovasc Res, 2011. **91**(1): p. 99-107.
37. Schepers, K., et al., *Myeloproliferative neoplasia remodels the endosteal bone marrow niche into a self-reinforcing leukemic niche.* Cell Stem Cell, 2013. **13**(3): p. 285-99.
38. Kramann, R., D.P. DiRocco, and B.D. Humphreys, *Understanding the origin, activation and regulation of matrix-producing myofibroblasts for treatment of fibrotic disease.* J Pathol, 2013. **231**(3): p. 273-89.
39. Le, Y.Z., et al., *Mouse opsin promoter-directed Cre recombinase expression in transgenic mice.* Mol Vis, 2006. **12**: p. 389-98.
40. Duffield, J.S., *Cellular and molecular mechanisms in kidney fibrosis.* J Clin Invest, 2014. **124**(6): p. 2299-306.
41. Fabian, S.L., et al., *Hedgehog-Gli pathway activation during kidney fibrosis.* Am J Pathol, 2012. **180**(4): p. 1441-53.
42. Michelotti, G.A., et al., *Smoothened is a master regulator of adult liver repair.* J Clin Invest, 2013. **123**(6): p. 2380-94.
43. Kusano, K.F., et al., *Sonic hedgehog myocardial gene therapy: tissue repair through transient reconstitution of embryonic signaling.* Nat Med, 2005. **11**(11): p. 1197-204.
44. Pola, R., et al., *The morphogen Sonic hedgehog is an indirect angiogenic agent upregulating two families of angiogenic growth factors.* Nat Med, 2001. **7**(6): p. 706-11.
45. Pola, R., et al., *Postnatal recapitulation of embryonic hedgehog pathway in response to skeletal muscle ischemia.* Circulation, 2003. **108**(4): p. 479-85.
46. Goel, H.L. and A.M. Mercurio, *VEGF targets the tumour cell.* Nat Rev Cancer, 2013. **13**(12): p. 871-82.
47. Brownell, I., et al., *Nerve-derived sonic hedgehog defines a niche for hair follicle stem cells capable of becoming epidermal stem cells.* Cell Stem Cell, 2011. **8**(5): p. 552-65.

48. Merchant, A., et al., *Gli1 regulates the proliferation and differentiation of HSCs and myeloid progenitors.* Blood, 2010. **115**(12): p. 2391-6.

49. Takanaga, H., et al., *Gli2 is a novel regulator of sox2 expression in telencephalic neuroepithelial cells.* Stem Cells, 2009. **27**(1): p. 165-74.

50. Liao, R., et al., *Cardiac-specific overexpression of GLUT1 prevents the development of heart failure attributable to pressure overload in mice.* Circulation, 2002. **106**(16): p. 2125-31.

51. Malinda, K.M., *In vivo matrigel migration and angiogenesis assay.* Methods Mol Biol, 2009. **467**: p. 287-94.

52. Zhu, H., et al., *A protocol for isolation and culture of mesenchymal stem cells from mouse compact bone.* Nat Protoc, 2010. **5**(3): p. 550-60.

53. Bunster, E. and R.K. Meyer, *An improved method of parabiosis.* Anat. Rec. , 1933. **57**: p. 339-343.

54. Ruckh, J.M., et al., *Rejuvenation of regeneration in the aging central nervous system.* Cell Stem Cell, 2012. **10**(1): p. 96-103.

55. Koh, W., et al., *In vitro three dimensional collagen matrix models of endothelial lumen formation during vasculogenesis and angiogenesis.* Methods Enzymol, 2008. **443**: p. 83-101.

56. Simoes, A.E., et al., *Efficient recovery of proteins from multiple source samples after TRIzol((R)) or TRIzol((R)) LS RNA extraction and long-term storage.* BMC Genomics, 2013. **14**: p. 181.

57. Zhang, Y., et al., *Validation of the wall motion score and myocardial performance indexes as novel techniques to assess cardiac function in mice after myocardial infarction.* Am J Physiol Heart Circ Physiol, 2007. **292**(2): p. H1187-92.

3

GLI1^{+} MESENCHYMAL STROMAL CELLS ARE A KEY DRIVER OF BONE MARROW FIBROSIS AND AN IMPORTANT CELLULAR THERAPEUTIC TARGET

Rebekka K. Schneider,[1, 2*#], Ann Mullally,[3] Aurelien Dugourd,[4] Fabian Peisker,[5] Remco Hoogenboezem,[1] Paulina M. H. Van Strien,[1] Eric M. Bindels,[1] Dirk Heckl,[6] Guntram Büsche,[7] David Fleck,[8] Gerhard Müller-Newen,[8] Janewit Wongboonsin,[10] Monica Ventura Ferreira,[2] Victor G. Puelles,[5] Julio Saez-Rodriguez,[4] Benjamin L. Ebert[3], Benjamin D. Humphreys[11] and Rafael Kramann[5*]

[1]Department of Hematology, Erasmus MC Cancer Institute, Rotterdam, The Netherlands;
[2]Department of Hematology, Oncology, Hemostaseology, and Stem Cell Transplantation, RWTH Aachen University, Aachen, Germany;
[3]Division of Hematology, Brigham and Women's Hospital, Department of Medicine, Harvard Medical School, Boston, Massachusetts, USA;
[4]RWTH Aachen University, Faculty of Medicine, Joint Research Centre for Computational Biomedicine;
[5]Division of Nephrology and Clinical Immunology, RWTH Aachen University, Aachen, Germany;
[6]Division of Pediatric Hematology and Oncology, Hannover Medical School, Germany;
[7]Institute of Pathology, Hannover Medical School, Hannover, Germany;
[8]Institute of Biology II, Department of Chemosensation, RWTH Aachen, Germany;
[9]Institute of Biochemistry and Molecular Biology, RWTH Aachen University, Aachen Germany;
[10]Department of Medicine, University of Minnesota, Minneapolis, MN and Department of Internal Medicine, Faculty of Medicine Siriraj Hospital, Mahidol University, Bangkok, Thailand;
[11]Division of Nephrology, Department of Medicine, Washington University School of Medicine, USA
lead author

Running title: Gli1 MSC drive bone marrow fibrosis

Corresponding author:

*Rebekka K. Schneider, MD
Department of Hematology
Erasmus Medical Center Cancer Institute
Phone: +31-10-704 3769
Email: r.k.schneider@erasmusmc.nl

or

*Rafael Kramann, MD
Division of Nephrology and Clinical Immunology,
Medical Faculty RWTH Aachen University,
Pauwelsstrasse 30, 52074 Aachen, Germany
Phone.: 0049-241-80 37750
Fax.: +49-241-80-82446
E-mail: rkramann@gmx.net

Cell Stem Cell 2017 20(6):785-800

SUMMARY

Bone marrow fibrosis (BMF) develops in various hematological and non-hematological conditions and is a central pathological feature of myelofibrosis. Effective cell-targeted therapeutics are needed, but the cellular origin of BMF remains elusive. Here, we show using genetic fate tracing in two murine models of BMF that Gli1$^+$ mesenchymal stromal cells (MSCs) are recruited from the endosteal and perivascular niche to become fibrosis-driving myofibroblasts in the bone marrow. Genetic ablation of Gli1$^+$ cells abolished BMF and rescued bone marrow failure. Pharmacological targeting of Gli proteins with GANT61 inhibited Gli1$^+$ cell expansion and myofibroblast differentiation, and attenuated fibrosis severity. The same pathway is also active in human BMF and Gli1 expression in BMF significantly correlates with the severity of the disease. In addition, GANT61 treatment reduced the myofibroblastic phenotype of human MSCs isolated from patients with BMF, suggesting that targeting of Gli proteins could be a relevant therapeutic strategy.

INTRODUCTION

Bone marrow fibrosis is characterized by the increased deposition of reticulin fibers or collagen fibers. A number of hematologic and non-hematologic disorders are associated with increased bone marrow fibrosis [3-8] which is a central pathological feature and WHO major diagnostic criterion of myelofibrosis (MF). Myelofibrosis (MF) refers to BCR-ABL1-negative myeloproliferative neoplasms (MPN). Polycythemia vera (PV), essential thrombocythemia (ET), and primary myelofibrosis (PMF) constitute the BCR-ABL1-negative MPN, which are clonal disorders of hematopoiesis arising in the hematopoietic stem cell (HSC) compartment . The majority of patients with MF carry mutations that activate JAK–STAT signaling; 60% of patients with MF harbor the JAK2V617F mutation, approximately 30% carry a calreticulin mutation (CALR), and 8% carry a myelo-proliferative leukemia virus oncogene (MPL) mutation . PMF is the least common of the three classic MPNs; however, it is the most aggressive and is associated with a significantly shortened survival [11, 12]. PMF is characterized by malignant clonal hematopoiesis, bone marrow fibrosis, extramedullary hematopoiesis, splenomegaly and abnormal cytokine expression leading to significant systemic symptoms, risk of transformation to acute leukemia, and reduced survival.

Although the somatic mutations that drive the development of MPN have been largely defined, the cellular targets of bone marrow fibrosis still remain obscure and are poorly understood compared with solid organ fibrosis. The HSC niche has recently emerged as an oncogenic unit that promotes malignant hematopoiesis at the expense of normal hematopoiesis [13]. In MPN, mesenchymal stromal cells (MSCs), key components of the HSC niche, have recently been shown to acquire a secretory, extracellular matrix remodelling phenotype and lose their hematopoiesis-supporting capacity [15]. A recent study using a knockin Jak2V617F MPN mouse model demonstrated that MPN progression in the bone marrow creates neuropathic changes in the BM niche, which affect the activity of perivascular MSCs and alter the function of the HSC niche [16, 17]. Identifying the cells that drive the development of a fibrotic bone marrow niche with its detrimental consequences for the maintenance of HSCs is a prerequisite for the development of novel targeted therapeutics.

Multiple genetic fate tracing studies have been performed to elucidate the cellular origin of fibrosis driving myofibroblasts in solid organs . The recent identification of perivascular $Gli1^+$ MSC-like cells as a major cellular origin of organ fibrosis and as a relevant therapeutic target to prevent solid organ dysfunction after injury provides significant potential to identify the origin of fibrosis-driving cells in bone marrow fibrosis [15, 18, 19]. $Gli1^+$ cells are (1) intimately associated with the microvasculature and in direct contact with $CD31^+$ endothelial cells or (2) localized in the adventitia of arteries distant from endothelial cells, highlighting their perivascular origin. $Gli1^+$ cells were defined as MSCs by accepted criteria for their identification and they consistently express the mesenchymal marker PDGFR-β. Given that the Hedgehog (Hh) signaling pathway regulates mesenchyme cell fate during

development and in view of growing evidence implicating a critical role for Hh in solid organ fibrosis and cancer , these findings provide a rationale for potential targeting of the Hedgehog (Hh) pathway in bone marrow fibrosis.

Currently, the clonal myeloid neoplasm is the primary therapeutic target in MPN. The discovery of the JAK2V617F mutation has led to rapid development of therapies with positive impact on patients with myelofibrosis [17]. Currently, the only potentially curative therapy for patients with PMF is allogeneic hematopoietic stem cell transplantation, a high risk procedure with significant associated morbidity and mortality. Establishing new modalities to directly block the cellular changes occuring in the malignant BM niche, including the inhibition of aberrant MSC differentiation into fibrosis-driving cells could have a substantial therapeutic impact in the treatment of bone marrow fibrosis.

RESULTS

Perivascular and endosteal localization of Gli1⁺ cells in the bone marrow niche

Having identified Gli1 as a faithful marker for fibrosis-driving MSCs in solid organs , we sought to characterize Gli1⁺ cells in the bone marrow niche more thoroughly. To comprehensively study Gli1⁺ cells in the bone barrow, Gli1CreER^{t2} driver mice were crossed to a tdTomato reporter for inducible genetic labeling. Gli1⁺ cells in the bone marrow either align against bone (Figure 1A) or are associated with the vasculature (Figure 1B-C). Quantification of Gli1⁺ cell distribution in bigenic Gli1CreER;tdTomato mice indicated that the majority of Gli1⁺ cells reside in the endosteal niche whereas a smaller fraction is associated with bone marrow sinusoids and arterioles (Fig 1D). Clearing of a sternal bone with deep imaging of the bone marrow further illustrated the endosteal or perivascular localization of Gli1⁺ cells (Figure S1A-B). We next assessed the expression of markers that have been reported for stromal and perivascular cells by immunostaining and confocal microscopy. We observed high CD105 and moderate NG2 expression in perisinusoidal and periarteriolar Gli1⁺ cells while expression of both markers was almost absent in endosteal Gli1⁺ cells (Figure 1E-G). Nestin expression was detected in many endosteal and perivascular Gli1⁺ cells; however, we also observed Gli1⁺ cells in both niches that did not co-express Nestin (Figure 1H). Of note, we did not detect leptin receptor expression in Gli1⁺ cells (Figure S1C). While we detected sympathic innervation of periarteriolar and to a lesser extent perisinusoidal Gli1⁺ cells, endosteal Gli1⁺ cells did not show adjacent sympathic nerves (Figure 1I). Similarly, many perivascular but not endosteal Gli1⁺ cells were adjacent to Schwann cells (Figure 1J). We further studied the surface profile of Gli1⁺ cells isolated from bone chips of bigenic Gli1CreER;tdTomato mice by flow cytometry. We observed high expression of pericyte markers such as CD73, mesenchymal markers such as platelet derived growth factor receptor alpha PDGFRα (CD140a), the mesenchymal stem cell markers CD105, CD44, CD29, Sca1 and CD51 while we did not observe expression of the endothelial cell lineage marker CD31 (Figures 1K, S1D). To study Gli1 expression in human bone marrow, we validated Gli1 staining in human glioblastoma multiforme tissue that had been EDTA treated (Figure S1E). Immunostaining of human bone marrow indicates Gli1 expression in spindle shaped stromal cells (1) aligning the bone (endosteal niche) or (2) associated with the vasculature (Figure 1L). Image quantification of human bone marrow demonstrated that 68.1±2.7% of Gli1⁺ cells are in an endosteal and 31.9±2.7% in perivascular localization, comparable to the findings in murine bone marrows. Co-staining for Nestin and Gli1 indicated co-expression in some but not all Gli1 expressing cells (Figure S1F), whereas no leptin receptor expression or NG2 expression in Gli1 expressing cells of human bone marrow was observed (Figure S1F). When isolated from human bone marrow, Gli1⁺ cells express CD90, CD105 and Nestin, consistent with their pericyte/MSC origin (Figure 1M, S1G).

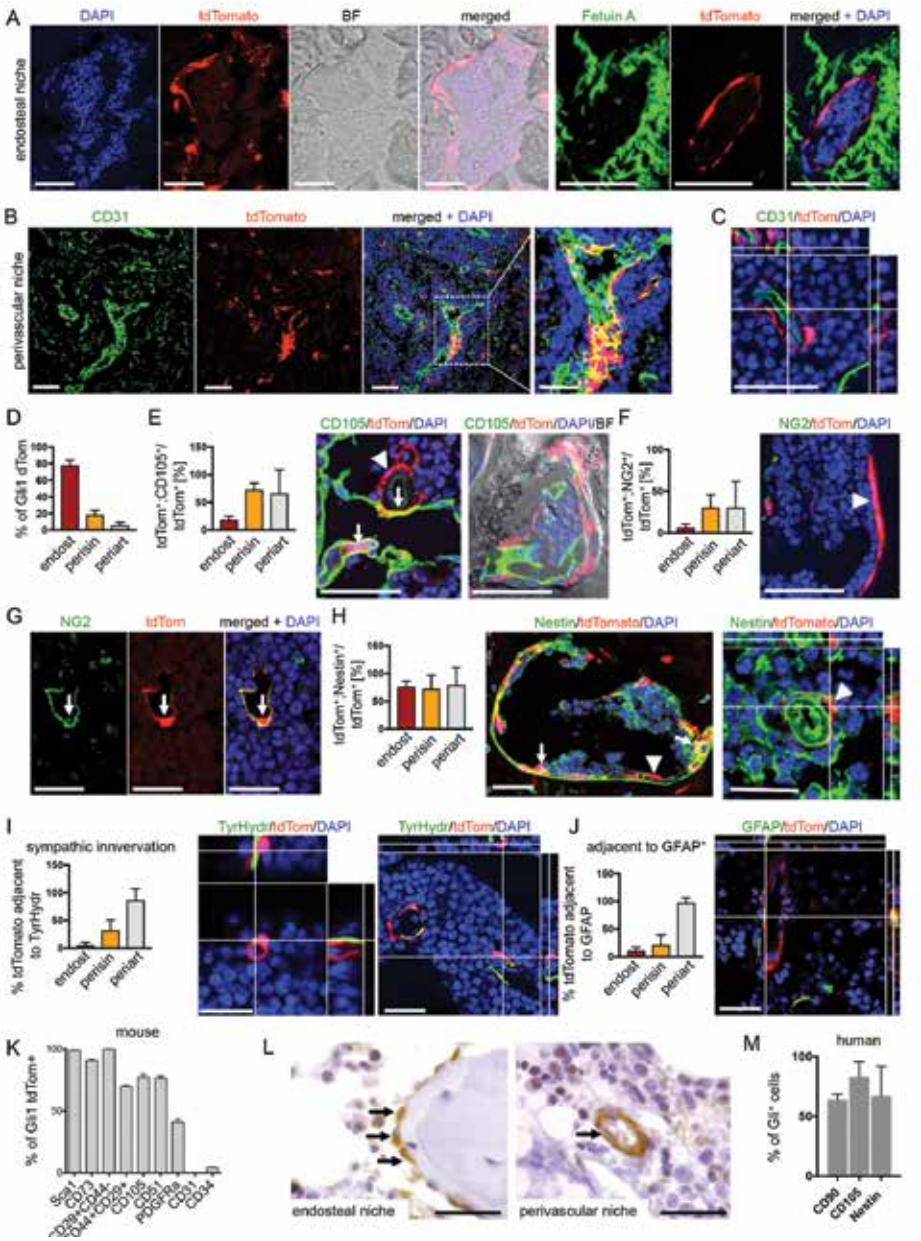

Figure 1: Gli1⁺ cells reside in the perivascular and endosteal bone marrow niche in human and mice

(A) Representative images of bone marrows from bigenic Gli1CreER^{t2};tdTomato mice 10 days after tamoxifen application (3x10mg p.o.). Brightfield (BF) and Fetuin A stained images show Gli1⁺ cells lining the bone in the endosteal niche. Scale bars 50µm **(B-C)** Representative images and Z-Stack analyses of the perivascular bone marrow niche indicate close association of Gli1⁺ cells with CD31⁺ endothelial cells. Of note, the Z-Stack analysis shows no-colocalization of CD31 and tdTomato. Scale bars 50µm. **(D)** Distribution of Gli1⁺ cells in the endosteal (endost), perisinusoidal (perisin) and periarteriolar (periart) niche; mean±SEM. **(E-H)** CD105, NG2 and Nestin expression by Gli1⁺ cells in the endosteal, perisinusoidal and periarteriolar niche; mean±SEM; arrows indicate co-epression in Gli1⁺ cells; arrowheads indicate no-expression in Gli1⁺ cells; scale bars 50µm in E-F, 25µm in G-H; mean±SEM. **(I)** Representative Z-Stack images and quantification of Gli1⁺ cell innervation by tyrosine hydroxylase (TyrHydr)-

positive sympathic nerve fibres. Scale bars 25µm; mean±SEM. **(J)** Representative Z-Stack image and quantification of Gli1$^+$ cells adjacent to glial fibrillary acidic protein (GFAP)-expressing glia cells. Scale bars 25µm. **(K)** Surface expression pattern of tdTomato$^+$ cells from bigenic Gli1CreER^{t2}; tdTomato mice as assessed by flow cytometry; mean±SEM. (**L**) Representative images of human bone marrows stained for Gli1. Arrows indicate Gli1 expressing cells. Scale bars: 50µm**. (M)** Surface expression profile of human Gli1$^+$ MSCs; mean±SEM. See also Figure S1.

Gli1$^+$ cells are myofibroblast precusors in myelofibrosis

To determine if Gli1$^+$ cells have a fibrosis-inducing role in bone marrow fibrosis, we performed genetic fate tracing experiments in a murine model of thrombopoeitin (ThPO)-induced myelofibrosis. Overexpression of ThPO, a c-mpl ligand and physiological regulator of platelet production, results in a myeloproliferative phenotype characterized by thrombocytosis, leukocytosis, dysplastic megakaryocytes, extramedullary hematopoiesis and high grade myelofibrosis with osteosclerosis with short latency [24]. To trace the fate of Gli1$^+$ cells, bigenic Gli1CreER$^{t2+/-}$;tdTomato$^{+/-}$ recipient mice received tamoxifen to induce cell-specific expression of the tdTomato fluorochrome and were subjected to lethal irradiation followed by transplantation of ThPO overexpressing or control bone marrow (Figure 2A, B). We transduced hematopoietic stem and progenitor cells from Gli1CreER$^{t2-/-}$;tdTomato$^{-/-}$ (wildtype-WT littermates) with ThPO overexpressing cDNA (pRRL.PPT.SFFV.Thpo.iGFP) or control (pRRL.PPT.SFFV.MCS.iGFP). The irradiation was performed at least 10 days after the last tamoxifen dose to eliminate any possibility of Cre recombination after injury.

ThPO overexpression induced significant myeloproliferative features including thrombocytosis and leukocytosis (Figure S2A). Hemoglobin (Hb) decreased over time in ThPO overexpressing mice and the percentage of ThPO-GFP$^+$ overexpressing cells in these mice (gene marking) also significantly decreased suggesting the replacement of hematopoietic cells in the bone marrow by fibrosis (Figure S2A-B). The decrease of marrow hematopoiesis was accompanied by extramedullary hematopoeisis in the spleen with significant increase in spleen weight (Figure S2C) and presence of lineage^{low}Sca1$^+$ckit$^+$ hematopoietic stem and progenitor cells in the spleen (Figure S2D). Trichrome staining indicated marked remodeling of the spleen, however without development of collagen fibrosis (Figure S2E).

The bone marrow of ThPO overexpressing mice showed abundant reticulin and trichrome$^+$ fibrosis (Figures 2C, S2F-G). Flow cytometric analysis of the genetically marked tdTomato$^+$ population and GFP$^+$ hematopoeisis demonstrated a significant increase in the frequence of Gli1$^+$ stromal cells in the bone marrow cavity in ThPO-induced myelofibrosis (Figure 2D). Interestingly, while Gli1$^+$ cells express markers of both MSCs and OBCs, primarily MSC marker expressing Gli1$^+$ cells expanded in fibrosis (Figure 2E).

Confocal imaging further demonstrated that Gli1$^+$ cells are activated by the malignant hematopoietic clone, undergo tremendous expansion, and acquire expression of alpha smooth muscle actin (α-SMA) indicating myofibroblast differentiation (Figure 2F-H, S2H). Of note, quantification indicated that approximatively half of all myofibroblasts were derived from the Gli1 lineage (Figure 2H). Quantification of Gli1$^+$ cell distance to bone and endothelial cells by image analysis indicated that Gli1$^+$ cells are mobilized from their endosteal and perivascular niche (Figure 2I).

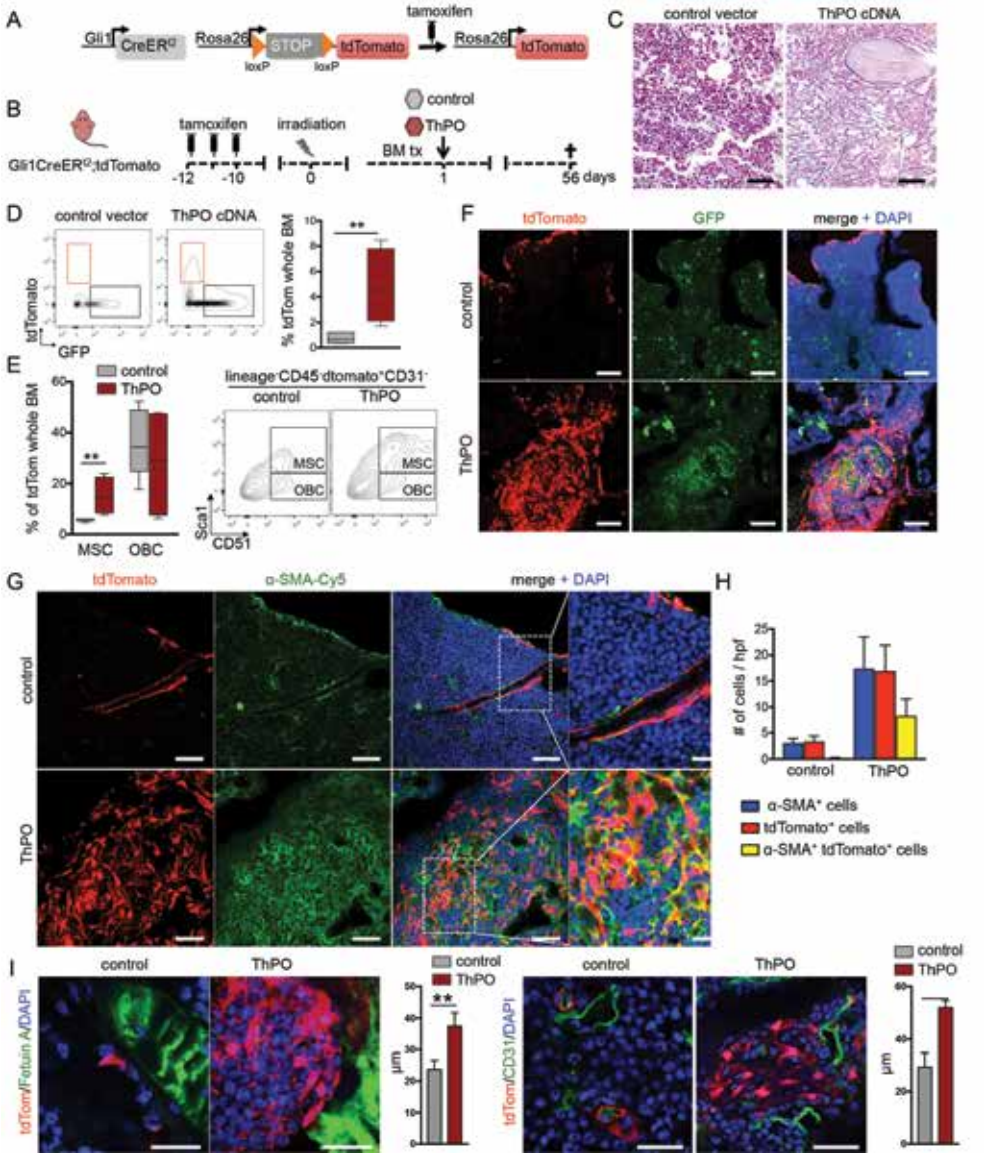

Figure 2: Gli1$^+$ cells expand and become myofibroblasts in thrombopoietin (ThPO) induced bone marrow fibrosis
(A-B) Bigenic Gli1CreER;tdTomato mice were injected with tamoxifen (3x10mg p.o.) at 8 weeks of age, lethally irradiated at 10 days after the last tamoxifen dose and received c-kit enriched hematopoietic stem cells from wildtype littermates expressing either Thrombopoietin-cDNA (ThPO, n=5, 3 males) or control cDNA (control, n=5, 3 males; both lentiviral SFFV-iGFP vector backbone). Mice were sacrificed at 56 days after transplantation. **(C)** Representative images of reticulin stained bone marrows from control and ThPO group 56 days after transplantation. Scale bars 200μm. **(D)** Representative flow cytometric plots and quantification of tdTomato$^+$ cells in the bone marrow of control and ThPO group 56 days after transplantation. **p<0.01 by t-test. (box plot and whiskers, min to max). **(E)** Representative flow cytometric plots and quantification of the contribution of tdTomato$^+$ cells to MSCs, and OBCs contained in the endosteal (Lin-/CD45-) BM stromal fraction in the control and ThPO group 56 days after transplantation. MSCs are tdTom$^+$lin$^-$CD45$^-$CD31$^-$Sca1$^+$CD51$^+$; OBCs are tdTom$^+$lin$^-$CD45$^-$ CD31$^-$Sca1$^-$CD51$^+$; **p<0.01

by t-test. (box plot and whiskers, min to max). **(F)** Representative confocal images of bone marrows from control and ThPO group indicating tremendous expansion of Gli1$^+$ cells following ThPO overexpression. Scale bars 50µm. **(G-H)** Representative images and quantification of bone marrows from the control and ThPO group stained for alpha smooth muscle actin (α-SMA). *p<0.05, ***p<0.001 versus the control group by t-test; scale bars 50µm, inserts 20µm. **(I)** Representative images of bone marrows from the control and ThPO group stained for Fetuin A (left panel) and CD31 (right panel). The distance of Gli1$^+$ cells to bone (Fetuin A$^+$) and vasculature (CD31$^+$) was quantified. **p<0.01 by t-test; mean±SEM; scale bars 25µm. See also Figure S2.

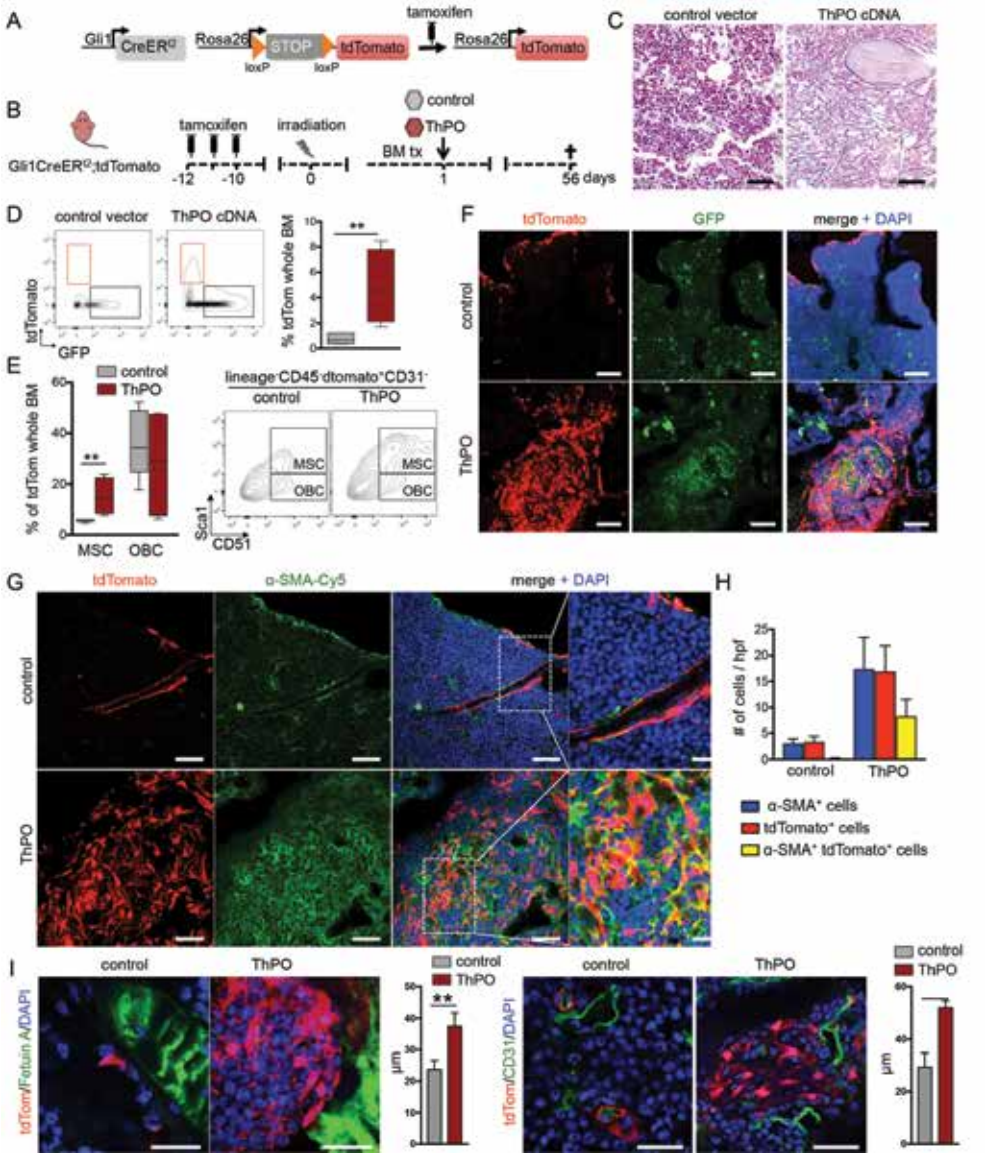

Figure 2: Gli1$^+$ cells expand and become myofibroblasts in thrombopoietin (ThPO) induced bone marrow fibrosis (A-B) Bigenic Gli1CreER;tdTomato mice were injected with tamoxifen (3x10mg p.o.) at 8 weeks of age, lethally irradiated at 10 days after the last tamoxifen dose and received c-kit enriched hematopoietic stem cells from wildtype littermates expressing either Thrombopoietin-cDNA (ThPO, n=5, 3 males) or control cDNA (control, n=5,

3 males; both lentiviral SFFV-iGFP vector backbone). Mice were sacrificed at 56 days after transplantation. **(C)** Representative images of reticulin stained bone marrows from control and ThPO group 56 days after transplantation. Scale bars 200µm. **(D)** Representative flow cytometric plots and quantification of tdTomato$^+$ cells in the bone marrow of control and ThPO group 56 days after transplantation. **p<0.01 by t-test. (box plot and whiskers, min to max). **(E)** Representative flow cytometric plots and quantification of the contribution of tdTomato$^+$ cells to MSCs, and OBCs contained in the endosteal (Lin-/CD45-) BM stromal fraction in the control and ThPO group 56 days after transplantation. MSCs are tdTom$^+$lin$^-$CD45$^-$CD31$^-$Sca1$^+$CD51$^+$; OBCs are tdTom$^+$lin$^-$CD45$^-$ CD31$^-$Sca1$^-$CD51$^+$; **p<0.01 by t-test. (box plot and whiskers, min to max). **(F)** Representative confocal images of bone marrows from control and ThPO group indicating tremendous expansion of Gli1$^+$ cells following ThPO overexpression. Scale bars 50µm. **(G-H)** Representative images and quantification of bone marrows from the control and ThPO group stained for alpha smooth muscle actin (α-SMA). *p<0.05, ***p<0.001 versus the control group by t-test; scale bars 50µm, inserts 20µm. **(I)** Representative images of bone marrows from the control and ThPO group stained for Fetuin A (left panel) and CD31 (right panel). The distance of Gli1$^+$ cells to bone (Fetuin A$^+$) and vasculature (CD31$^+$) was quantified. **p<0.01 by t-test; mean±SEM; scale bars 25µm. See also Figure S2.

Genetic ablation of Gli1$^+$ cells abolishes myelofibrosis and rescues bone marrow failure

Having shown by inducible genetic lineage tracing that Gli1$^+$ cells are myofibroblast progenitors during ThPO-induced myelofibrotic transformation, we next asked if Gli1$^+$ cells are required for the development of bone marrow fibrosis and whether genetic ablation of Gli1$^+$ cells affects fibrosis severity and bone marrow function. We therefore generated a mouse model with inducible Gli1$^+$ cell-specific expression of the human symian diphtheriatoxin receptor (iDTR) - Gli1CreER$^{t2+/-}$;iDTR$^{+/-}$ (Figure 3A). In this model, Gli1$^+$ cells express the iDTR after tamoxifen induced recombination and subsequent diphtheria toxin (DTX) injection will specifically ablate the Gli1$^+$ cell population but no other cells as normal mouse cells lack expression of a diphtheria toxin receptor. Bigenic Gli1CreER$^{t2+/-}$;iDTR$^{+/-}$ mice received tamoxifen and underwent bone marrow transplantation receiving ckit$^+$ HSPCs expressing either the empty vector or ThPO overexpressing cDNA from wildtype littermates. Mice were randomized on their Hb level at 4 weeks after bone marrow transplantation and received DTX (50ng/kgBW) in order to ablate the Gli1$^+$ cells (Figure 3B).

Mice that received ThPO overexpressing marrow in the presence of Gli1$^+$ cells (ThPO+vehicle) developed a severe bone marrow fibrosis, as indicated by significant decrease in the Hb counts over time and replacement of hematopoietic cells in bone marrow and spleen by reticulin fibrosis as well as significant splenomegaly, while the white blood cell and platelet counts were not affected (Figure 3C-F; Figure S3A). Ablation of Gli1$^+$ cells completely abolished this fibrotic phenotype (ThPO+DTX, Figure 3C-F) as determined by stabilization of the Hb counts, complete absence of reticulin fibrosis in bone marrow and spleen, normalized spleen weights and reduced osteosclerosis (Figure S3B-C). mRNA expression of iDTR further demonstrated significant expansion of Gli1$^+$ cells in ThPO-induced bone marrow fibrosis with sufficient ablation following DTX injection (Figure 3G). Genetic ablation of the Gli1$^+$ cell population also reduced the fibrotic readouts α-SMA, collagen 3α1 (Col3α1) and fibronectin (Figure 3 H-J), which were all significantly increased following ThPO overexpression in the bone marrow.

These experiments provide the first *in vivo* functional evidence that Gli1$^+$ cells are fibrosis-driving cells in bone marrow fibrosis and thus represent a novel cellular target. Importantly,

the ablation of Gli1$^+$ cells in normal hematopoiesis (control+DTX) did not have detrimental effects on differentiated lineages (Figure S3D-H) nor on hematopoietic stem and progenitor cells (Figure 3K). Furthermore, we did not observe a significant effect of Gli1$^+$ cell ablation on marrow vascularization (CD31 surface area), sympathic nerve fibres (tyrosine hydroxylase surface area) or glia cells (GFAP surface area) (Figure S3I-K).

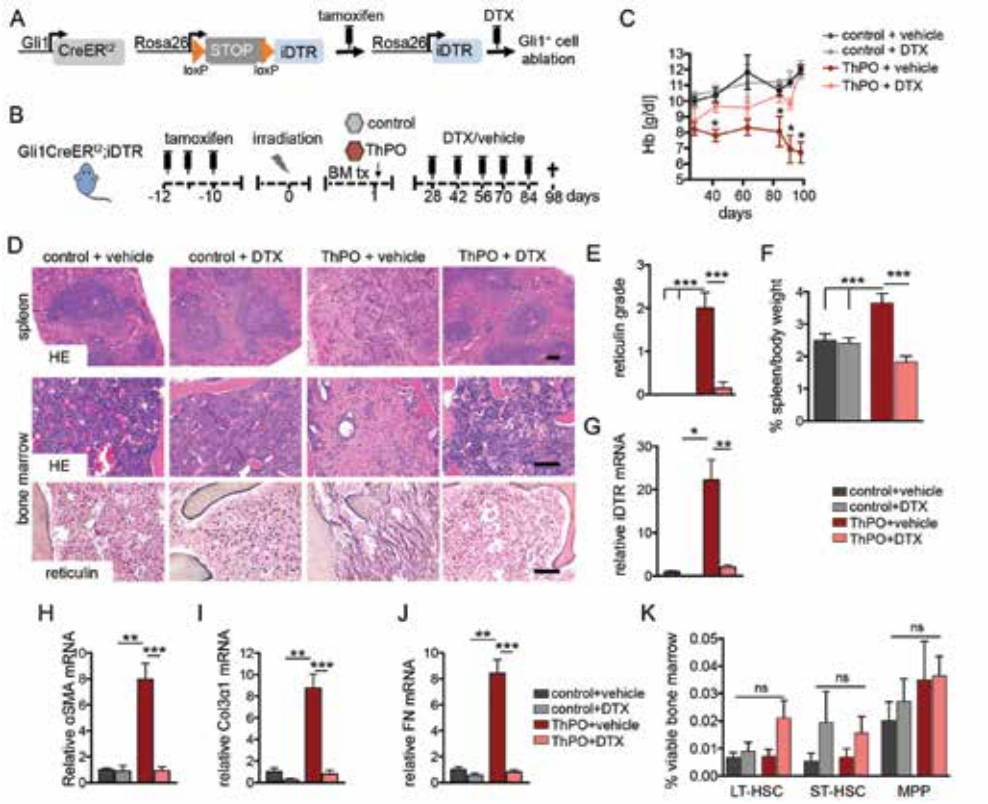

Figure 3: Genetic ablation of Gli1$^+$ cells abolishes bone marrow fibrosis and rescues thrombopoietin induced bone marrow failure. (A-B) Bigenic Gli1CreER^{t2};iDTR mice received tamoxifen (3x10mg p.o.), were lethally irradiated at 10 days after the last tamoxifen dose and transplanted with 2x10^5 c-kit purified bone marrow cells from wild type littermates transduced with either control or ThPO cDNA. Mice were injected with diphtheriatoxin in order to ablate Gli1$^+$ cells (DTX, 50ng/kg body weight i.p.) or vehicle (PBS) as indicated (control + vehicle n=3, 2 males; control+DTX n=4, 2 males; ThPO + vehicle n=9, 5 males; ThPO + DTX n=6, 4 males). **(C)** Time course of hemoglobin counts. *p<0.05 by t-test**;** mean±SEM. **(D)** Representative hematoxylin & eosin (HE) and reticulin stained images from spleen and bone marrows. Scale bars 300µm. **(E)** Scoring of reticulin fibrosis grade. ***p<0.001 by one way ANOVA with posthoc Tukey; mean±SEM. **(F)** Spleen weight relative to body weight among the groups. ***p<0.001 by one way ANOVA with posthoc Tukey**;** mean±SEM. **(G)** mRNA expression of the symian diphtheriatoxin receptor (iDTR). *p<0.05 **p<0.01 by one way ANOVA with posthoc Tukey; mean±SEM. **(H-J)** Relative mRNA expression for the fibrotic readouts alpha smooth muscle actin (α-SMA), collagen 3α1 (Col3α1) and fibronectin. **p<0.01, ***p<0.001 by one way ANOVA with posthoc Tukey; mean±SEM. **(K)** Analysis of the HSC compartment, defined as long-term (LT; lin^{low}Sca1$^+$ckit$^+$CD48$^-$CD150$^+$), short-term (ST; lin^{low}Sca1$^+$ckit$^+$CD48$^-$CD150$^-$) HSCs and multipotent progenitor cells (MPP, lin^{low}Sca1$^+$ckit$^+$CD48$^+$CD150$^-$) in the bone marrow within the four different groups. mean±SEM; ns=non-significant by one way ANOVA with posthoc Tukey. See also Figure S3.

Pharmacological targeting of Gli1$^+$ cells with GANT61 amelioreates myelofibrosis

Having shown that Gli1$^+$ cells are the key myofibroblast progenitors of the bone marrow and that ablation of these cells abolishes bone marrow fibrosis and restores hematopoiesis in ThPO-overexpression induced myelofibrosis, we next asked whether Gli1$^+$ cells can be targeted pharmacologically in a more physiological myelofibrosis model. As 60% of patients with myelofibrosis harbor the JAK2(V617F) mutation, we introduced the mutation in a retroviral vector (MSCV-IRES-GFP, MIG) in ckit$^+$ HSPCs [26, 27]. Gli antagonist 61 (GANT61) was identified in a screen to be a direct small molecule compound inhibitor of Gli proteins and has been reported as a promising treatment of fibrosis in lung and kidney [28]. To elucidate whether pharmacologic inhibition of Gli proteins is a therapeutic strategy in myelofibrosis, we performed a genetic fate tracing experiment of Gli1$^+$ cells in a JAK2V617F myelofibrosis model combined with GANT61 treatment. Bigenic Gli1CreER$^{t2+/-}$;tdTomato$^{+/-}$ mice received tamoxifen and were transplanted with bone marrow of WT littermates retrovirally transduced with either WT Jak2 control vector or Jak2(V617F). Treatment with either GANT61 or vehicle was initiated at 8 weeks after onset of the disease in the Jak2(V617F) group (Figure 4A, S4A). Mice were randomized based on the Hb level to receive either GANT61 or vehicle every other day.

Mice transplanted with Jak2(V617F) presented with significantly elevated hemoglobin levels (Hb) compared to the control groups (Figure S4A), reflecting erythroid hyperplasia, while treatment with GANT61 rescued this phenotype with a significant decrease of Hb to levels comparable to the control groups. Analysis of the bone marrow at 17 weeks after transplantation showed a significant expansion of genetically tagged Gli1$^+$ cells with subsequent development of reticulin fibrosis and splenomegaly (Figures 4B-F, S4B-C) in the Jak2(V617F) transplanted mice compared to the WT controls.

Co-staining with α-SMA demonstrated that Gli1$^+$ cells differentiated into myofibroblasts and represented a significant part of the myofibroblast population (Figure 4E, F and S4C). Notably, treatment with GANT61 resulted in significantly reduced numbers of Gli1$^+$-tdTomato$^+$ and Gli1$^+$-tdTomato$^+$-αSMA$^+$ cells and abolished development of reticulin fibrosis (Figure 4B-F, S4B-C). Distance measurements of Gli1$^+$ cells to bone and endothelial cells revealed that the presence of a Jak2(V617F) hematopoietic clone resulted in Gli1$^+$ cell mobilization from both the endosteal and the perivascular niche which was ameliorated by GANT61 treatment (Figure S4D-E).

Moreover, while Jak2(V617F) transplantation resulted in signifcantly increased spleen weight and numbers of long-term hematopoietic stem cells (LT-HSCs), multipotent progenitor cells (MPPs) and erythroid progenitors as typical for a polycythemia vera (PV), GANT61 reversed this phenotype (Figure 4G, S4F-G) suggesting an effect of GANT61 on both Gli1$^+$ cells and the malignant hematopoietic clone. To assess the relative effect of GANT61 treatment on Jak2(V617F) expressing hematopoietic cells, we treated transduced (GFP$^+$) and non-transduced (GFP$^-$) c-kit+ HSPCs *in vitro*. GANT61 specifically reduced Jak2(V617F) expressing

cells and induced significant apoptosis (Figure 4H and Figure S4H). We then analyzed the down-stream effects of Jak2(V617) and observed a significant down-regulation of STAT5 phosphorylation by GANT61 treatment (Figure 4I). Jak2(V617F) induced expression of the phosphatidylinositol-3-kinase (PI3K), which was also inhibited by GANT61 treatment (Figure 4J). As the PI3K/Akt axis was shown to activate Gli in a non-canonical fashion, we analyzed Akt and Gli1 expression. Jak2(V617F) in HSPCs induced increased (but not significant) expression of both Akt and Gli1 which was in tendency decreased by GANT61 treatment (Figure 4J). These results suggest that GANT61 might partially also inhibit expansion of the malignant clone by inhibition of signal transduction pathways and induction of apoptosis.

These data suggest that targeting Gli proteins by GANT61 is a novel therapeutic approach in myelofibrosis that affects both expansion of myelofibrosis driving Gli1^{+} myofibroblasts and the expansion of the malignant hematopoietic clone.

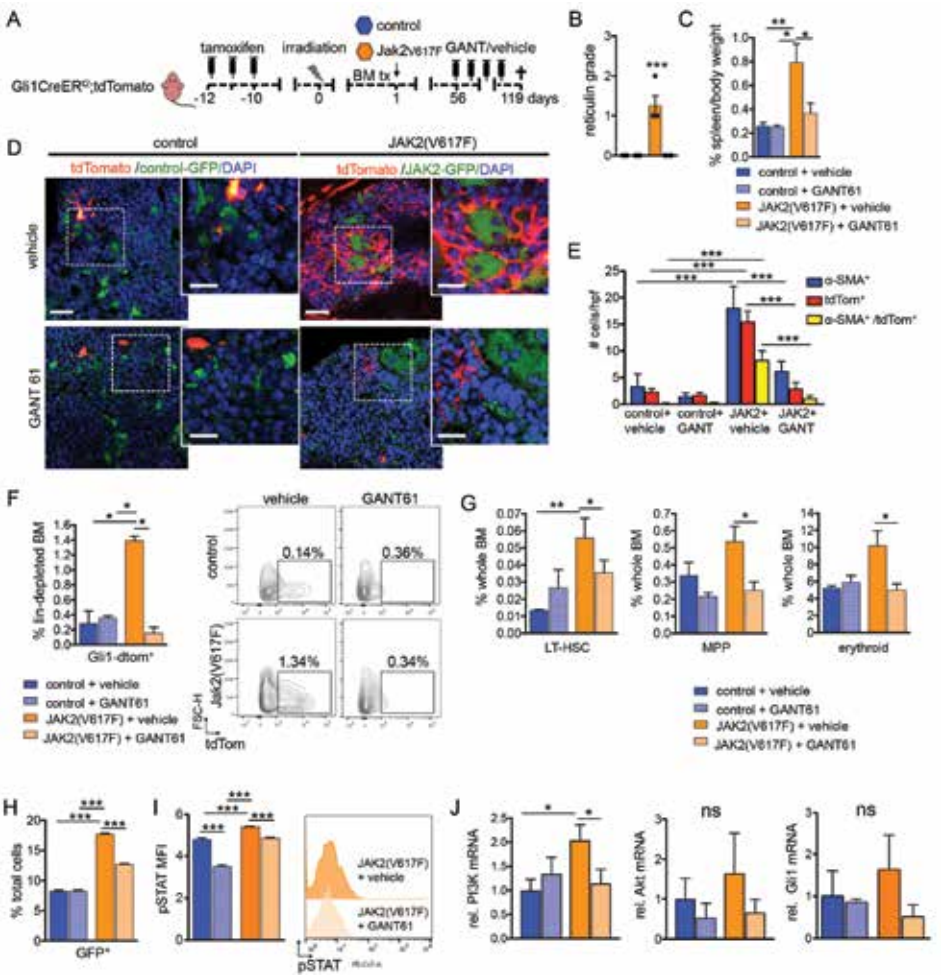

Figure 4: Gli1$^+$ cells are myofibroblast precursors in JAK2(V617F) induced myelofibrosis and can be targeted pharmacologically by GANT61
(A) Bigenic Gli1CreER^{t2};tdTomato mice received tamoxifen (3x10mg p.o.) and were lethally irradiated 10 days after the last tamoxifen dose and transplanted with 2x10^5 c-kit purified bone marrow cells from wild type littermates that had been transduced with either control (n=10) or Jak2(V617F) (n=10) cDNA (both MCSV-IRES-GFP retroviral backbone vector). Mice were injected with GANT61 (50mg/kg body weight) or vehicle (corn oil / ethanol) every other day between 8 and 17 weeks after transplantation (control + vehicle n=3, 2 males; control+GANT61 n=5, 3 males; Jak2(V617F) + vehicle n=4, 3 males; Jak2(V617F) + GANT61 n=4, 3 males). **(B)** Grading of reticulin fibrosis. ***p<0.001 versus all other groups by one way ANOVA with posthoc Tukey; mean±SEM**. (C)** Spleen weight was determined as a percentage of the body weight. *p<0.05, **p<0.001 by one way ANOVA with posthoc Tukey; mean±SEM. **(D)** Representative images of sternal bones. Scale bars 50μm, inserts 25μm. **(E)** Quantification of all alpha smooth muscle actin expressing cells (α-SMA$^+$), Gli1 cells (tdTomato$^+$) and Gli1-derived myofibroblasts (α-SMA$^+$/ tdTomato$^+$) in the bone marrow of mice transplanted with Jak2(V617F) (Jak2) or control that have been treated with GANT61 or vehicle. ***p<0.001 by one way ANOVA with posthoc Tukey; mean±SEM. **(F)** Representative flow cytometric plots and quantification of Gli1$^+$ cells and within the lineage depleted bone marrow. *p<0.05 by one way ANOVA with posthoc Tukey; mean±SEM. **(G)** Analysis of long-term (LT; lin^{low}Sca1$^+$ckit$^+$CD48$^-$CD150$^+$) and multipotent progenitor cells (MPP, lin^{low}Sca1$^+$ckit$^+$CD48$^+$CD150$^-$) as well as erythroid cells (Gr1$^-$CD11b$^-$CD3$^-$CD19$^-$Ter119$^+$) by flow cytometry. *p<0.05, **p<0.01 by one way ANOVA with posthoc Tukey; mean±SEM. **(H)** c-kit$^+$ purified HSPCs from wild type mice were transduced with either control or Jak2(V617F) cDNA (both MCSV-IRES-GFP retroviral backbone vector). 48 hours after transduction, cells were treated with GANT61 or vehicle. The gene marking (GFP$^+$) was quantified by flow cytometry 48 hours after treatment. ***p<0.001 versus all other groups by one way ANOVA with posthoc Tukey; mean±SEM**. (I)** Quantification of the mean fluorescence intensity (MFI) and representative flow cytometric analysis of levels of phospho-STAT5 (p-STAT5) in c-kit+ cells transduced with Jak2(V617F) or control (GFP$^+$) 48 hours after treatment with GANT61 or vehicle. GFP$^+$ cells are shown in the histogram. ***p<0.001 versus all other groups by one way ANOVA with posthoc Tukey; mean±SEM**. (J)** c-kit$^+$ purified HSPCs were transduced with Jak2(V617F) or control cDNA, were sort-purified by GFP-expression 48 hours after transduction and treated with GANT61 or vehicle 24 hours later. 24 hours after treatment, cells were harvested for RNA isolation and qt-RT-PCRs. Relative mRNA expression for Phosphatidylinositol-4,5-bisphosphate 3-kinase (PI3K), Akt and Gli1 is shown. *p<0.05 ns=non-signifcant by one way ANOVA with posthoc Tukey; mean±SEM. See also Figure S4.

Gli1$^+$ cells undergo distinct transcriptional changes in bone marrow fibrosis

To determine whether and how Gli1$^+$ stromal cells are altered in bone marrow fibrosis, we performed RNA sequencing on sort-purified lineage$^-$GFP$^-$Gli1-tdtom$^+$ cells from controls and ThPO-overexpressing mice with bone marrow fibrosis (at 10 weeks after bone marrow transplantation). Principal component analysis and hierarchical cluster analysis revealed that Gli1$^+$ cells in bone marrow fibrosis are drastically distinct from Gli1$^+$ cells in homeostasis (Figure 5A-B). Statistical analysis revealed that 1597 genes were differentially expressed between the Gli1$^+$ cells in control conditions and Gli1$^+$ cells in bone marrow fibrosis (0.5 log2 fold, Benjamini Hochberg-FDR corrected p-value 0.05), with 924 up-regulated and 673 down-regulated genes. To uncover differentially altered mechanisms in the Gli1$^+$ stromal cells in bone marrow fibrosis and potential pathways of activation by the malignant hematopoietic clone, we performed gene set analysis using PIANO [30, 31] with a pathway collection adapted for mouse . We found up-regulated pathways that play a critical role in cytokine-cytokine receptor interaction but also in the inflammatory response, specifically the leukotriene (LOX) and prostaglandin (COX) pathways, both of which use the same primary precursor, arachidonic acid (Figures 5C, S5). There is evidence that bone marrow stromal cells actively metabolize arachidonic acid and that metabolites are important for the regulation of hematopoeisis [32, 33]. Arachidonate 12-lipoxgenase

(ALOX12) was significantly up-regulated in bone marrow fibrosis and is, together with ALOX5, known to be pro-carcinogenic and implicated to play a role in myeloid malignancy [34-37]. Differential gene expression analysis demonstrated that megakaryocyte-associated genes were significantly up-regulated, in particular the chemokine Cxcl4 (cytokine-cytokine receptor interaction pathway, Figure 5C-D) and the Arachidonate lipoxygenase enzyme ALOX12 (KEGG MM Leukotriene Metabolism, KEGG MM Prostaglandin Formation from Arachidonate), which have been implicated to play a role in fibrosis , hematopoietic stem cell regulation and are linked to platelet and stromal cell biology [40]. These findings are in line with previous studies showing that MPN and myelofibrosis are linked to defective megakaryopoiesis [41], and our genetic fate tracing analysis demonstrating close association of $Gli1^+$ cells to abnormal megakaryocytes.

We further observed increased metabolic activity in $Gli1^+$ stromal cells in bone marrow fibrosis (Figure 5C), in particular of fatty acid metabolism. Peroxisome proliferator-activated receptors (PPARs) are activated by fatty acids and their derivates and have emerged as links between disturbed metabolism and inflammation. PPARγ, the master switch of lipogenic differentiation in MSCs, was further significantly induced in bone marrow fibrosis and recently described to play a role in pulmonary fibrosis [12]. To validate this finding and to identify a potential lipogenic phenotype of $Gli1^+$ MSCs in bone marrow fibrosis, we performed co-staining with the neutral lipid stain (LipidTOX) as recently described in pulmonary fibrosis [34-37]. Indeed, we observed sparsely LipidTOX positive $Gli1^+$ cells in bone marrow from ThPO-overexpressing mice (Figure 5E).

In line with previous studies of niche cells in bone marrow fibrosis , we found altered expression of many HSC-regulatory genes and cytokines, including a broad down-regulation of HSC retention factors, in particular Cxcl12 (Figure 5C,F).

As CXCL4 was implicated as a marker for fibrosis in multiple organ systems, including bone marrow fibrosis , is a regulator of hematopoiesis and a chemotactic factor, we hypothesized that Cxcl4 plays a crucial role in the activation of $Gli1^+$ cells from their niche and in the fibrotic transformation process. Interestingly Cxcl4 was among 4 up-regulated cytokines in a cytokine array from medium supernatant of both ThPO and Jak2(V617F) overexpressing cells (Figure 5G). Based on previously published data and our findings, we propose a model of abnormal release of Cxcl4 (and also of the related chemokine platelet basic protein, PPBP/CXCL7) from α-granules from atypical megakaryocytes and platelets in MPN [35] (Figure 5H). In turn, Cxcl4 as a CXC chemokine contributes to the activation of $Gli1^+$ cells and their transdifferentiation into α-SMA^+ myofibroblasts. In fibrosis progression, thrombin and collagen contribute to the activation of arachidonic acid metabolism which transforms stromal cells into inflammatory, metabolically active cells which lose their hematopoiesis-supporting capacity, further contributing to abnormal hematopoeisis in MPN (Figure 5H).

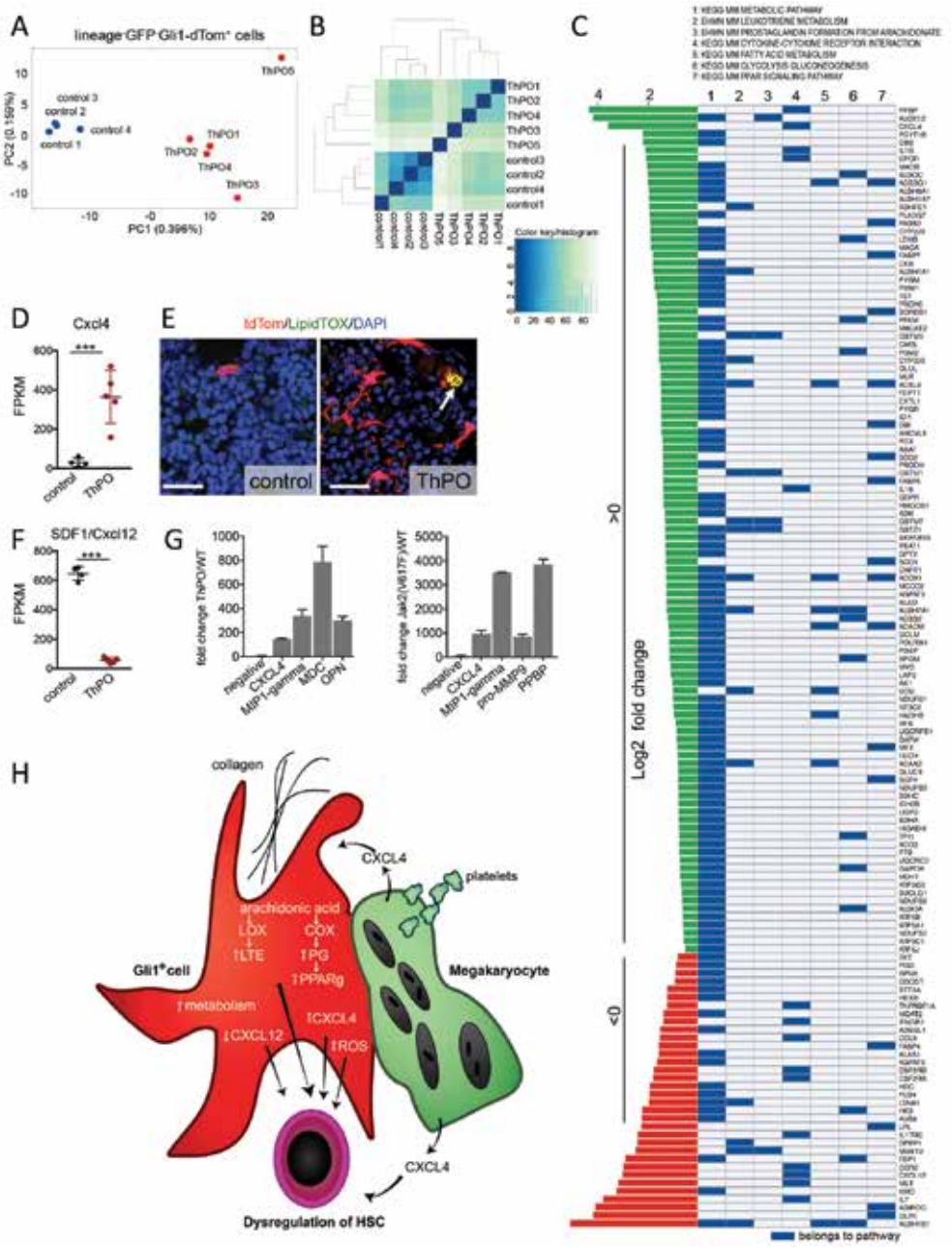
A
lineage GFP Gli1-dTom+ cells
PC2 (0.159%)
PC1 (0.396%)
control 3
control 2
control 4
control 1
ThPO5
ThPO1
ThPO2
ThPO4
ThPO3
B
ThPO1
ThPO2
ThPO4
ThPO3
ThPO5
control3
control2
control4
control1
Color key/Histogram
C
1: KEGG MM METABOLIC PATHWAY
2: EHMN MM LEUKOTRIENE METABOLISM
3: EHMN MM PROSTAGLANDIN FORMATION FROM ARACHIDONATE
4: KEGG MM CYTOKINE-CYTOKINE RECEPTOR INTERACTION
5: KEGG MM FATTY ACID METABOLISM
6: KEGG MM GLYCOLYSIS GLUCONEOGENESIS
7: KEGG MM PPAR SIGNALING PATHWAY
>0
<0
Log2 fold change
belongs to pathway
D
Cxcl4
FPKM
control
ThPO
E
tdTom/LipidTOX/DAPI
control
ThPO
F
SDF1/Cxcl12
FPKM
control
ThPO
G
fold change ThPO/WT
negative
CXCL4
MIP1-gamma
MDC
OPN
fold change Jak2(V617F)/WT
negative
CXCL4
MIP1-gamma
pro-MMP9
PPBP
H
collagen
CXCL4
platelets
arachidonic acid
LOX
COX
↑LTE
↑PG
↑PPARg
Gli1+cell
Megakaryocyte
↑metabolism
↓CXCL12
↑CXCL4
↑ROS
CXCL4
Dysregulation of HSC

Figure 5: Gli1$^+$ cells in bone marrow fibrosis are transcriptionally distinct from Gli1$^+$ cells in homeostasis. Bigenic Gli1CreER;tdTomato mice were injected with tamoxifen (3x10mg p.o.) at 8 weeks of age, lethally irradiated at 10 days after the last tamoxifen dose and received c-kit enriched hematopoietic stem cells from wildtype littermates expressing either Thrombopoietin-cDNA (ThPO, n=5, 3 males) or control-cDNA (control, n=4, 3 males; both lentiviral SFFV-iGFP vector backbone). Mice were sacrificed at 70 days after transplantation. Gli1$^+$ cells were sort-purified as lin$^-$GFP$^-$dtTomato$^+$ and subjected to RNA sequencing **(A)** Principal component analysis (PCA). **(B)** Heatmap representation with hierarchical clustering **(C)** Significantly directional enriched (median FDR >0.05) pathways. **(D)** Fragments per kilobase of exon per million fragments mapped (FPKM) values of CXCL4 in control and ThPO group; mean±SEM. **(E)** Representative images of bone marrow from Gli1CreER^{t2};tdTomato mice transplanted with bone marrow from wildtype littermates expressing either ThPO or control-cDNA stained with the neutral lipid staining LipidTOX. Scale bars 50µm. Arrow indicating LipidTOX positive Gli1$^+$ cells. **(F)** FPKM value of stromal derived factor 1 (SDF 1/ CXCL12) in control and ThPO group; mean±SEM. **(G)** Cytokine analysis in serum and cytokine-free medium supernatant of ckit+ cells expressing ThPO or control (lentiviral SFFV-iGFP vector backbone) or Jak2(V617F) or control (both MCSV-IRES-GFP retroviral backbone). n=2. **(H)** Model for stroma-hematopoiesis interactions in bone marrow fibrosis. See also Figure S5.

To validate the findings of the RNA sequencing and to dissect the direct interaction of stromal cells and hematopoietic cells in bone marrow fibrosis *in vitro*, we co-cultured ThPO overexpressing c-kit+ hematopoietic stem and progenitor cells (HSPCs) and Gli1$^+$ isolated stromal cells. As GANT61 ameliorates bone marrow fibrosis, we further tested the effect of GANT61 treatment on differentially expressed genes (Figure 6A). The co-culture with ThPO overexpressing HSPCs significantly induced expression of Cxcl4 in stromal cells, which was completely normalized by GANT61 treatment. Endothelin 1 and MMP9 as pro-fibrotic readouts associated with increased Cxcl4 expression in organ fibrosis [43-45], were significantly up-regulated in stromal cells exposed to ThPO overexpressing HSPCs and were normalized after GANT61 treatments (Figure 6A). ALOX12 and PPARγ as targets of activated arachidonic acid were up-regulated in stromal cells in the presence of ThPO overexpressing HSPCs and normalized by GANT61 treatment. As previous studies suggested that GANT61 leads to apoptosis and cell cycle arrest, we analyzed the anti-apoptotic gene Bcl2 and the cyclin-dependent kinase inhibitor p21. Bcl2 was significantly decreased after treatment with GANT61 and p21 significantly induced, suggesting that GANT61 induces apoptosis and might affect cell-cycle (Figure 6A).

We validated in co-culture experiments that the exposure of Gli1$^+$ cells with ThPO overexpressing HSPCs induces differentiation into α-SMA$^+$ myofibroblasts and that GANT61 inhibits the differentiation or induces apoptosis in differentiated cells (Figure 6B). We analyzed apoptosis in Gli1$^+$ and Gli1$^-$ stromal cells and confirmed that GANT61 induces apoptosis specifically in Gli1$^+$ stromal cells (Figure 6C). GANT61 further induced apoptosis in hematopoietic cells, suggesting that part of the positive effect of GANT61 in bone marrow fibrosis can be explained by reduction of the malignant hematopoietic clone (Figure 6D). Interestingly, we observed a direct effect of GANT61 on megakaryocyte ploidy, suggesting inhibition of megakaryocyte maturation (Figures 6E, S6). This data further validates that GANT61 affects both Gli1$^+$ stromal cells and the malignant hematopoietic clone.

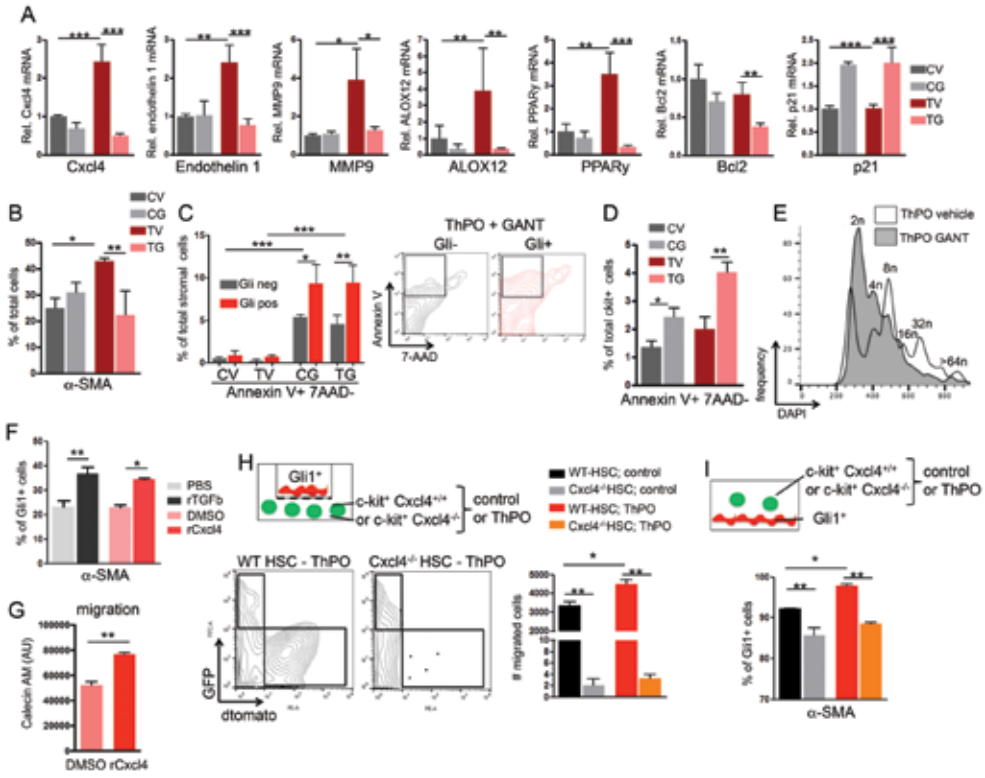

Figure 6: Cxcl4 induces migration and myofibroblastic differentiation of Gli1⁺ cells (A-E) tdTomato-Gli1⁺ stromal cells co-cultured with c-kit⁺ hematopoietic stem and progenitor cells (HSPCs) expressing either Thrombopoietin-cDNA (ThPO) or control cDNA (control vector=CV) were treated for 24 hours with vehicle or GANT61. CV= control vector, vehicle; CG= control vector and GANT61; TV= ThPO overexpression and vehicle; TG= ThPO overexpression and GANT61. **(A)** Relative mRNA expression in tdTomato-Gli1⁺ stromal cells is shown for platelet-factor 4 (Cxcl4), endothelin 1, matrix metalloproteinase 9 (MMP9), Arachidonate 12-lipoxygenase (ALOX12), Peroxisome proliferator-activated receptor gamma (PPARγ), B-cell lymphoma gene 2 (Bcl2) and p21. **p<0.01, ***p<0.001 by one way ANOVA with posthoc Tukey; mean±SEM. n=3. **(B)** Quantification of td-Tomato⁺⁺α-SMA⁺ myofibroblasts in stromal cells co-cultured with HSPCs (expressing control or ThPO cDNA) and treated with GANT61. *p<0.05, **p<0.01 by one way ANOVA with posthoc Tukey; mean±SEM. n=3. **(C)** Quantification and representative flow blots of early apoptosis (AnnexinV⁺7AAD⁻) in td-Tomato⁺ and td-Tomato⁻ stromal cells co-cultured with HSPCs and treated with GANT61. *p<0.05, **p<0.01, ***p<0.001 by one way ANOVA with posthoc Tukey; mean±SEM. n=3. **(D)** Quantification of early apoptosis (AnnexinV⁺7AAD⁻) in c-kit⁺ HSPCs (expressing control or ThPO cDNA) co-cultured with stromal cells. *p<0.05, **p<0.01 by one way ANOVA with posthoc Tukey; mean±SEM. n=3. **(E)** Representative histogram showing ploidy in CD41⁺ ThPO-overexpressing megakaryocytes treated with GANT61 or vehicle. Representative data from one of three experiments. **(F)** Flow cytometric quantification of α-SMA⁺ in stromal cells treated with recombinant platelet factor 4 (rCxcl4) or TGFβ as a known stimulus for myofibroblastic differentiation (or respective controls). *p<0.05, **p<0.01 by t-test; mean±SEM. n=3. **(G)** Quantification of migration of tdTomato-Gli1⁺ stromal cells towards an rCxcl4 or control (DMSO) gradient. AU= arbitrary unit; mean±SEM; **p<0.01 by t-test. n=2 **(H)** Schematic, representative flow blots and quantification of tdTomato⁺ Gli1⁺ migration towards c-kit+ HSPCs isolated from Cxcl4⁻/⁻ mice or littermate controls (Cxcl4⁺/⁺) expressing either ThPO or control cDNA (GFP⁺). **p<0.01 by one way ANOVA with posthoc Tukey; mean±SEM, n=3. **(I)** Schematic and quantification of α-SMA⁺ myofibroblast differentiation (flow cytometry) of tdTomato⁺ Gli1⁺ stromal cells co-cultured with c-kit⁺ HSPCs isolated from Cxcl4⁻/⁻ mice or littermate controls expressing either ThPO or control cDNA (GFP⁺). *p<0.05, **p<0.01 by one way ANOVA with posthoc Tukey; mean±SEM. n=3. See also Figure S6

Cxcl4 is necessary and sufficient for the migration of Gli1$^+$ stromal cells and induces their myofibroblastic differentiation

To confirm that Cxcl4 induces migration and myofibroblastic differentiation of Gli1$^+$ cells, we exposed Gli1$^+$ cells to recombinant Cxcl4 and analyzed myofibroblast differentiation and cell migration towards a Cxcl4 gradient. Recombinant Cxcl4 (rCxcl4) significantly induced myofibroblast differentiation of Gli1$^+$ cells comparable to induction with TGFβ, a known stimulus for differentiation of MSCs into myofibroblast (Figure 6F). In a chemotactic migration assay, Cxcl4 significantly increased the migration of Gli1$^+$ cells towards the rCxcl4 gradient (Figure 6G) Having established that Cxcl4 induces migration and myofibroblast differentiation of Gli1$^+$ cells, we sought to confirm the hypothesis that Cxcl4 in hematopoietic cells in bone marrow fibrosis induces the migration and differentiation process of Gli1$^+$ stromal cells. We tested if genetic knockdown of Cxcl4 in hematopoeitic cells can ameliorate the migration and myofibroblastic differentiation of Gli1$^+$ cells. We thus performed a migration assay with Gli1$^+$ cells on a transwell membrane and hematopoietic cells isolated from Cxcl4$^{-/-}$ mice and WT controls, expressing control or ThPO cDNA, in the lower compartment as a chemotactic gradient (Figure 6H). The migration of Gli1$^+$ cells was significantly increased with ThPO overexpressing cells as the migratory stimulus and the migration activity was almost absent in conditions with Cxcl4$^{-/-}$ hematopoietic cells as the chemoattractant, demonstrating that Cxcl4 is necessary for the migration of Gli1$^+$ stromal cells induced by ThPO overexpressing HSPCs (Figure 6H). We next analyzed whether the genetic knockout of Cxcl4 in hematopoietic cells had an effect on pre-activated Gli1$^+$ myofibroblasts in a direct co-culture model. The absence of Cxcl4 in hematopoeitic cells ameliorated myofibroblastic differentiation, but did not completely inhibit the differentiation process (Figure 6I), indicating that myofibroblastic differentiation results from multiple interplaying cytokines secreted by the hematopoietic clone. In summary, these data show that the atypical megakaryocytes and platelets play an important role in the activation and recruitment of Gli1$^+$ stromal cells from their niche, and that Cxcl4 in the hematopoietic clone is a strong chemotactic factor and contributes to fibrotic transformation.

Gli1$^+$ cells expand in human MPN and can be targeted therapeutically

Given that Gli1$^+$ cells are important myofibroblast progenitors and show efficacy as a therapeutic target in two distinct mouse models of myelofibrosis, we next asked whether the same pathway might be active in human myelofibrosis. Bone marrow punch biopsies were collected from MPN patients (n=60) and age-matched, normal bone marrow biopsies without a primary hematological disease (healthy controls; n=33), stained for reticulin and scored blindly by pathologists for the severity of myelofibrosis and Gli1 expression (Figure 7A and S7A; Table S1). Gli1$^+$ cells aligned the bone and sinusoids in healthy controls as demonstrated in Figure 7A. Comparable to the findings in murine MPN models, the frequency of spindle-shaped Gli1$^+$ cells significantly increased in MPN (Figure 7A, B). Gli1$^+$

cells were diffusely present in the hematopoietic marrow, and not restricted to their localization in the endosteal and vascular niche. Gli1$^+$ cells were found in cellular areas with storifomous growth pattern or positioned within amorphous matrix deposits (Figure 7A). The frequency of Gli1$^+$ cells positively correlated with an increase in reticulin grading of myelofibrosis, independent of the MPN classification (Figure 7C). The frequency of Gli1$^+$ cells did not correlate with JAK2(V617F) or calreticulin gene (CALR) mutation status (Fig. S7B), suggesting a common pathobiological pathway that regulates the interaction between the malignant hematopoietic clone, atypical megakaryocytes and their niche.

Next, we isolated MSCs from bone marrow biopsies of MPN patients (MPN-MSC; n=4) and healthy control donors (n=4). Interestingly, we observed both up-regulation of Gli1 and aSMA mRNA in MSCs from MPN patients when compared to MSCs of healthy donors, just as we observed in the murine models (Figure 7D). MSCs from MPN patients also up-regulated mRNA expression of extracellular matrix proteins such as collagens and fibronectin (Figure 7D). Cells with myofibroblast morphology were only observed in MPN as shown by staining of α-SMA$^+$ stress fibres (Figure 7E), α-SMA gene expression (Figure 7F) and an α-SMA population by flow cytometry (Figure 7G). Strikingly, treatment with GANT61 significantly reduced both α-SMA and Gli1-expression in MPN-MSCs on protein and gene expression level (Figure 7F-G). Furthermore, we observed a significant increase in apoptosis (AnnexinV$^+$7AAD$^-$) specifically in MPN-MSCs treated with GANT61 (Figure 7H). These results suggest that GANT61 induces apoptosis in Gli1-expressing myofibroblasts. Expression of the MSC marker nestin has been shown to be significantly reduced in MPN and to contribute to the disease progression by causing neuropathic changes in the bone marrow . We asked how Gli1 and nestin expression are related in myelofibrotic transformation. Flow cytometry confirmed that Gli1 cells express nestin under steady state conditions and that nestin expression is lost in MPN wheras Gli1 expression is increased, indicating that Gli1 promotes the myelofibrotic transformation (Figure 7I). In summary, these data suggest that targeting Gli1$^+$ MSCs by GANT61 might be a potential novel therapy in human bone marrow fibrosis.

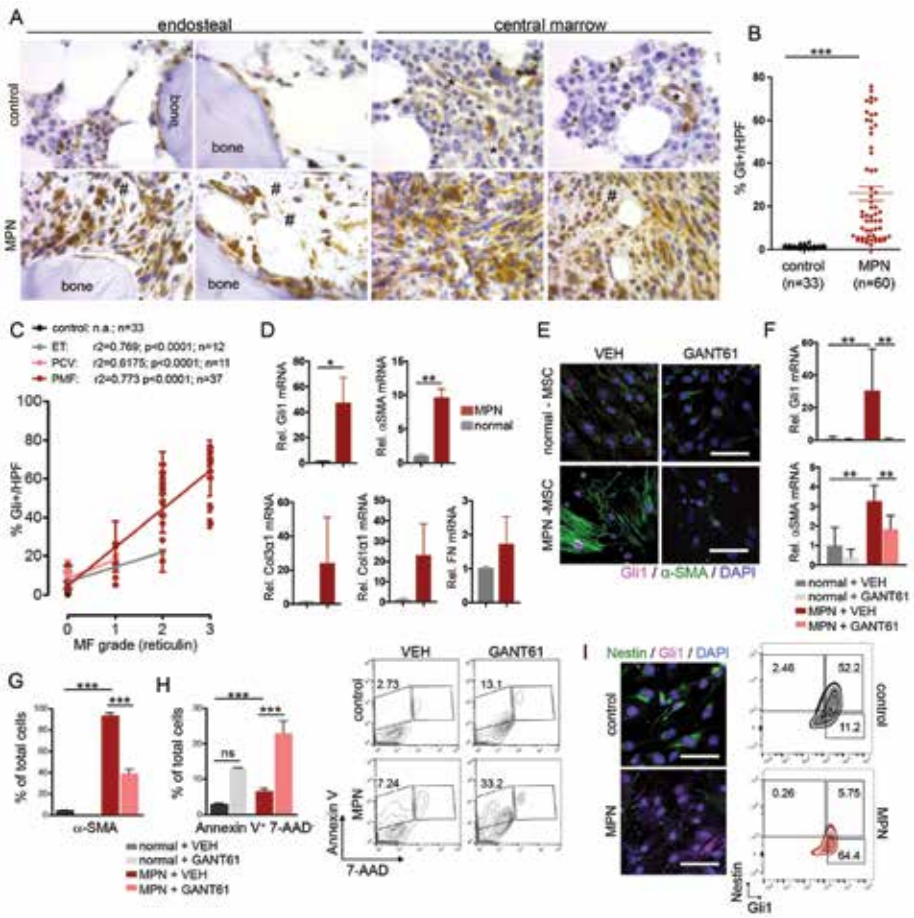

Figure 7: Increased Gli1 frequency correlates with fibrosis grade in human bone marrows and can be targeted pharmacologically

(A) Representative images of human bone marrow biopsies from control patients (MF=0) and patients with myelofibrosis stained for Gli1. *= sinusoids; #= amorphous matrix. Scale bars: 200µm. **(B)** Quantification of Gli1$^+$ cell frequency in human bone marrows from healthy control patients (healthy) and MPN patients. 3 high power fields (HPF) (400x) were counted for each patient and the mean value calculated; each dot represents one patients (n=33 control; n=60 MPN patients p<0.05, ****p<0.0001 by t-test; mean±SEM**. (C)** Correlation of Gli1$^+$ cell frequency and myelofibrosis (MF) grade in human bone marrow; mean±SEM. The myelofibrosis (MF)/reticulin grade was graded by hematopathologists at different institutions. Each dot represents one patient. ET: Essential Thrombocythemia; PCV: Polycythemia Vera; PMF: Primary Myelofibrosis. **(D)** Relative mRNA expression of Gli1 and the fibrotic readouts alpha smooth muscle actin (α-SMA), collagen3α1 (Col3α1), collagen1α1 (Col1α1) and fibronectin (FN) in human mesenchymal stem cells (MSCs) isolated from bone marrows of patients with myeloproliferative neoplasia (MPN, n=4) or healthy controls (control, n=4). *p<0.05, **p<0.001 by t-test; mean±SEM, **(E)** Representative imagesof human mesenchymal stem cells (MSCs) from bone marrow biopsies of patients with myeloproliferative neoplasia (MPN-MSCs, n=4) or healthy controls (control MSCs, n=4) stained for alpha-smooth muscle actin (α-SMA) and Gli1 24 hours after treatment with GANT61 (10µM) or vehicle (DMSO, VEH). **p<0.01 by one way ANOVA with posthoc Tukey. Scale bars 20µm. **(F)** Relative Gli1 and alpha smooth muscle actin (α-SMA) expression in human MSCs from healthy donors (control) and MPN patients after treatment with GANT61 (n=4 each) or vehicle (DMSO, VEH, n=4 each). **p<0.01 by one way ANOVA with posthoc Tukey. **(G)** Flow cytometric quantification of aSMA after treatment with GANT61 (n=3 each) or vehicle (DMSO, VEH, n=3 each). ***p<0.001 by one way ANOVA with posthoc Tukey. **(H)** Flow cytometric quantification and representative flow blots of Annexin V staining after treatment with GANT61 (n=4 each) or vehicle (DMSO, VEH, n=4 each). ***p<0.001 by one way ANOVA with posthoc Tukey. **(I)** Representative images and flow cytometric plots of MSCs from healthy donors (control) and MPN patients co-stained for Gli1 and Nestin. Scale bars 20µM mean±SEM. See also Figure S7 and supplementary table S1/S2 for patient characteristics.

DISCUSSION

Our studies strongly suggest a critical role for Gli1$^+$ stromal cells in the pathogenesis of bone marrow fibrosis. Genetic ablation and pharmacological targeting of Gli1$^+$ cells in two mouse models of bone marrow fibrosis/myelofibrosis and in human samples, reversed the myofibroblast phenotype and matrix production, two central mechanisms in the progression of bone marrow fibrosis.

Across different organ systems (e.g. heart, lung and liver) most investigators agree that myofibroblasts cause fibrosis, however the functional contribution of myofibroblasts in bone marrow fibrosis remained unclear. Electron-microscopy studies from the last century and more recent immunohistochemical stainings suggested an increase of myofibroblasts in human bone marrow fibrosis . Our inducible genetic fate tracing data and ablation studies show a functional contribution of Gli1$^+$ stromal cells as progenitors of myofibroblasts in bone marrow fibrosis. The fact that genetic ablation of Gli1$^+$ cells abolishes bone marrow fibrosis and restores hematopoiesis indicates that Gli1$^+$ MSCs are a promising cellular therapeutic target.

Gli1$^+$ cells have trilineage (multipotent) differentiation potential and readily differentiate into adipocytes, chrondroblasts as well as osteoblasts . Frenette et al. reported Nes^{peri} cells; periarteriolar Nestin GFP$^+$ (bright) cells along arterioles that co-express NG2 and are associated with sympathic nerves and GFAP$^+$ glia . Furthermore, they report Nes^{reti} cells; Nestin-GFP$^+$ (dim) cells aligned with sinusoids and co-expression of leptin receptor. While there might be an overlap of periarteriolar Gli1$^+$ cells and Nes^{peri} cells, we did not observe leptin receptor expression in Gli1$^+$ cells (Figure S1C). The majority of Gli1$^+$ cells in the endosteal niche was not associated with GFAP$^+$ glia or sympathic nerve fibres and only partially expressed Nestin. Thus, these cells might be partially distinct from the reported Nestin$^+$ populations.

A subpopulation of Gli1$^+$ MSCs expresses CD51 (and Sca1^{low}), the marker combination for osteoblastic lineage cells (OBC). Schepers et al. elegantly demonstrated that osteoblastic lineage cells are derived from multipotent stromal cells and that the *BCR-ABL*$^+$ clone in chronic myelogenous leukemia (CML) leads to expansion of OBC resulting in matrix production, bone marrow fibrosis and trabecular thickening [14]. We hypothesize that Gli1$^+$ cells are precursor cells for myofibroblasts and OBC, providing a mechanistic basis for both myelofibrosis as well as also preceeding osteosclerosis.

It was recently shown that HSCs carrying a *JAK2*(V617F) mutation induce significant neuroglial damage, reduction of Nestin$^+$ MSCs and Schwann cell death that contributes to

the pathogenesis of the disease by causing a neuropathic changes and is itself a promising therapeutic target [36]. Both Schepers et al. and Arranz et al. point to the potential for the microenvironment as a critical cooperator in the malignant process in MPN and emphasize a two-way perturbation process required for MPN. HSCs acquire a mutation (e.g., *JAK2-V617F, BCR-ABL* mutation) that leads to cell expansion and the mutant HSC perturbs the bone marrow niche, which further drive HSCs into neoplasia. The elegant study by Arranz et al. proposed that neural-glial protective agents and β3-adrenergic agonists may subvert the process and be therapeutically useful [34, 35]. It remained an open question which cells are the origin of bone marrow fibrosis. We demonstrate that in steady state conditions, a subfraction of Gli1$^+$ cells co-expresses nestin$^+$. Upon myelofibrotic transformation, Gli1$^+$ cells expand while nestin$^+$ cells decrease, suggesting that neuropathic changes lead to dysregulation of the niche accompanied by unregulated expansion and myofibroblast differentiation of Gli1$^+$ MSCs.

Already 30 years ago studies indicated that abnormal megakaryocytes in myelofibrosis stimulate the proliferation of fibrosis-driving fibroblasts, partially mediated by Cxcl4 . A central role of Cxcl4 in fibrosis was confirmed in solid organs and it was demonstrated that Cxcl4 is not only secreted by activated platelets but also plasmacytoid dendritic cells and fibroblasts [12, 14]. We demonstrated that Cxcl4 induces migration of Gli1$^+$ stromal cells and myofibroblastic differentiation, thus mediating central cellular processes in bone marrow fibrosis. We further observed significant down-regulation of the chemokine stromal-cell derived factor (SDF)-1 (CXCL12), in line with previous studies characterizing niche cells in MPN [14, 49]. Deletion of Cxcl12 in stromal cells was shown to increase circulating platelets [50] and studies in patients with myelofibrosis suggest that the bone marrow microenvironment is deprived of active CXCL12 [51]. Based on our data and previous studies, we propose that Gli1$^+$ stromal cells are activated from their niche by atypical platelets/megakaryocytes (mediated by Cxcl4), which leads to a cascade of myofibroblastic differentiation, metabolic reprogramming and down-regulation of CXCL12.

Our studies in MPN patient samples demonstrated that the frequency of Gli1$^+$ cells did not correlate with the mutation status, suggesting a common pathobiological pathway activates Gli1$^+$ cells. Previous studies have shown that unifying pathobiological pathways lead to abnormal megakaryocyte development in mouse models of myelofibrosis and in primary myelofibrosis patients, as reviewed in [52]. Thrompoietin (ThPO) exerts major extrinsic control on megakaryocytopoiesis. Hyperactive ThPO signals can be represented by activating mutations of MPL, its downstream effector JAK2 or calreticulin (CALR) mutations [20, 21, 53].

Currently, the standard therapies for MF can be divided into two catergories: clonal eradication or targeting bone marrow fibrosis. In PMF, the only therapy with a curative potential is allogenic hematopoietic stem cell transplantation leading to eradication of the malignant clone and reversal of bone marrow fibrosis . With the introduction of selective JAK inhibitors over the last 10 years, initial expectation of clonal suppression as measured by elimination of molecular and karyotypic abnormalities was dampened by the observations of persistent clonal hematopoiesis and unaltered MPN bone marrow pathological features. Although JAK inhibitors have been shown to improve patient constitutional symptoms and reduce splenomegaly, JAK inhibitor monotherapy does not significantly reduce mutant allele burden in the majority of MPN patients.

The therapeutic window for JAK inhibitors is limited due to the essential role of the JAK-STAT signaling pathway in normal hematopoiesis, which has been observed in the clinic where these inhibitors have been associated with dose limiting toxicities. Therefore, there is a need to identify additional pathways that might be involved in the development and maintenance of MPN mutant clones, which could be targeted in combination with JAK2 for improved therapeutic benefit.

An increase in the expression of hedgehog target genes has been observed in granulocytes isolated from MPN patients [28]. So far, the exact role of the Hh pathway in MF and its contribution to bone marrow fibrosis is not fully understood. Here, we show that Gli1-expression is significantly increased in stromal cells from MPN patients and that $Gli1^+$ MSCs are activated from their niche in the bone marrow upon expansion of the malignant clone, migrate into the hematopoietic marrow where they differentiate into matrix-producing myofibroblasts. Combinations of JAK2 inhibitors with inhibitors of the Hh pathway could provide an avenue of targeting stem cell–derived clonal myeloproliferation (which evades JAK2-targeted monotherapy). Preclinical and clinical data suggest that hedgehog pathway inhibitors have therapeutic activity in MF. To date, only smoothened (SMO)-inhibitors have been tested in MF with varying success [28]. We hypothesize that Gli proteins in $Gli1^+$ cells can be activated independent of canonical Hh signaling, explaining the mixed response in patients with MF, e.g. by PI3K/AKT signaling. Our data provide a rationale for targeted therapy of $Gli1^+$ cells in bone marrow fibrosis, as monotherapy or combined therapy with other agents.

Author contributions

R.K.S. designed and carried out experiments, analyzed results and wrote the manuscript, A.M., B.L.E. and B.D.H. contributed to experimental design, data interpretion and writing of the manuscript, J.S.R, R.H., A.D. and J.W. analyzed data and reviewed the manuscript, G.B. selected patient specimen, analyzed and interpreted histopathology and reviewed

the manuscript, G.M.N. contributed to confocal imaging and reviewed the manuscript, P.M.H.V-S, E.M.B., F.P, M.V.F., D.F. and V.P. carried out experiments, analyzed the data and reviewed the manuscript, R.K. designed and carried out experiments, analyzed results and wrote the manuscript.

Acknowledgements

This work was supported by a grant of the German Research Foundation (SCHN 1188/5-1), a grant of the Interdisciplinary Center for Clinical Research (IZKF) RWTH Aachen (O1-5), a clinical research grant of the European Hematology Association (EHA) and a Max Eder Grant of German Cancer Aid (Deutsche Krebshilfe 111750), all to RKS and by Grants of the German Research Foundation (KR-4073/3-1, SFBTRR57, SCHN 1188/5-1), a Grant of the European Research Council (ERC-StG 677448), a START Grant of the RWTH Aachen University (101/15) and a Grant of the State of North Rhine-Westphalia (Return to NRW) all to RK and by the NIH/NIDDK (DK088923, DK103740 and DK103050) and by an Established Investigator Award of the American Heart Association (EIA14650059) to BDH and by the confocal microscopy facility, a core facility of the IZKF Aachen. This project has received funding from the European Union´s Horizon 2020 research and innovation programe under grant agreement No 675585 (Marie-Curie ITN “SymBioSys”). Author AD is a Marie-Curie ESR at RWTH (Germany). We thank Willi Jahnen-Dechent (RWTH Aachen) for kindly providing labeled Fetuin A.

CONTACT FOR REAGENT AND RESOURCE SHARING

As Lead Contact, Rebekka K Schneider (Erasmus Medical Center, Rotterdam) is responsible for all reagent and resource requests. Please contact Rebekka K Schneider at r.k.schneider@erasmusmc.nl with requests and inquiries.

EXPERIMENTAL MODEL AND SUBJECT DETAILS

Mice

All mouse experiments were performed according to the animal experimental guidelines issued by the Animal Care and Use Committee at Harvard University, the Boston Childrens Hospital or the German government authorities (Landesamt für Natur, Umwelt und Verbraucherschutz Nordrhein Westfalen). Gli1CreER^{t2} (i.e. Gli1$^{tm3(re/ERT2)Alj}$/J, JAX Stock #007913), Rosa26tdTomato (i.e. B6-Cg-Gt(ROSA)26Sort$^{tm(CAG-tdTomato)Hze}$/J JAX Stock # 007909) and iDTR mice (i.e. C57BL/6-Gt(ROSA)26Sor$^{tm1(HBEGF)Awai}$/J, JAX Stock # 007900) were purchased from Jackson Laboratories (Bar Harbor, ME, USA). Offspring were genotyped by PCR according to the protocol from the Jackson laboratory. Males and females were used for the experiments as stated in the figure legends. Animals were maintained on the same 12hr light-dark cycle and received water and standard chow at libitum. For lineage tracing studies, 6-7 week old mice received 3x10 mg tamoxifen in corn oil / 3% ethanol (Sigma) via

oral gavage 10 days before lethal irradiation (1050 Rads). Mice received $5x10^5$ cells from 8 week old wild type littermates that had been harvested 48 hours prior to transplantation and were transduced with (1) Jak2(V617F) (JAK2) or control (control; WT Jak2) cDNA retrovirus or (2) ThPO or control (empty vector) lentivirus. Mice were randomly assigned to groups by choosing from a list of animal numbers with four digits. Mice were sacrificed 8 weeks after bone marrow transplantation in the ThPO fate tracing experiments and 17 weeks after bone marrow transplantation in the JAK2 experiments, when a significant decrease in the hemoglobin counts was observed. For RNA-Sequencing mice were sacrificed 10 weeks after bone marrow transplantation.

For the ablation experiments, bigenic Gli1CreER^{t2}; iDTR mice received tamoxifen (3x 10mg per oral gavage) 10 days prior to irradiation and bone marrow transplantation and were injected with diphtheriatoxin dissolved in PBS (List Biological Laboratories) at a dose of 50ng/g body weight intraperitoneally (i.p.) as indicated (Figure 3B). Mice were sacrificed 14 weeks after bone marrow transplantation. Mice were equally assigned to DTX or vehicle groups based on their Hb to control for significant differences before start of the treatment (at 4 weeks after bone marrow transplantation). GANT61 Cayman Chemical) was dissolved in ethanol and stored at -80°C. The ethanol solution was further diluted in corn oil (1:4) immediately before injections. Mice were injected with 50mg/kg-body weight of GANT61 (s.c.) or vehicle (corn oil / ethanol) every other day starting 8 weeks after bone marrow transplantation until sacrifice at 119 days after transplantation.

Human specimen

Patients samples originated form RWTH Aachen University Hospital and Hannover Medical School and the study was approved by the Ethical board of the RWTH Aachen Medical Faculty (ethical votes 173/06, 206/09, 300/13, 94/16) and the Hannover Medical School (ethical vote 3381-2016). Samples were deidentified at the time of inclusion. All patients provided informed consent and the study was performed in accordance with the Declaration of Helsinki. Bone marrow biopsies for histological examination (tissue microarrays and whole punch biopsies) were chosen from archived patient samples of paraffin-embedded tissue from the Institute of Pathology at RWTH Aachen University Hospital, Aachen, Germany and from the Biobank of Dr. G. Büsche at the Department of Pathology, Hannover Medical School, Hannover, Germany. Biopsies were primarily taken during earlier hospitalization. Patient characteristics of biopsy specimen are reported in Table S1. Isolated human MSCs were studied from 4 healthy donors (age 62±10, 2 males) and 4 MPN patients (51±10, 2 males) as outlined in Table S2. To establish the Gli1 antibody staining human glioblastoma multiforme tissue was accessed from the RWTH Aachen Biobank.

METHOD DETAILS

Human cell isolation and GANT61 treatment

Human MSCs (MPN patients or controls from hip replacement surgeries) were isolated by tissue culture plastic adherence after the mononuclear cell fraction was separated by Ficoll. Cells were seeded at a density of $5x10^6$ cells/flask. MSCs were maintained in medium (Mesenpan; PAN Biotech) containing 10% fetal bovine serum (Life Technologies), 1% penincilin-streptomycin-glutamine (Life Technologies). Medium was changed every third day and cells were split at near confluence. MSC surface phenotype was assessed at passage 1 using antibodies against the following antigens: CD45 (clone HI30), CD105 (SN6), CD73 (AD2). Antibodies were purchased from BD Biosciences (San Jose, USA) or eBiosciences (San Diego, USA). To study the effect of GANT61, cells were treated for 24-48h with 10 µM GANT61 (Sigma) in DMSO versus vehicle (DMSO).

Isolation of Gli1$^+$ cells

Gli1$^+$ cells were isolated from the compact bone of 8-10 week old bigenic, male, Gli1CreER;tdTomato mice after receiving 3x10mg Tamoxifen p.o. Compact bones including femur, tibia, pelvis and vertebrae were crushed by mortar and pestle until only small fragments were left. The fragments were digested at 37°C in 10ml collagenase 2 (1mg/ml, Invitrogen) DMEM (Gibco) solution with 10% FBS (Gibco) for 90min. Following digestion the fragments were washed three times with PBS and then transferred to a 15cm cell-culture dish. The bone chips were cultured in alpha MEM (GlutaMAX, Life Technologies) containing 20% MSC qualified FBS (Life Technologies), 2% Penicillin Streptomycin (Life Technologies),1ng/ml murine basic fibroblast growth factor (Thermo Fisher Scientific) and 5ng/ml murine epidermal growth factor (Peprotech). To study the effect of TGFβ or CXCL4, primary Gli1$^+$ bone marrow cells were seeded at a density of 60.000 cells/well in 6-well plates and cytokine treatment was started 24h later. The cytokines were added in fresh medium every 24 hours, for a total of 72 hours, at the following concentrations: TGFβ1 (100-21-10UG, Peprotech) 10ng/ml medium, CXCL4 (795-P4-025, R&D Systems) 400ng/ml. PBS (solvent for TGFβ) and DMSO (solvent for CXCL4) were added as controls. After 72 hours cells were subjected to flow cytometry for α-SMA as described below.

Viral transduction

For retro- and lentiviral transductions, ckit$^+$ cells from wild type littermates were isolated using the autoMACS pro Separator after crushing the compact bone (Miltenyi Biotec). Ckit$^+$ bone marrow cells were pre-stimulated for 24 hours in StemSpan™ Serum-Free Expansion Medium (Stem Cell Technology, Vancouver, Canada) supplemented with murine thrombopoietin (m-tpo) (50 ng/mL; Peprotech), murine stem cell factor (m-scf) (50 ng/mL; Peprotech), IL-6 ng/ml and 10ng/ml IL-3 (both Peprotech). Oncoretroviral vectors were

pseudotyped with ecotropic envelope and produced using standard protocols. Retroviral transduction was performed on retroNectin (Takara Bio) coated cell culture dishes loaded with unconcentrated virus. Cells were then resuspended in virus containing medium in the presence of 10µg/ml polybrene (final concentration). Lentiviral particles were produced by transient transfection with lentiviral plasmid together with pSPAX and VSVG packaging plasmids using TransIT-LT (Mirus). Lentiviral and retroviral particles were concentrated using ultracentrifugation. Lentiviral transduction was performed with concentrated lentiviral supernatant in the presence of 2 µg/ml Polybrene using spin-infection for 90 minutes at 2,200rpm at 37°C.

Co-culture of HSCs and MSCs

For co-culture of Gli1$^+$ stromal cells with c-kit+ hematopoietic stem and progenitor cells expressing control cDNA or ThPO/Jak2(V617F), c-kit+ cells were isolated and pre-stimulated for 24 hours in StemSpan™ Serum-Free Expansion Medium (Stem Cell Technology, Vancouver, Canada) supplemented with murine thrombopoietin (m-tpo) (50ng/mL; Peprotech), and murine stem cell factor (m-scf) (50ng/mL; Peprotech). C-kit cells were then transduced with concentrated lentivirus and 4µg/ml polybrene for 24 hours. Next, the cells were washed and co-cultured with Gli1$^+$ stromal cells which were seeded at a density of 50 000 cells/well in alpha MEM (GlutaMAX, Life Technologies) containing 10% MSC qualified FBS (Life Technologies). For the analysis of stromal cells, hematopoietic cells were washed away (or harvested) and stromal cells were recovered by trypsinization. For the GANT61 experiments cells were treated for the last 48h with 10µM GANT61 in DMSO versus vehicle (DMSO) alone.

Migration assay

Lentivirally transduced c-kit$^+$ cells from wild type littermates of Gli1CreER;tdTomato mice were seeded at 50,000 cells/well in a 24 well plates 24 hours after transduction. Primary Gli1$^+$ bone marrow cells were seeded at 50,000 cells/well in transwells of the InnoCyte Cell Migration Assay (Millipore, #CBA017) above the ckit+ cells (bottom well). Cell migration was measured by flow cytometry from the bottom well. Alpha MEM (GlutaMAX, Life Technologies) containing 20% MSC qualified FCS (Life Technologies), 2% Penicillin Streptomycin (Life Technologies) was used as medium in this system.

In another set of experiments, solely Gli1$^+$ cells were cultured in the transwell (600,000 cells/well) and recombinant Cxcl4 (95-P4-025, R&D Systems) in DMSO was added at 400ng/ml to the medium in the bottom well versus DMSO alone. After 12 hours of incubation, cell migration was measured by either flow cytometry or according to the manufacturer's instructions on a plate reader (BMG Labtech, Clariostar).

Cytokine array

C-kit+ HSC were isolated from 8 week old wild type C57Bl6/J mice (males) as described above and lentivirally or retrovirally transduced with ThPO or Jak2(V617F) versus controls (empty backbone or WT Jak2, respectively). Cells were cultured in StemSpan™ serum-free expansion medium (Stem Cell Technology, Vancouver, Canada) supplemented with murine thrombopoietin (m-tpo) (50ng/mL; Peprotech), and murine stem cell factor (m-scf) (50ng/mL; Peprotech). After 7 days the cells were washed 3 times in PBS and starved in RPMI (Gibco) with 0.5% MSC-FCS (Life Technologies). The supernatant was harvested and incubated with the membranes of the mouse cytokine array (C2000 AAM-CYT-2000-2, Ray Biotech) according to the manufacturer's instructions. Imaging was achieved by chemiluminescence detection with the ChemiDoc imager (BioRad) and quantification by analyzing the pictures with the Protein Array Analyzer plugin for ImageJ.

RNA-Sequencing and bioinformatics

For RNA-Sequencing 6-7 week old bigenic Gli1CreER;tdTomato mice were injected with tamoxifen (3x10mg p.o.), subjected to lethal irradiation 10 days after the last tamoxifen dose and received bone marrow of wildtype littermates that had been transduced with ThPO or control (empty backbone) lentivirus as described above. 10 weeks after bone marrow transplantation mice were sacrificed**,** whole bone marrow samples were lineage-depleted using paramagnetic microbeads and an autoMACS pro magnetic separator (Miltenyi Biotec). $Gli1^+$ cells were sorted as $lineage^-$, GFP^-, $tdTomato^+$ on a FACS Aria II (BD Bioscience) into PBS (5% FBS) and frozen in liquid nitrogen as pellets. RNA was extracted using TRIZOL Reagent (Life Technologies) according to the manufacturer's instructions. cDNA libraries were generated using the Smart-Seq V4 ultra low input RNA kit (Clontech Laboratories) according to manufacturer instructions. Subsequently, amplified cDNA libraries were further processed using the Truseq Nano DNA sample prep guide (Illumina) generating Illumina Hiseq compatible pooled libraries that were sequenced paired-end (2x75 cycles) on a Hiseq2500 platform (Illumina).

The unprocessed data resulting from Hiseq2500 (Ilumina) were demultiplexed using casava (Ilumina). Quality metrics of the resulting fastq files were measured using the programs fastqc (Babraham bioinformatics) and multiqc (http://multiac.info). The later program summarizes the result of the first. An insert size estimate was performed by aligning the reads to a reference transcriptome using BWA (http://bio-bwa.sourceforge.net) and the actual insert size estimate was done with the program collectInsertSizeMetrics from the picard tools suite. The splicing aware alignment was performed using Tophat2 (https://ccb.jhu.edu/software/tophat/index.shtml) using the previously computed estimate for the insert size. Prior to the alignment the SMARTer adapters were trimmed. Gene and isoform abundance estimation was performed using cufflinks (http://cole-trapnell-lab.github.io/cufflinks/). Gene counts that were used in the differential expression analysis, clustering

and principle component plots were obtained using HTseq counts (http://www-huber.embl.de/HTSeq/doc/count.html) using the intersect strict settings. Finally principle component analysis and clustering was performed using R (https://www.r-project.org/).

Directional pathway enrichment analysis was performed using the PIANO R package (Bioconductors, https://bioconductor.org/packages/release/bioc/html/piano.html, *[1-3]* and a collection of pathway adapted to mus musculus (GSKB R package, Bioconductors, https://bioconductor.org/packages/release/data/experiment/html/ gskb.html). PIANO compute the significance of the directional enrichment of a pathway by aggragating (here through the median) the FDR corrected p-values yielded by a set of enrichment methods. The method used here are : mean, median, sum, maxmean, stoufer, fisher, tail strength, wilcoxon and PAGE. The detailed explanation of the different methods can be found in . The collection of pathway used here as gene sets is derived from MSigDB canonical pathway complemented by a few other currated pathway databases and metabolic reaction networks (see GSKB R package). Reactome was discarded from the pathway sources as it was too much redundant with itself and other pathway ressources. The script of the pathway enrichment analysis is available at GITHUBADRESS.

Flow cytometry

Bone marrow (BM) cells were isolated by flushing and crushing pelvis and hind leg bones with PBS (GIBCO) + 2% FBS + Penicillin/Streptomycin (GIBCO). Whole bone marrow was lysed on ice with red blood cell (RBC) lysis solution (Invitrogen/Life Technologies), and washed in PBS (GIBCO) + 2% FBS. Single-cell suspensions of spleen were prepared by pressing tissue through a cell strainer followed by red blood cell lysis. Cells were labeled with the following monoclonal, directly fluorochrome conjugated antibodies: anti-mouse: Ter119 (eBioscience efluor 450), Gr1 eBioscience (efluor 450), CD11b (eBioscience, efluor 450), B220 (efluor 450 eBioscience), CD3 (efluor 450 eBioscience), CD150 (PeCy7 BioLegend), CD48 (APCCy7 Biolegend), CD34 (Alexa Fluor 700 eBioscience), ckit (APC eBioscience), Sca1 (PE, eBioscience), Gr1 (Alexa Fluor 700, eBioscience), CD11b (APC, eBioscience), CD3 (PE, eBioscience), CD19 (PeCy7 eBioscience), Ter119 (FITC, eBioscience), CD31 (APC, Biolegend), CD34 (FITC, eBioscience), CD29 (APC, eBioscience), Sca1 (APC-Cy7, Biolegend), CD44 (PE-Cy7 eBioscience); CD105 (PE-Cy7, Biolegend), CD73 (APC, Biolegend), PDGFR**α** (APC, Biolegend), CD31 (APC, Biolegend), CD34 (FITC, eBioscience), CD29 (APC, eBioscience), Sca1 (APC-Cy7, Biolegend), CD44 (PE-Cy7 eBioscience); CD105 (PE-Cy7, Biolegend), CD73 (APC, Biolegend), PDGFR**α** (APC, Biolegend). Anti-human: CD90 (PeCy7, BD Pharmingen), CD105 (V450, BDPharmingen), Nestin (PE, RnD Systems). Further the following primary non-conjugated antibodies were used: Nestin (1:100, Abcam), CD51 (1:100, Biolegend), **α**SMA (1:100 Sigma), Gli1 (1:100, Novus biological). For flow cytometry, cells were stained in antibodies diluted as 1:100 in 2% FBS/PBS for 30 min on ice.

The staining of the intracellular antigens was performed after fixation and permeabilization of the cells (Cytofix/Cytoperm solution, BD Biosciences). Following incubation with primary antibodies, cells were washed in PBS and incubated with the appropriate AF647/AF488 secondary antibodies (Jackson Immuno) at 1:200 for 15min on ice. For detection of apoptosis, the APC Annexin V antibody (BD Bioscience, #550474) was used together with the Annexin V Binding Buffer (BD Bioscience, #556454) and co-staining for DAPI or 7AAD (BD Bioscience, #559925) was performed according to the manufacturer's instructions. For staining of pSTAT5, cells were fixed in 4% paraformaldehyde (Sigma) for 10 minutes followed by permeabilization with 90% ice cold methanol (Sigma) for 30 minutes followed by staining with the pSTAT5 antibody (PE-Cy7, 1:100, BD Bioscience #560117) in PBS. To increase the flow efficiency, whole bone marrow samples were lineage-depleted (for HSC staining and stromal cells) or –enriched (lineages) using paramagnetic microbeads and an autoMACS pro magnetic separator (Miltenyi Biotec). All flow cytometric analyses were performed at the LSR II Flow Cytometer or Canto II (both BD Biosciences). For flow cytometric analyses DAPI (1mg/ml 1:1000) was added in order to exclude dead cells. Data were analyzed by using Flow Jo software (Version 9.6.2, Tree Star Inc).

Viral vector cloning

The murine Jak2 cDNA was cloned into the retroviral vector MSCV-IRES EGFP (a gift from Tannishtha Reya Addgene #20672). The V617F mutation in Jak2 was achieved using site-directed mutagenesis (Quikchange-XL; Agilent). The murine Thrombopoietin cDNA (MGC clone 3593885, GE Dharmacon) was PCR amplified using the primer sequences 5'-AGACCGGTGCCACCATGGAGCTGACTGATTTGCTCC-3' and 5'-TCACGCGTCTATGTTTCCTGAGACAAATTCC-3'. Subsequently, the PCR product was digested with AgeI and XhoI and cloned into the pRRL.PPT.SFFV.IRES2.EGFP.PRE (kindly provided by A. Schambach and C. Baum, Hannover Medical School, Hannover, Germany).

Histological an immunohistochemical analysis

For histological and immunohistochemical analyses, murine organs were fixed in 4% formaldehyde overnight, dehydrated and prepared for paraffin embedding. H&E staining and reticulin staining was done according to routine protocols. Human bone marrow biopsies were fixed for 24 hours using 12% buffered formaldehyde plus 64% methanol, decalcified (EDTA), dehydrated and embedded in paraffin. For immunohistochemistry, samples were deparaffinized and stained as follows.

Immunohistochemical analysis was performed using a primary antibody for Gli1 (Novus biological, NG-600-600, 1:100). Antigen demarcation was achieved by pressure cooker treament in citrate buffer (Vector Antigen unmasking solution). After blocking (Blocking Kit; Vector Laboratories) and 3%H2O2 treatment, sections were incubated with the primary antibody. Biotinylated monoclonal goat-anti-rabbit (Vector Laboratories) was

used as a secondary antibody. Detection was performed using the Vectastin ABC Kit (Vector Laboratories). Slides were counterstained with hematoxylin. Cell numbers and co-staining was evaluated in 400x magnification at the Keyence BZ9000 by a blinded pathologist. Co-staining by immunohistochemistry in human bone marrow biopsies was achieved by using the regular staining as described above for the first antigen (Leptin Receptor, 1:100, Santa Cruz sc-1834; Nestin 1:100, Abcam Ab134017; NG2 1:100, Millipore AB5320) followed by staining of the second antigen (Gli1 1:100, Novus biological, NG-600-600) with the ImmPRESS-AP Anti Rabbit IgG (alkaline phosphatase) polymer detection kit (Vector MP-5401) and the Vector Red Alkalkine Phosphatase (Red AP) Substrate Kit (#SK5100).

For immunofluorescence studies, tissue was fixed in 4% paraformaldehyde on ice for 1 hour, then incubated in 30% sucrose in PBS at 4°C overnight. OCT-embedded (Sakura Finetek) tissues were cryosectioned into 6µm sections and mounted on Superfrost slides (Fisher Scientific). Sections were washed in 1X PBS, blocked in 10% normal goat serum (Vector Labs) and incubated with primary antibodies specific for alpha SMA (1:200, Sigma, # A2547), CD31 (1:100, ebioscience, #14-0311 and AF3628 1:100 R&D Systems), leptin receptor (1:100; sc-1834, Santa Cruz), CD105 (1:100, MAB 1320, R&D Systems), Nestin (1:100, abcam ab134017), NG2 (AB5320 Millipore tyrosine hydroxylase (1:100, #AB152 millipore), GFAP (1:100; DAKO Z0334). Secondary antibodies were FITC-, or Cy5-conjugated (Jackson ImmunoResearch). To stain lipid droplets OCT sections were incubated with LipidTox Deep Red neutral lipid stain (Invitrogen, H34477) at 1:200 in PBS for 1 hour. To stain bone, we used Fetuin A from fetal bovine serum (Sigma aldrich #F2379) which was purified over HiLoad 16/60 Superdex 200pg columns (GE Healthcare #28989335) in an ÄKTA Purifier (GE Healthcare #28406264) and then conjugated with Alexa Fluor 647 NHS Ester (Invitroagen #A37573), according to the manufacturer's instructions. All sections were counterstained with DAPI (4´,6´-´diamidino-2-phenylindole) and mounted in Prolong Gold (Life Technologies). Images were obtained by confocal microscopy (Nikon C1 eclipse and Zeiss LSM 710).

Clearing and imaging of mouse bone

Solvent-based optical clearing was performed using a sequence of dehydration steps in ethanol (50% for 12 hours, 70% for 6 hours, and 100% for 6 hours), followed by direct immersion on ethyl cinnamate (Sigma, #112372) for 12 hours in order to render the bone transparent. Vasculature was labeled with a CD31-AF647 antibody (BioLegend, #102516). Imaging was performed using an upright scanning confocal microscope (Leica TCS SP8; Leica Microsystems, Wetzlar, Germany). Optical sections were acquired with an optimised step-size of 2µm for a total depth of 120µm. Image post-processing and 3D rendering was performed with Imaris (Bitplane, v8.1).

Real Time PCR Experiments

Tissue was harvested and immediately snap frozen in liquid nitrogen. RNA from was extracted according to the manufacturer instructions using the RNeasy Mini Kit (Qiagen)

and 600ng of total RNA was reverse transcribed with iScript (BioRad). During the RNA extraction DNA was removed by a DNAse digestion step (Life Technologies). Quantitative polymerase chain reactions were carried out with iQ-SYBR Green supermix (BioRad) and the Applied Biosystems, 7300 Teal-Time PCR System. Cycling conditions were 95°C for 3 minutes then 40 cycles of 95°C for 15 seconds and 60°C for 1 minute, followed by one cycle of 95°C for 10 seconds. Glyceraldehyde-3-phosphate dehydrogenase (GAPDH) was used as a housekeeping gene. Data was analyzed using the $2^{-\Delta\Delta ct}$ method. Primers are listed in tables S3-S4.

Immunocytochemistry

Human MSCs (n=4 healthy; n=4 MPN patients) were seeded at a density of $1x10^5$ cells/well in chamber slides (Nunc, lab tek, Thermo Fischer Scientific, Darmstadt, Germany), the next day cells were treated for 24 hours with 10 μM Gant61 (Sigma, Munich, Germany). After washing and fixation steps, cells were stained with α-SMA antibody (Sigma, Munich, Germany) at 1:400 for 3h at RT, and co-stained with the fluorescent secondary-labeled antibody donkey anti-mouse Alexa Fluor 488 (Thermo Fischer Scientific, Darmstadt, Germany) at 1:200 for 1h at RT. After washing, cells were stained with the primary unconjugated antibody Gli1 (Novus Biologicals, Wiesbaden Nordenstadt, Germany) at 1:100 overnight at 4 degree and stained with the fluorescent secondary-labeled antibody goat anti-rabbit Alexa Fluor 633 (Thermo Fischer Scientific, Darmstadt, Germany) at 1:200 for 1h at RT. Nuclear staining was performed with DAPI at 1ug/mL for 15 minutes at RT and mounting with Vectashield (#H-1000, Biozol, Eching, Germany). Images were acquired with a confocal laser scanning microscope (LSM 710; Zeiss, Germany) running the Zen 2012 (Zeiss) software.

Image Quantification

The distance to either $CD31^+$ endothelial cells or Fetuin A^+ bone was performed by ImageJ. Random images were acquired by the LSM710 confocal microscope (Zeiss) with a magnification of 800x (at least 3-4 images of 3 mice per group). All images were processed by ImageJ. First, all images were split into RGB channels. Gaussian blur was applied to adjust background noise in all channels. Auto-threshold was used to convert intensity values of CD31 staining and $tdTomato^+$ area into binary data. Then a distance map was created from the binary data. One maximum intensity point was selected as the representative point of each nucleus. These points were used to divide the binary $tdTomato^+$ area into smaller areas representing single $tdTomato^+$ cells. Selected nuclei and the divided $tdTomato^+$ areas were overlayed on a CD31 or Fetuin A generated distance map. The distance value from each nucleus to the nearest CD31 or Fetuin A positive area was calculated.

Quantification of $GFAP^+$ and tyrosine $hydroxylase^+$ areas was performed by Image J using the Gaussian blur and auto-threshold function. The number of $tdTomato^+$, αSMA^+ and αSMA^+ /$tdTomato^+$ cells were calculated by Image J using split single channels (RGB). Auto-threshold was again used to identify αSMA^+ and $tdTomato^+$ binary area and the overlying

point of maximal intensity of each nucleus was used to quantify the number of each cell population. CD31 surface area from immunohistochemistry was calculated using the number of stained pixels per total pixels in Adobe Photoshop CS5 (Adobe Systems Inc.). Reticulin staining (myelofibrosis grade) was quantified by a blinded hematopathologist based on the WHO criteria. $Gli1^+$ cells in human bone marrow biopsies were counted by a blinded hematopathologist in at least 3 random high power fields (400x) per patient. The association to bone and vasculature was noted during counting. Gli1-$tdTomato^+$ cell distribution and co-localization with marker expression was counted in backbone and sternal bone sections (at least 4/mouse) using the LSM710 confocal microscope.

QUANTIFICATION AND STATISTICAL ANALYSIS

Data are presented as mean±SEM . Comparison of two groups was performed using unpaired t-test. Paired t-test was used for comparsion of repeated measured in the same group. For multiple group comparison analysis of variance with posthoc Tukey correction was applied. Statistical analyses were performed using GraphPad Prism 5.0c (GraphPad Software Inc., San Diego, CA). A p value of less than 0.05 was considered significant.

DATA AND SOFTWARE AVAILABILITY

RNA Sequencing data is available online through the European Nucleotide Archive, which is hosted by the European Bioinformatics Institute (EBI). Accession number: ERA829202

SUPPLEMENTARY FIGURES:

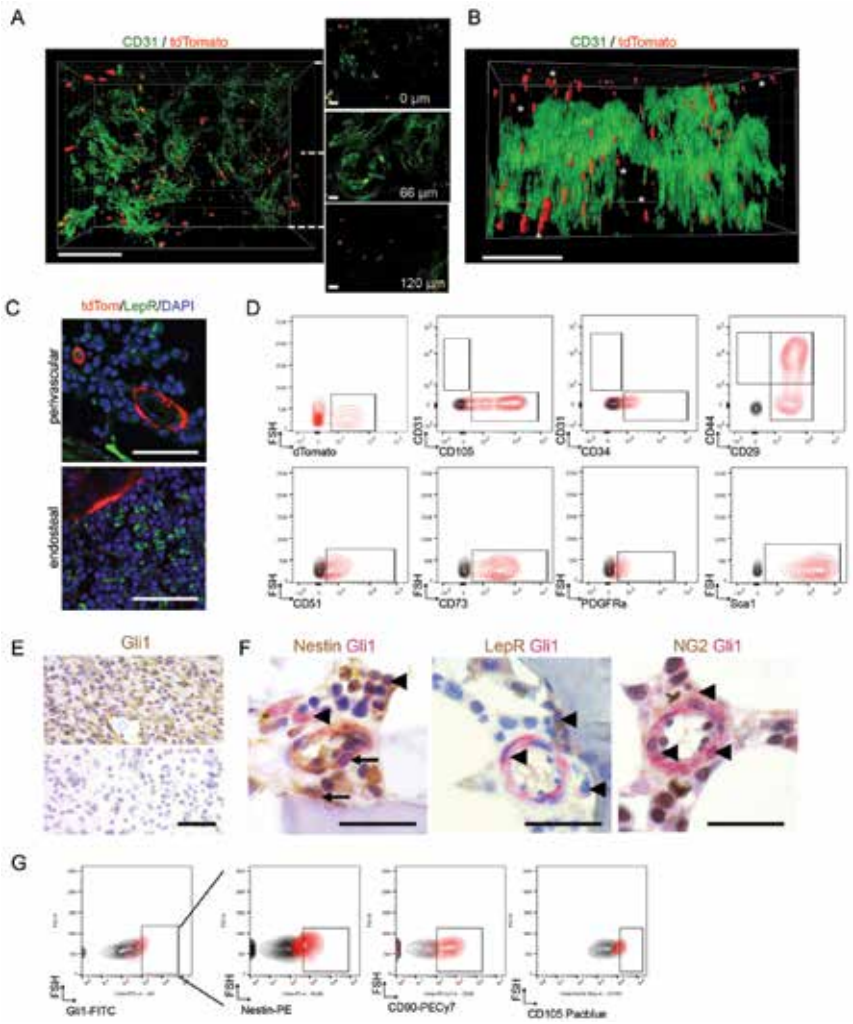

Figure S1: Gli1^{+} cells in mouse and human (related to Figure 1)
(A-B) Confocal Z-stack (120µm) of mouse sternal bone after clearing and CD31 staining. Mid panel shows representative 2D images from the top, middle and bottom of the Z-stack. Asterisks mark the endosteal niche. Of note, many Gli1^{+} cells that are in the endosteal niche are not associated with the vasculature. Scale bars 50 µm. **(C)** Representative images of leptin-receptor (LepR) staining. Scale bars 30 µm. **(D)** Representative flow cytometric plots of markers expressed in tdTomato^{+} cells from whole bone marrow of bigenic Gli1CreER^{t2};tdTomato mice at 10 days after tamoxifen pulse (3x10mg p.o.). tdTomato^{+} cells were gated as shown in the first panel, and then co-expression of other markers was analyzed. The black population indicates the unstained, isotype control. **(E)** Validation of the Gli1 antibody for immunohistochemistry in EDTA-decalcified human glioblastoma multiforme tissue (upper panel). Negative control (only secondary antibody) to exclude endogenous peroxidase activity on the lower panel. Scale bar 50 µm. **(F)** Representative images of human bone marrow from healthy subjects co-stained for Gli1 (red) and Nestin, leptin receptor (LepR) and NG2 (brown). Arrows indicating double positive cells and arrow heads indicating cells that express only one of the antigens. Scale bars 50µm. **(G)** Representative flow cytometric plots and gating of human Gli1 expressing MSC (black indicating negative control). Quantification is illustrated in Figure 1M.

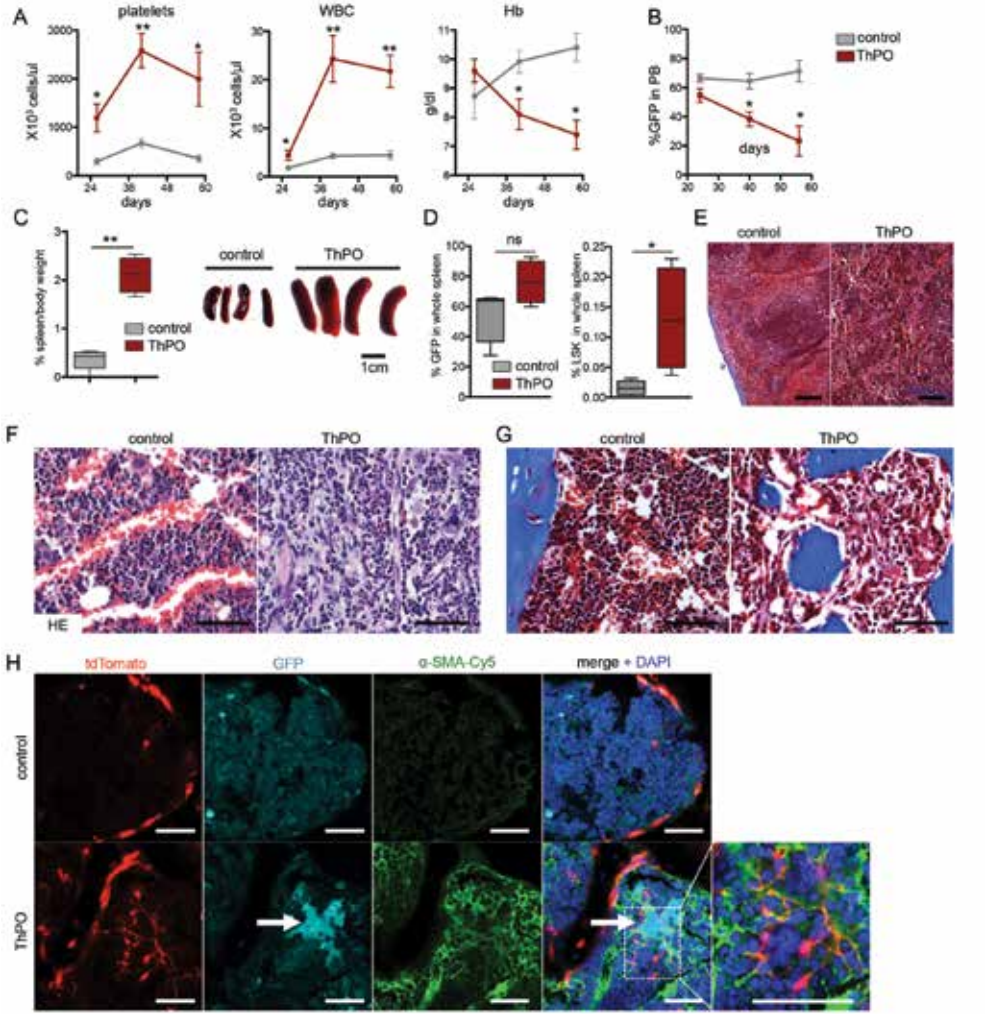

Figure S2: Fate tracing of Gli1^{+} cells in thrombopoietin induced myelofibrosis (related to Figure 2)
(A) Time course of platelets, white blood cells (WBC) and hemoglobin (Hb) following bone marrow transplantation of thrombopoietin (ThPO) expressing or control cells in bigenic Gli1CreER;tdTomato mice (see Figure 2). *p<0.05, *p<0.01 by t-test, mean±SEM. **(B)** Time course of green fluorescent protein (GFP) expressing cells (gene marking) in peripheral blood (PB) *p<0.05 by t-test, mean±SEM**. (C)** Spleen weight standardized to body weight and representative spleen images in the control and thrombopoietin (ThPO) group. *p<0.01 by t-test, box plot and whiskers, min to max. **(D)** Percentage of GFP^{+} and lineage^{low}Sca1^{+},c-kit^{+} (LSK) hematopoietic stem cells in the spleen of mice transplanted with control or thrombopoietin (ThPO) expressing cells. **p<0.01 by t-test, box plot and whiskers, min to max. **(E-G)** Representative images of trichrome stained spleens and trichrome and hematoxylin-eosin (HE) stained bone marrows of control and thrombopoietin group (ThPO). Scale bars 100µm. **(H)** Representative images of sternal bones from control and thrombopoietin (ThPO) overexpressing bone marrows stained for alpha smooth muscle actin (αSMA-Cy5). Arrow shows GFP expressing ThPO+ megakaryocytes. Scale bars 50µm.

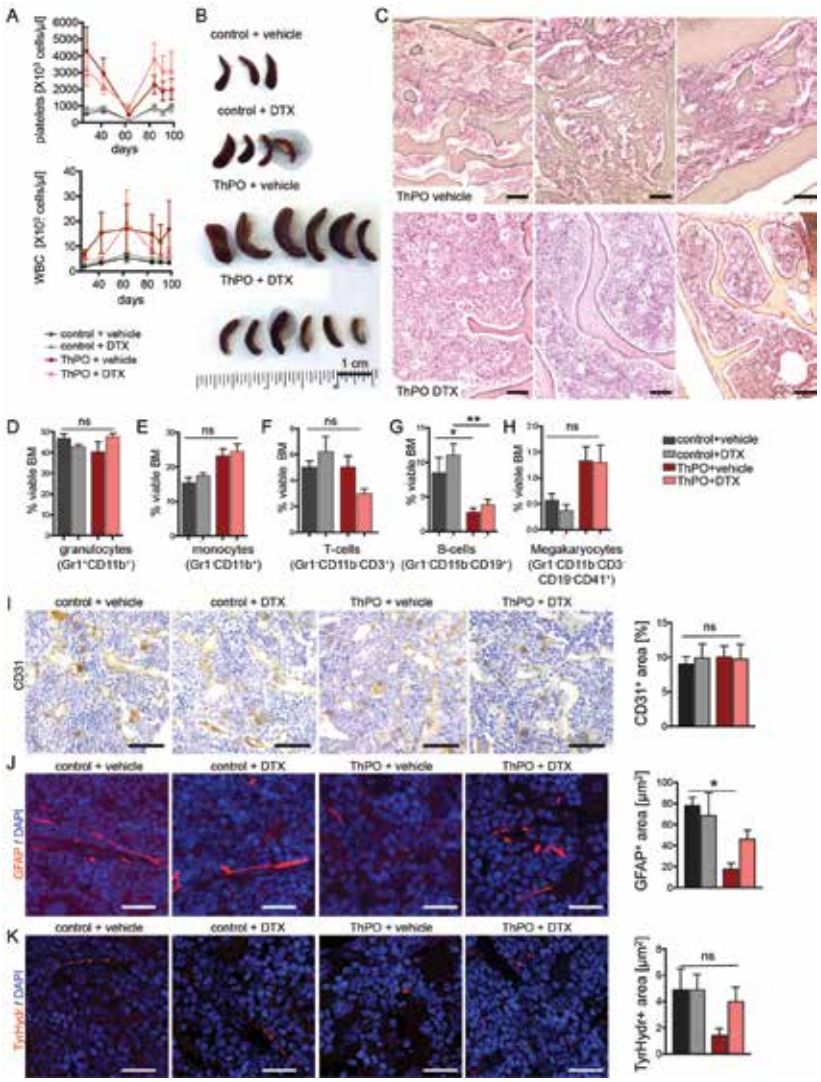

Figure S3: Ablation of Gli1⁺ cells does not affect myeloid lineages (related to Figure 3)
(A) Time course of platelets and white blood cells (WBC) in mice transplanted with bone marrow cells expressing thrombopoietin (ThPO) or control plasmids, with and without ablation of Gli1⁺ cells in bigenic Gli1CreER;iDTR mice. (DTX, diphtheriatoxin; ThPO, thrombopoietin; vehicle, PBS). **(B)** Representative images of spleens following ablation of Gli1⁺ cells in bigenic Gli1CreER;iDTR mice. (DTX, diphtheriatoxin; ThPO, thrombopoietin; vehicle, PBS). **(C)** Representative images of reticulin stained sections from ThPO overexpressing mice that received vehicle or diphtheriatoxin (DTX) injection indicating severe osteosclerosis in the vehicle group whereas after DTX injection almost no osteosclerosis was detectable. Scale bars 100µm. **(D-H)** Quantification of granulocytes, monocytes, CD3⁺ T-cells, CD19+ B-cells and megakaryocytes as a percentage of viable bone marrow cells following ablation of Gli1⁺ cells in control and thrombopoietin overexpression group by diphtheriatoxin (DTX) versus vehicle (PBS). mean±SEM. **(I)** Representative images and surface area quantification of CD31 stained bone marrows with and without ablation of Gli1⁺ cells in bigenic Gli1CreER;iDTR mice. Scale bars 25µm. Mean±SEM. **(J-K)** Representative images and surface area quantification of glial fibrillary acidic protein (GFAP) and tyrosine hydroxylase stained bone marrows with and without ablation of Gli1⁺ cells in bigenic Gli1CreER;iDTR mice. Scale bars 25µm. Mean±SEM.*p<0.05 by one way ANOVA with posthoc Tukey, mean±SEM.

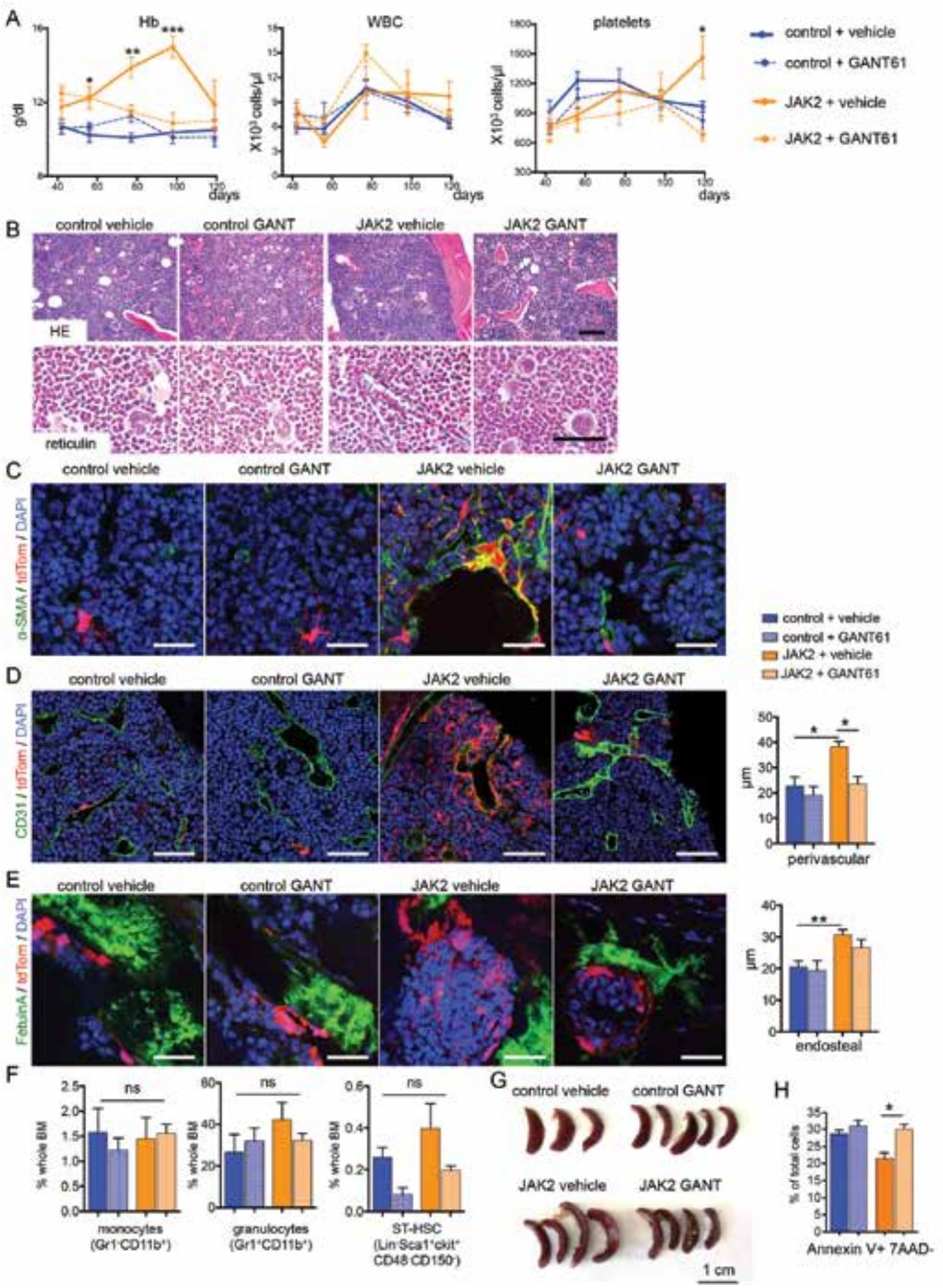
A
Hb
WBC
platelets
g/dl
X10³ cells/µl
days
control + vehicle
control + GANT61
JAK2 + vehicle
JAK2 + GANT61
B
control vehicle
control GANT
JAK2 vehicle
JAK2 GANT
HE
reticulin
C
α-SMA / tdTom / DAPI
D
CD31 / tdTom / DAPI
µm
perivascular
E
FetuinA / tdTom / DAPI
endosteal
F
% whole BM
ns
monocytes (Gr1⁺CD11b⁺)
granulocytes (Gr1⁺CD11b⁺)
ST-HSC (Lin⁻Sca1⁺ckit⁺ CD48⁻CD150⁺)
G
1 cm
H
% of total cells
Annexin V+ 7AAD-

Figure S4: GANT61 treatment ameliorates myelofibrosis by inhibiting both Gli1$^+$ cell expansion and the malignant hematopoietic clone (related to Figure 4)
(A) Time course of hemoglobin (Hb), white blood cells (WBC) and platelets following bone marrow transplantation of hematopoietic stem cells retrovirally transduced with Jak2(V617F) (JAK2) or control cDNA (both MCSV-IRES-GFP retroviral backbone vector) in bigenic Gli1CreER;tdTomato mice treated with GANT61 or vehicle (corn oil/ethanol).*p<0.05; **p<0.01, ***p<0.001 by one way ANOVA with posthoc Tukey, mean±SEM. **(B)** Representative images of hematoxylin and eosin (HE) or reticulin stained bone marrows from Gli1CreER;tdTomato mice transplanted with JAK2(V617F) (JAK2) or control cDNA expressing bone marrow and treated with GANT61 (GANT) or vehicle. Scale bars 100µm. **(C)** Representative images of alpha smooth muscle actin (α-SMA) staining in bone marrows from bigenic Gli1CreER;tdTomato mice transplanted with Jak2(V617F) (JAK2) or control cDNA expressing bone marrow and treated with GANT61 (GANT) or vehicle. Scale bars 50µm. For quantification see Figure 4E. **(D-E)** Representative images of CD31 and Fetuin A stained bone marrows from bigenic Gli1CreER;tdTomato mice transplanted with Jak2(V617F) (JAK2) or control cDNA expressing bone marrow and treated with GANT61 (GANT) or vehicle. Distance to either CD31$^+$ endothelial cells or Fetuin A$^+$ bone was measured by Image J. Scale bars 50µm in D and 100µm in E, *p<0.05; **p<0.01 by one way ANOVA with posthoc Tukey, mean±SEM. **(F)** Frequency of monocytes, granulocytes and short term hematopoietic stem cells (ST-HSC) as percentage of whole viable bone marrow (BM) from Gli1CreER;tdTomato mice transplanted with Jak2(V617F) (JAK2) or control cDNA expressing bone marrow and treated with GANT61 (GANT) or vehicle; mean±SEM.**(G)** Representative images of spleens from Gli1CreER;tdTomato mice transplanted with JAK2 WT (control) or JAK2(V617F) (JAK2) expressing bone marrow and treated with GANT61 (GANT) or vehicle. (H) Quantification of early apoptosis (AnnexinV$^+$7AAD$^-$) in sort-purified c-kit$^+$ HSPCs [expressing control or Jak2(V617F) cDNA] treated with GANT61 or vehicle. *p<0.05, by one way ANOVA with posthoc Tukey; mean±SEM. n=3.

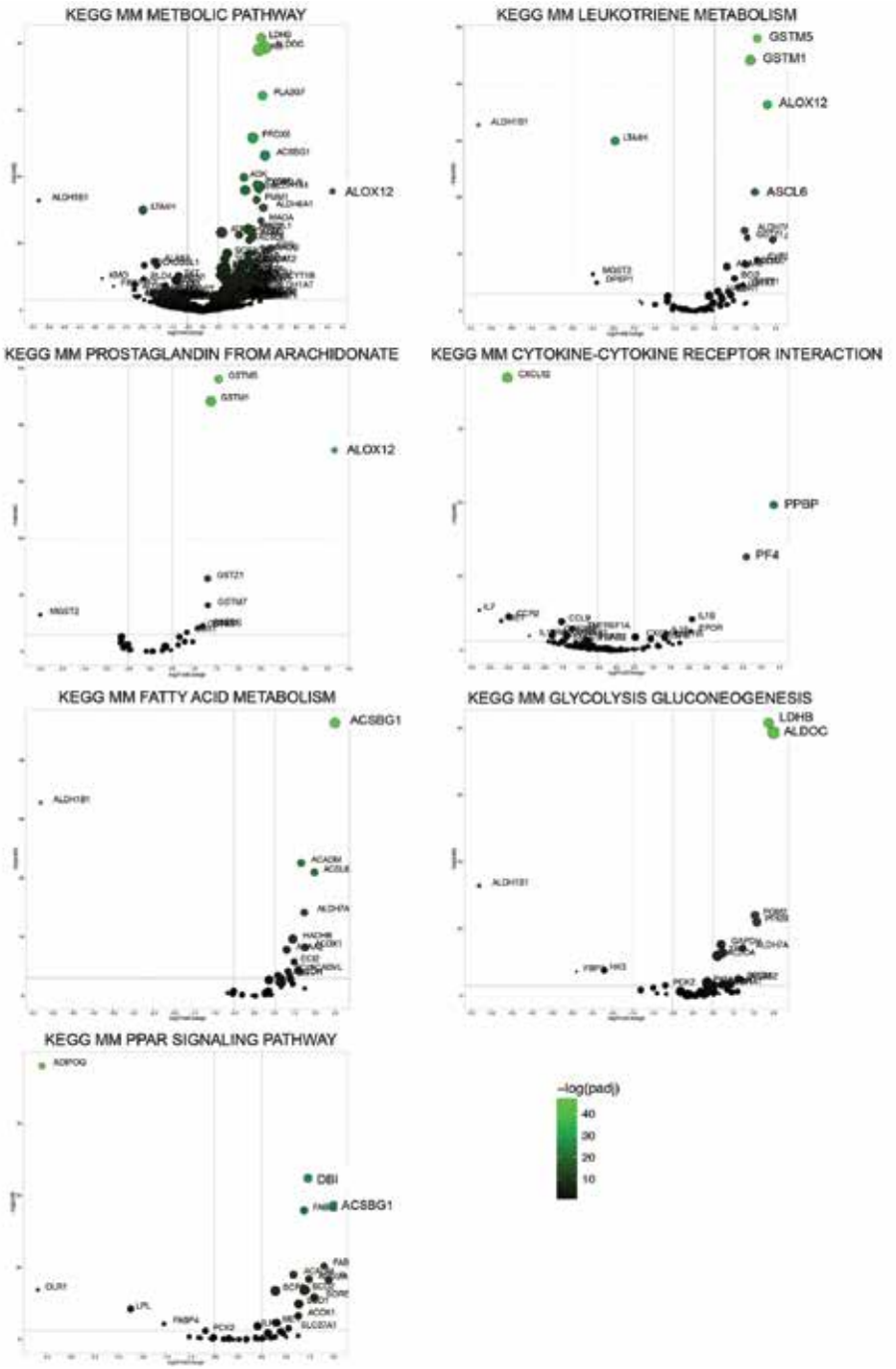

Figure S5: Thrombopoietin overexpression in hematopoietic stem cells leads to distinct transcriptional changes in Gli1^{+} cells (related to Figure 5)
Volcano plots highlighting the distinct pathways from Figure 5.

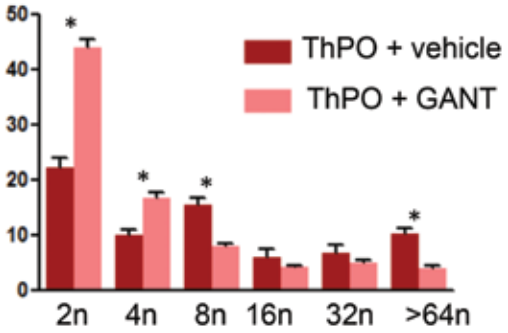

Figure S6: GANT61 reduces the ploidy of ThPO overexpressing megakaryocytes (related to Figure 6)
Quantification of megakaryocyte ploidy after permeabilization, staining for CD41 and DAPI of c-kit+ HSC from wildtype mice that have been transduced with thrombopoietin (ThPO) and treated with GANT61 (10µM) or vehicle (DMSO) for 48h. *p<0.05 by t-test, mean±SEM.

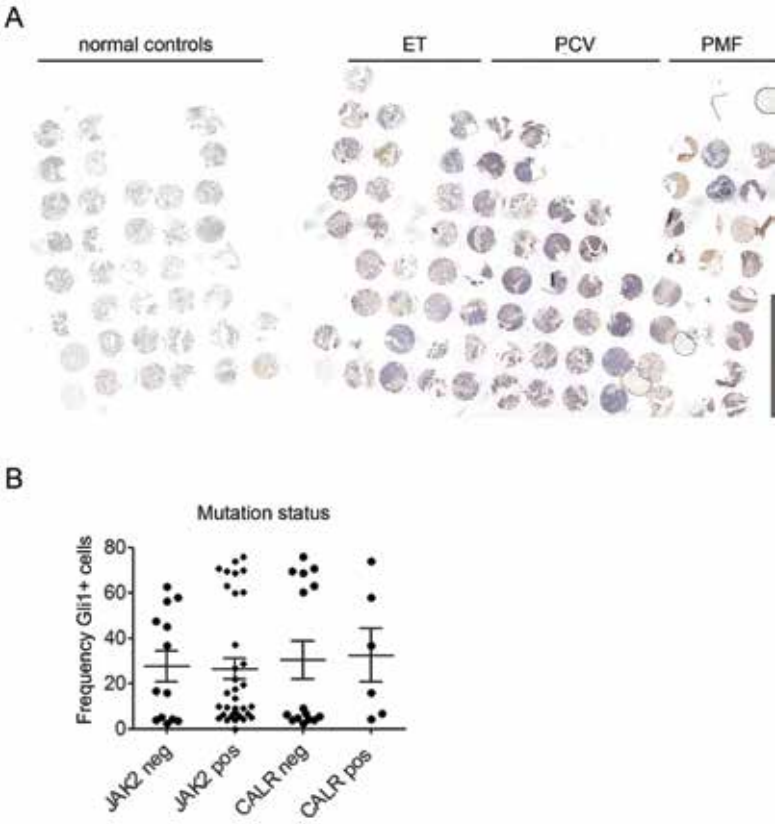

Figure S7: Gli1 expression in human bone marrow biopsies (related to Figure 7)
(A) Overview of tissue microarrays from healthy controls (no primary bone marrow disease) and patients with essential thrombocythemia (ET), polycythemia vera (PCV) and primary myelofibrosis (PMF) stained for Gli1. **(B)** Gli1^{+} cells frequency in the bone marrow of patients with regards to their mutation status. mean±SEM. See Table S1 for patient characteristics.

REFERENCES

1. Kuter, D.J., et al., *Bone marrow fibrosis: pathophysiology and clinical significance of increased bone marrow stromal fibres.* Br J Haematol, 2007. **139**(3): p. 351-62.
2. Tefferi, A., et al., *Proposals and rationale for revision of the World Health Organization diagnostic criteria for polycythemia vera, essential thrombocythemia, and primary myelofibrosis: recommendations from an ad hoc international expert panel.* Blood, 2007. **110**(4): p. 1092-7.
3. Levine, R.L., *JAK-mutant myeloproliferative neoplasms.* Curr Top Microbiol Immunol, 2012. **355**: p. 119-33.
4. Klampfl, T., et al., *Somatic mutations of calreticulin in myeloproliferative neoplasms.* N Engl J Med, 2013. **369**(25): p. 2379-90.
5. Tefferi, A., et al., *CALR and ASXL1 mutations-based molecular prognostication in primary myelofibrosis: an international study of 570 patients.* Leukemia, 2014. **28**(7): p. 1494-500.
6. Tefferi, A., et al., *The prognostic advantage of calreticulin mutations in myelofibrosis might be confined to type 1 or type 1-like CALR variants.* Blood, 2014. **124**(15): p. 2465-6.
7. Nangalia, J., et al., *Somatic CALR mutations in myeloproliferative neoplasms with nonmutated JAK2.* N Engl J Med, 2013. **369**(25): p. 2391-405.
8. Levine, R.L. and D.G. Gilliland, *Myeloproliferative disorders.* Blood, 2008. **112**(6): p. 2190-8.
9. Mehta, J., et al., *Epidemiology of myeloproliferative neoplasms in the United States.* Leuk Lymphoma, 2014. **55**(3): p. 595-600.
10. Tefferi, A., *Primary myelofibrosis: 2012 update on diagnosis, risk stratification, and management.* Am J Hematol, 2011. **86**(12): p. 1017-26.
11. Schmidt, T., et al., *Loss or inhibition of stromal-derived PlGF prolongs survival of mice with imatinib-resistant Bcr-Abl1(+) leukemia.* Cancer Cell, 2011. **19**(6): p. 740-53.
12. Schepers, K., et al., *Myeloproliferative neoplasia remodels the endosteal bone marrow niche into a self-reinforcing leukemic niche.* Cell Stem Cell, 2013. **13**(3): p. 285-99.
13. Schneider, R.K., et al., *Activated fibronectin-secretory phenotype of mesenchymal stromal cells in pre-fibrotic myeloproliferative neoplasms.* J Hematol Oncol, 2014. **7**(1): p. 92.
14. Arranz, L., et al., *Neuropathy of haematopoietic stem cell niche is essential for myeloproliferative neoplasms.* Nature, 2014. **512**(7512): p. 78-81.
15. Kramann, R., D.P. DiRocco, and B.D. Humphreys, *Understanding the origin, activation and regulation of matrix-producing myofibroblasts for treatment of fibrotic disease.* J Pathol, 2013. **231**(3): p. 273-89.
16. Schepers, K., T.B. Campbell, and E. Passegue, *Normal and leukemic stem cell niches: insights and therapeutic opportunities.* Cell Stem Cell, 2015. **16**(3): p. 254-67.
17. Kramann, R., et al., *Perivascular Gli1+ progenitors are key contributors to injury-induced organ fibrosis.* Cell Stem Cell, 2015. **16**(1): p. 51-66.
18. Yu, J., T.J. Carroll, and A.P. McMahon, *Sonic hedgehog regulates proliferation and differentiation of mesenchymal cells in the mouse metanephric kidney.* Development, 2002. **129**(22): p. 5301-12.
19. Aberger, F. and I.A.A. Ruiz, *Context-dependent signal integration by the GLI code: the oncogenic load, pathways, modifiers and implications for cancer therapy.* Semin Cell Dev Biol, 2014. **33**: p. 93-104.
20. Harrison, C., et al., *JAK inhibition with ruxolitinib versus best available therapy for myelofibrosis.* N Engl J Med, 2012. **366**(9): p. 787-98.
21. Harrison, C.N., et al., *Long-term findings from COMFORT-II, a phase 3 study of ruxolitinib vs best available therapy for myelofibrosis.* Leukemia, 2016.

22. Yan, X.Q., et al., *A model of myelofibrosis and osteosclerosis in mice induced by overexpressing thrombopoietin (mpl ligand): reversal of disease by bone marrow transplantation.* Blood, 1996. **88**(2): p. 402-9.
23. Villeval, J.L., et al., *High thrombopoietin production by hematopoietic cells induces a fatal myeloproliferative syndrome in mice.* Blood, 1997. **90**(11): p. 4369-83.
24 .Wernig, G., et al., *Efficacy of TG101348, a selective JAK2 inhibitor, in treatment of a murine model of JAK2V617F-induced polycythemia vera.* Cancer Cell, 2008. **13**(4): p. 311-20.
25. Lauth, M., et al., *Inhibition of GLI-mediated transcription and tumor cell growth by small-molecule antagonists.* Proc Natl Acad Sci U S A, 2007. **104**(20): p. 8455-60.
26. Moshai, E.F., et al., *Targeting the hedgehog-glioma-associated oncogene homolog pathway inhibits bleomycin-induced lung fibrosis in mice.* Am J Respir Cell Mol Biol, 2014. **51**(1): p. 11-25.
27. Kramann, R., et al., *Pharmacological GLI2 inhibition prevents myofibroblast cell-cycle progression and reduces kidney fibrosis.* J Clin Invest, 2015. **125**(8): p. 2935-51.
28. Varemo, L., J. Nielsen, and I. Nookaew, *Enriching the gene set analysis of genome-wide data by incorporating directionality of gene expression and combining statistical hypotheses and methods.* Nucleic Acids Res, 2013. **41**(8): p. 4378-91.
29. Bares, V. and X. Ge, *gskb: Gene Set data for pathway analysis in mouse.* R package version 1.6.1., 2015.
30. Abraham, N.G., et al., *Modulation of erythropoiesis by novel human bone marrow cytochrome P450-dependent metabolites of arachidonic acid.* Blood, 1991. **78**(6): p. 1461-6.
31. Desplat, V., et al., *Incorporation and effect of arachidonic acid on the growth of human myeloma cell lines.* Mediators Inflamm, 1999. **8**(2): p. 115-8.
32. Chen, Y., D. Li, and S. Li, *The Alox5 gene is a novel therapeutic target in cancer stem cells of chronic myeloid leukemia.* Cell Cycle, 2009. **8**(21): p. 3488-92.
33. Chen, Y., et al., *Loss of the Alox5 gene impairs leukemia stem cells and prevents chronic myeloid leukemia.* Nat Genet, 2009. **41**(7): p. 783-92.
34. Zaldivar, M.M., et al., *CXC chemokine ligand 4 (Cxcl4) is a platelet-derived mediator of experimental liver fibrosis.* Hepatology, 2010. **51**(4): p. 1345-53.
35. van Bon, L., et al., *Proteome-wide analysis and CXCL4 as a biomarker in systemic sclerosis.* N Engl J Med, 2014. **370**(5): p. 433-43.
36. Burstein, S.A., et al., *Platelet factor-4 excretion in myeloproliferative disease: implications for the aetiology of myelofibrosis.* Br J Haematol, 1984. **57**(3): p. 383-92.
37. Leoni, P., et al., *Platelet abnormalities in idiopathic myelofibrosis: functional, biochemical and immunomorphological correlations.* Haematologica, 1994. **79**(1): p. 29-39.
38. Bruns, I., et al., *Megakaryocytes regulate hematopoietic stem cell quiescence through CXCL4 secretion.* Nat Med, 2014. **20**(11): p. 1315-20.
39. Desplat, V., et al., *Effects of lipoxygenase metabolites of arachidonic acid on the growth of human blood CD34(+) progenitors.* Blood Cells Mol Dis, 2000. **26**(5): p. 427-36.
40. Varricchio, L., A. Mancini, and A.R. Migliaccio, *Pathological interactions between hematopoietic stem cells and their niche revealed by mouse models of primary myelofibrosis.* Expert Rev Hematol, 2009. **2**(3): p. 315-334.
41. El Agha, E., et al., *Two-Way Conversion between Lipogenic and Myogenic Fibroblastic Phenotypes Marks the Progression and Resolution of Lung Fibrosis.* Cell Stem Cell, 2016.

42. Vannucchi, A.M., et al., *Pathogenesis of myelofibrosis with myeloid metaplasia: lessons from mouse models of the disease.* Semin Oncol, 2005. **32**(4): p. 365-72.
43. Biagini, G., et al., *Stromal cells in primary myelofibrosis: ultrastructural observations.* Virchows Arch B Cell Pathol Incl Mol Pathol, 1985. **48**(1): p. 1-8.
44. Thiele, J., et al., *Ultrastructure of bone marrow tissue in so-called primary (idiopathic) myelofibrosis-osteomyelosclerosis (agnogenic myeloid metaplasia). I. Abnormalities of megakaryopoiesis and thrombocytes.* J Submicrosc Cytol Pathol, 1991. **23**(1): p. 93-107.
45. Schmitt-Graeff, A.H., R. Nitschke, and R. Zeiser, *The Hematopoietic Niche in Myeloproliferative Neoplasms.* Mediators Inflamm, 2015. **2015**: p. 347270.
46. Kunisaki, Y., et al., *Arteriolar niches maintain haematopoietic stem cell quiescence.* Nature, 2013. **502**(7473): p. 637-43.
47. Boulais, P.E. and P.S. Frenette, *Making sense of hematopoietic stem cell niches.* Blood, 2015. **125**(17): p. 2621-9.
48. Mendez-Ferrer, S., et al., *Mesenchymal and haematopoietic stem cells form a unique bone marrow niche.* Nature, 2010. **466**(7308): p. 829-34.
49. Tzeng, Y.S., et al., *Loss of Cxcl12/Sdf-1 in adult mice decreases the quiescent state of hematopoietic stem/progenitor cells and alters the pattern of hematopoietic regeneration after myelosuppression.* Blood, 2011. **117**(2): p. 429-39.
50. Migliaccio, A.R., et al., *Altered SDF-1/CXCR4 axis in patients with primary myelofibrosis and in the Gata1 low mouse model of the disease.* Exp Hematol, 2008. **36**(2): p. 158-71.
51. Elf, S., et al., *Mutant Calreticulin Requires Both Its Mutant C-terminus and the Thrombopoietin Receptor for Oncogenic Transformation.* Cancer Discov, 2016. **6**(4): p. 368-81.
52. Rondelli, D., et al., *Allogeneic hematopoietic stem-cell transplantation with reduced-intensity conditioning in intermediate- or high-risk patients with myelofibrosis with myeloid metaplasia.* Blood, 2005. **105**(10): p. 4115-9.
53. Verstovsek, S., et al., *A double-blind, placebo-controlled trial of ruxolitinib for myelofibrosis.* N Engl J Med, 2012. **366**(9): p. 799-807.
54. Bhagwat, N., et al., *Improved Efficacy Of Comibnation Of JAK2 and Hedgehog Inhibitors in Myelofibrosis.* Blood, 2013. **122**(21).
55. Sasaki, K., et al., *Phase II evaluation of IPI-926, an oral Hedgehog inhibitor, in patients with myelofibrosis.* Leuk Lymphoma, 2015. **56**(7): p. 2092-7.

4

PARABIOSIS AND SINGLE-CELL RNA-SEQUENCING REVEAL A LIMITED CONTRIBUTION OF MONOCYTES TO MYOFIBROBLASTS IN KIDNEY FIBROSIS

Rafael Kramann,[1*] Flavia Machado,[2] Haojia Wu,[2] Tetsuro Kusaba,[3] Konrad Hoeft,[1] Rebekka K Schneider,[4,5] and Benjamin D. Humphreys[2*]

[1]Division of Nephrology and Clinical Immunology RWTH Aachen University, 52074 Aachen, Germany
[2]Division of Nephrology, Department of Medicine, Washington University School of Medicine, St Louis, MO 63110, USA
[3]Department of Nephrology, Graduate School of Medical Science, Kyoto Prefectural University of Medicine, Kyoto, Japan
[4]Department of Hematology, Erasmus MC Cancer Institute, 3015CN Rotterdam, the Netherlands
[5]Division of Hematology, RWTH Aachen University, 52074 Aachen, Germany

Running title: Circulating myofibroblast precursors

Corresponding author:
*Rafael Kramann, MD
Division of Nephrology and Clinical Immunology,
Medical Faculty RWTH Aachen University,
Pauwelsstrasse 30, 52074 Aachen, Germany
Phone.: 0049-241-80 37750
Fax.: 617-525-5965
E-mail: rkramann@gmx.net

or

* Benjamin D. Humphreys, MD, PhD
Divison of Nephrology
Washington University School of Medicine
660 S. Euclid Ave., CB8129
St. Louis, MO 63110
humphreysbd@wustl.edu

ABSTRACT

Fibrosis is the common final pathway of virtually all chronic injury to the kidney. While it is well accepted that myofibroblasts are the scar-producing cells in the kidney, their cellular origin is still hotly debated. The relative contribution of proximal tubular epithelium and circulating cells including mesenchymal stem cells, macrophages and fibrocytes to the myofibroblast pool remains highly controversial. Using inducible genetic fate tracing of proximal tubular epithelium we confirm that proximal tubule does not contribute to the myofibroblast pool. However, in parabiosis models in which one parabiont is genetically labeled and the other is unlabeled and undergoes kidney fibrosis, we demonstrate that a small fraction of genetically labeled renal myofibroblasts derive from the circulation. Single cell RNA-Sequencing confirms this finding but indicates that these cells are circulating monocytes, express few extracellular matrix or other myofibroblast genes and do express many proinflammatory cytokines. We conclude that this small circulating myofibroblast progenitor population contributes to renal fibrosis by paracrine rather than direct mechanisms.

INTRODUCTION

Chronic kidney disease (CKD) affects 10% of the population in Europe and the United States and disease prevalence is increasing steadily. Renal interstitial fibrosis correlates well with kidney functional decline and inhibition of fibrosis is a promising strategy to slow down progression of CKD. While it is well accepted that myofibroblasts are the cells that cause fibrosis, the cellular origin of kidney myofibroblasts is still very controversial . We have reported that approximately half of all kidney myofibroblasts are derived from the pericyte lineage . However, the origins of the other half remains unclear. A precise definition of the cellular origins of kidney myofibroblasts represents a key step to understand fibrosis and develop novel therapeutics to slow progression of CKD.

The contribution of proximal tubular epithelium to the myofibroblast pool via epithelial to mesenchymal transition (EMT) has been controversial for almost 20 years and is ongoing. Genetic fate tracing experiments come to different conclusions reporting either no contribution [11] a major contribution [2, 12, 13] or a minor contribution of the epithelium .

Similarly, the degree to which circulating progenitor cells contribute to the myofibroblast pool has also been debated for many years . Bone marrow derived mesenchymal stem cells (MSCs) have been reported to contribute to as much as 35% of the renal myofibroblast pool [15, 16]. Furthermore, fibrocytes and macrophages have also been defined as kidney myofibroblast progenitors. Fibrocytes were originally described more than two decades ago as a leukocyte-derived population of fibroblast-like cells in subcutaneously implanted wound chambers that express extracellular matrix proteins such as collagen I . Regarding a contribution of fibrocytes to the myofibroblast pool in kidney fibrosis, studies from different groups have led to different conclusions. While bone marrow transplantation experiments using Collagen 1a1 or Collagen 1a2 reporter chimeras suggest no significant contribution of circulating bone marrow derived cells to the myofibroblast pool, [17-24] other groups have reported a major contribution of hematopoietic lineage-derived fibrocytes and macrophages to kidney fibrosis .

Most studies to date have relied heavily on confocal microscopy and/or bone marrow transplantation experiments. Discriminating myofibroblasts from hematopoietic lineage cells by confocal microscopy is technically challenging due to their thin, branched architecture and by their abundance in the renal interstitium after injury. Furthermore, bone marrow transplantation experiments using genetic reporters result in engraftment solely of hematopoietic stem cells whereas other bone marrow cells such as MSCs do not engraft well, [26] [4] precluding analysis of the contribution of MSC lineage cells to the myofibroblast pool. Using a novel inducible genetic fate tracing model we confirm that proximal tubular epithelium does not contribute to the myofibroblast pool. In order to dissect the contribution of any circulating cells to the renal myofibroblast pool we have performed parabiosis and single cell RNA-Sequencing experiments. Our data indicate that

monocytes contribute a small fraction of myofibroblast in kidney fibrosis whereas most myofibroblasts are derived from resident mesenchymal cells such as pericytes and resident fibroblasts.

RESULTS

Inducible genetic fate tracing indicates no contribution of proximal tubular epithelium to the myofibroblast pool in kidney fibrosis.

We recently developed a novel inducible and proximal tubule specific Cre driver [27] by knocking a CreER^{t2} cassette into the sodium-dependent inorganic phosphate transporter SLC34a1 locus which is expressed only in the proximal tubule. In order to perform inducible genetic fate tracing of proximal tubular epithelium we generated bigenic SLC34a1-GFPCreER^{t2}; tdTomato mice (Figure 1A). 8 week old mice were pulsed with high dose tamoxifen and subjected to UUO surgery at 10 days after the last tamoxifen dose (Figure 1B). Careful evaluation and quantification of kidney sections co-stained for α-SMA indicated that proximal tubular epithelial cells do not become interstitial myofibroblasts (Figure 1C-D

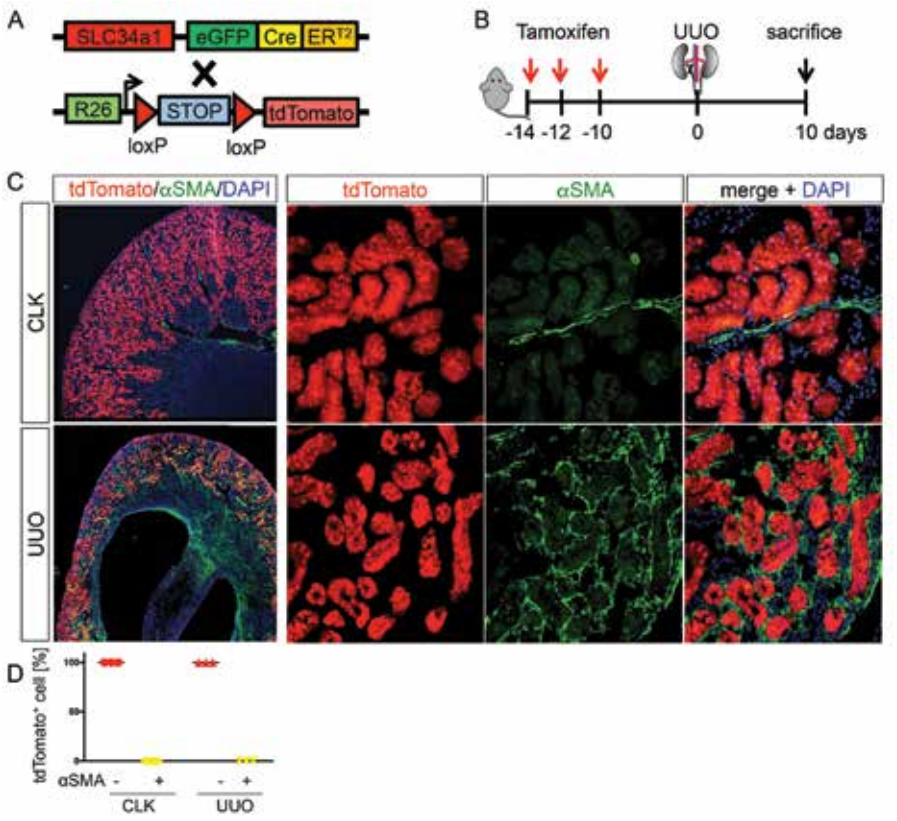

Figure 1 Inducible genetic fate tracing indicates no contribution of proximal tubular epitelium to kidney myofibroblasts.
(**A**) Scheme of SCL34a1GFPCreERt2; tdTomato mice
(**B**) Scheme of the genetic fate tracing experiment, 8 week old SLC34a1GFPCreER;tdTomato mice (n=3 males) were pulsed with tamoxifen (3x10mg p.o.) and subjected to UUO surgery at 10 days after the last tamoxifen dose. Mice were sacrified 10 days after surgery.
(**C**) Representative pictures of contralateral non-injured (CLK) and injured (unilateral ureteral obstruction, UUO) kidneys stained for α-SMA.
(**D**) Quantification of tdTomato+ and α-SMA$^+$ versus α-SMA$^-$ cells. All data represents mean±SD

Parabiosis model with fate tracing of all cells from one mouse and kidney fibrosis induction in the other.

To quantitate and better describe the contribution of circulating cells to the kidney myofibroblast pool, we performed parabiosis experiments with generalized genetic cell fate tracing in one parabiont and induction of kidney fibrosis in the other. To ubiquitously genetically label cells with the bright red fluorochrome tdTomato, bigenic Rosa26CreER;tdTomato mice received tamoxifen and underwent parabiosis surgery at 10 days after the last tamoxifen dose (Figure 2A). The Rosa26CreER;tdTomato mice were then conjoined with B6-CD45.1$^+$ mice which do not express tdTomato but express a different isoform of the pan-leukocyte marker CD45, which can be discriminated by flow cytometry, (B6-CD45.1$^+$ as opposed to Rosa26CreER;tdTomato-CD45.2$^+$) (Figure 2A). Shared circulation and recombination efficiency were verified 4 weeks after parabiosis surgery and before induction of kidney fibrosis (Figure 2B-C). The analysis showed a good cross circulation indicated by an almost 1:1 ratio of CD45.1$^+$ and CD45.2$^+$ cells and a recombination efficiency of >90% (Figure 2B-C). The B6-CD45.1 parabiont was then subjected to unilateral ureteral obstruction (UUO) surgery to ask whether any circulating tdTomato$^+$ cells from the Rosa26CreER;tdTomato (CD45.2$^+$) parabiont would contribute to the myofibroblast pool during kidney fibrosis. Mice were sacrificed 10 days after UUO surgery. The contralateral non-injured kidney (CLK) served as an internal control. Development of fibrosis in the UUO model was confirmed by trichrome staining and quantification (Supplementary Figure 1A-B). Flow cytometric evaluation of the PBS perfused spleen from the CD45.1 mice showed a cross-circulation with CD45.1$^+$ and CD45.2$^+$ leukocytes from both mice and confirmed efficient recombination (Figure 2D-E). As expected, UUO surgery resulted in tremendous influx of leukocytes into the UUO kidneys. More than half of the leukocytes were derived from the CD45.2 (Rosa26CreER;tdTomato) parabiont (Figure 2F-H), confirming effectiveness of the cross-circulation and an optimal experimental set-up to study influx of circulating cells from the conjoined mouse. Representative gating on living, single kidney cells is shown in Supplementary Figure 1C.

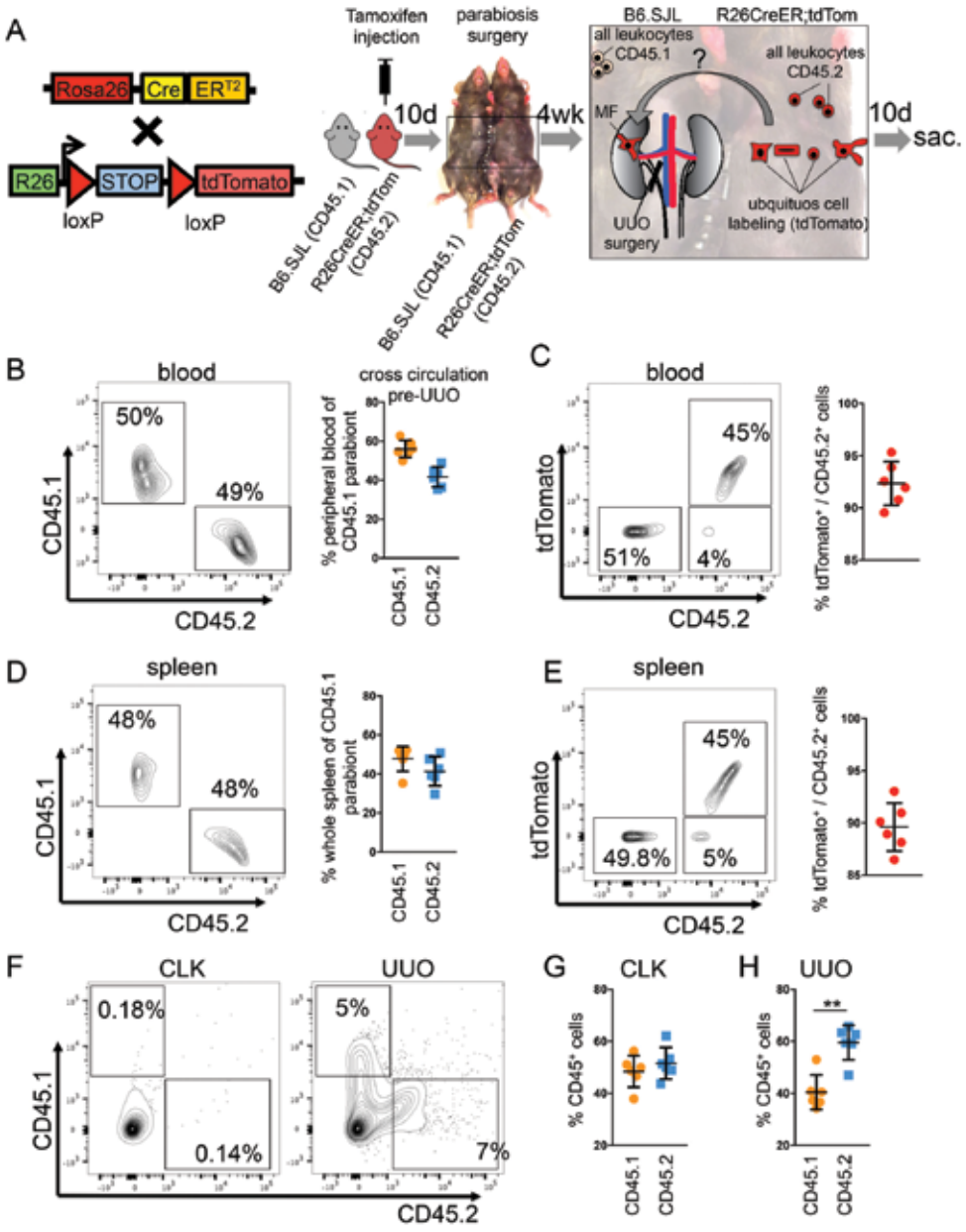

Figure 2 Parabiosis with genetic fate tracing to dissect the contribution of circulating cells to kidney fibrosis
(**A**) n=8 Rosa26CreER;tdTomato mice (all females, 8 week of age) received tamoxifen (4x10mg p.o. every other day) to genetically tag all cells and were conjoined with B6.SJL (CD45.1) mice at 10 days after the last tamoxifen dose. Four weeks after parabiosis surgery the B6.SJL parabiont was subjected to unilateral ureteral obstruction (UUO) surgery to induce kidney fibrosis. Mice were sacrificed 10 days after UUO surgery. n=2 mice died during the experiment, final data represents n=6 parabiosis pairs in all readouts. MF, myofibroblast
(**B**) Representative flow cytometric plot and quantification of CD45.1$^+$ versus CD45.2$^+$ cells in the blood of the B6.SJL (CD45.1) parabiont at 4 weeks after parabiosis surgery.

(**C**) Representative flow cytometric plot and quantification of recombination efficiency (i.e. tdTomato$^+$) of CD45.2$^+$ cells in the blood of the B6.SJL parabiont at 4 weeks after parabiosis surgery.
(**D**) Representative flow cytometric plots and quantification of CD45.1$^+$ versus CD45.2$^+$ cells in the spleen of the B6.SJL (CD45.1) parabiont after sacrification.
(**E**) Representative flow cytometric plot and quantification of recombination efficiency (i.e. tdTomato$^+$) of CD45.2$^+$ cells in the spleen of the B6.SJL parabiont after sacrification.
(**F-H**) Representative flow cytometric plots and quantification of CD45.1$^+$ versus CD45.2$^+$ leukocyte influx into the contralateral non-injured (CLK) and fibrotic UUO kidneys.
All data represents mean±SD, **p<0.01 by unpaired t-test, n=6 in each graph.

Circulating cells contribute to a minor fraction of renal myofibroblasts.

We next measured the contribution of circulating cells (tdTomato$^+$) to the myofibroblast lineage. Half of the fibrotic (UUO) and control (CLK) kidneys were subjected to flow cytometric evaluation and co-staining with the myofibroblast marker alpha-smooth muscle actin (α-SMA). Flow-cytometric evaluation after gating on single and living (DAPI-) cells indicated that indeed a small fraction of renal myofibroblasts was derived from circulation (tdTomato$^+$/α-SMA$^+$) (Figure 3A-F). While we observed a tremendous increase of both tdTomato$^+$ cells (influx of all circulating cells) and α-SMA$^+$ cells (expansion of myofibroblasts) after UUO, as expected, only a small fraction of myofibroblasts co-expressed tdTomato, indicating an origin from the Rosa26CreER;tdTomato parabiont (Figure 3A-F). Confocal microscopy of the Rosa26CreER;tdTomato (CD45.2) kidney confirmed the recombination efficiency and showed that all cells were tdTomato$^+$ (Figure 3G).

To confirm the flow cytometric data we used high-resolution confocal-microscopy (Airyscan detector) to localize tdTomato$^+$ myofibroblasts that were derived from circulation. While we only observed sparse tdTomato$^+$ cells in the CLK kidneys of the B6-CD45.1 parabiont, high resolution confocal microscopy confirmed areas with large numbers of tdTomato$^+$ cells in the UUO kidneys. Importantly, we observed some tdTomato$^+$ cells that indeed co-expressed perinuclear α-SMA (Figure 3H arrows), thus confirming the flow cytometric data with high resolution imaging of renal interstitium.

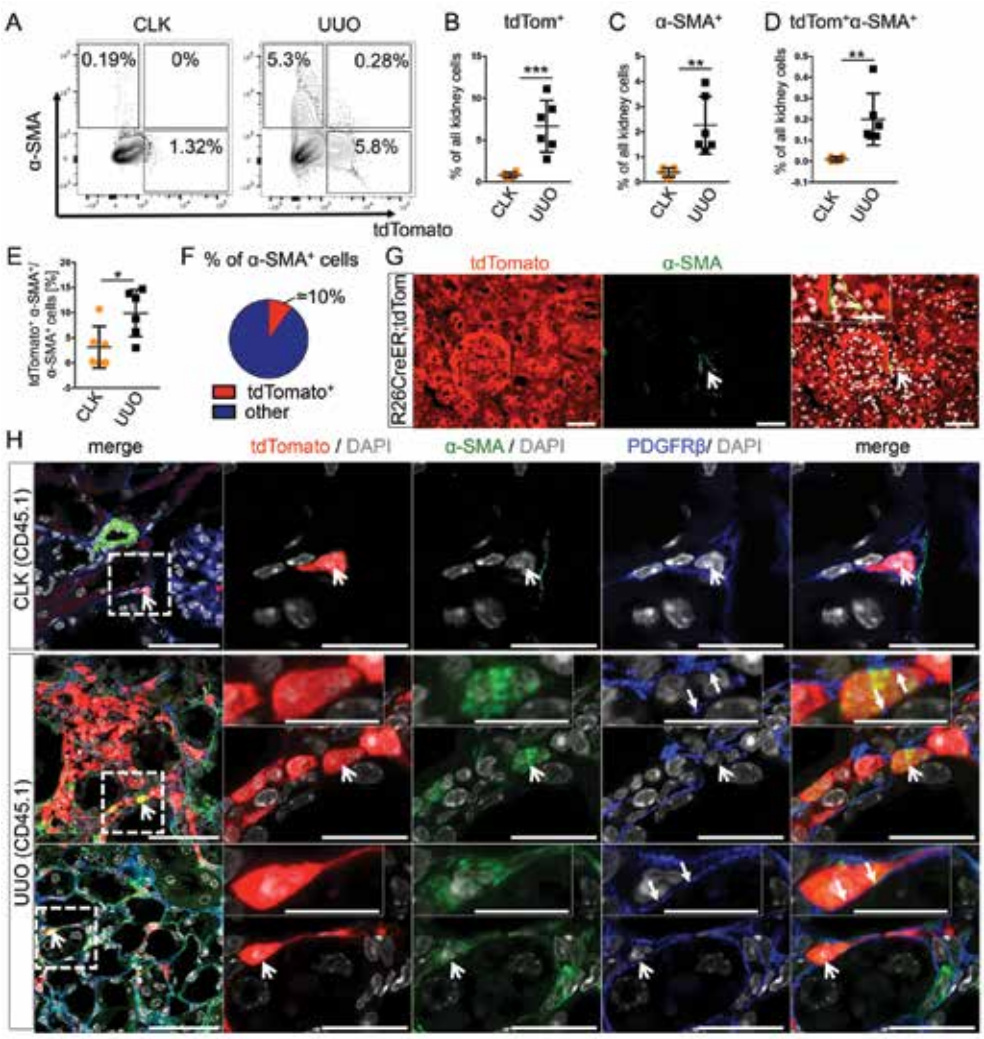

Figure 3 A small fraction of kidney myofibroblasts is derived from circulation

(**A**) Flow cytometric plots of myofibroblasts (α-SMA$^+$), circulating cells (tdTomato$^+$) and overlap i.e. myofibroblast derived from circulation in non-injured contralateral kidneys (CLK) and fibrotic - unitlateral ureteral obstruction (UUO) kidneys from B6.SJL (CD45.1) mice (n=6).

(**B**) Fraction of circulating tdTomato$^+$ cells from all kidney cells in non-injured contralateral kidneys (CLK) and fibrotic - unitlateral ureteral obstruction (UUO) kidneys from B6.SJL (CD45.1) mice (n=6).

(**C**) Fraction of myofibroblasts (α-SMA$^+$) from all kidney cells in non-injured contralateral kidneys (CLK) and fibrotic - unitlateral ureteral obstruction (UUO) kidneys from B6.SJL (CD45.1) mice(n=6).

(**D**) Fraction of myofibroblasts derived from circulation (α-SMA$^+$/tdTomato$^+$) from all kidney cells in non-injured contralateral kidneys (CLK) and fibrotic - unitlateral ureteral obstruction (UUO) kidneys from B6.SJL (CD45.1) mice(n=6).

(**E-F**) Fraction of myofibroblasts derived from circulation (tdTomato$^+$/ α-SMA$^+$) from all myofibroblasts α-SMA$^+$ (n=6)..

(**G**) Representative image of the non-injured kidney of the Rosa26CreER;tdTomato parabiont. Scale bars 50µm, insert 25µm.

(**H**) High resolution confocal microscopy (Airyscan) images of non-injured contralateral kidneys (CLK) and fibrotic

- unitlateral ureteral obstruction (UUO) kidneys from B6.SJL (CD45.1) mice co-stained for α-SMA and PDGFRβ. Large arrows indicate tdTomato$^+$ cell co-expressing α-SMA and PDGFRβ. Small arrows indicate the area of thin membranous PDGFRβ signal. Scale bars 50μm left panel, 10μm inserts, 20μm all others. All data represents mean±SD, *p<0.05, **p<0.01, ***p<0.001 all by unpaired t-test.

Flow cytometric analysis revealed that all cells in the UUO kidneys that were derived from circulation (tdTomato$^+$) also co-expressed CD45.2 (Figure 4A-B) and thus were of hematopoetic lineage. Co-staining for CD45 with subsequent confocal microscopy indeed showed that tdTomato$^+$ cells in the kidneys showed a thin layer of CD45 membrane staining confirming their hematopoietic origin (Figure 4C-D inserts). We next aimed to identify a combination of surface markers that would allow isolation of myofibroblasts from circulation in comparison to non-circulating myofibroblasts. As we have previously reported that all renal myofibroblasts co-express the mesenchymal marker PDGFRβ [28] and PDGFRβ has also been described as a marker of circulating fibrocytes [29] a combination of PDGFRβ with CD45 would allow to isolate circulating hematopoietic myofibroblasts (PDGFRβ$^+$,CD45$^+$) and resident non-hematopoetic (PDGFRβ+,CD45-) cells. Co-staining of kidneys for PDGFRβ indeed indicated that the tdTomato$^+$/α-SMA$^+$ population of myofibroblasts derived from circulation co-expresses PDGFRβ (Figure 3H). Thus, our data suggest that costaining for the pan leukocyte marker CD45 and the mesenchymal marker PDGFRβ can be used to isolate both resident and circulating kidney myofibroblasts.

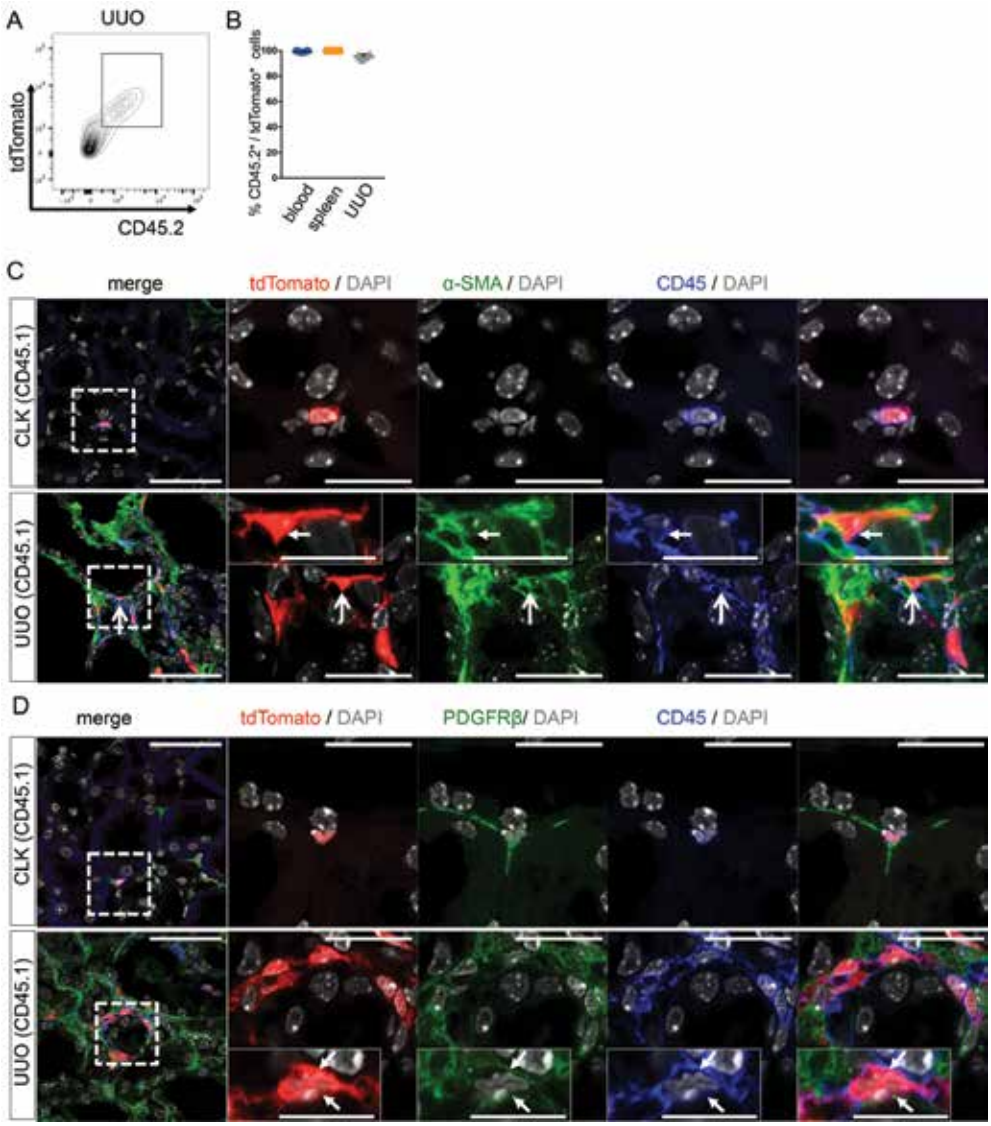

Figure 4 Myofibroblasts derived from circulation co-express PDGFRβ and CD45

(**A-B**) Representative flow cytometric plot and quantification of tdTomato$^+$ and CD45.2$^+$ cells in blood, spleen and UUO kidneys of the B6.SJL (CD45.1) mice (n=6).

(**C**) Representative high resolution confocal microscopy images of contralateral non-injured kidney (CLK) and fibrotic unilateral ureteral obstruction (UUO) kidneys from B6.SJL (CD45.1) mice costained for α-SMA and CD45. Scale bars 50μm left panel, 10μm inserts, 20μm all others. Large arrows indicate tdTomato$^+$ cell co-expressing α-SMA and CD45. Small arrows indicate the area of thin membranous CD45 signal.

(**D**) Representative high resolution confocal microscopy images of contralateral non-injured kidney (CLK) and fibrotic unilateral ureteral obstruction (UUO) kidneys from B6.SJL (CD45.1) mice costained for PDGFRβ and CD45. All data represents mean±SD of n=6. Small arrows indicate the area of thin membranous CD45 and PDGFRβ signal in the tdTomato$^+$ cell. Scale bars 50μm left panel, 20μm all others

Single cell RNA-Sequencing confirms a contribution of circulating CD45$^+$ cells to the myofibroblast pool.

We next turned to an unbiased non-parabiosis approach to confirm our genetic fate tracing parabiosis results with single cell RNA-sequencing (scRNA-seq) from FACS isolated PDGFRβ$^+$,CD45$^+$ and PDGFRβ$^+$,CD45$^-$ cells. C57Bl6 wildtype mice were subjected to UUO surgery and sacrificed 10 days after surgery. We sorted either myofibroblasts that were derived from circulation (PDGFRβ$^+$/CD45$^+$) or all other myofibroblasts (PDGFRβ$^+$/CD45$^-$) as singlets into individual wells of 96-well plates (Supplementary Figure 2A). We sorted two 96 well plates of each population from whole digested UUO kidney samples and subjected the samples to scRNA-seq. The kidney samples were pooled from three different mice. Cells from two different plates were distributed evenly in the clusters of the tSNE analysis excluding batch effects (Supplementary Figure 2B). The tSNE analysis resulted in two distinct clusters that were almost identical with the two sorted cell-populations of PDGFRβ$^+$/CD45$^+$ and PDGFRβ$^+$/CD45$^-$ cells (Figure 5A). The top 30 upregulated genes in both clusters are outlined in Supplementary Figure 2C. Importantly, the sc-RNA-seq data confirmed the parabiosis fate-tracing experiment and demonstrated that the great majority of myofibroblasts identified by expression of α-SMA (Acta2) and or collagen (Col1a1, Col3a1) were among the PDGFRβ$^+$/CD45$^-$ population or resident kidney cells whereas only a few myofibroblasts were among the population of circulating hematopoietic PDGFRβ$^+$/CD45$^+$ cells (Figure 5B-E). The PDGFRβ$^+$/CD45$^-$ population showed expression of markers that have been associated with pericytes and myofibroblasts such as Timp1, Col1a1, Col3a1, Rgs5, desmin, CSPG4 and the mesenchymal marker vimentin (Figure 5B-H and Supplementary Figure 2C) whereas the population of myofibroblasts derived from circulation (PDGFRβ$^+$/CD45$^+$) showed high expression of the monocyte marker CD68 (Figure 5F).

We next examined expression of extracellular matrix proteins as well as chemokines and cytokines that have been associated with fibrosis. Interestingly the resident PDGFRβ$^+$/CD45$^-$ population showed strong expression of various collagens and fibronectin as well as connective tissue growth factor (CTGF) as well as transforming growth factor beta 3 (TGFb3) whereas the circulating population of PDGFRβ$^+$/CD45$^+$ cells primarily expressed various chemokines and interleukins with significantly lower or absent expression of extracellular matrix components compared to the population of resident myofibroblasts (Figure 5J). This data indicate that circulating PDGFRβ$^+$/CD45$^+$ only contribute a minor fraction to the myofibroblast pool but might regulate kidney fibrosis in a paracrine fashion by secretion of proinflammatory and pro-fibrotic chemokines. We hypothesized therefore that circulating PDGFRβ$^+$/CD45$^+$ might interact with resident PDGFRβ$^+$/CD45$^-$ cells and looked into receptor-ligand interactions between the two cell-populations within the scRNA-Seq dataset. Interestingly, we observed strong expression of multiple receptor-ligand pairs between both cell populations (Figure 5K). Among the observed ligands we found CXCL4/PF4 expression in the circulating cells (PDGFRβ$^+$/CD45$^-$) and we have recently reported that CXCL4 can induce

myofibroblast differentiation in Gli1^{+} bone marrow cells [30]. This data suggested that the circulating population might be involved in activation and myofibroblast differentiation of the resident population of myofibroblast precursors. We also checked the relative proliferative state of the two populations based on the scRNA-seq data indiciating that both populations have a high percentage of cells in the G2/M and S phase of the cell cycle and thus are cells that show a proliferative response to kidney injury (Figure 6A)

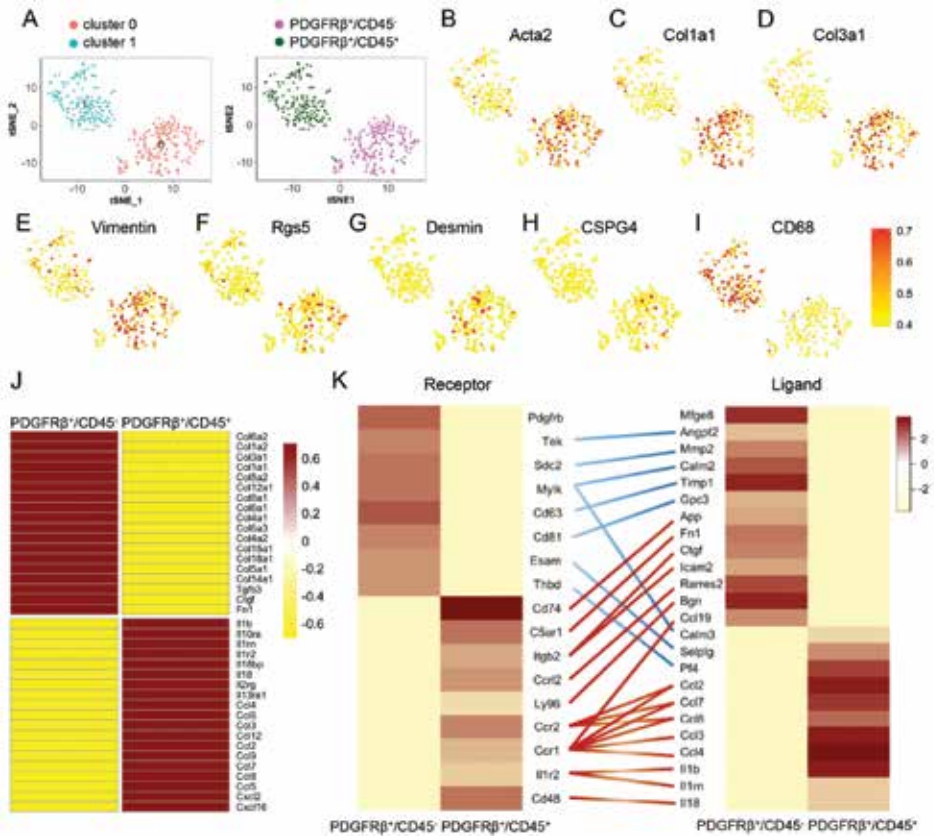

Figure 5 Single cell RNA-Sequencing reveals that the majority of kidney myofibroblasts is derived from resident pericytes while a small fraction is derived from circulation.

(**A**) Single-cell RNA-Sequencing was performed PDGFRβ^{+}/CD45^{-} cells (myofibroblasts derived from circulation) and PDGFRβ^{+}/CD45^{+} cells (all other myofibroblasts) of whole fibrotic (UUO unilateral ureteral obstruction) kidneys. Kidneys were pooled from 3 mice and two 96 well plates were sorted from each population. tSNE analysis clusters two distinct cell populations congruent with the sorted populations.

(**B-I**) Expression levels of genes that define myofibroblasts, pericytes or macrophages in both tSNE clusters. (Acta2, alpha smooth muscle actin; Col1a1, collagen 1 alpha 1; Col3a1, collagen 3 alpha 1) Color key denotes the z-score normalized average expression value of selected differentially expressed genes between PDGFRβ^{+}/CD45^{-} and PDGFRβ^{+}/CD45^{+} cells.

(**J**) Expression levels of extracellular matrix components and proinflammatory, profibrotic cytokines and growth factors between the two cell populations.

(**K**) Ligand-receptor pair expression according to cell type. Ligands are indicated on the right panel, receptors on the left panel. Straight lines indicate ligand-receptor pairs. Color key denotes the z-score normalized average expression value.

The circulating myofibroblasts are of monocyte origin.

Since transcription factors drive cell identity, we next estimated transcription factor activity based on their target gene expression in the scRNA-seq data. We aimed to identify key transcription factors that would define the two cell populations (Figure 6B-C, Supplementary Tables 1-2). The data showed two entirely distinct landscapes of transcription factor activity in the two cell populations further indicating that the two cell populations of resident (PDGFRβ$^+$/CD45$^-$) and circulating myofibroblasts (PDGFRβ$^+$/CD45$^+$) are distinct from each other. In line with their expression of proinflammatory cytokines and their hematopoietic origin from circulation the analysis revealed transcription factors that have been reported to be critical in the inflammatory response and macrophage activation such as ATF3 [31], Fos [32], Jun/Junb [33], Maf [34] and EGR1 [35-37] among others were central in the landscape of transcription factor activity of the PDGFRβ$^+$/CD45$^+$ population (Figure 6A-B and Supplementary Table 1).

In contrast, the resident population of myofibroblasts (PDGFRβ$^+$/CD45$^-$) was characterized by transcription factors that have been reported to define tissue resident cardiac fibroblasts / myofibroblasts as Tcf21, or mesenchymal stem cells such as Prrx1 or Hoxd10 Furthermore the data suggested high activity of the nuclear receptor subfamily 2 group member 2 (Nr2f2) in the resident PDGFRβ$^+$/CD45$^-$ population. Nr2f2 is an important inhibitor of adipogenesis and has been recently reported to be highly expressed in Gremlin 1$^+$ bone marrow MSC [39]. These findings are in line with our previously reported fate tracing experiments that kidney Gli1$^+$ pericytes represent a population of MSC and are a major source of myofibroblasts [18, 23, 24, 40]. We have further reported that Hedgehog-Gli signaling is a critical regulator of Gli1$^+$ cell expansion and inhibition of Gli proteins is a therapeutic strategy in kidney fibrosis . Consistent with these observations, the Hh pathway member and transcriptional repressor of Hh signaling Glis2 was among other transcription factors enriched in the PDGFRβ$^+$/CD45$^-$ population.

Gene ontology (GO) analysis revealed that genes involved in extracellular matrix formation, collagen production, metabolism and growth factor binding were significantly overrepresented in the resident myofibroblast population (PDGFRβ$^+$/CD45$^-$) reflecting their major contribution to fibrosis formation (Supplementary Figure 3A). The circulating myofibroblast population of PDGFRβ$^+$/CD45$^+$ cells mostly showed expression of genes that were associated with immune response mechanism, reflecting their mechanism of activation and homing to the injured kidney (Supplementary Figure 3).

We next asked which circulating blood population might give rise to the small kidney PDGFRβ$^+$/CD45$^+$ myofibroblast population. We compared a published dataset of human peripheral blood mononuclear cells (PBMCs) to the resident (PDGFRβ$^+$/CD45$^-$) and circulating (PDGFRβ$^+$/CD45$^+$) kidney myofibroblast dataset (Figure 6D). Importantly, we did not observe any overlap of the PBMCs with the resident kidney myofibroblast population whereas the circulating myofibroblast population of PDGFRβ$^+$/CD45$^+$ cells correlated strongly with human monocytes (Figure 6D). Altoghether this data indicates circulating monocytes contribute a

minor population of myofibroblasts while they do not secrete much extracellular matrix they produce high amounts of proinflammatory cytokines that might activate resident myofibroblasts. We next asked whether circulating myofibroblast population of PDGFRβ^{+}/CD45^{+} shows expression of genes that have been reported to characterize M1 or M2 macrophages. Interstingly, PDGFRβ^{+}/CD45^{+} cells primarily showed expression of classically activated, pro-inflammatory M1 macrophages such as Socs3, Tlr2, Il1b, TNFa,Ccl2 and Ccl8 (Supplementary Figure 3B).

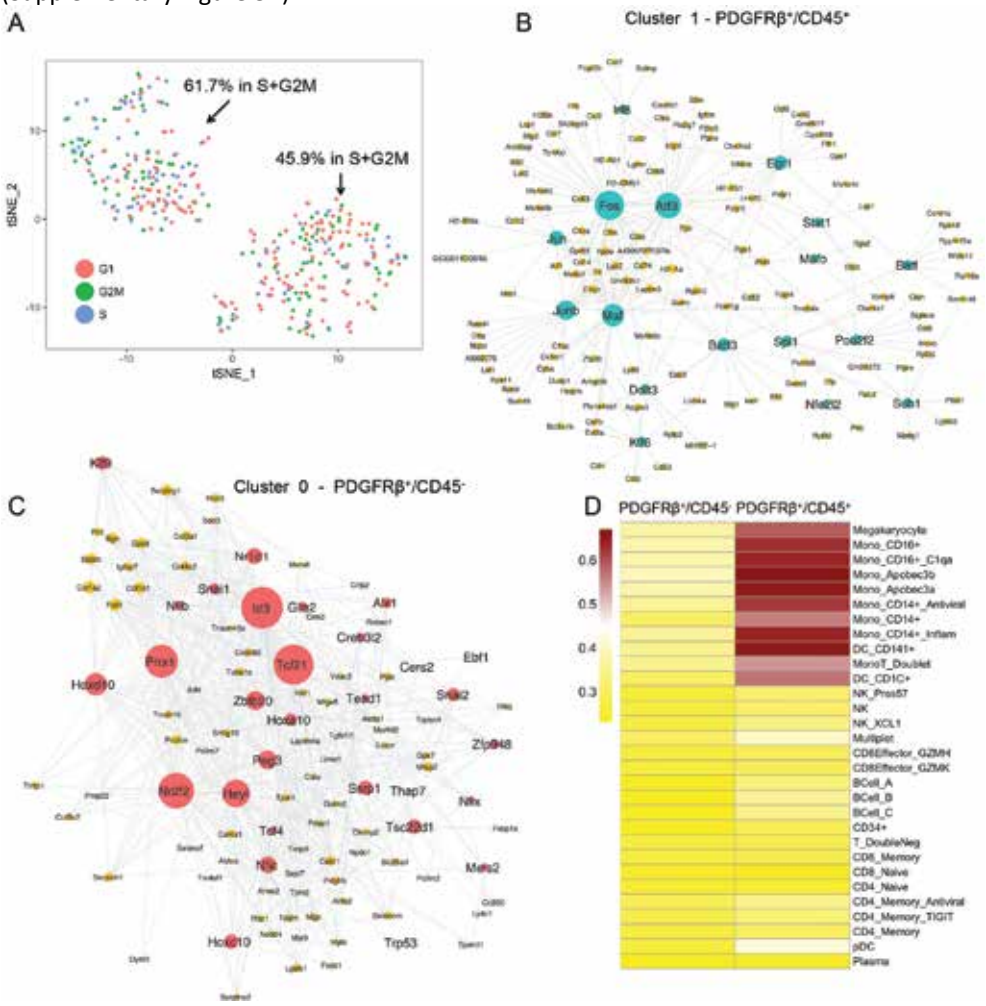

Figure 6 Single RNA-Sequencing data identifies circulating myofibroblast progenitors as monocytes
(**A**) Proliferative state in the two cell-clusters based on gene expression.
(**B-C**) Transcription factor (TF) activity network based on mRNA expression of TF target genes in the two cell populations.
(**D**) Comparison of both cell populations with a Drop-Seq data set (10x genomics) of human peripheral blood mononuclear cells (n=33,000 cells, healthy donor).The color key denotes the Pearson's correlation coefficient (rho) between mouse and human cells. Rho has a value between -1 and 1. Greater rho value indicates higher correlation between the two cell types.

DISCUSSION

Our data indicates that proximal tubular epithelium does not contribute to the myofibroblast pool whereas circulating monocytes contribute a minor population of αSMA$^+$ myofibroblasts. A contribution of monocytes and macrophages to the myofibroblast pool has been described from several groups . However, Reich et al. have reported that fibrocytes independent of monocyte lineages are an important source of kidney myofibroblasts [2, 41]. As macrophages are a major site of collagen internalization and degradation, antibody staining for matrix proteins might be difficult to interpret . Importantly, there is an ongoing debate whether there is a direct contribution of myeloid leukocytes to myofibroblast pool at all and many reported effects might have been results of indirect mechanisms [11]. In this work, we show, using two powerful and complementary approaches, that indeed a small percentage of kidney myofibroblasts derive from monocytes. However, importantly, these myeloid-derived myofibroblasts express very few matrix genes – suggesting they do not play a direct role in interstitial matrix accumulation. The data indicates that PDGFRβ$^+$/CD45$^+$ monocytes primarily secrete high amounts of proinflamatory pro-fibrotic cytokines that have been reported to activate resident myofibroblasts suggesting paracrine communications between circulating-monocytes and resident myofibroblasts driving fibrosis as well. Thus the direct contribution of circulating monocytes to the myofibroblast pool and matrix production is minor compared to their paracrine effects. This single cell RNA-Sequencing dataset confirms that the great majority of kidney myofibroblasts are of resident kidney origin.

A contribution of circulating bone marrow MSCs to the kidney myofibroblast pool has been discussed for several years as well . After parabiosis two mice share one blood circulation which allows rapid exchange of blood, cells and particles such as ultrasound-bubbles from one mouse to the other independent of cell size [4, 13]. Therefore our parabiosis approach with induced labeling of all cells (90% recombination efficiency) in one mouse and induction of kidney fibrosis in the other mouse allows quantitative tracking of all circulating cells which would in theory also include MSCs. However, we performed two independent experiments both indicating that only CD45$^+$ and thus hematopoietic (non-mesenchymal) cells contribute a small population of myofibroblast. Of note, CD45 expression is an exclusion criterion for MSC.

First, the parabiosis experiments demonstrate that circulating tdTomato$^+$ cells in blood, spleen and kidney are all CD45$^+$ and all circulating myofibroblasts we observed (tdTomato$^+$/αSMA$^+$) in the UUO kidneys also showed co-expression of CD45. However, in the parabiosis experiments our recombination efficiency was 90% and thus, although unlikely, we can not exclude that among the non-labeled cells some non-hematopoetic cells might have contributed to the myofibroblast pool.

Second, since we have previously reported that all kidney myofibroblasts express PDGFRβ [4] we performed non-biased sc-RNA-seq of PDGFRβ$^+$ cells that were either CD45$^+$

(hematopoetic) or CD45$^-$ (non-hematopoietic) to profile all kidney myofibroblasts. The data indicate that the vast majority of kidney myofibroblasts are of resident origin while a minor fraction of circulating hematopoetic (CD45$^+$) cells also expressed the myofibroblast marker αSMA. Importantly, when comparing the dataset to a human PBMC sc-RNA-seq dataset only the circulating (PDGFRβ$^+$/CD45$^+$) population showed a strong correlation and the comparison identified monocytes as the origin of circulating myofibroblasts. Thus our data indicates that circulating MSC do not contribute to the myofibroblast pool.

Importantly, we have also recently reported bone marrow transplantation and parabiosis experiments indicating that Gli1$^+$ MSC do not circulate [45, 46] and a recent study reports no evidence for circulating MSC in patients with organ injury unless they do not suffer from sever trauma with multiple fractures which leads to mechanical disruption of bone marrow with embolism . However, the sc-RNA seq experiment was not performed as a time course and thus we cannot account for dynamic changes in expression of the markers over the course of the experiment.

In conclusion, kidney myofibroblasts arise primarily from resident mesenchymal cells whereas circulating monocytes contribute a minor fraction. Importantly, these circulating myofibroblasts primarily secrete proinflammatory cytokines and do not appreciably contribute to extracellular matrix production.

METHODS

Mice

All mouse experiments were performed according to the animal experimental guidelines issued by the Animal Care and Use Committee at Harvard University and the Washington University. Rosa26CreER^{t2} (JAX #008463), Rosa26tdTomato (JAX #007909), B6-CD45.1 (JAX #002014) and C57BL/6J (JAX #000664) mice were purchased from Jackson Laboratories (Bar Harbor, ME). In the parabiosis experiment bigenic Rosa26CreER;tdTomato mice (females, 8 weeks of age) received tamoxifen (4x10mg in corn oil with 3% ethanol) per oral gavage (every other day) and were conjoined with B6-CD45.1 mice (8 week old females) 10 days after the last tamoxifen dose. Parabiosis was performed as previously described.[47]

Anasthesia was achieved by intraperitoneal injection of ketamine (100mg/kg bodyweight), xylazine (10mg/kg) and acepromacine (3mg/kg). Buprenorphine (0.05mg/kg), meloxicam (1mg/kg) and lidocaine (1%) was given subcutaneously to achieve analgesia.

The entire flanks of the mice were shaved and the skin was cleaned with triple applications of a povidine iodine soap alternating with an alcohol rinse. Thereafter matching skin incisions were made from the elbow to the knee joint of each mouse. The right olecranon of one animal was attached to the left olecranon of the other by a single 4-0 suture and tie. Similarly, the partners' knee joints were connected. The dorsal and ventral skin was then anastomosed by staples and suture. Four weeks after parabiosis surgery blood was drawn from the retro-orbital vein plexus to check cross-circulation efficiency. Thereafter the B6-CD45.1 mice underwent unilateral ureteral obstruction surgery as follows: Anasthesia and analgesia was achieved in the parabiosis pair as described above. After flank incision the right kidney was exposed and freed from the peri-renal fat tissue, the ureter was tied off at the level of the lower pole using two 4.0 silk ties. Wounds were closed by staples. Mice were sacrificed at 10 days after UUO surgery. UUO surgeries in C57Bl6 wildtype mice were performed at 8 weeks of age using the same technique.

Statistical Analysis

Data are presented as mean±SD . Comparison of two groups was performed using unpaired t-test. Paired t-test was used for comparison of repeated measured in the same group. Statistical analyses were performed using GraphPad Prism 5.0c (GraphPad Software Inc., San Diego, CA). A p-value of less than 0.05 was considered significant.

Tissue Preparation and Histology

Mice were anesthetized with isofluorane (Baxter) and subsequently perfused via the left ventricle with 4°C PBS for 1 minute. For histological analyses, tissue sections were fixed in 10% formaldehyde for 1 hour, paraffin embedded, cut with a rotating microtome at a thickness of 3 µm, and stained according to routine histological protocols. For immunofluorescence

studies kidneys were fixed in 4% paraformaldehyde on ice for 1 hour, then incubated in 30% sucrose in PBS at 4°C overnight. OCT-embedded (Sakura Finetek) tissues were cryosectioned into 5 µm sections and mounted on superfrost slides (Fisher Scientific). Sections were washed in 1X PBS, blocked in 10% normal goat serum (Vector Labs) and incubated with primary antibodies specific for α-SMA-FITC (mouse, 1:100, sigma cat no. F3777), PDGFRb (rabbit, 1:100, Abcam cat. no. ab32570), CD45 (rat, 1:100, Novusbio, NB100-77417). Secondary antibodies were FITC- or Cy5-conjugated (Jackson ImmunoResearch). Sections were then stained with DAPI (4´,6´-´diamidino-2-phenylindole) and mounted in Prolong Gold (Life Technologies). All images were obtained by confocal (Zeiss LSM880 equipped with an Airyscan detector) trough the Washington University Center for Cellular Imaging (WUCCI). Fibrosis was scored at x400 magnification using a counting grid with 117 intersections. The number of grid intersections overlying trichrome-positive interstitial areas was counted and expressed as a percentage of all grid intersections. Intersections that were in tubular lumen and glomeruli were substracted from the total number of grid-intersections.

Flow Cytometry and cell sorting

For flow cytometric analysis or fluorescence activated cell sorting (FACS) mice were euthanized as described above, perfused with sterile PBS via the left ventricle and the kidneys were placed in PBS with 5% FBS. After thoroughly mincing the tissue/organ using a sterile scalpel (Feather), the tissue/organ was placed in gentleMACS C Tubes (Miltenyi Biotec) containing 1.5ml DMEM (Life Technologies) with 0.1mg/ml Liberase TL (Roche). The tissue was then dissociated using the D program of the gentleMacs dissociator (Miltenyi Biotec) followed by 30 min incubation at 37°C. Following washing steps with FACS buffer and centrifugation (1500 rpm 5 min) the solution was filtered twice trough a 40µm cell strainer (BD Biosciences) and transfered to 5ml Polystyrene Round-Bottom FACS tube (BD Biosciences). For flow cytometric studies the samples were stained in 100-500µl FACS Buffer using the following fluorochrome conjugated antibodies: CD45.1 (APC-Cy7, ebioscience #25045382), CD45.2-FITC (ebioscience #110454), α-SMA-FITC (sigma # F3777) PDGFRb-APC (Biolegend, #136008), CD45-BV421 (Biolegend, #103133) all 1:100 for 30 min followed by a washing step with PBS. Cytofix/Cytoperm solution (BD Biosciences) was used to achieve staining for intracellular α-SMA. All flow cytometric analyses were performed at a Canto II analyzer (BD Biosciences). For sorting DAPI (1mg/ml 1:1000) was added in order to exclude dead cells. Single cell sorting was performed at the Siteman Flow Cytometry Core (Washington University) using an iCyt Synergy sorter (Sony). Single cells were sorted directly into 10x lysis buffer (Clontech) in 96well PCR plates. Data were analyzed by using Flow Jo software (Version 9.6.2, Tree Star Inc).

Single cell RNA-seq and data pre-processing

96-well plates with single cell in each well were sealed and sent to the sequencing core at Washington University in St Louis (Genome Technology Access Center, GTAC). RNA from individual wells were processed with the Clonetech Smarter system and ligated with unique barcodes. Each plate was then pooled into one library and the resulting pools were then ligated to adapters containing unique 7bp index sequences so that samples originating from a single plate can be identified by Illumina conventional indexing strategies and each individual well is defined by barcoades sequenced on the first read of a paired end read pair.

Al plates were pooled into a single library and subjected to Illumina sequencing (HiSeq2500 2x50bp). The resulting sequencing read were demultiplexed by index with a custom Phython demultiplexing script and further demultiplexed by barcode with a custom Perl demultiplexing script. The RNA-Seq reads were then aligned to the Mus musculus Ensembl release 76 top-level assembly with STAR version 3.0.4.b. Gene counts were derived from the number of uniquely aligned unambiguous reads by Subread:featureCount version 1.4.5. Sailfish version 0.6.3. was used to produce isoform estimated counts. Gene and isoform counts were further transformed into counts-per-million (CPM), log 2 CPM with a prior count of 2 (moderated log2CPM), and RPKM with custom Rscripts. Sequencing performance was assessed for total number of aligned reads, total number of uniquely aligned reads, genes and transcripts detected, ribosomal fraction, known junction saturation and read distribution over known gene models with RSeQC version 2.3. The single cell RNA-Seq raw data is available in the gene expression omnibus (GEO) database: accession number GSE112033.

Bioinformatics

1. Unsupervised clustering and differential gene analysis

We used Seurat software in R to identify cell clusters, performed differential gene analysis, and generated the top gene heatmap. In brief, gene expression matrix with gene names as rows and cell names as columns was input into Seurat. Before clustering, we removed low expressed genes and low quality cells by filtering out genes that were expressed in less than 10 cells and cells that had greater than 20% mitochondrial gene content, resulting in 14,062 genes and 357 cells. After filtering, we normalized the expression values for each cell by the total expression, multiplied this by 10,000, and log-transformed the result. Next, we performed dimensionality reduction on the scaled data by computing the significant principal components (PC) on highly variable genes. Graph-based clustering analysis were performed on the first 10 PCs and clusters were visualized in tSNE. To examine potential batch effect, cells were colored by plates and plotted in the same tSNE. Differential gene analysis was performed using the FindAllMarkers function in Seurat (likelihood-ratio test). Differentially expressed genes that were expressed at least in 25% cells within the cluster and with a fold change more than 0.25 (log scale) were considered to be marker

genes. Marker genes in each cluster were visualized by two different ways: we used the DoHeatmap function (Seurat) to show the top 30 genes for each cluster, and the FeaturePlot function (Seurat) to plot the well-known markers. To compare the relative expression of pro-fibrotic genes and pro-inflammatory genes between clusters, we selected genes that are components of extracellular matrix and genes that are known as cytokines/chemokines from the differential gene list. Average expression level of these selected genes was z-score normalized and visualized using the pheatmap package in R. To classify the gene function of the marker genes, we uploaded the differential gene list onto ToppGene suite (https://toppgene.cchmc.org) for gene sets functional enrichment analysis. The top 5 enriched GO terms from each category (molecular function, cellular components, and biological function) were compared between clusters and bar plots were shown using the ggplot2 package.

2. Comparison of fibrocytes and a public PBMC dataset

Cell-type-specific expression patterns of the cell clusters identified in our dataset were compared to signatures previously defined in a PBMC dataset by calculating the pairwise Pearson correlations coefficients between each pair of cell types for the same set of genes. First, a precomputed Seurat object containing cell cluster information for 33K human PBMCs was downloaded from Satija's lab (http://satijalab.org/seurat/get_started.html). Second, mouse genes were converted to human equivalent genes using a R package biomaRt. Only genes that are detected in our dataset and the PBMC dataset were used for downstream correlation analysis. Third, Pearson correlation was computed between the cell clusters in our dataset and the cell clusters identified in the PBMC dataset, using the previously defined cell-type annotations and normalized average gene expression values for each cell type. Data was shown by pheatmap R package.

3. Construction of transcription network by driving force analysis

To identify the key regulators that control the cell states, we established the relationship between transcription factors (TFs) and their target genes (TGs) following the SINCERA pipeline [49]. This approach consists of three main steps. First, the candidate TFs and TGs were extracted from the DEG list identified in each cluster. Second, cell type specific transcription regulatory network (TRN) was constructed by establishing the interaction between TF-TF and TF-TG as previously described [1-3]. TG-TF and TF auto-regulations were not considered in the present study. Finally, the key TFs were selected based on their network node importance, and ranked by integrating six node importance metrics including Degree Centrality (DC), Closeness Centrality (CC), Betweenness Centrality (BC), Disruptive Fragmentation Centrality (DFC), Disruptive Connection Centrality (DCC) and Disruptive Distance Centrality (DDC). The TRN igraph object obtained from SINCERA was converted to JSON using a R package RJSONIO, and imported into Cytoscape (version 3.4.0) for network visualization.

Ligand-receptor interaction analysis

To study ligand-receptor interactions between myofibroblast and fibrocyte, we used a human ligand–receptor list comprising 2,557 ligand–receptor pairs curated by the Database of Ligand−Receptor Partners (DLRP), IUPHAR and Human Plasma Membrane Receptome (HPMR). We selected the receptors that were only differentially expressed in each cell type. To determine the ligand-receptor pairs to plot on the heatmap, we required that (i) the receptors are uniquely expressed in each cell type (q-val<0.05 and logFC>0.6); (ii) Each receptor should have at least one corresponding ligand to pair with. We used heatmap.2 function from gplots package to visualize the ligand-receptor pairs.

Statistical analysis

Data are presented as mean±SD . Comparison of two groups was performed using unpaired t-test. Statistical analyses were performed using GraphPad Prism 5.0c (GraphPad Software Inc., San Diego, CA). A p-value of less than 0.05 was considered significant.

Study approval

All mouse experiments were performed according to the animal experimental guidelines issued by the Animal Care and Use Committee at Harvard University, Boston (#04474) and the Washington University St Louis (#A-3381-01).

Author contributions

R.K. designed and carried out experiments, analyzed results and wrote the manuscript, F.M., K.H.,T.K. and R.K.S. carried out some of the experiments, analyzed the data and reviewed the manuscript, H.W. contributed to the single cell RNA-Sequencing experiment and performed the bioinformatics, B.D.H. designed experiments, analyzed results and contributed to writing of the manuscript.

The authors have declared that no conflict of interest exists.

Acknowledgments

This work was supported by Grants of the German Research Foundation (KR-4073/3-1, SCHN1188/5-1, SFB/TRR57) a Grant of the European Research Council (ERC-StG 677448), a START Grant of the RWTH Aachen University (101/15) and a Grant of the State of Northrhinewestfalia (Return to NRW) to RK and by the NIH/NIDDK (DK088923, DK103740 and DK103050) and by an Established Investigator Award of the American Heart Association (EIA14650059) to BDH. We thank the Genome Technology Access Center in the Department of Genetics at Washington University school of Medicine for help with genomic analysis. The Center is partially supported by NCI Cancer Center Support Grant #P30 CA91842 to the Siteman Cancer Center and by ICTS/CTSA Grant #UL1 TR000448 from the National Center

for Research Resources (NCRR), a component of the NIH, and NIH Roadmap for Medial Research. This publication is solely the responsibility of the authors and does not necessarily represent the official view of the NCRR or NIH. Experiments were performed in part through the use of Washington University Center for Cellular Imaging (WUCCI).

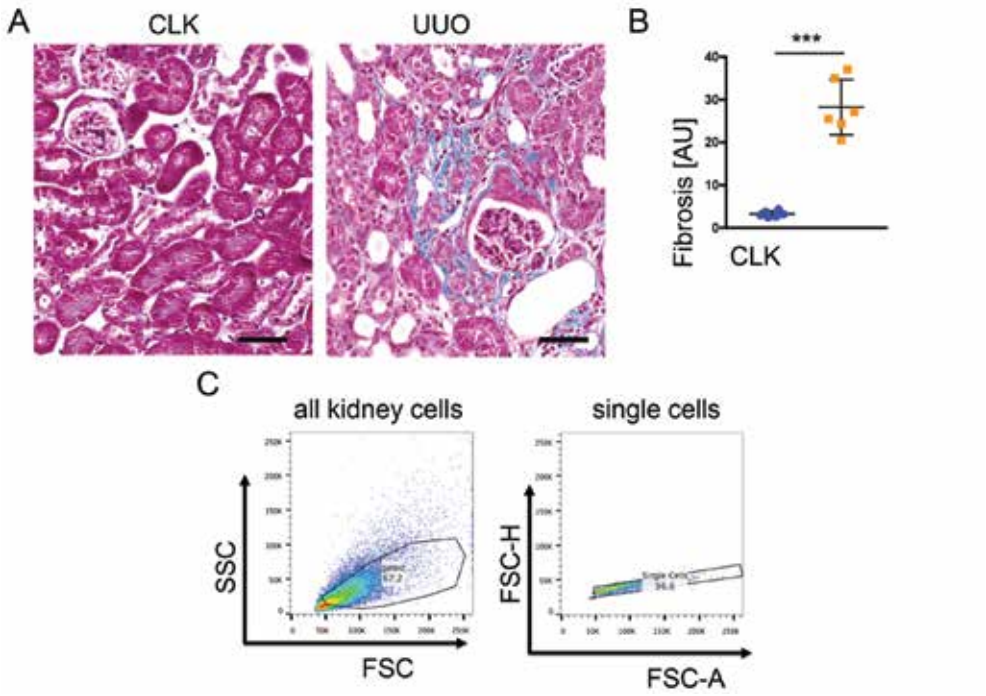

Supplementary Figure S1 Trichrome staining and representative gating for flow cytometry of whole kidneys
(**A-B**) Non-injured contralateral (CLK) kidneys and injured unilateral ureteral obstructed (UUO) kidney of the CD45.1 parabiont were trichrome stained and the interstitial fibrosis was quantified. Scale bars 50µm. ***p<0.001 by unpaired t-test.
(**C**) Representative gating for flow-cytometric analysis of the whole kidneys.

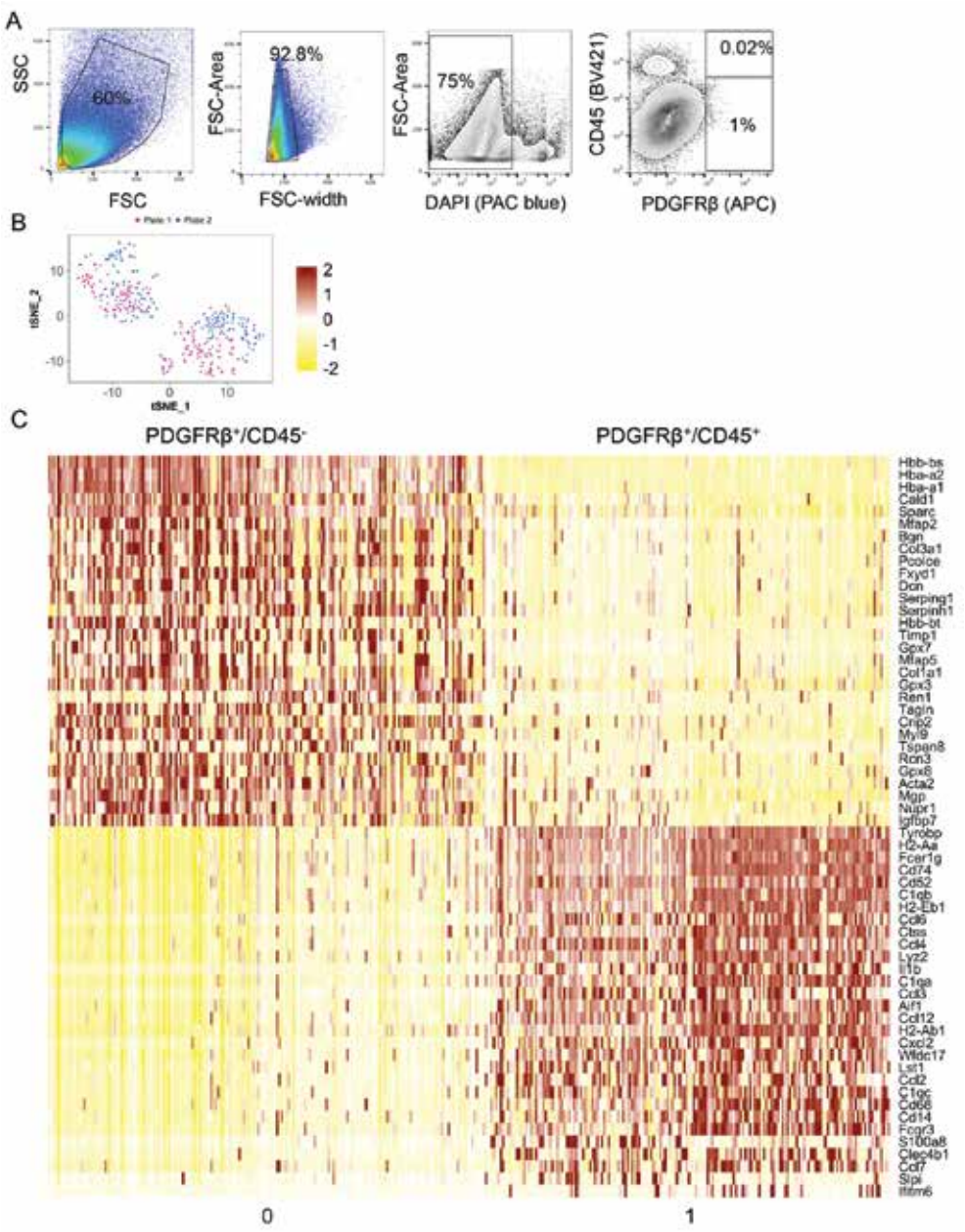

Supplementary Figure S2 Representative gating for FACS and top upregulated genes in single cell RNA-Sequencing clusters of resident and circulating myofibroblasts

(**A**) Representative gating for the sorting (FACS) of whole kidneys on single/living (DAPI-) PDGFRβ+/CD45+ and PDGFRβ-/CD45- cells

(**B**) tSNE analysis clusters with respect to the batch.

(**C**) Top 30 expressed genes in the two tSNE clusters.

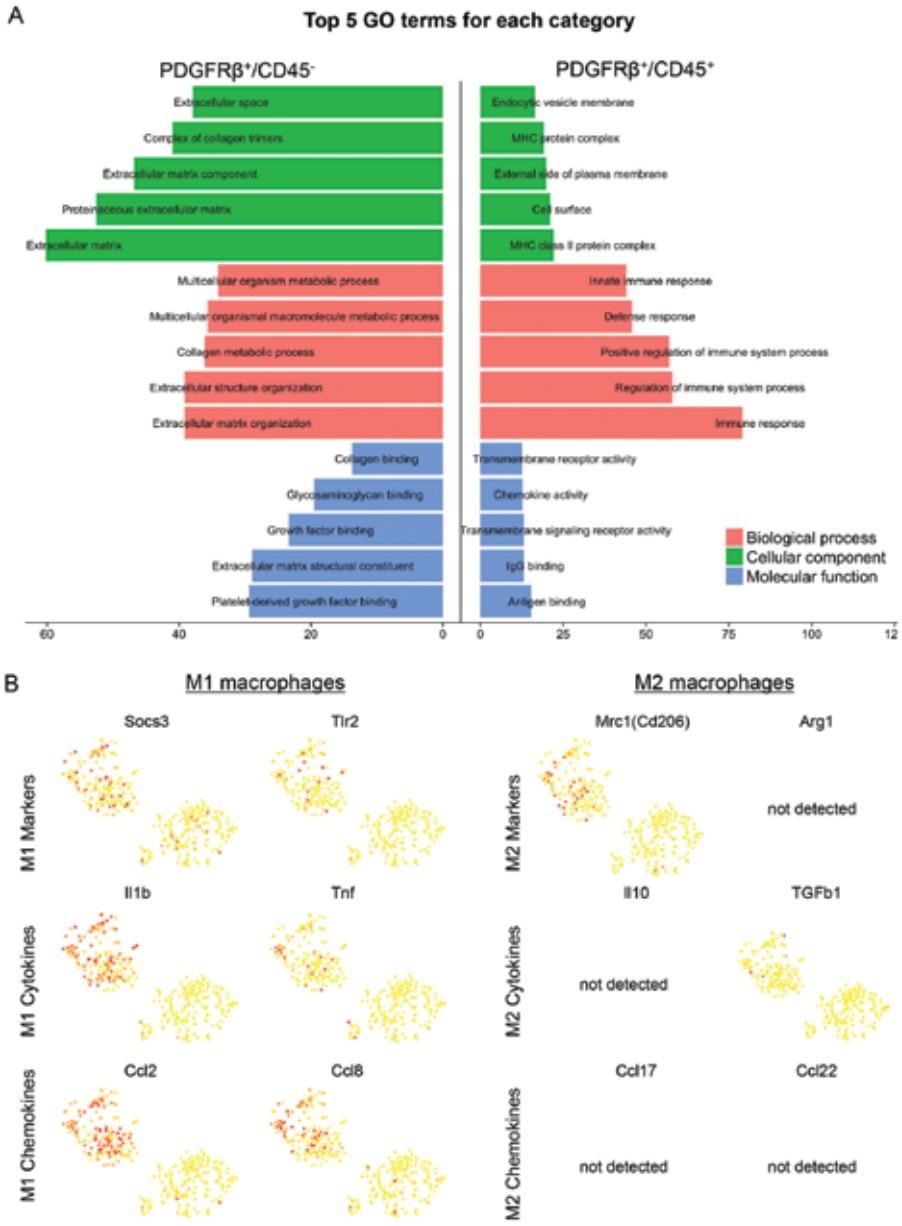

Supplementary Figure S3 Top gene ontology terms and macrophage polarization markers in the two clusters.
(**A**) Top 5 gene ontology (GO) terms of the two tSNE cluster for the categories biological process, cellular component and molecular function.
(**B**) Expression levels of genes that define M1 and M2 macrophages in both tSNE clusters. (Socs3, suppressor of cytokine signaling 3; Tlr2, toll-like receptor 2; Il1b, Interleukin 1b; Tnf, tumor necrosis factor alpha; Ccl2, cc-chemokine ligand 2; Ccl8, cc-chemokine ligang 8; Mrc1, mannose receptor 1; Arg1, arginase 1; Il10, Interleukin 10; TGFb1, transforming growth factor beta 1; Ccl17, cc-chemokine ligand 17; Ccl22, cc-chemokine ligand 22 Color key denotes the z-score normalized average expression value of selected differentially expressed genes between PDGFRβ^{+}/CD45^{-} and PDGFRβ^{+}/CD45^{+} cells.

Supplementary Table 1: Transcription factors for PDGFRb+/CD45+ cell population in kidney fibrosis

TF	DC	CC	BC	DFC	DCC	DDC	AVG.RANK
Fos	1	2	1	1	1	1	1
Atf3	2	1	2	3	3	2	2
Junb	4	3	3	2	2	3	3
Egr1	6	6	5	4	4	4	4
Maf	3	4	4	6	7	5	4
Batf3	7	5	6	8	9	9	6
Pou2f2	9	7	9	6	7	8	7
Batf	11	12	8	5	5	6	8
Spi1	8	8	7	11	6	7	8
Jun	5	12	11	11	12	12	10
Sub1	11	16	10	8	9	11	11
Irf8	14	14	12	8	9	10	12
Ddit3	11	9	14	11	12	13	13
Stat1	14	10	13	11	12	14	14
Klf6	9	15	15	11	12	15	15
Nfe2l2	17	17	17	11	12	17	16
Mafb	16	11	16	17	17	16	17

TF: transcription factor; **DC**: Degree Centrality; **CC**: Closeness Centrality; **BC**: Betweenness Centrality; **DFC**: Disruptive Fragmentation Centrality; **DCC**: Disruptive Connection Centrality; **DDC**: Disruptive Distance Centrality; **AVG.RANK**: Average Ranking.

Supplementary Table 2: Transcription factors for the PDGFRb+/CD45- cell population in kidney fibrosis

TF	DC	CC	BC	DFC	DCC	DDC	AVG.RANK
Id3	2	1	1	4	4	2	1
Prrx1	4	5	2	1	1	1	1
Nr2f2	3	2	3	4	4	4	3
Tcf21	1	3	5	4	4	6	4
Tsc22d1	10	6	4	2	2	3	5
Heyl	5	4	6	4	4	5	6
Peg3	8	11	7	2	2	7	7
Nfic	7	8	8	4	4	8	8
Zbtb20	8	12	9	4	4	10	9
Hoxd10	6	13	11	4	4	12	10
Hoxa10	14	17	10	4	4	9	11
Snai2	12	15	15	4	4	15	12
Nr1d1	11	19	13	4	4	16	13
Ssrp1	12	14	16	4	4	17	13
Tcf4	19	16	14	4	4	11	15
Nfib	17	18	12	4	4	13	15
Hoxc10	17	7	21	4	4	18	17
Creb3l2	21	9	20	4	4	14	18
Alx1	21	10	22	4	4	19	19
Snai1	15	20	19	4	4	21	20
Zfp948	19	21	18	4	4	22	21
Meis2	24	23	17	4	4	20	22
Klf9	15	22	24	4	4	23	22
Glis2	21	25	23	4	4	24	24
Tead1	24	24	27	4	4	25	25
Thap7	26	27	26	4	4	26	26
Nfix	27	26	25	4	4	27	26
Cers2	27	28	28	4	4	28	28
Ebf1	29	29	29	4	4	29	29
Trp53	30	30	30	4	4	30	30

TF: transcription factor; **DC**: Degree Centrality; **CC**: Closeness Centrality; **BC**: Betweenness Centrality; **DFC**: Disruptive Fragmentation Centrality; **DCC**: Disruptive Connection Centrality; **DDC**: Disruptive Distance Centrality; **AVG.RANK**: Average Ranking.

REFERENCES

1. El Agha, E., et al., *Mesenchymal Stem Cells in Fibrotic Disease.* Cell Stem Cell, 2017. 21(2): p. 166-177.
2. Duffield, J.S., *Cellular and molecular mechanisms in kidney fibrosis.* J Clin Invest, 2014. **124**(6): p. 2299-306.
3. Falke, L.L., et al., *Diverse origins of the myofibroblast-implications for kidney fibrosis.* Nat Rev Nephrol, 2015. **11**(4): p. 233-44.
4. Kramann, R., et al., *Perivascular Gli1+ progenitors are key contributors to injury-induced organ fibrosis.* Cell Stem Cell, 2015. **16**(1): p. 51-66.
5. Kriz, W., B. Kaissling, and M. Le Hir, *Epithelial-mesenchymal transition (EMT) in kidney fibrosis: fact or fantasy?* J Clin Invest, 2011. **121**(2): p. 468-74.
6. Menon, M.C. and M.J. Ross, *Epithelial-to-mesenchymal transition of tubular epithelial cells in renal fibrosis: a new twist on an old tale.* Kidney Int, 2016. **89**(2): p. 263-6.
7. Zhao, Y., et al., *MiR-30c protects diabetic nephropathy by suppressing epithelial-to-mesenchymal transition in db/db mice.* Aging Cell, 2017. **16**(2): p. 387-400.
8. Grande, M.T., et al., *Snail1-induced partial epithelial-to-mesenchymal transition drives renal fibrosis in mice and can be targeted to reverse established disease.* Nat Med, 2015. **21**(9): p. 989-97.
9. Humphreys, B.D., et al., *Fate tracing reveals the pericyte and not epithelial origin of myofibroblasts in kidney fibrosis.* Am J Pathol, 2010. **176**(1): p. 85-97.
10. Iwano, M., et al., *Evidence that fibroblasts derive from epithelium during tissue fibrosis.* J Clin Invest, 2002. **110**(3): p. 341-50.
11. LeBleu, V.S., et al., *Origin and function of myofibroblasts in kidney fibrosis.* Nat Med, 2013. **19**(8): p. 1047-53.
12. Kramann, R., et al., *Matrix Producing Cells in Chronic Kidney Disease: Origin, Regulation, and Activation.* Curr Pathobiol Rep, 2013. **1**(4).
13. Kramann, R., D.P. DiRocco, and B.D. Humphreys, *Understanding the origin, activation and regulation of matrix-producing myofibroblasts for treatment of fibrotic disease.* J Pathol, 2013. **231**(3): p. 273-89.
14. Bucala, R., et al., *Circulating fibrocytes define a new leukocyte subpopulation that mediates tissue repair.* Mol Med, 1994. **1**(1): p. 71-81.
15. Roufosse, C., et al., *Bone marrow-derived cells do not contribute significantly to collagen I synthesis in a murine model of renal fibrosis.* J Am Soc Nephrol, 2006. **17**(3): p. 775-82.
16. Lin, S.L., et al., *Pericytes and perivascular fibroblasts are the primary source of collagen-producing cells in obstructive fibrosis of the kidney.* Am J Pathol, 2008. **173**(6): p. 1617-27.
17. Reich, B., et al., *Fibrocytes develop outside the kidney but contribute to renal fibrosis in a mouse model.* Kidney Int, 2013. **84**(1): p. 78-89.
18. Wang, Y.Y., et al., *Macrophage-to-Myofibroblast Transition Contributes to Interstitial Fibrosis in Chronic Renal Allograft Injury.* J Am Soc Nephrol, 2017. **28**(7): p. 2053-2067.
19. Broekema, M., et al., *Bone marrow-derived myofibroblasts contribute to the renal interstitial myofibroblast population and produce procollagen I after ischemia/reperfusion in rats.* J Am Soc Nephrol, 2007. **18**(1): p. 165-75.
20. Chen, G., et al., *CXCL16 recruits bone marrow-derived fibroblast precursors in renal fibrosis.* J Am Soc Nephrol, 2011. **22**(10): p. 1876-86.
21. Yan, J., et al., *JAK3/STAT6 Stimulates Bone Marrow-Derived Fibroblast Activation in Renal Fibrosis.* J Am Soc Nephrol, 2015. **26**(12): p. 3060-71.
22. Li, J., et al., *The contribution of bone marrow-derived cells to the development of renal interstitial fibrosis.* Stem Cells, 2007. **25**(3): p. 697-706.

23. Yang, J., et al., *Adiponectin promotes monocyte-to-fibroblast transition in renal fibrosis.* J Am Soc Nephrol, 2013. **24**(10): p. 1644-59.
24. Wang, S., et al., *TGF-beta/Smad3 signalling regulates the transition of bone marrow-derived macrophages into myofibroblasts during tissue fibrosis.* Oncotarget, 2016. **7**(8): p. 8809-22.
25. Cilloni, D., et al., *Limited engraftment capacity of bone marrow-derived mesenchymal cells following T-cell-depleted hematopoietic stem cell transplantation.* Blood, 2000. **96**(10): p. 3637-43.
26. Kusaba, T., et al., *Differentiated kidney epithelial cells repair injured proximal tubule.* Proc Natl Acad Sci U S A, 2014. **111**(4): p. 1527-32.
27. Aono, Y., et al., *Role of platelet-derived growth factor/platelet-derived growth factor receptor axis in the trafficking of circulating fibrocytes in pulmonary fibrosis.* Am J Respir Cell Mol Biol, 2014. **51**(6): p. 793-801.
28. Schneider, R.K., et al., *Gli1+ Mesenchymal Stromal Cells Are a Key Driver of Bone Marrow Fibrosis and an Important Cellular Therapeutic Target.* Cell Stem Cell, 2017. **20**(6): p. 785-800 e8.
29. Thompson, M.R., D. Xu, and B.R. Williams, *ATF3 transcription factor and its emerging roles in immunity and cancer.* J Mol Med (Berl), 2009. **87**(11): p. 1053-60.
30. Zenz, R., et al., *Activator protein 1 (Fos/Jun) functions in inflammatory bone and skin disease.* Arthritis Res Ther, 2008. **10**(1): p. 201.
31. Fontana, M.F., et al., *JUNB is a key transcriptional modulator of macrophage activation.* J Immunol, 2015. **194**(1): p. 177-86.
32. Cao, S., et al., *The protooncogene c-Maf is an essential transcription factor for IL-10 gene expression in macrophages.* J Immunol, 2005. **174**(6): p. 3484-92.
33. Decker, E.L., C. Skerka, and P.F. Zipfel, *The early growth response protein (EGR-1) regulates interleukin-2 transcription by synergistic interaction with the nuclear factor of activated T cells.* J Biol Chem, 1998. **273**(41): p. 26923-30.
34. Kanisicak, O., et al., *Genetic lineage tracing defines myofibroblast origin and function in the injured heart.* Nat Commun, 2016. **7**: p. 12260.
35. Kumar, A., et al., *Specification and Diversification of Pericytes and Smooth Muscle Cells from Mesenchymoangioblasts.* Cell Rep, 2017. **19**(9): p. 1902-1916.
36. Greenbaum, A., et al., *CXCL12 in early mesenchymal progenitors is required for haematopoietic stem-cell maintenance.* Nature, 2013. **495**(7440): p. 227-30.
37. Ackema, K.B. and J. Charite, *Mesenchymal stem cells from different organs are characterized by distinct topographic Hox codes.* Stem Cells Dev, 2008. **17**(5): p. 979-91.
38. Worthley, D.L., et al., *Gremlin 1 identifies a skeletal stem cell with bone, cartilage, and reticular stromal potential.* Cell, 2015. **160**(1-2): p. 269-84.
39. Kramann, R., et al., *Pharmacological GLI2 inhibition prevents myofibroblast cell-cycle progression and reduces kidney fibrosis.* J Clin Invest, 2015. **125**(8): p. 2935-51.
40. Nikolic-Paterson, D.J., S. Wang, and H.Y. Lan, *Macrophages promote renal fibrosis through direct and indirect mechanisms.* Kidney Int Suppl (2011), 2014. **4**(1): p. 34-38.
41. Nelson, P.J., *The contentious ontogeny of fibrosis in the kidney.* Kidney Int, 2013. **84**(1): p. 14-5.
42. Gibney, B.C., et al., *Cross-circulation and cell distribution kinetics in parabiotic mice.* J Cell Physiol, 2012. **227**(2): p. 821-8.
43. Wu, J.M., et al., *Circulating cells contribute to cardiomyocyte regeneration after injury.* Circ Res, 2015. **116**(4): p. 633-41.
44. Hoogduijn, M.J., et al., *No evidence for circulating mesenchymal stem cells in patients with organ injury.* Stem Cells Dev, 2014. **23**(19): p. 2328-35.
45. Bunster, E. and R.K. Meyer, *An improved method of parabiosis.* Anat. Rec. , 1933. **57**: p. 339-343.

46. Ruckh, J.M., et al., *Rejuvenation of regeneration in the aging central nervous system.* Cell Stem Cell, 2012. **10**(1): p. 96-103.

47. Guo, M., et al., *SINCERA: A Pipeline for Single-Cell RNA-Seq Profiling Analysis.* PLoS Comput Biol, 2015. **11**(11): p. e1004575.

48. Lebre, S., *Inferring dynamic genetic networks with low order independencies.* Stat Appl Genet Mol Biol, 2009. **8**: p. Article 9.

49. Ramilowski, J.A., et al., *A draft network of ligand-receptor-mediated multicellular signalling in human.* Nat Commun, 2015. **6**: p. 7866.

5

GLI2 REGULATES MYOFIBROBLAST CELL-CYCLE PROGRESSION IN KIDNEY FIBROSIS AND IS A NOVEL THERAPEUTIC TARGET

Rafael Kramann[1,2], Susanne V. Fleig[1,4], Rebekka K. Schneider[3], Steven L. Fabian[1], Derek P. DiRocco[1], Omar Maarouf[1], Janewit Wongboonsin[1], Yoichiro Ikeda[1], Dirk Heckl[3], Steven L. Chang[5], Helmut G. Rennke[6], Sushrut S. Waikar[1] and Benjamin D. Humphreys[1,7*]

[1]From the Renal Division, Brigham and Women's Hospital, Department of Medicine, Harvard Medical School, Boston, Massachusetts;
[2]Division of Nephrology and Clinical Immunology RWTH Aachen University Medical Faculty RWTH Aachen University, Pauwelsstrasse 30, 52074 Aachen, Germany
[3] Division of Hematology, Brigham and Women's Hospital, Department of Medicine, Harvard Medical School, Boston, Massachusetts;
[4]Division of Nephrology and Hypertension, Hannover Medical School, Hannover, Germany
[5]Divison of Urology, Brigham and Women's Hospital
[6]Department of Pathology, Brigham and Women's Hospital
[7] Harvard Stem Cell Institute, Cambridge, Massachusetts

Corresponding author:
*Benjamin D Humphreys, MD, PhD
Renal Division, Department of Medicine,
Washington University School of Medicine;
Box 8126
600 South Euclid Avenue
St. Louis, Missouri 63110
Tel: 314 362 8233
FAX: 314 362 8237
E-mail: bhumphre@dom.wustl.edu

J Clin Invest 2015 Aug 3;125(8):2935-51

ABSTRACT

Chronic kidney disease is characterized by interstitial fibrosis with proliferation of scar-secreting myofibroblasts, ultimately leading to end stage renal disease. The hedgehog pathway transcriptional effectors Gli1 and Gli2 are expressed in myofibroblast progenitors but their role during fibrogenesis is poorly understood. We demonstrate that Gli2, but not Gli1, drives myofibroblast cell cycle progression *in vitro*. Hedgehog pathway suppression by expression of Gli3 repressor in Gli1+ myofibroblast progenitors prevented fibrosis, an effect mimicked by cell-specific knockout of Gli2 but not Gli1. The mechanism of fibrosis inhibition was through induction of myofibroblast-specific cell-cycle arrest. Pharmacologic targeting of this pathway with darinaparsin, an arsenical in clinical trials, reduced fibrosis through reduction of Gli2 protein levels with a subsequent cell-cycle arrest of myofibroblasts. Gli2 overexpression rescued the cell-cycle effect of darinaparsin in vitro. While darinaparsin ameliorates fibrosis in wildtype and Gli1 knockout mice it does not show an effect in conditional Gli2 knockout mice pointing towards Gli2 as a molecular target of darinaparsin. The Gli inhibitor GANT61 also reduced fibrosis in mice and we demonstrate increased expression of Gli1 and Gli2 in human kidney fibrosis. Gli inhibition is a promising novel therapeutic strategy to target myofibroblast proliferation in kidney fibrosis.

INTRODUCTION

The rising incidence of diabetes and hypertension in our aging population have led to increased rates of both chronic kidney disease (CKD) and end-stage renal disease (ESRD) Estimates of CKD prevalence approach 10% in the United States, with more than 600,000 patients living with ESRD[4]. These patients suffer substantial morbidity and mortality while on dialysis, and kidney transplant list wait times number in years because there are not enough kidneys available. The cost to care for patients with ESRD also consumes a disproportionate fraction of healthcare budgets [4, 5]. For these reasons, novel therapeutic strategies to slow down CKD progression and reduce the incidence of ESRD are urgently needed.

Kidney fibrosis is the common final pathway for nearly all progressive kidney diseases. Inhibiting kidney fibrosis therefore represents a logical strategy to slow the progression of CKD to ESRD. However, there are currently no approved drugs available to treat kidney fibrosis . Myofibroblasts are widely accepted as the cell type responsible for the secretion of matrix proteins that drive kidney fibrosis [6] and we have recently shown that Gli1 expression identfies a perivascular mesenchymal stem cell (MSC)-like progenitor population that gives rise to myofibroblasts in solid organ injury [7]. Genetic ablation of these cells ameliorates heart and kidney fibrosis, providing a proof-of-principle for therapeutic targeting of these cells [8]. The specificity of Gli1 expression in these myofibroblast progenitors prompted us to investigate the functional role of hedgehog-Gli pathway in these cells during fibrosis.

In vertebrates three members of the Gli transcription factor family exist - Gli1, Gli2 and Gli3, likely derived from duplications of a single ancestral Gli gene [8-12]. All Gli proteins contain a C-terminal activator domain, whereas only Gli2 and Gli3 possess an N-terminal repressor domain . Mouse mutants suggest that Gli2 is important for the activator function in response to Hh signaling while Gli3 is the major repressor; Gli1 primarily amplifies the transcriptional response . The Hh receptor Patched (Ptc) is localized in and around the primary cilium. Upon binding of a Hh ligand (sonic, desert or indian Hh), Ptc releases tonic inhibition of the transmembrane protein smoothened (Smo) and leaves the cilium. Smo activation results in accumulation of suppressor of fused (SUFU)-Gli2 and SUFU-Gli3 complexes in the cilium, which otherwise would have been ubiquitinated and degraded . Following dissociation from SUFU, Gli2 (and Gli3) translocate into the nucleus where they activate the expression of Hh target genes, including Gli1 and Ptc1 .

In mammals, Gli1 is not required for Shh signaling and Gli1-knockout mice develop normally, unless one copy of Gli2 is defective [15, 16], whereas Gli2-knockout mice die at birth with severe skeletal and neural defects [12]. Studies in mutant mice where the zinc finger encoding exons have been removed from either Gli1 or Gli2 genes suggest that Gli2 can rescue most Gli1 functions whereas Gli1 cannot rescue Gli2 function [4, 5, 8, 18, 19]. Interestingly, when Gli1 is expressed from the endogenous Gli2 locus it can rescue the *in vivo*

function of Gli2 suggesting that only the activator form of Gli2 is required for development .

The Hh pathway regulates mesenchyme cell fates during kidney and ureteric development and growing evidence implicates a critical role of Hh in solid organ fibrosis and cancer . We and others have reported a role of the Hh pathway in renal fibrosis . While some evidence suggests upregulation of Hh ligands during kidney fibrosis, accumulating data indicates that Gli proteins can also be activated in a ligand-independent fashion by transforming growth factor beta (TGF-β) [25, 26], platelet derived growth factor (PDGF) signaling [27-32], epidermal growth factor receptor, RAS and AKT/PI3K pathways , all of which have also been reported to contribute to progression of fibrosis.

Given the specific expression Gli1 and Gli2 in myofibroblasts and their precusors [26, 33, 34], the important role of Hh signaling in cell proliferation and the possibility of direct activation of Gli proteins by known pro-fibrotic pathways, we investigated the role of Gli1 and Gli2 in myofibroblast function in kidney fibrosis. We demonstrate that conditional knockout of Gli2 or inhibition of Gli proteins by overexpression of the Gli3 repressor in Gli1 haploinsufficient mice, but not knockout of Gli1 alone, induces a specific myofibroblast cell-cycle arrest with reduced fibrosis. Furthermore, direct targeting of Gli proteins with darinaparsin, a novel organic arsenical with optimized pharmacokinetic properties that is currently undergoing clinical studies in hematologic malignancies and solid tumors [9, 26, 33, 37-39], inhibits hedgehog effectors Gli1 and Gli2 during kidney fibrosis and prevents myofibroblast proliferation. Darinaparsin acts by directly binding to Gli2 and inducing a Gli-dependent cell cycle arrest in kidney myofibroblasts. GANT61, a small molecule inhibitior of Gli, also ameliorates renal fibrosis in mice even when administered after injury. Furthermore, we demonstrate that Gli1 and Gli2 expression is also increased in fibrotic human kidneys suggesting that a similar mechanism might be involved in human kidney fibrosis progression.

RESULTS

Knockdown of Gli2 but not Gli1 induces a G0/G1 cell-cycle arrest in vitro

There are many examples of Hh-dependent regulation of cell proliferation in development and disease . *Gli2*$^{-/-}$ skin transplants are characterized by growth arrest in hair follicle development while constitutively active Gli2 induces skin proliferation in Shh null mice, suggesting that Gli2 is the effector of Hh-induced proliferation [6, 20]. Our own recent data indicates that pharmacologic inhibition of Gli proteins reduces the self-renewal capacity of Gli1^{+} MSC-like myofibroblast precursors . To evaluate the role of Gli1 versus Gli2 on cell proliferation *in vitro,* we performed siRNA knockdown experiments in the MSC-like cell line 10T1/2 (Figures 1, S1). Treatment with siRNA against Gli1 reduced mRNA and protein levels of Gli1 alone, while siRNA directed against Gli2 reduced both Gli1 and Gli2 expression, consistent with Gli1 as a downstream transcriptional target of Gli2 (Figure 1 A-B, S1 B-C). Flow cytometric analysis of cell-cycle distribution revealed that knockdown of Gli2 (or both Gli1 and Gli2) resulted in G0/G1 arrest with fewer cells in S and G2/M phases, whereas siRNA against Gli1 alone had no effect (Figure 1 C-D). Knockdown of Gli2 or both Gli1 and Gli2 reduced levels of phosphorylated retinoblastoma (Ser780) with increased levels of the cyclin dependent kinase inhibitor p21, suggesting that cells exited the cell cycle at the G1 restriction point (Figures 1E, S1D-E).

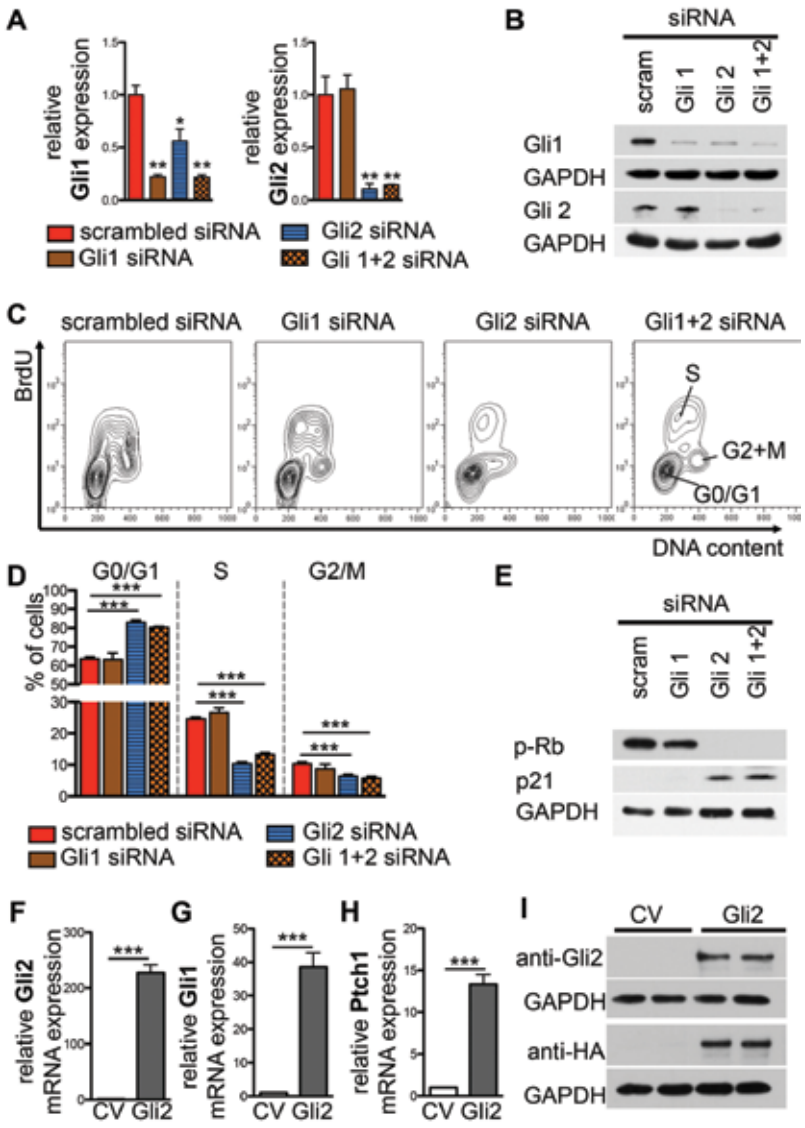

Figure 1: Lowering Gli2 but not solely Gli1 by RNAi induces a cell-cycle arrest of MSC-like cells *in vitro*

A-B: mRNA and protein levels of Gli1 and Gli2 in 10T1/2 cells treated with siRNA as indicated. Shh was added to the medium to increase Gli protein levels for better detection (the experiment was repeated in n=3 biological replicates, Quantification of western blot data from three replicates is shown in figure S1)

C-D: Representative flow cytometric cell-cycle plots and quantification of 10T1/2 cells after siRNA mediated knockdown of Gli1, Gli2 or both Gli1/Gli2 compared to scrambled siRNA (n=3 replicates).

E: Representative western blot of the cell-cycle regulators at the G1 restriction point phosphorylated retinoblastoma (pRb) and p21 following knockdown of Gli1, Gli2 or Gli1/2. Quantification of western blot data from three replicates is shown in figure S1

F-I: Overexpression of Gli2 by retroviral delivery activates the hedgehog pathway with increased downstream expression of Gli1 and patched 1 (Ptch1).

*p<0.05, **p<0.01, ***p<0.001, A by t-test, D by one way ANOVA with posthoc Bonferroni , data presented as mean±SEM

Overexpression of Gli2 drives cell proliferation

We next investigated whether overexpression of Gli2 by retroviral delivery (Figure S2 A-D) drives proliferation and could rescue the effect of siRNA knockdown. Gli2 overexpression caused activation of the Hh pathway as reflected by increased mRNA expression of Gli1 and Ptch1 (Figure 1 F-I) as expected. Importantly Gli2 overexpression increased cell-proliferation and was able to rescue the effect of Gli2 or Gli1 and Gli2 knockdown by RNAi, confirming the specificity of the siRNA approach and pointing towards Gli2 as a key regulator of cell proliferation (Figure S2E-F).

Conditional knockout of Gli2 or overexpression of the Gli3 repressor in Gli1^{+} cells reduces kidney fibrosis, but knockout of Gli1 has no effect

Interstitial myofibroblasts and their perivascular precursors are the only cells in the mouse kidney that express Gli1 and Gli2 [21] and it has been reported that knockout of Gli1 ameliorates kidney fibrosis in mice [12, 14]. Since Gli2 can compensate for Gli1 function in development, we asked whether conditional knockout of Gli2 in Gli1^{+} cells would provide further additive protection against fibrosis compared to Gli1 knockout alone. To repress the entire Gli family, we also crossed *Gli1-CreER^{t2}* mice against the *R26-Gli3T* strain, in which the Gli3 repressor is expressed from Rosa26 locus following Cre-mediated recombination. UUO experiments in *Gli1-nLacZ* and *Gli2-nLacZ* mice and co-staining for α-SMA and β-Galactosidase confirmed that expression of Gli1 and Gli2 is restricted to the myofibroblast lineage after kidney injury (Figure S3A-B). Western blot of whole kidney lysates after sham and UUO surgery confirms upregulation of endogenous Gli1 and Gli2 protein after kidney injury (Figure S3C).

Wildtype littermates, *Gli1KO*, conditional *Gli2 KO*, *Gli1/2 KO* or *Gli3T* mice were injected with tamoxifen as indicated, underwent unilateral ureteral obstruction (UUO) surgery and were sacrificed at day 10 following UUO (Figure 2A).

As expected, Gli1 knockout mice lacked Gli1 expression (Figures 2B-D, S4). *Gli2KO* and *Gli3T* mice showed substantially reduced expression of Gli1, suggesting that upstream Gli2 regulates basal Gli1 levels. *Gli2KO*, *Gli1/2KO* and *Gli3T* mice exhibited significantly reduced expression of Gli2 compared to *Gli1KO* whereas Gli2 levels were unaffected (Figures 2 C-D, S4). While *Gli2 KO*, *Gli1/2KO* and *Gli3T* mice showed reduced fibrosis severity, knockout of Gli1, surprisingly, had no appreciable effect when compared to wildtype littermates (Figures 2 E-H, S4). This data indicates that knockout of Gli1 in the presence of Gli2 has no effect on kidney fibrosis, while inhibition of both Gli1 and Gli2 by *Gli3T* or conditional knockout of Gli2 (in haploinsufficient Gli1 knockout mice) reduced fibrosis severity. These observations are in line with previous reports that Gli1 knockout mice show no developmental phenotype in the presence of Gli2 [21], suggesting that Gli2 may rescue Gli1 functions, while Gli1 cannot rescue Gli2 functions in the absence of Gli2.

A possible explanation for Gli1 knockout being not protective following UUO in our hands is the different background of the *Gli1CreER*^{t2} mice compared to *Gli1-nLacZ* mice previously used to knockout Gli1 . We therefore utilized *Gli1-nLacZ* mice to knockout Gli1, however again we could not detect a difference in fibrosis severity when comparing *Gli1-nLacz*$^{+/+}$ mice to wildtype littermates (Figure S5).

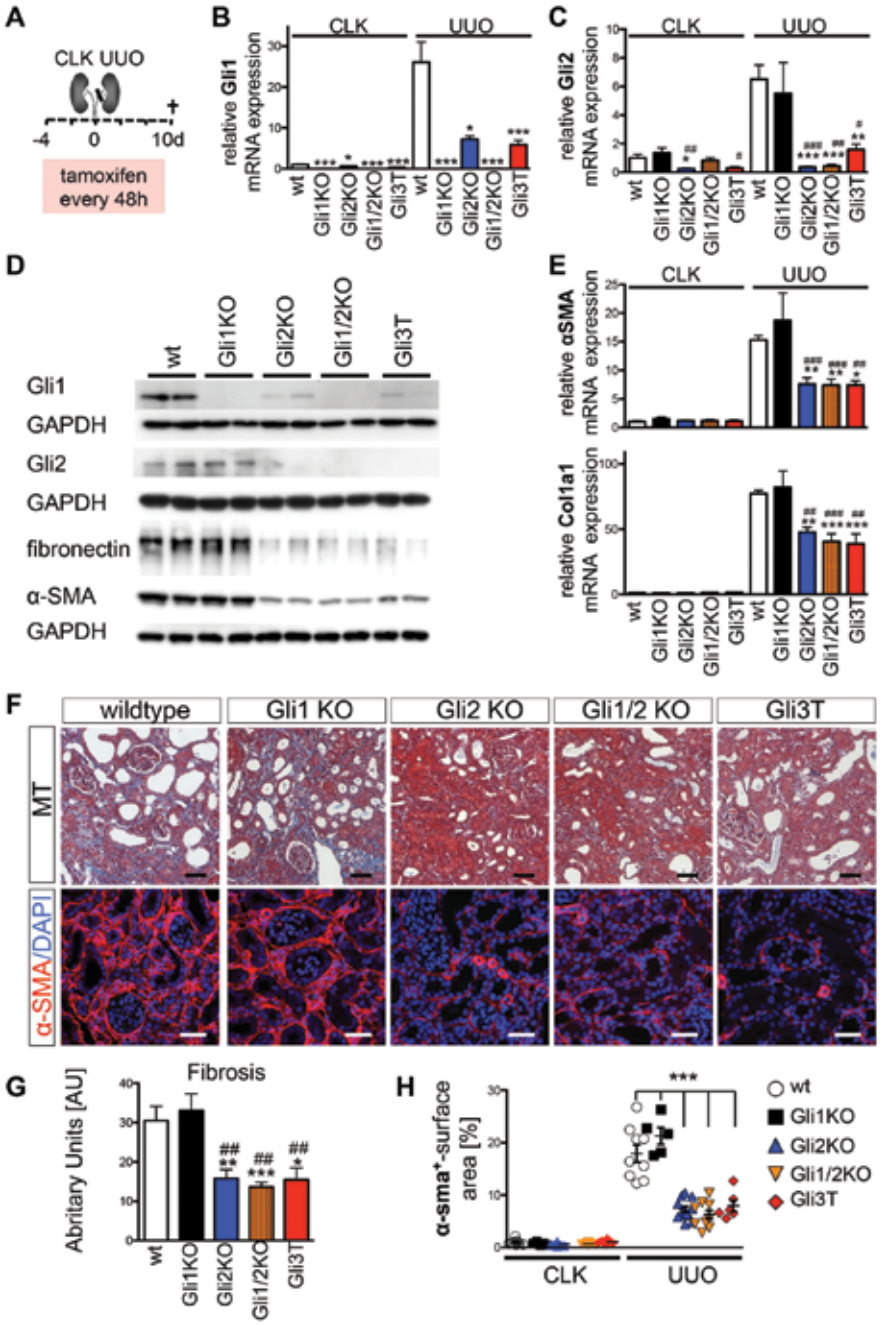

Figure 2: Conditional knockout of Gli2 or overexpression of the Gli3 repressor in Gli1^{+} cells ameliorates kidney fibrosis following UUO

A: Wildtype littermates (wt, n=9, 5 males), Gli1KO (Gli1CreER$^{t2+/+}$;Gli2flox$^{-/-}$, n=5, 3 males), conditional Gli2 KO (Gli1CreER$^{t2+/-}$;Gli2flox$^{+/+}$, n=12, 7 males), Gli1/2 KO (Gli1CreER$^{t2+/+}$;Gli2flox$^{+/+}$, n=9, 5 males), or Gli3T mice (Gli1CreERt2$^{+/-}$;Gli3T$^{+/-}$, n=6, 4 males) were injected with tamoxifen, underwent unilateral ureteral obstruction

(UUO) surgery as indicated and were sacrificed at 10 days after UUO. All used transgenic mice underwent surgery at 8-10 weeks of age and can be considered as mixed background with C57Bl/6J and 129S. Wildtype controls were littermates of the transgenic mice used in the experiments. **B-C:** Quantitative realtime PCR for mRNA expression of Gli1 and Gli2 in whole kidney lysates of conditional knockout experiments. **D:** Western blots for Gli1 effector proteins and fibrotic readouts fibronectin and alpha-smooth muscle actin (α-SMA) in UUO kidneys. Representative western blots for the non-injured contralateral kidneys (CLK) and quantification by integrated optical densitiy is presented in figure S4. **E:** Quantitative realtime PCR for mRNA expression of fibrotic readouts α-SMA and collagenIαI (CollaI). **F:** Representative images of trichrome or α-SMA stained UUO kidneys at 10 days after surgery. **G-H:** Quantification of interstitial fibrosis and α-SMA$^+$ surface area. *p<0.05, **p<0.01, ***p<0.001 versus wt, #p<0.05, ##p<0.01, ###p<0.001 versus Gli1KO, by one way ANOVA with posthoc Bonferroni , data presented as mean ±SEM

Conditional knockout of Gli2 or expression of the Gli3 repressor in Gli$^+$ cells halts kidney fibrosis progression by inducing myofibroblast-specific cell-cycle arrest

Since our *in vitro* data suggested that Gli2 is required for cell-cycle progression in MSC-like cells, we next asked whether Gli2 knockout or Gli3T expression reduces fibrosis severity by halting myofibroblast cell-cycle progression *in vivo*. Wildtype littermates, *Gli1KO*, *Gli2KO*, *Gli1/2KO* and *Gli3T* mice received tamoxifen, underwent UUO surgery and were euthanized at day 3 following surgery. BrdU was administered 3 hours before sacrifice. We performed co-staining for BrdU (S-Phase) with phospho-histone H3 (p-H3, G2/M Phase) and α-SMA (myofibroblasts, Figure 3A). Quantification of stained tubular-epithelial cells and interstitial α-SMA$^+$ cells revealed a G0/G1 cell cycle arrest specifically in the interstitial α-SMA$^+$ population (myofibroblasts) of Gli2KO, Gli1/2 KO and Gli3T mice (Figure 3B). Costaining and quantification of α-SMA$^+$ with Ki67 confirmed this data and indicated fewer cycling myofibroblasts after conditional knockout of Gli2 (Gli2KO; Gli1/2KO) or Gli3T expression (Figure S6 A-C). Importantly, cell-cycle distribution of tubular-epithelial cells or interstitial non-myofibroblast cells (α-SMA-) was not affected (Figures 3C, S6C-D, S7A-B), consistent with recombination specifically in interstitial myofibroblasts and their Gli1$^+$ precursors.

Protein analysis of whole kidney lysates showed increased levels of the cyclin dependent kinase inhibitor p21 and decreased levels of p-Rb following conditional knockout of Gli2 or expression of the Gli3 repressor (Figures 3D-H, S7C). Together with our quantification of cell-cycle stages in kidney cells, the results suggest that interstitial myofibroblasts left the cell-cycle at the G1 restriction point before the phosphorylation of retinoblastoma at Ser780 and consistent with our *in vitro* findings after siRNA mediated knockdown of Gli2.

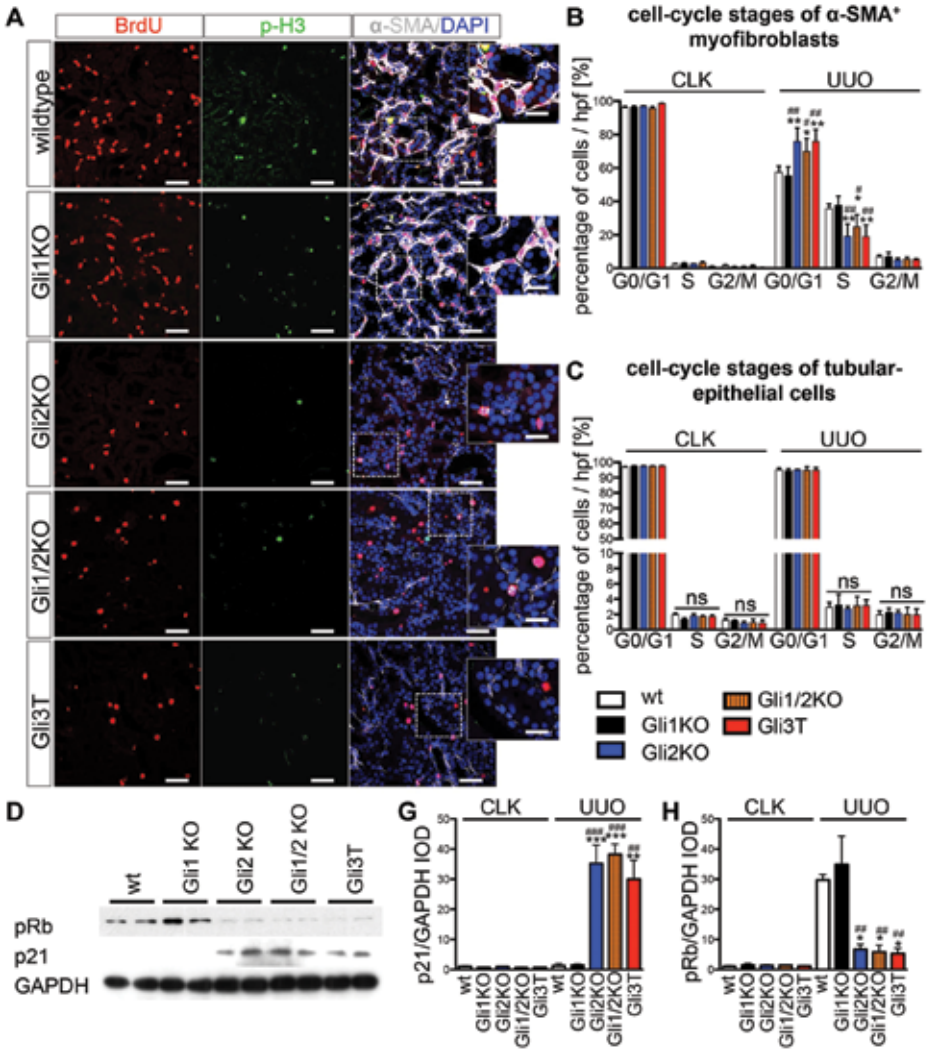

Figure 3: Conditional knockout of Gli2 or overexpression of the Gli3 repressor in Gli1⁺ cells induces a myofibroblast specific cell-cycle arrest

A: Wildtype littermates, Gli1KO, Gli2KO, Gli1/2KO and Gli3T mice (n=5 each, mixed background of 129S and C57Bl/6J, 8-10 weeks of age, 3 males 2 females each) received tamoxifen, underwent UUO surgery and were euthanized at day 3 following surgery. BrdU was administered 3 hours before sacrifice. Representative images of UUO kidneys after co-staining for BrdU (S-Phase), phospho-histone H3 (p-H3, G2/M Phase) and alpha smooth muscle actin (α-SMA /myofibroblasts). (Representative images and quantification of Ki67+ cells are shown in figures S6-S7)

B: Cell counting and quantification of myofibroblasts cell cycle (S-phase = α-SMA⁺/BrdU⁺; G2/M phase = α-SMA⁺/p-H3⁺; G0/G1phase= α SMA⁺ - SMA⁺/BrdU⁺ - α-SMA⁺/p-H3⁺).

C: Cell counting and quantification of tubular epithelial cell-cycle (S-phase = tubule epithelial cells-TE/BrdU⁺; G2/M phase = TE/p-H3⁺; G0/G1phase= TE – TE/BrdU⁺ - TE/p-H3⁺).

D: Western blot of whole UUO kidney lysates for phosphorylated retinoblastoma (pRb) and p21.

G-H: Quantification of western blots for phosphorylated retinoblastoma (pRb) and p21 by integrated optical densitiy (IOD). Representative western blots of non-injured CLK kidneys are shown in figure S7C).

*p<0.05, **p<0.001 versus wt, #p<0.05, ##p<0.001 versus Gli1KO, by one way ANOVA with posthoc Bonferroni , data presented as mean±SEM, all scale bars 50µm, inserts 25µm.

The novel organic arsenic darinaparsin reduces Gli1 and Gli2 protein levels and induces a cell-cycle arrest of MSC-like cells in vitro

We were next interested in determining whether this Gli2-dependent pro-fibrotic pathway in kidney myofibroblasts could be targeted therapeutically. Arsenic trioxide (ATO) is used clinically to treat acute promyelocytic leukemia and was recently shown to antagonize both Gli1 and Gli2 [43]. We therefore investigated if darinaparsin (S-dimethylarsino-glutathione), a novel arsenic-based drug with a favorable systemic toxicity profile and currently undergoing clinical studies in hematologic malignancies and solid tumors, [44] inhibits hedgehog effectors Gli1 and Gli2 and affects proliferation of MSC like cells *in vitro*. Indeed, darinaparsin was recently shown to modulate Gli protein levels in prostate cancer cell lines [46].

The MSC-like, pericyte-like cell line 10T1/2 was treated with darinaparsin or vehicle and flow cytometric cell-cycle analysis revealed that darinaparsin (0.5μM) induces a G0/G1 cell cycle arrest of 10T1/2 cells in vitro (Figure 4A, B). We next asked if darinaparsin treatment of 10T1/2 cells alters Gli protein levels and the regulator proteins of cell-cycle G1/S transition in a similar fashion as our RNAi studies. Western blot analysis revealed that darinaparsin reduced the protein levels of Gli1 and Gli2 with a subsequent upregulation of p21 and decreased levels of p-Rb (Figures 4C-E, S8A-B). Interestingly, while darinaparsin treatment decreased Gli1 mRNA, Gli2 mRNA remained unchanged (Figure 4F-G) suggesting an effect of darinaparsin on Gli2 protein stability. To evaluate the effect of darinaparsin on Gli2 protein stability we transfected human 293T cells with a full length Gli2 (pcDNA3.1-His [47]), added darinaparsin over a time-course of 24-72 hours and performed Western blots to determine Gli2 protein levels. Quantification of this data indicated a significant decrease of Gli2 protein levels over time (Figure S8C). This data suggested together with our previous RNAi results that the cell-cycle effect of low dose darinaparsin might be related to its effect on Gli2 protein level.

Overexpression of Gli2 rescues the cell-cycle inhibitory effect of darinaparsin

Our results identify Gli2 as a critical regulator of mesenchymal cell proliferation because reduction of Gli2 protein level by either RNAi, conditional knockout or darinaparsin treatment caused cell-cycle arrest and overexpression of Gli2 drove proliferation. We next investigated whether overexpression of Gli2 was sufficient to rescue the inhibitory effect of darinaparsin. Gli2 was overexpressed in 10T1/2 cells by retroviral delivery (Figures 1F-I, S2A-D), increased cell proliferation and rescued the cell-cycle effect of darinaparsin treatment (Figure 4 H-I) pointing towards Gli2 as the molecular target of darinaparsin. We next performed siRNA knockdown experiments in 10T1/2 cells treated with darinaparsin or vehicle (Figure S9). While darinaparsin treatment induced a G0/G1 cell-cycle arrest in cells treated with control siRNA and siRNA against Gli1, it did not have an appreciable effect in cells treated with siRNA against Gli2 or both Gli1 and Gli2 (Figure S9) further confirming a central role for Gli2 in the cell-cycle inhibitory effect of darinaparsin.

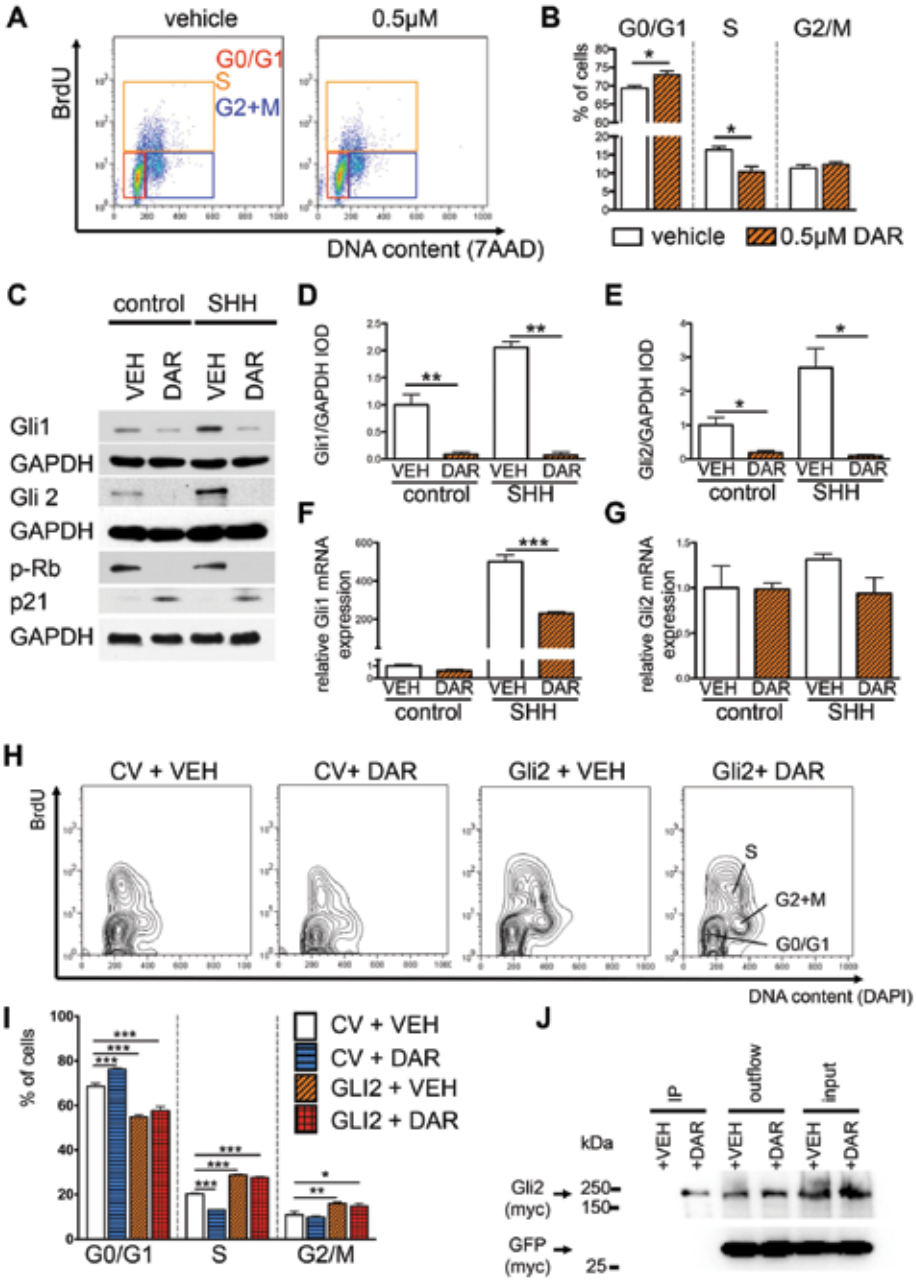

Figure 4: Darinaparsin reduces Gli protein levels and induces a cell-cycle arrest in vitro while overexpression of Gli2 rescues this cell-cycle effect of darinaparsin.

A-B: Darinaparsin (DAR) induces a G0/G1 cell cycle arrest in the mouse MSC-like, pericyte-like 10T1/2 cell-line (BrDU, Bromdesoxyuridin, S-Phase; 7AAD,7-aminoactinomycin, DNA content)

C: Representative western blots of whole cell-lysate from 10T1/2 cells treated with DAR or vehicle (VEH) in presence or absence of sonic hedgehog (Shh). (Quantification for p21 and p-Rb of western blots of 3 biological replicates is shown in figure S8).

D-E: Quantification of Gli1 and Gli2 protein levels by integrated optical density (IOD) of 2 pooled experiments with a total of n=3 biological replicates indicating reduced Gli1 and Gli2 protein levels after treatment with darinaparsin.
F-G: Quantitative realtime PCR for mRNA expression of Gli1 and Gli2 in 10T1/2 cells after treatment with vehicle (VEH) or darinaparsin (DAR) in presence or absence of sonic hedgehog (SHH, n=3 replicates).
H-I: Retroviral expression of Gli2 rescues the cell cycle effect of darinaparsin and drives proliferation of 10T1/2 cells. (CV-control virus; DAPI 4',6-diamidino-2-phenylindole, DNA content, data of n=3 biological replicates, gating Figure S4).
J: 293T cells were transfected with full length Gli2-myc, co-transfected with GFP-myc as a control protein and treated with darinaparsin (DAR) or vehicle (VEH). Glutathione-S-transferase (GST) agarose beads were added to the cell lysate to bind the glutathione moiety of DAR. The immunoblot for myc suggests that in presence of DAR GST is able to pull down Gli2 (myc) indicating DAR binding to Gli2 (IP + DAR). Importantly the GFP-myc control protein was not detectable indicating the specificity of the IP. *p<0.05, **p<0.01, ***p<0.001, A by t-test, B-F by t-test, I by two way ANOVA with posthoc Bonferroni, data presented as mean±SEM.

Coimmunoprecipitation suggests that Darinaparsin might bind Gli2 in vitro

Although these results implicate Gli2 as a target of darinaparsin, and arsenicals are known to antagonize Gli1 and Gli2, arsenic also inhibits a number of other pathways and could have been inhibiting Gli2 indirectly. On the other hand, arsenic has been proposed to bind to thiol groups on critical cysteine residues located in the Gli zinc finger domains [48], by extension of its known binding to zinc fingers of the promyelocytic leukemia protein [49]. To test whether darinaparsin directly binds to Gli2, we overexpressed myc-tagged Gli2 (pCS2-MT Gli2FL) [6, 20] and myc-tagged eGFP (pEGFP-C1-myc, as a control protein) in human 293T cells. After 72 hours, cells were treated overnight with 0.5µM darinaparsin or vehicle, and the cell-lysate was incubated with glutathione-s-transferase (GST) agarose beads. Since the arsenic in darinaparsin (S-methylarsino-glutathione) is bound to glutathione moieties we expected that GST would bind the glutathione, allowing pull-down of darinaparsin itself and of any protein bound to the arsenic. Indeed, using this strategy we observed that GST beads pulled down Gli2 only in the presence of darinaparsin, but not in its absence, suggesting that darinaparsin indeed binds to Gli2 (Figure 4J). Importantly, we did not detect the eGFP control-protein in the immunoprecipitation (Figure 4J). This suggested, together with our previous data, that darinaparsin might reduce Gli2 protein stability by a direct effect. However, this experiment cannot rule out that darinaparsin might also bind other zinc finger proteins including Gli1 or that darinaparsin might bind to a second protein that actually binds Gli2. Because reduced Gli2 also causes a reduction in Gli1 we cannot rule out that reduction of both proteins is needed for a cell cycle effect.

Darinaparsin prevents the increase of Gli1 and Gli2 normally observed during fibrosis and ameliorates fibrosis even when administered after injury

Having established that darinaparsin lowers Gli protein levels in vitro, we next investigated whether it would reduce the expression of Gli1 and Gli2 *in vivo* and most importantly, reduce the severity of kidney fibrosis. Wildtype mice were treated daily with darinaparsin or vehicle starting 2 days prior to UUO surgery and sacrificed at day 10 (Figure 5A). Western blot analysis revealed a significant reduction of endogenous Gli1 and Gli2 protein levels in the UUO kidneys of darinaparsin treated mice compared to the UUO kidneys of the control

group (Figures 5B, S10). A similar experiment in LacZ reporter mice for Gli1 and Gli2 (Gli1-nLacZ, Gli2-nLacZ) demonstrated that darinaparsin treatment reduces the number of Gli expressing interstitial cells after UUO (Figure S10). Furthermore darinaparsin treatment resulted in reduced mRNA expression of Hh readouts Gli1 and Ptch1 (Figure S10).
Strikingly, the severity of fibrosis was significantly reduced in the darinaparsin treatment group (Figures 5C-G, S11). To determine whether darinaparsin ameliorates fibrosis in a therapeutic rather than preventative dosing strategy, we repeated the UUO experiment but started darinaparsin treatment two days after the ureteral ligation surgery. We again observed substantial reductions in fibrotic readouts using this protocol (Figure S12 A-F).

In order to test whether darinaparsin not only improves fibrosis but preserves kidney function in a therapeutic model, we used a severe bilateral ischemia-reperfusion injury (IRI) model that causes substantial fibrosis and CKD at four weeks as previously reported as an acute kidney injury (AKI) to CKD model . A total of 19 mice underwent surgery and were randomized at day 7 after the surgery to two groups with no difference in their day 1 and day 7 blood urea nitrogen (BUN) levels (Figures 5H-I, S12I). After randomization mice were treated daily with darinaparsin or vehicle and sacrificed at day 28 (Figure 5H). Mice in the treatment group showed reduced interstitial fibrosis and reduced expression of fibrotic readouts (Figures 5J-L, S12). Importantly, the anti-fibrotic effect of darinaparsin was accompanied by lower BUN and creatinine levels at late timepoints after injury, when compared to the vehicle group (Figures 5I, S12J). Our data so far indicated darinaparsin as a novel antifibrotic therapy and pointed towards Gli2 inhibition as the molecular mechanism of its action. To prove this, we subjected Gli1KO mice or conditional Gli2KO mice to UUO surgery and treated them with darinaparsin or vehicle starting 2 days prior to surgery (Figure S13). Importantly, darinaparsin treatment ameliorated fibrosis severity in Gli1KO mice whereas it did not show an appreciable effect in Gli2KO mice (Figure S13), confirming a central role of Gli2 in mediating the effect of darinaparsin.

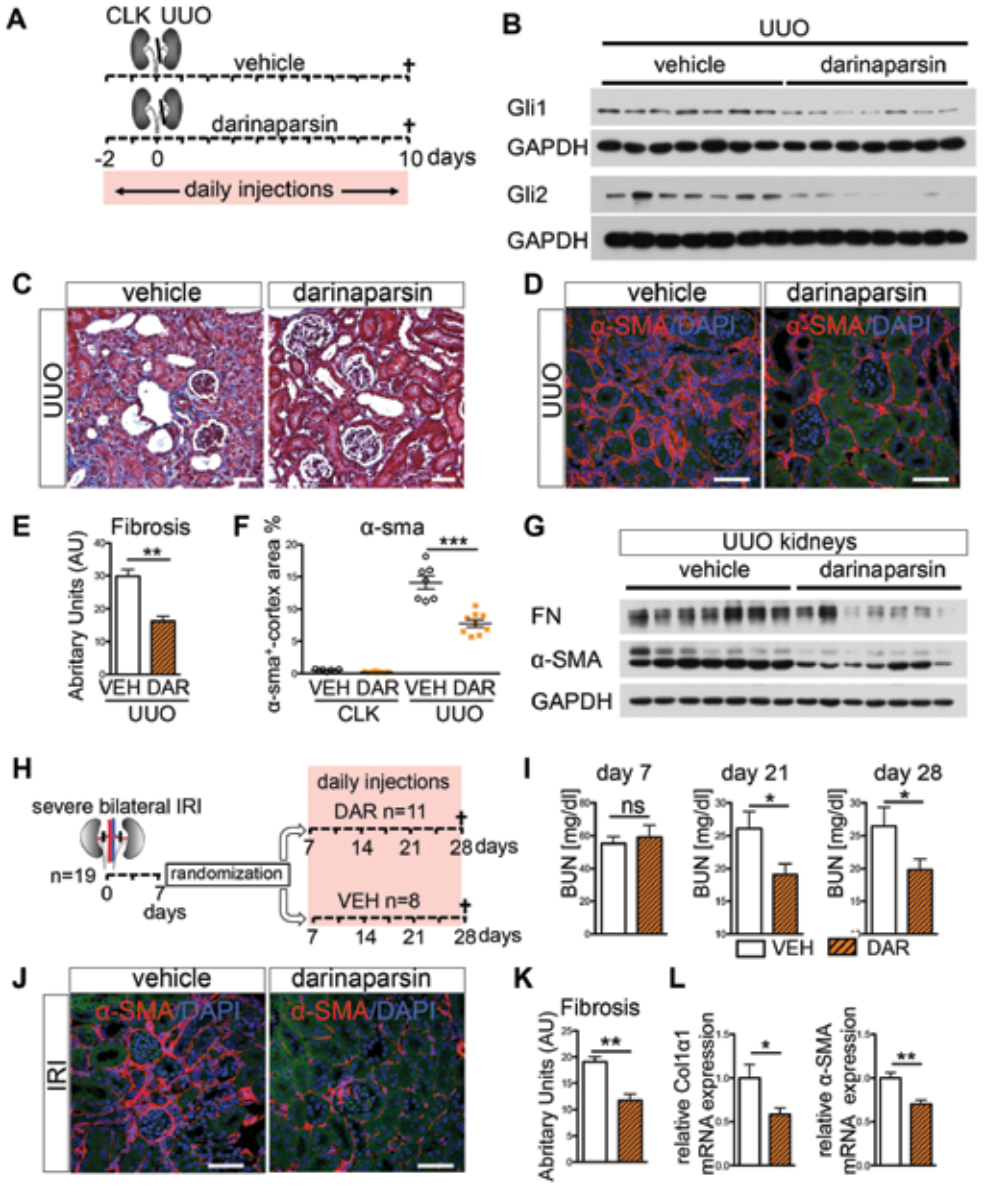

Figure 5: Darinaparsin treatment ameliorates renal interstitial fibrosis after unilateral ureteral obstruction and AKI to CKD progression after severe ischemia reperfusion injury.

A: Wildtype mice (C57Bl/6J, 8-10 weeks old, all males) were treated with darinaparsin (50mg/kg, n=9) or vehicle (normal saline, n=7) as indicated, underwent unilateral ureteral obstruction (UUO) surgery and were sacrificed at day 10 after surgery.

B: Representative western blots of whole UUO kidney lysates for Gli1 and Gli2 (CLK kidneys and quantification by integrated optical density (IOD) is shown in figure S10).

C-D: Representative trichrome stained and alpha smooth muscle actin (α-SMA) immunostained UUO kidneys.

E-F: Quantification of interstitial fibrosis and α-SMA$^+$ surface area.

G: Representative western blot of whole UUO kidney lysates for fibronectin and α-SMA. (CLK kidneys and quantification by integrated optical density (IOD) is shown in figure S11).

H: Wildtype mice (C57Bl/6J, n=19, all 8-10 week old males) underwent severe bilateral ischemia reperfusion injury (IRI) and were randomized based on their day 1 and 7 blood urea nitrogen (BUN, Figure S8) to darinaparsin (DAR) or vehicle treatment (VEH).
I: BUN measurement at randomization (day 7) and after 14 or 21 days of treatment (BUN at baseline, day 1 and 14, bodyweight and creatinine data is shown in figure S12).
J: representative image of α-SMA immunostained kidneys after IRI
K: Quantification of interstitial fibrosis (n=11 DAR; n=8 VEH).
L: relative mRNA expression for Collagen Iαl, and α-SMA (n=11 DAR; n=8 VEH).
*p<0.05,**p<0.01, ***p<0.0 01 vs vehicle treated mice, by t-test, data is presented as mean±SEM, all scale bars 50μm.

Darinaparsin induces a myofibroblast-specific cell cycle arrest in vivo

Since our previous results indicated that cell specific knockout of Gli2 led to a myofibroblast-specific cell-cycle arrest, we next sought to determine the effect of darinaparsin treatment on myofibroblast proliferation *in vivo*. C57Bl6 mice were injected with darinaparsin or vehicle starting 2 days prior to UUO surgery and sacrificed at day 3. BrdU was administered 3 hours before sacrifice. We performed the same co-staining experiments as in the *in vivo* knockout experiments and quantified stained tubular and interstitial α-SMA^{+} myofibroblasts and α-SMA^{-} (non-myofibroblasts) cells to calculate the cell-cycle stages for these cell-types (Figures 6A-D, S14A-E).

Importantly, darinaparsin treatment resulted in a G0/G1 cell-cycle arrest of interstitial myofibroblasts (Figure 6B) without altering the cell-cycle distribution of other kidney cell-types (Figures 6C, S14A-E)**,** suggesting that myofibroblasts are uniquely sensitive to darinaparsin and consistent with our previous finding that myofibroblasts and their precursors are the only kidney cell type expressing Gli proteins during fibrosis (Figure S3) [43, 50]. We also measured proliferation of kidney cell-types in mice treated with darinaparsin or vehicle in a therapeutic regime from day 2-10 after UUO surgery (Figures S15-16). Again, we detected significantly decreased proliferation of interstitial myofibroblasts in the darinaparsin treatment arm with no appreciable effect on other kidney cells (Figures S15-16).

Western blot analysis of whole kidney lysates at day 10 after UUO revealed significantly increased expression of the cyclin dependent kinase inhibitor p21 in the darinaparsin treated UUO kidneys compared to the vehicle treated group (Figure 6D). The upregulation of p21 was accompanied by reduced phosphorylated retinoblastoma protein (p-Rb, Ser780) (Figure 6D, CLK kidneys S16D). Together with the determination of cell-cycle stages of different kidney cell-types (myofibroblasts, tubular-epithelial cells, interstitial non-myofibroblasts) this data suggested that most likely myofibroblasts in darinaparsin-treated UUO kidneys exited the cell cycle at the G1 restriction point. These results are consistent with our previous experiments with blockade of the hedgehog-pathway on the level of Gli through conditional knockout of Gli2 or expression of the Gli3 repressor suggesting that the *in vivo* antifibrotic effect of darinaparsin is indeed mediated trough lowering Gli2 protein levels with a subsequent cell-cycle arrest of myofibroblasts.

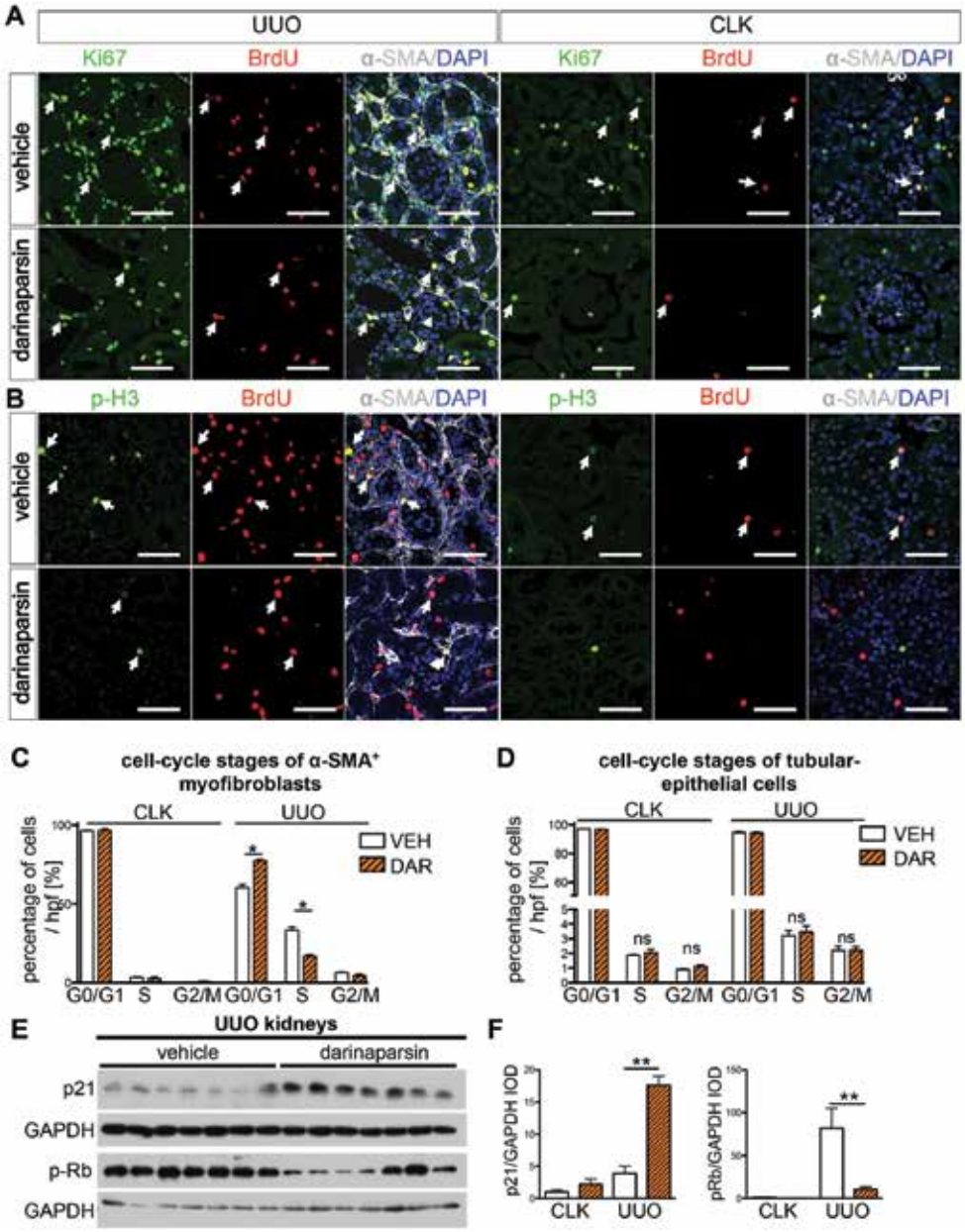

Figure 6: Darinaparsin induces a myofibroblast specific cell-cycle arrest while it does not affect the cell-cycle of tubular-epithelial cells

Wildtype mice (C57Bl/6J, 8-10 weeks old, all males) were treated with darinaparsin (50mg/kg, n=6) or vehicle (n=6) starting 2 days prior to unilatereal ureteral obstruction (UUO) surgery and sacrified at day 3 after surgery. Bromdesoxyuridin (BrDU) was injected (100mg/kg) 3 hours prior to sacrification.

A: Representative images of kidney sections from UUO and non-injured contralateral kidneys (CLK) costained for Ki67, BrdU and alpha smooth muscle actin (α-SMA) demonstrating reduced proliferation of interstitial

myofibroblasts in UUO kidneys of the darinaparsin treated group compared to the vehicle treated group. (For quantification of Ki67+ cells see figure S14.)

B-D: Co-staining of sections from the UUO and CLK kidneys for BrDU (cells in S-Phase), phospho histone H3 (p-H3, G2/M Phase) and alpha-smooth muscle actin (α-SMA) allowed quantification of cell-cycle stages for interstitial myofibroblasts (α-SMA$^+$) and tubular epithelial cells. Darinaparsin treatment resulted in a specific G0/G1 cell-cycle arrest of interstitial myofibroblasts in UUO kidneys (C), whereas the cell-cycle distribution of tubular-epithelial cells was not effected (D). (A similar analysis was performed in mice treated from day 2 until day 10 after UUO see figures S15-S16).

E-F: Representative Western blots and quantification by integrated optical density of whole UUO kidney lysates for the cyclin dependent kinase inhibitor p21/Cip1 and phosphorylated retinoblastoma (p-Rb), (CLK kidneys are shown in Supplementary Figure S16). ***p<0.001 by t-test data is presented as mean±SEM, all scale bars 60µm)

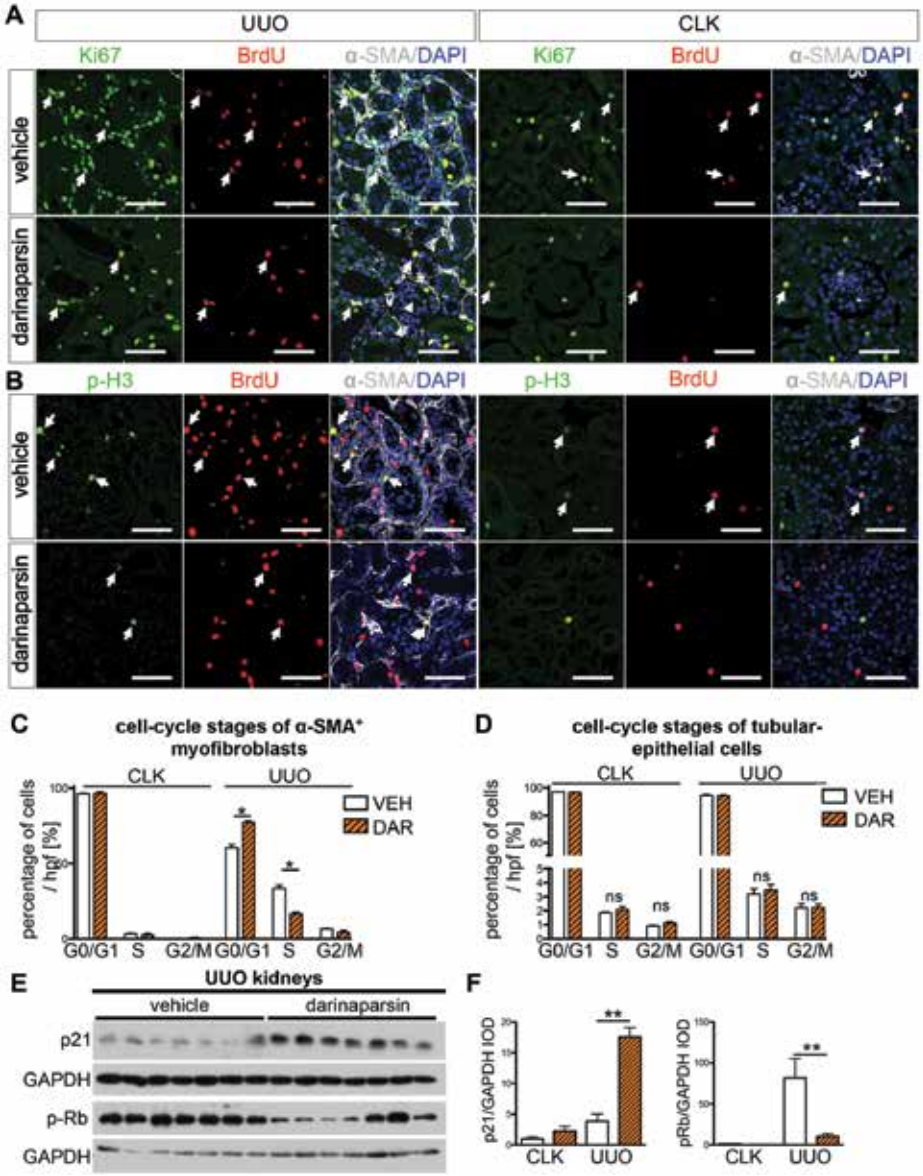

Figure 6: Darinaparsin induces a myofibroblast specific cell-cycle arrest while it does not affect the cell-cycle of tubular-epithelial cells
Wildtype mice (C57Bl/6J, 8-10 weeks old, all males) were treated with darinaparsin (50mg/kg, n=6) or vehicle (n=6) starting 2 days prior to unilatereal ureteral obstruction (UUO) surgery and sacrified at day 3 after surgery. Bromdesoxyuridin (BrDU) was injected (100mg/kg) 3 hours prior to sacrification.
A: Representative images of kidney sections from UUO and non-injured contralateral kidneys (CLK) costained for Ki67, BrdU and alpha smooth muscle actin (α-SMA) demonstrating reduced proliferation of interstitial myofibroblasts in UUO kidneys of the darinaparsin treated group compared to the vehicle treated group. (For quantification of Ki67+ cells see figure S14.)
B-D: Co-staining of sections from the UUO and CLK kidneys for BrDU (cells in S-Phase), phospho histone H3 (p-H3, G2/M Phase) and alpha-smooth muscle actin (α-SMA) allowed quantification of cell-cycle stages for interstitial myofibroblasts (α-SMA$^+$) and tubular epithelial cells. Darinaparsin treatment resulted in a specific G0/G1 cell-cycle arrest of interstitial myofibroblasts in UUO kidneys (C), whereas the cell-cycle distribution of tubular-epithelial cells was not effected (D). (A similar analysis was performed in mice treated from day 2 until day 10 after UUO see figures S15-S16).
E-F: Representative Western blots and quantification by integrated optical density of whole UUO kidney lysates for the cyclin dependent kinase inhibitor p21/Cip1 and phosphorylated retinoblastoma (p-Rb), (CLK kidneys are shown in Supplementary Figure S16). ***p<0.001 by t-test data is presented as mean±SEM, all scale bars 60μm)

Treatment with GANT61, a specific small-molecule Gli antagonist, ameliorates kidney fibrosis following unilateral ureteral obstruction surgery

Collectively these results suggest that Gli2 is a novel therapeutic target in kidney fibrosis, however darinaparsin is an arsenical with an uncertain long term safety profile even though it has reduced toxicity when compared to ATO [6]. This could complicate efforts to develop darinaparsin as an anti-fibrotic treatment for patients with CKD. Therefore we investigated whether targeting of Gli proteins using the specific Gli antagonist 61 (GANT61) might inhibit fibrosis in a similar fashion as darinaparsin.

Mice underwent UUO surgery and were treated using a therapeutic dosing strategy beginning after surgery as indicated (Figure 7). Scoring of trichrome stained sections revealed significantly reduced interstitial fibrosis (Figure 7B, C). Expression of fibrotic readouts Col1α1, α-SMA and fibronectin were significantly reduced in UUO kidneys of GANT61 treated mice when compared to the UUO kidneys of the vehicle treated mice (Figure 7 D-G). Treatment with GANT61 resulted in significantly reduced Gli1 and Gli2 protein levels of UUO kidneys, accompanied by a reduced mRNA expression of hedgehog readouts Gli1 and Ptch1 (Figure 7 H-N) confirming its ability to antagonize Gli proteins *in vivo.*

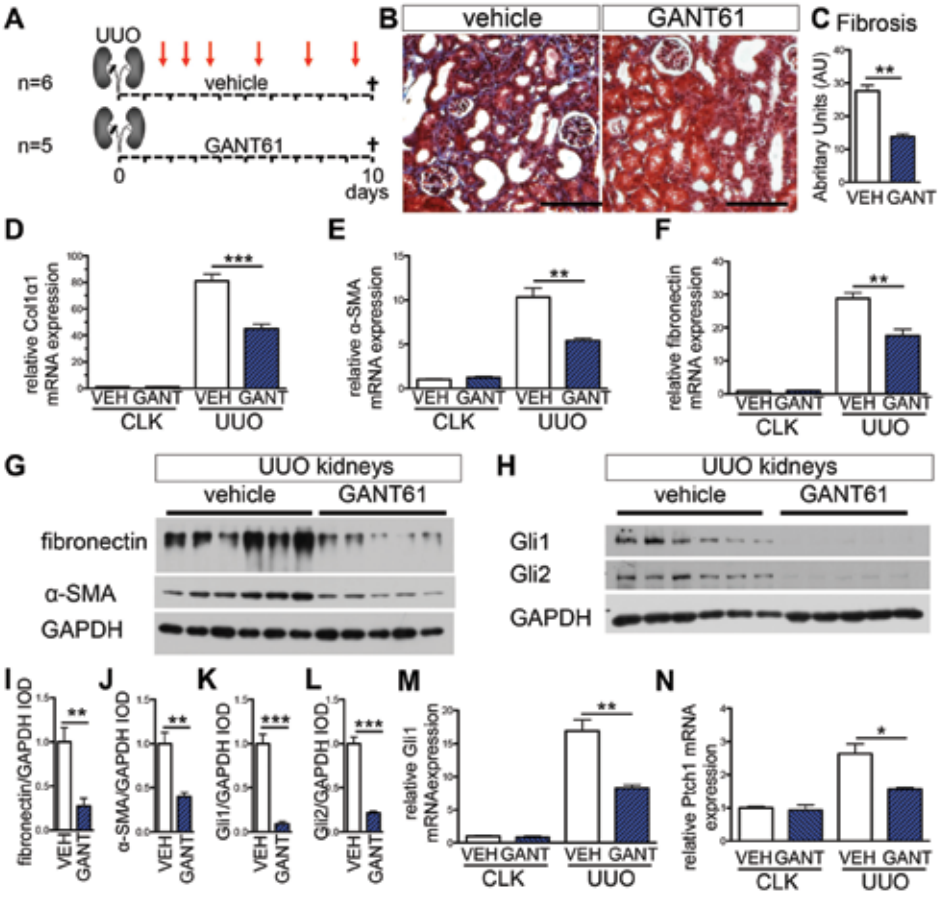

Figure 7: Targeting of Gli proteins by GANT61 ameliorates renal fibrosis following unilateral ureteral obstruction
A: To test whether specific inhibition of Gli ameliorates renal fibrosis wildtype mice (C57Bl/6J, 8-10 weeks old, all males) were subjected to unilateral ureteral obstruction (UUO) surgery and treated on indicated days (arrows) with either GANT61 (n=5) or vehicle (ethanol / corn oil 1/4; n=6) subcutaneously at 50mg/kg bodyweight. **B-C:** Trichrome staining and scoring for interstitial fibrosis in UUO kidneys revealed significantly less fibrosis in GANT61 treated mice. **D-F:** Determination of mRNA expression demonstrated a significant lower expression of the fibrotic readouts (D) collagen-1-alpha-1 (Col1α1), (E) alpha smooth muscle actin (α-SMA) and (F) fibronectin in the unilateral ureteral osbtruction (UUO) kidneys of GANT61 (GANT) treated animals when compared to vehicle (VEH) treated animals. **G-L:** Representative western blots and quantification by integrated optical density (IOD) for fibronectin, α-SMA, Gli1 and Gli2 from whole UUO kidney lysates demonstrating reduced protein expression of both Gli1 and Gli2 as well as reduced fibrotic readouts.. **I-J:** GANT61 treatment resulted in significant reduction of the increased mRNA expression of hedgehog pathway readouts Gli1 and Ptch1 following UUO. *p<0.05,** p<0.01, ***p<0.001, by t-test, data presented as mean±SEM, Scale bars 100µm

Gli expression is increased in human kidney fibrosis

Given our data on Gli inhibition as a novel antifibrotic therapy in mouse kidney fibrosis we next asked whether the same pathway might be upregulated in human kidney fibrosis. Kidney specimens were freshly obtained from tumor nephrectomies of 10 patients (Supplementary Table 3) and immediately processed for histology and RNA extraction.

Fibrosis severity was scored in Trichrome stained sections by a trained kidney pathologist blinded to mRNA results and clinical details. The kidney specimen were stratified into a low grade fibrosis group (fibrosis grade ≤20%) and high grade fibrosis group (fibrosis grade ≥40%) (Figure 8 A-B). In line with the histologic scoring we determined increased mRNA expression of fibrotic readouts collagen1a1, fibronectin and αSMA in the high grade fibrosis group (Figure 8C). Importantly, we determined increased expression of Gli1, Gli2 and Ptch1 mRNA in the high-grade fibrosis group compared to the low-grade fibrosis group. This data suggests activation of the Hh pathway with increased expression of Gli1 and Gli2 in human kidney fibrosis (Figure 8).

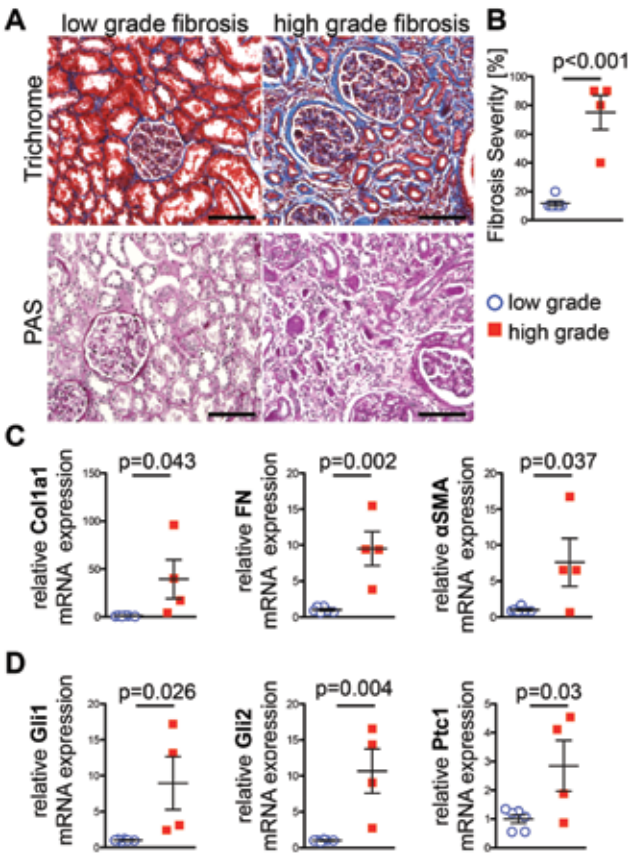

Figure 8: Upregulation of Gli in human kidney fibrosis

A-B: Human kidney tissue was obtained from tumor nephrectomies of n=10 patients and scored by an experienced kidney pathologist for the degree of interstitial fibrosis. (A) Representative images of trichrome and Periodic acid-Schiff (PAS) stained sections of specimen assigned to the high-grade fibrosis versus low-grade fibrosis group PAS) (B) Based on the fibrosis severity n=4 specimen were assigned to the high-grade fibrosis (interstitial fibrosis > 40%) and n=6 specimen to the low grade fibrosis group (interstitial fibrosis < 20%). (Clinical data of the patients is shown in supplementary table 3).**C:** Quantitative realtime PCR indicates significant higher mRNA expression of fibrotic readouts collagen1a1 (Col1a1), fibronectin (FN) and alpha smooth muscle actin (α-SMA) in the high-grade fibrosis group compared to the low-grade fibrosis group, as expected.

D: Quantitative realtime PCR indicated a significant upregulation of Gli1, Gli2 and patched1 (Ptch1) mRNA expression in the high-grade fibrosis group compared to the low-grade fibrosis group.

p-value as indicated by t-test, data presented as mean±SEM, Scale bars 100µm

DISCUSSION

We have recently demonstrated that Gli1$^+$ perivascular cells are an important kidney myofibroblast progenitor population [12, 14-16]. Our results here demonstrate that Gli2 plays a critical functional role in regulating the proliferation of these cells and represents a novel therapeutic target in renal fibrosis. Conditional knockout of Gli2 or overexpression of the Gli3 repressor in Gli1$^+$ cells ameliorates kidney fibrosis by inducing a myofibroblast-specific cell-cycle arrest. The same effects are achieved by Gli2 inhibition via darinaparsin, which we show might directly bind Gli2. Notably, this drug inhibits myofibroblasts specifically and had no appreciable effect on tubular epithelium, consistent with the absence of active Hh-Gli signaling in tubule.

The absence of Gli1 had no effect on kidney fibrosis in contrast to the report of Ding et al. . The reason for this discrepancy is unclear but we cannot rule out a contribution from differing mouse background. On the other hand, our results strongly implicate Gli2 over Gli1 as the critical mediator of pro-fibrotic signaling in kidney, and our findings were consistent across different mouse strains *in vivo* as well as in our cell-culture model. This conclusion confirms previous reports that Gli2 is the major transcriptional activator of Hh signaling, and is consistent with the observations that Gli1 is not required for development whereas Gli2 knockout mice die at birth .

Arsenic trioxide (ATO) is an established therapy for acute promyelocytic leukemia and acts via degradation of the oncoprotein AML-RXRα [43, 51, 52]. Darinaparsin does not act via AML-RXRα degradation, however, and ATO resistant myeloma cell-lines are susceptible to darinaparsin . These findings suggest that darinaparsin has a different mechanism of action than ATO. Darinaparsin was designed as a novel organic arsenic by conjugating dimethylarsenic to glutathione, shows a significantly lower systemic toxicity with a 50-fold higher tolerated maximum dose when compared to ATO . Tian *et al.* reported no significant side effect of darinaparsin on fast cycling cell populations such as the bone marrow or intestine [41, 42]. Darinaparsin is currently being tested in phase 2 clinical trials for solid tumors and hematopoietic malignancies [52], however, its molecular mechanism of action has not been fully elucidated . It has been reported that ATO antagonizes both Gli1 and Gli2 [44] and a very recent report also suggests that darinaparsin might reduce Gli2 protein levels in prostate tumor initiating cells .

The mechanism by which arsenicals inhibit Gli2 function is not defined, but probably involves effects on protein stability and subcellular localization. Kim *et al.* analyzed the effect of arsenic trioxide (ATO) on Hh signaling based on malformations in developing embryos after treatment with arsenic compounds showing a typical Hh dependent pattern . They reported that short term ATO reduces ciliary accumulation of Gli2 leading to Hh pathway inhibition and long term ATO treatment reduced steady-state levels of Gli2, suggesting a direct affect on Gli2 protein stability . This is in line with our observation that darinaparsin

treatment reduces Gli2 protein levels over time, with subsequent reduction of downstream Gli1 mRNA and protein expression, whereas Gli2 gene-expression remained unchanged. Our data suggests that darinaparsin might affect Gli2 protein stability by directly binding to Gli2. Importantly, darinaparsin treatment mimics both the cell-cycle effect of RNAi against Gli2 *in vitro* or conditional Gli2 knockout *in vivo* and induces a myofibroblasts specific cell cycle arrest with upregulation of p21 and reduced pRb. The cell-restricted expression of Gli1 and Gli2 in kidney myofibroblasts and their precursors might explain the specific effect of darinaparsin on kidney myofibroblasts while we did not observe cell-cycle alterations in tubular epithelial cells by darinaparsin treatment.

Hh signaling controls proliferation of diverse cell types during embryogenesis [58-60], it regulates proliferation of cancer cells and mounting evidence implicates Hh-Gli signaling in cell cycle progression at the restriction point. In Drosophila Hh signaling induces expression of Cyclin D and Cyclin E, both inhibitors of Rb [26]. Nagao *et al.* reported that Gli2 knockdown prevented human osteosarcoma growth by inducing a G1 cell-cycle arrest via upregulation of p21 with subsequent reduction of Rb phosphorylation [63]. Similar effects involving a G0/G1 arrest by p21 upregulation and reduced levels of phosphorylated Rb have been reported by knockdown of Gli2 in human vascular smooth muscle cells [64], human hepatocellular carcinoma cells [65] and human MSC [66]. All of these findings support our observation that lowering Gli2 protein level by darinaparsin treatment or siRNA induces a cell-cycle arrest of myofibroblasts at the restriction point by upregulation of p21/Cip1 with subsequent inhibition of Rb phosphorylation whereas overexpression of Gli2 increases proliferation. Of note, because in all our experiments lowering Gli2 protein levels always resulted in reduced downstream Gli1 expression we cannot determine whether reduction of solely Gli2 with normal Gli1 levels would have an appreciable effect. However, our data clearly suggests that inhibition of Gli2 with downstream reduced Gli1 is a promising therapeutic target in kidney fibrosis.

GANT61 was found in a compound screen as a direct Gli antagonist with selectivity for the Hh pathway [67]. It has been reported that GANT61 induced a G0/G1 arrest with upregulation of p21 in human colon cancer cells [14]. Importantly, in bleomycin induced lung fibrosis GANT61 decreased fibrosis severity, while inhibition of smoothened via GDC-0449 did not show this effect [20]. Our data demonstrates that directly targeting Gli proteins is a promising and novel therapeutic strategy in kidney fibrosis. The ability of a Gli inhibitor that is structurally distinct from darinaparsin to ameliorate fibrosis strongly supports the central role of Gli in kidney fibrosis and as a novel therapeutic target in CKD.

In conclusion, Gli2 regulates kidney myofibroblast proliferation and is a novel therapeutic target. Gli2 inhibition with downstream reduction of Gli1, via darinaparsin, reduces fibrosis in two kidney fibrosis models even when administered after the onset of fibrosis by reducing myofibroblasts proliferation. Furthermore, antagonizing Gli proteins with GANT61 also ameliorated renal fibrosis confirming the relevance of Gli proteins in kidney

fibrosis and providing a more specific compound with potentially fewer side effects than arsenics. Importantly, our data also suggests that this pathway is upregulated in human kidney fibrosis, providing strong support for future investigation of Gli inhibition to slow CKD progression in humans.

METHODS

Animal Experiments

All mouse experiments were performed according to the animal experimental guidelines issued by the Animal Care and Use Committee at Harvard University. Wild type mice were 8-10 weeks old males C57Bl/6J from Charles River Laboratories (Wilmington, MA). Gli1CreERt2 (i.e. Gli1tm3(re/ERT2)Alj/J, JAX Stock #007913), Gli2 floxed (i.e. Gli2^{tm6ALj}/J, JAX Stock #007926), Gli3T (i.e. Gt(ROSA)26Sor$^{tm3(Gli3)Amc}$/J JAX Stock #013124), Gli1-nLacZ (JAX Stock 008211), Gli2-nLacZ (JAX stock 0007922) were purchased from Jackson Laboratories (Bar Harbor, ME).

Gli1-KO mice were generated by generating homozygous Gli1CreER^{t2} mice or by breeding heterozygote Gli1-nLacZ (129S1/SvImJ background) that harbor a β-galactosidase knock-in at the transcriptional start site that abolishes Gli1 gene function.[68] Offspring were genotyped by PCR according to the protocol from the Jackson laboratory. Wild type littermates were used as controls in the conditional knockout experiments experiment and heterozygote littermates were used as controls for the quantification of LacZ positive cells. For the conditional knockout experiments all mice received tamoxifen (Cayman Chemicals in corn oil 3% ethanol, 0.4mg/kg bodyweight p.o.) as indicated.

All mice underwent UUO surgery at 8-10 weeks as previously described.[69] Briefly, after flank incision the left ureter was tied off at the level of the lower pole with two 4.0 silk ties. Mice were sacrificed at day 10 after surgery. For the quantification of proliferation mice were injected with Bromodeoxyuridine (BrdU; Sigma, 100mg/kg bodyweight in normal saline intraperitoneally) on day 3 after surgery and sacrificed 3 hours after BrdU injection. LacZ positive cells in Gli1-nLacZ +/+ vs Gli1-n-LacZ+/- mice were quantitated at day 7 after UUO surgery. For the bilateral ischemia re-perfusion injury (IRI) experiments surgery were performed as previously described.[70] Briefly, mice were anesthetized with pentobarbital sodium (60 mg/kg body weight, intraperitoneally), kidneys were exposed through flank incisions and mice were subjected to ischemia by clamping the renal pedicle with nontraumatic microaneurysm clamps (Roboz, Rockville, MD) for 26 min. Body temperatures were controlled at 36.5°C–37.5°C throughout the procedure. Mice were bled 7 days prior to surgery, at day 1,7,14,21 and 28 after surgery by tail vein bleeding. BUN was measured using the Infinity Urea assay (Thermo Scientific) according to the manufacturer instructions. Serum creatinine was assessed by HPLC [45] in the O´Brien Core Center for Acute Kidney Injury Research (University of Alabama, Birmingham School of Medicine).

Darinaparsin experiments

Darinaparsin (Zio-101, Ziopharm Oncology Inc., Cambridge, MA) was prepared freshly before treatment of cells or animals by dissolving in normal saline (vehicle). For animal experiments a 5mg/ml stock solution was prepared and animals were given daily 50mg/kg

body weight darinaparsin or vehicle per intraperitoneal injection. In the UUO experiments, mice were randomly assigned to the darinaparsin or vehicle group and treated starting 2 days before surgery (Experiment 1, Figure 1) or starting 2 days after surgery (Experiment 2 Supplementary Figure S2) . The last dose was given 4 hours before sacrifice. In the IRI experiment mice were treated daily starting at day 7 after surgery until they were sacrificed at day 28 after surgery. For the cell-culture experiments a 1mM stock solution was sterile filtered and a final concentration of 0.5-3µM was used in the cell-culture medium every 24h versus normal saline (vehicle).

GANT61 experiments

Gant61 (Cayman Chemical # 13841) was dissolved in ethanol and stored at -80°C. The ethanol solution was further diluted in corn-oil (1:4) immediately before subcutaneous injection (50mg / kg bodyweight) at day 1, 2, 3, 5, 7 and 9 after UUO surgery. Preparation of Gant61 in this ethanol / oil solution and delivery via subcutaneous injection in mice has been described previously by Lauth et al. [48] Control mice were injected with the vehicle (ethanol / corn oil 1:4) at the same time-points.

Tissue Preparation and Histology

Mice were anesthetized with isoflurane (Baxter) and subsequently perfused via the left ventricle with 4°C PBS for 1 minute. For histological analyses tissue sections were fixed in 10% formaldehyde for 1h, paraffin embedded and cut with a rotating microtome at 3µm thickness and stained according to routine histology protocols. For immunofluorescence studies kidneys were fixed in 4% paraformaldehyde on ice for 1 hour, then incubated in 30% sucrose in PBS at 4°C overnight. OCT-embedded (Sakura Finetek) kidneys were cryosectioned into 7 µm sections and mounted on Superfrost slides (Fisher Scientific). Sections were washed in 1X PBS, blocked in 10% normal goat serum (Vector Labs) and incubated with primary antibodies specific BrdU (1:100, Abcam # ab6326), phospho-Histone H3 (1:100, Santa Cruz Biotech, #SC-8656-R), alpha SMA (1:200, Sigma, Cat No. A2547), alpha SMA-Cy3 (1:200, Sigma, # C6198), Ki67 (1:100, Vector Laboratories #VP-K451), Laminin (1:100, Sigma-Aldrich #L9393). Secondary antibodies were FITC-, Cy3, or Cy5-conjugated (Jackson ImmunoResearch). Sections were then stained with DAPI and mounted in Prolong Gold (Life Technologies).

Quantification of BrdU+, phospho-Histone H3+ (p-H3+) tubular-epithelial cells and myofibroblasts (α-SMA+) was performed in 6 mice of each group. Pictures (400x, n=7/kidney) were taken randomly across the cortex of the UUO and CLK kidneys, positive cells were counted manually. Cell-cycle stages of myofibroblasts were calculated as follows: G0/G1 = all α-SMA$^+$cells - BrdU$^+$/α-SMA$^+$ cells - p-H3$^+$/α-SMA$^+$ cells; S= BrdU$^+$/α-SMA$^+$ cells; G2/M = p-H3$^+$/α-SMA$^+$ cells, cell cycle stages of tubular cells were calculated as follows: G0/G1 = all tubular cells - BrdU$^+$ tubular cells - p-H3$^+$ tubular cells ; S= BrdU$^+$ tubular cells ; G2/M =

p-H3^{+} tubular cells . Quantification of α-SMA positive surface area was performed by taking random cortical pictures (200x, n=7/kidney) in UUO and CLK kidneys of each mouse (n=7 vehicle vs n=9 darinaparsin) using the number of stained pixels per total pixels in Adobe Photoshop CS5 (Adobe Systems, Inc., San Jose, CA). All images were obtained by confocal (Nikon C1 eclipse, Nikon, Melville, NY) or standard microscopy (Nikon eclipse 90i).

Fibrosis severity was scored at 400x magnification using a counting grid with 117 intersections. The number of grid intersections overlying trichrome positive (blue) interstitial area was counted and expressed as a percentage of all grid intersections. For this calculation intersections that were in tubular lumen and glomeruli were subtracted from the total number of grid intersections.

To identify LacZ activity in kidney sections, PFA fixed frozen sections were incubated in standard 5-bromo-4-chloro-3-indolyl-β-d-galactoside (X-gal) for 48 hours, counterstained with nuclear fast red and mounted.

Cell Culture Experiments

All cell-lines used within this study were freshly ordered from ATCC and routinely checked for mycoplasma contamination in our laboratory. 10T1/2 cells (ATCC) and cultured in Basal Medium Eagle (BME, Gibco; Life Technologies) supplemented with 10% fetal bovine serum (FBS), penicillin and streptomycin and 2mmol/L glutamine (all Gibco). Sonic hedgehog conditioned media was produced from supernatant of confluent Cos7 cells stably transfected with pcDNA3-N-Shh or pcDNA3 control plasmid. For western blot experiments cells were grown on 10cm dishes, serum starved in 0.5% FBS for 12 hours and then incubated with darinaparsin (0.5μM) or vehicle with either Shh preconditioned medium or Cos7 control media (5x i.e. 2ml preconditioned media in 8ml BMW 0.5% FBS) for 72 hours.

For cell-cycle analysis cells were grown on 6 well plates until 50% confluency, serum starved in 0.5% FBS for 4h to synchronize the cell-cycle and then cultured for 48 hours in 10% FBS medium together with 0.5 μM darinaparsin or normal saline (vehicle). Before fixation cells were incubated for 75 minutes in 10μM BrdU and stained according to the BD APC BrdU Flow Kit (BD Bioscience #552598). Cells were analyzed by flow cytometry (FACS Canto II, BD Biosciences) within 1 hour after staining, and data were analyzed by using Flow Jo software (Version 7.5, Tree Star Inc).

SiRNA knockdown experiments

For siRNA experiments cells were transfected with siRNA against Gli1 (Life Sciences, siRNA ID: s66723, Sequence 5´3´ Sense: GCAGGUCUCCUAUCCUGAUtt, Antisense: nAUCAGGAUAGGAGACCUGCtg), Gli2 (Life Sciences, siRNA ID: s66726, Sequence 5´3´ Sense: GGAAAACUUCAACAAUACAtt, Antisense: UGUAUUGUUGAAGUUU UCCag), and both Gli1 and Gli2, scrambled siRNA was used as a negative control (Life Technologies, #AM4611) and Cy3 labeled siRNA against GAPDH (Life Technologies, #AM4649) was used as a positive

control for the transfection. Transfection was performed with a final concentration of 5nM of each siRNA according to the manufacturer instructions using Lipofectamine RNAiMAX transfection reagent (Life Technologies, #3778075). 72 hours after transfection cells were harvested for RNA or protein isolation. For cell cycle analysis cells were splitted 48h after transfection at a seeding density of 50%, 24h after the seeding cells were incubated for 75min with 10µM BrdU and subjected to cell-cycle analysis as described above.

Overexpression of Gli2 by retroviral delivery

The RSF91.IRES.EGFP retroviral vector was a kind gift of Dr. Axel Schambach and Dr. Christopher Baum (both Hannover Medical School, Hannover, Germany). The vector was modified with a multiple cloning site containing the SbfI and MluI restriction enzyme sites. The full length Gli2 cDNA was kindly provided by Dr. Hiroshi Sasaki (Riken database RDB #08065, Gene ID 14633).[71] The Gli2 cDNA was PCR amplified using Phusion Polymerase (New England Biolabs, #m0530) and a N-terminal HA-tag, a 5' SbfI, and 3' MluI site were added and the cDNA was inserted into the multiple cloning site. Ecotropic retroviral particles were produced by Calcium Phosphate based transient co-transfection of HEK293T cells with the retroviral constructs and packaging plasmid. Viral supernatants were collected at 36-48h post transfection and 0.22uM filtered. Cell transduction was performed by incubating the cells with serial dilutions of the retroviral supernatants in the presence of 4ug/ml Polybrene (Sigma-Aldrich, #107689). Cell-cycle flow-cytometric analysis was performed using 4',6-diamidino-2-phenylindole (DAPI) instead of 7AAD for detection of DNA content due to the viral GFP expression.

Gli2 darinaparsin binding assay

Human 293T/17 (HEK 293T/17, freshly ordered from ATCC) were grown in a 10 cm cell-culture dish until 80% confluent and transfected with pCS2-MT Gli2 FL kindly provided by Dr. Roessler [1, 2] (Addgene Plasmid 17648: pCS2-MT GLI2 FL) using Lipofectamine 2000 (Life Technologies) according to the manufacturer instructions. Cells were co-transfected with a myc tagged GFP plasmid (pEGFP-C1-myc), as a control protein. pEGFP-myc was generated using pEGFP-C1 (Clontech Laboratories, Palo Alto, CA) and addition of a Myc tag at the BspEi and BamHI restriction sites. 72 hours after transfection the cells were treated with 0.5µM darinaparsin or vehicle in DMEM 10% FBS for 12 hours, thereafter cells were resuspended in cold (4°C) PBS and washed twice with PBS. After centrifugation (1500rpm, 5 minutes) 1ml of IP-Lysis Buffer (Thermo Scientific) + proteinase inhibtor (Roche, #1183617000T) was added to the cell pellet and the suspension was homogenized using an insulin syringe. After centrifugation of the protein-solution (15min, 12000rpm) the supernatant was transferred into a fresh tube, an aliquot of 100µl was taken as input control (Figure 6) and the solution was incubated with 50µl GST-Agarose beads (Pierce GST Agarose #20211, Thermo Scientific) for 4 hours on a rotator at 4°C. Thereafter the bead-protein solution was centrifuged

(5000rpm, 3min) and the supernatant was taken as outflow control (Figure 6), the agarose beads were washed three times by adding 1ml of the above mentioned IP-Lysis buffer containing proteinase inhibitors followed by vortexing and centrifugation (5000rpm, 3min), the supernatant after each centrifugation was discarded. After 3 washes, the GST beads were cooked at 96°C for 7 minutes in 100µl Laemmli buffer (Bio-Rad). All protein samples (input, outflow and the final GST bead purification solution) were analysed by western blot with an antibody against c-myc (mouse monoclonal, 9E 10, DSHB, Iowa) the membrane was stained with Ponceau-S (Sigma) to show specificity (Figure 6H).

Real Time PCR Experiments

Kidney tissue or cell-pellets were harvested and immediately snap frozen in liquid nitrogen. RNA was extracted according to the manufacturer instructions using the RNeasy Mini Kit (Qiagen) and 600ng of total RNA was reverse transcribed with iScript (BioRad). Quantitative polymerase chain reactions were carried out with iQ-SYBR Green supermix (BioRad) and the BioRad CFX96 Real Time System with the C1000 Touch Thermal Cycler. Cycling conditions were 95°C for 3 minutes then 40 cycles of 95°C for 15 seconds and 60°C for 1 minute, followed by one cycle of 95°C for 10 seconds. Glyceraldehyde-3-phosphate dehydrogenase (GAPDH) was used as a housekeeping gene. Data was analysed using the $2^{-\Delta\Delta ct}$ method. Primers are listed in supplementary table 1 (mouse) and 2 (human).

Western Blot

Kidney tissue was snap frozen in liquid nitrogen and stored at -80°C immediately after mice were killed. Tissue samples were homogenized in lysis buffer containing 10mM HEPES, pH 7.4, 0.32M sucrose, 2mM EDTA, 1mM DTT, 1mM PMSF and 1 protease inhibitor tablet per 10ml of lysis buffer (Roche Cat. No. 11836153001). Samples were sonicated and protein concentration was determined by the Bradford Assay using Bio-Rad Protein Assay Dye (Biorad, Cat. No. 500-0006). 10-40µg of protein from lysates was loaded on a 7.5 or 10% polyacrylamide gel and separated by SDS electrophoresis. Proteins were transferred to a Immobilion membrane (Millipore) blocked in 5% milk in PBST, probed overnight at 4°C with the primary antibodies: mouse anti-αSMA at 1:4000 (Sigma, Cat. #A2547), rabbit anti-fibronectin at 1:4000 (Abcam, #ab23750), rabbit anti-p21at 1:200 (Santa Cruz, #sc-471), rabbit anti-phospho-retinoblastoma at 1:1000 (Cell Signaling #9307S, Ser780), rat anti-Gli1 at 1:1000 (R&D Systems #MAB3324, http://www.antibodypedia.com/binder_details.php?binder_id=701973), goat anti-Gli2 at 1:500 (R&D Systems #AF3635), rabbit anti-Cyclin E at 1:200 (Santa Cruz #sc-481), rabbit anti-Cyclin A at 1:200 (Santa Cruz #sc-751), rabbit anti-HA-Tag at 1:5000 (Cell Signaling #3724), mouse anti-c-myc (DSHB, Iowa, 9E 10) and rabbit anti-GAPDH at 1:4000 (Bethyl Laboratories, #A300-641A). Following incubation with primary antibody blots were washed probed with respective horseradish-peroxidase conjugated secondary antibodies at 1:5000 (Dako, Cat. No. P0447, P0448, P0450) for 1

hour at room temperature and then visualized using the Western Lightning ECL kit from PerkinElmer (#NEL100001EA). Quantification of western bands was performed using ImageJ (NIH).

Human kidney specimen

Human kidney specimens from 10 patients undergoing partial or total nephrectomy procedures for urologic indications (supplementary Table 3). Nephrectomy specimens were immediately placed on ice and within 15 minutes of surgical removal, three 5mm cubes of tissue were cut from portions of non-neoplastic tissue and placed into three separate containers with specific preservatives (neutral buffered formalin, 4% paraformaldehyde in phosphate-buffered saline, or RNA-Later). Trichrome-stained slides from formalin-preserved tissue were examined by a trained senior pathologist for semi-quantitative assessment of cortical tubulointerstitial fibrosis. The study was approved by the Institutional Review Board of Brigham and Women's Hospital and all patients provided written informed consent.

Statistical Analysis

All results are reported as mean ± SEM. Comparison of two groups was performed using unpaired t-test or Mann-Whitney U test where appropriate. For multiple group comparison analysis of variance with posthoc Bonferroni correction was applied. Statistical analyses were performed using GrapPad Prism 5.0c (GraphPad Software Inc., San Diego, CA). A p value of less than 0.05 was considered significant.

Study approval

All mouse experiments were approved by the Animal Care and Use Committee at Harvard University. The human study was approved by the Institutional Review Board of Brigham and Women's Hospital and all patients provided written informed consent.

Acknowledgements

This work was supported by NIH DK088923 (to BDH), NIH DK104308 (to BDH and SSW), by an Established Investigator Award of the American Heart Association (to BDH) and by a fellowship from the RWTH Aachen University (to RK) and the Deutsche Forschungsgemeinschaft (to RK, Kr 40731-1, RKS 188/3-1 and SF Fl 828/1-1). We acknowledge support from the UAB-UCSD O'Brien Core Center for Acute Kidney Injury Research (NIH P30-DK079337) for this project.

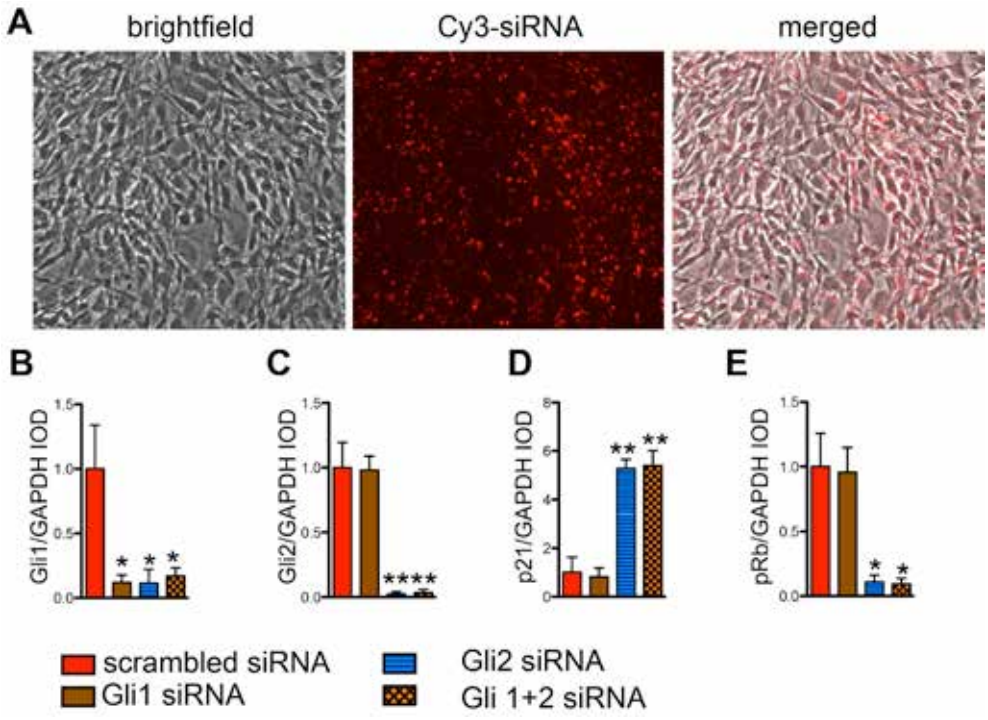

Figure S1: SiRNA knockdown of Gli2 induces p21 expression with reduced phosphorylation of retinoblastoma.
A: To monitor the efficiency of siRNA delivery to 10T1/2 cells we used a fluorochrome (Cy3) labeled siRNA against GAPDH. Pictures were taken after washing the cells with phosphate buffered saline indicating a successful and high efficient transfection.
B-E: Western blots from 2 experiments (total of n=3 biological replicates) of siRNA mediated knockdown of Gli1, Gli2 or Gli1+2 were quantified by integrated optical density (IOD). *p<0.05; **p<0.01 by one way ANOVA with posthoc Bonferroni , data presented as mean±SEM.

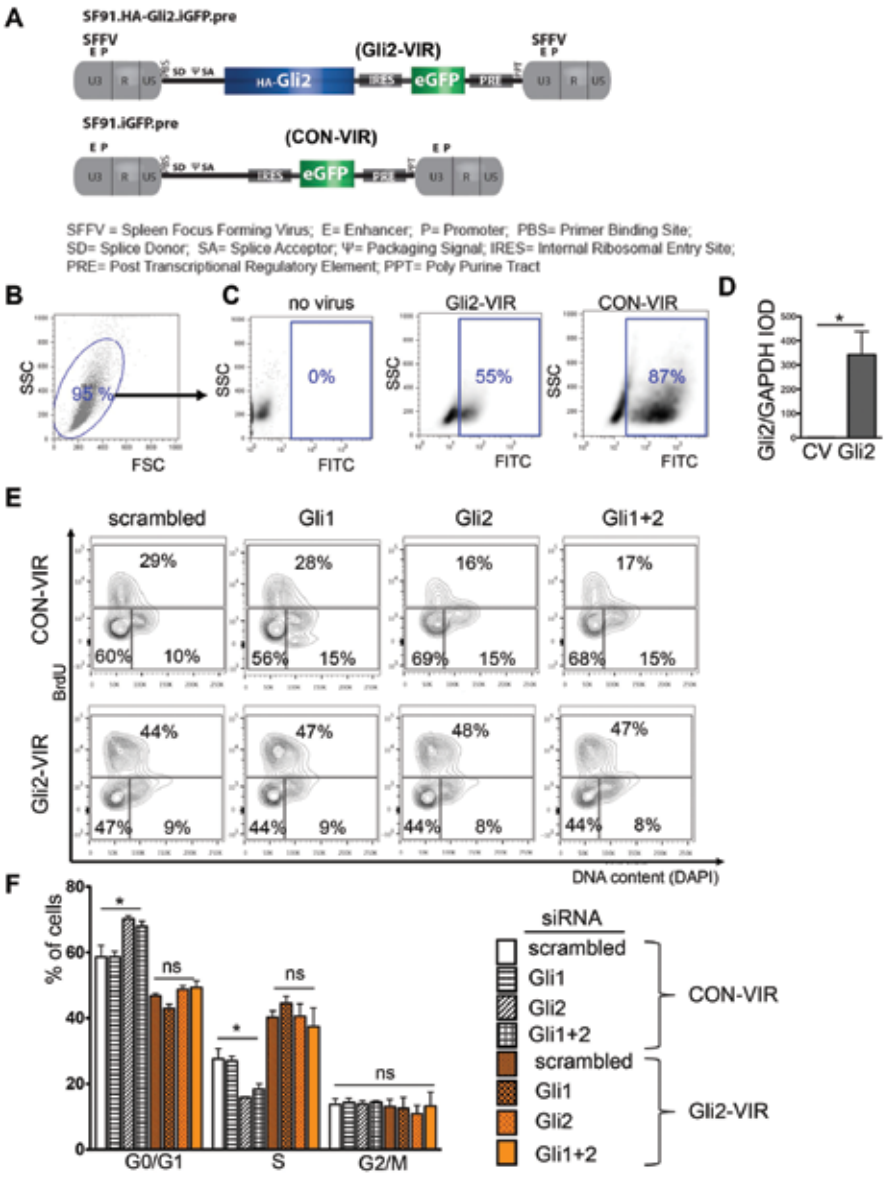

Figure S2: Gli2 overexpression induces proliferation and rescues the effect of siRNA knockdown
A: Scheme of the retrovirus used for overexpression of Gli2 (SF91.HA-Gli2.iGFP.pre) and the control virus (SF91.iGFP.pre). **B-C:** After initial gating of a population regarding forward and sideward scatter of the cells (FSC, SSC) (B) only the GFP expressing cells were included into further cell-cycle analysis (C). **D:** Western blots of 10T1/2 cells transduced with the Gli2 retrovirus (Gli2) and the control virus (CV) were quantified by integrated optical density (IOD) (data of 2 experiments with a total of n=4 biological replicates). **E:** Representative flow cytometric plots for cell-cycle analysis of 10T1/2 cells treated with siRNA against Gli1, Gli2, Gli1 and Gli2 or control (scrambled) with addition of a Gli2 expressing retrovirus (Gli2-VIR) versus a control virus (CON-VIR). **F:** Quantification of cell-cycle flow cytometry demonstrates a G0/G1 cell-cycle arrest in the control virus treated cells after knockout of Gli2 or Gli1 and Gli2 whereas overexpression of Gli2 (Gli2-VIR) increased proliferation and was able to rescue this effect of Gli2 siRNA.*p<0.05 by T-Test in D, by two way ANOVA with posthoc Bonferroni in F, data presented as mean±SEM.

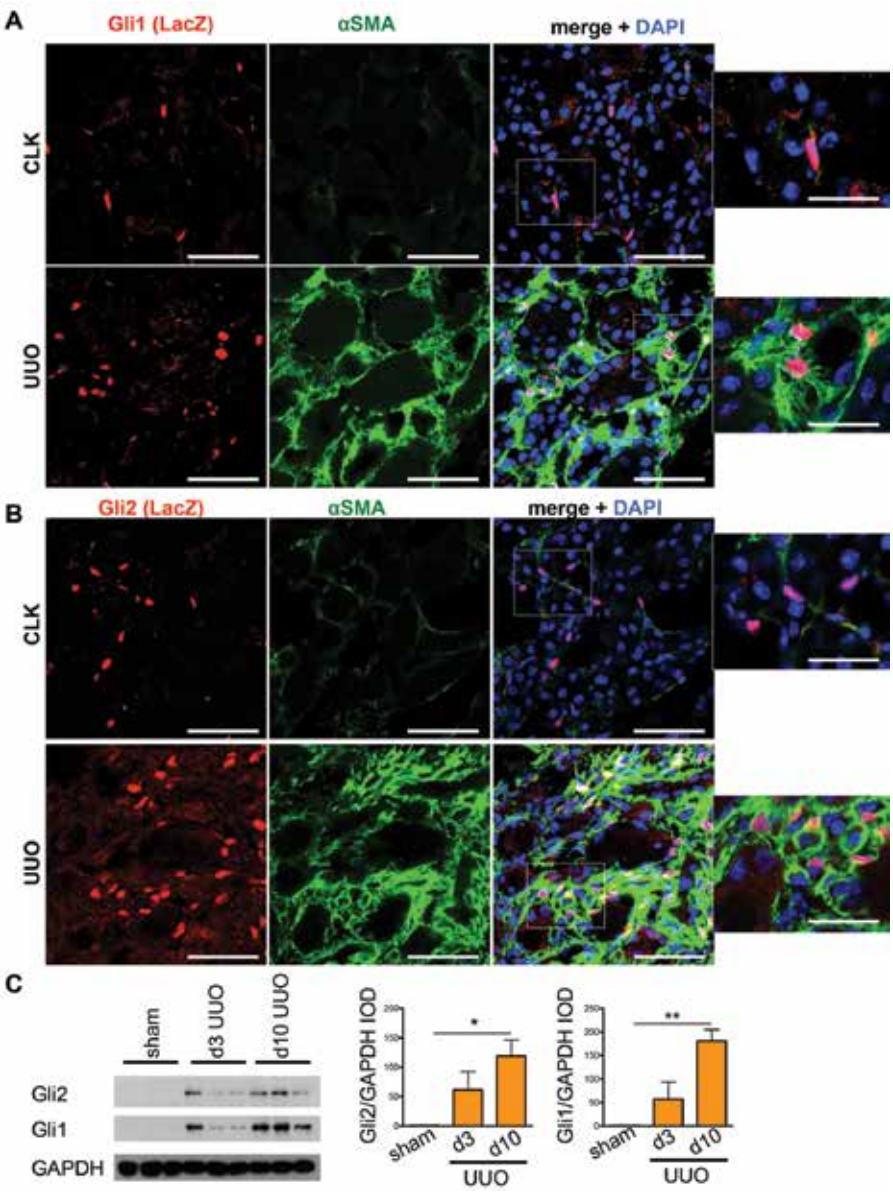

Figure S3: Increased expression of Gli1 and Gli2 in kidney fibrosis specifically expressed in interstitial myofibroblasts.

A-B: Representative images of day 10 UUO kidneys Gli1-nLacZ and Gli2-nLacZ mice (8-10 week of age, both transgenic lines are on a mixed background of 129S, Swiss Webster and C57Bl/6J) costained for β-galactosidase (LacZ) and alpha smooth muscle actin (α-SMA).

C: Representative western blots and quantification by integrated optical density (IOD) for Gli1 and Gli2 expression in wiltype mice (C57Bl/6J, all males 8-10 week of age) subjected to UUO (day 3 and day 10) or sham surgery (n=3 each). *p<0.05, **p<0.01 by one way ANOVA with posthoc Bonferroni. All scale bars 50μm, inserts 25μm.

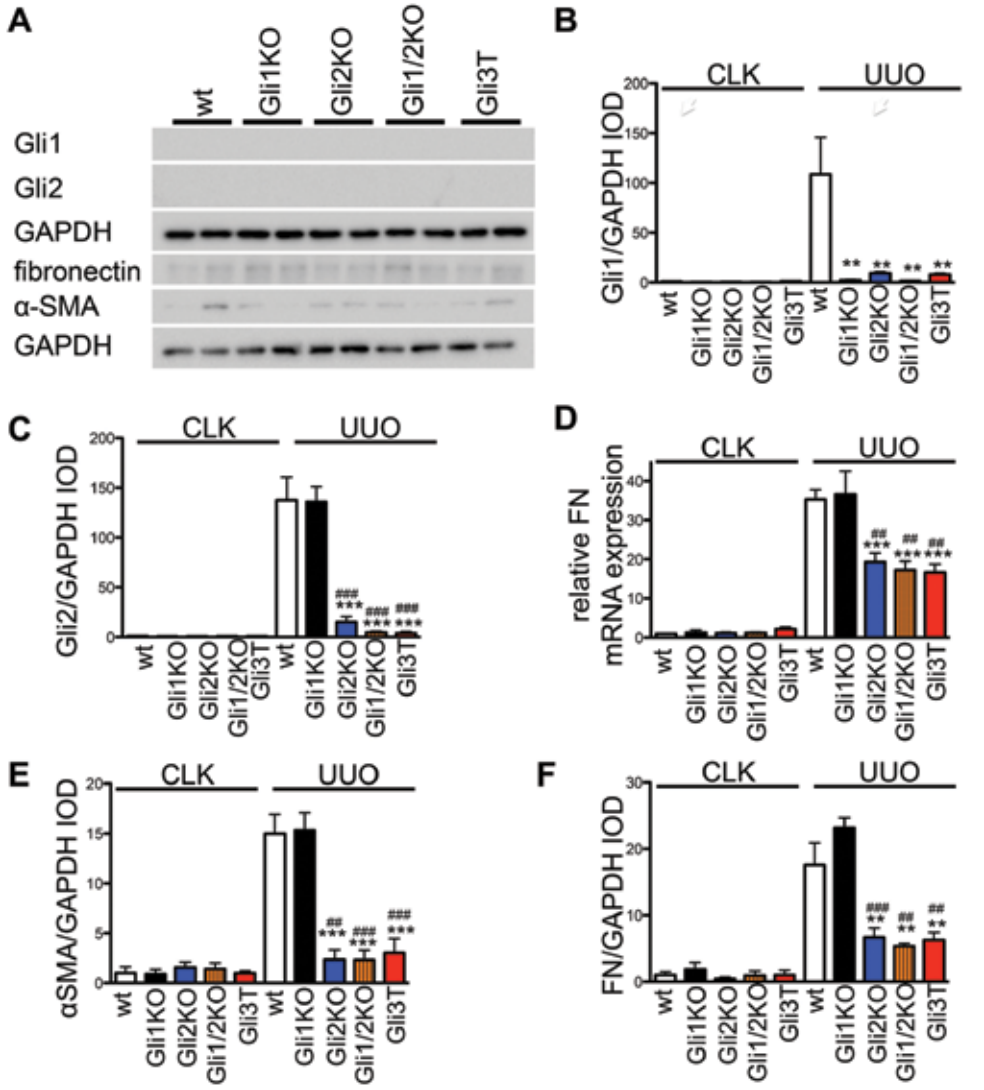

Figure S4: Reduced fibrosis severity following UUO in conditional knockout of Gli1 or Gli3 repressor expression in Gli1^{+} cells

A: Representative western blots of contralateral kidneys (CLK) from wildtype littermates (wt) compared to Gli1KO (Gli1CreER$^{t2+/+}$;Gli2flox$^{-/-}$); Gli2KO (Gli1CreER$^{t2+/-}$Gli2flox$^{+/+}$); Gli1/2KO (Gli1CreER$^{t2+/+}$Gli2flox$^{+/+}$) and Gli3T (Gli1CreER$^{t2+/-}$Gli3T$^{+/-}$) mice. Note: Gli proteins were not detectable in CLK kidneys. All used transgenic mice underwent surgery at 8-10 weeks of age and can be considered as mixed background with C57Bl/6J and 129S. Wildtype controls were littermates of the transgenic mice used in the experiments.

B-E: Protein levels from whole kidney lysates of CLK or unilateral ureteral obstruction (UUO) kidneys of n=4 mice from each group were quantified by integrated optical density -IOD Gli1, Gli2, fibronectin (FN) or αSMA /IOD glyceraldehyde-3-phosphate dehydrogenase (GAPDH).

F: Fibronectin mRNA expression in whole UUO and contralateral kidneys (CLK) of Gli1KO, Gli2KO, Gli1/2KO, Gli3T mice and wiltype littermates (wt). **p<0.05, ***p<0.001 versus wt, , ##p<0.01, ###p<0.001 versus Gli1KO, by one way ANOVA with posthoc Bonferroni , data presented as mean±SEM.

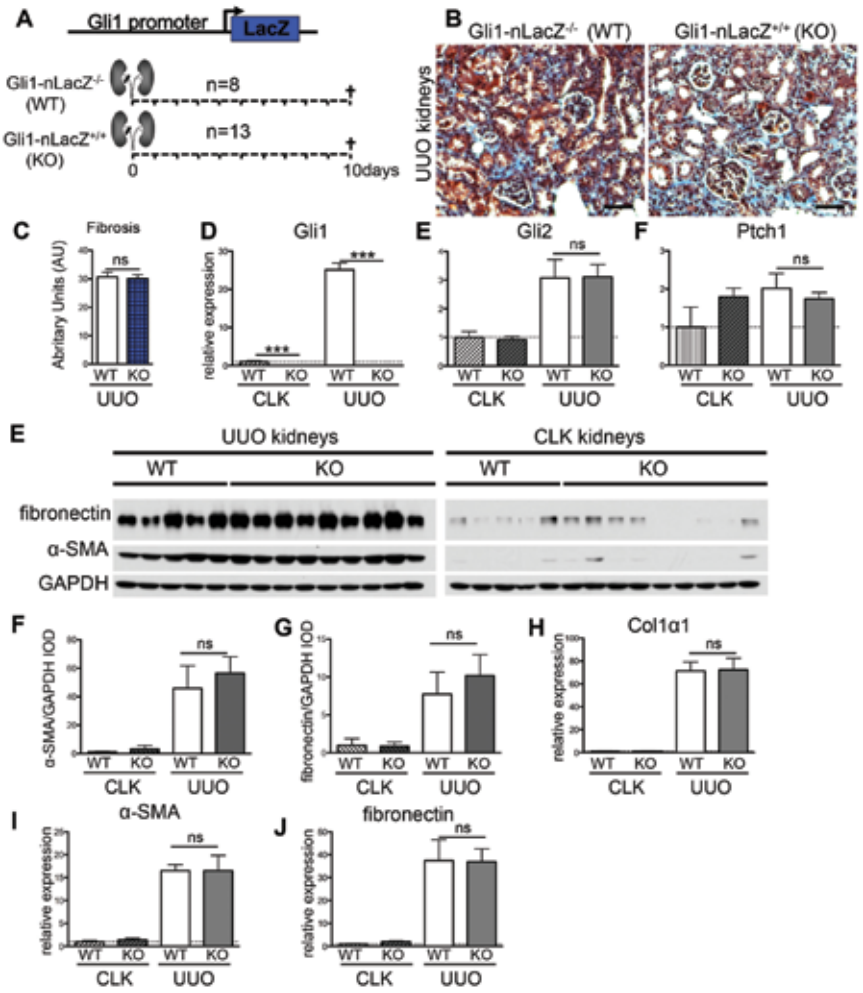

Figure S5: Knockout of the hedgehog effector Gli1 does not reduce renal fibrosis in unilateral ureteral obstruction (UUO)

A: Gli1 knockout (KO) was achieved by generating homozygous Gli1-nLacZ$^{+/+}$ mice (mixed background of 129S, Swiss Webster and C57Bl/6J) as their β-galactosidase knock-in mutation abolishes the Gli1 gene function. Gli1$^{+/+}$(KO) mice n=13 (all males, 8-10 weeks old) and their Gli1$^{-/-}$ wiltype (WT) littermates (n=8, all males, 8-10 weeks old) were subjected to UUO surgery and sacrificed at day 10 after surgery (A).

B-C: Knockout of Gli1 does not alter the extent of interstitial fibrosis. Trichrome stained kidney sections (B) were blindly scored for the extent of interstitial fibrosis (C)

D: Gli1 knockout abolishes the expression of Gli1 in UUO and contralateral control kidney (CLK), whereas the increased expression of Gli2 and Ptch1 in UUO was not effected. **E-G:** The increased expression of fibrotic readouts alpha smooth muscle actin (α-SMA) and fibronectin in UUO compared to CLK was not effected on protein level by knockout of Gli1 (Gli1$^{+/+}$; KO) compared to wildtype (Gli1$^{-/-}$; WT) littermates, as determined by Western blot (E) and quantified by integrated optical density (IOD) (F, G) IOD (α-SMA or IOD fibronectin/IOD glyceraldehydes-3-phosphate dehydrogenase (GAPDH)).

H-J: Quantification of mRNA expression by quantitative realtime PCR does not reveal a significant effect of Gli1 knockout (KO) on expression of increased fibrotic readouts collagen-1-alpha-1 (Col1α1, H), alpha smooth muscle actin (α-SMA, I) or fibronectin (J) in UUO kidneys compared to wildtype (WT) littermates. ns-non signficiant, ***p<0.001 by t-test, data is presented as mean±SD, scale bars 50μm.

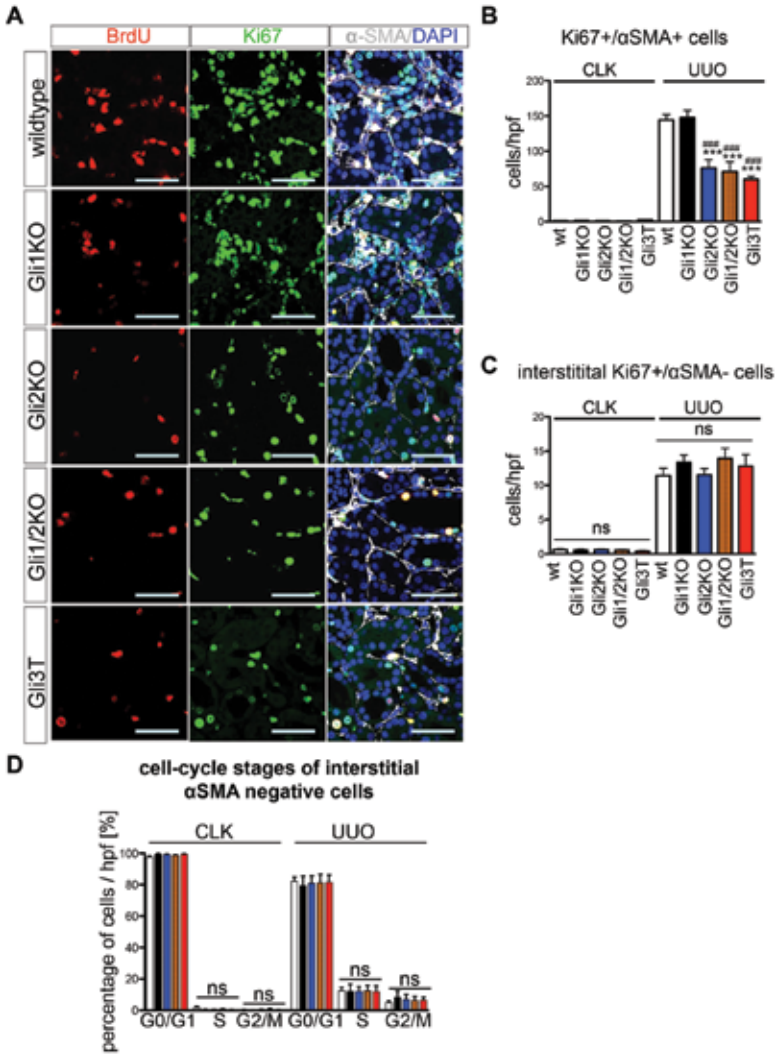

Figure S6: Conditional knockout of Gli2 or expression of the Gli3 repressor reduces proliferation of renal myofibroblasts.

A: Representative pictures of day 10 unilateral ureteral obstruction (UUO) kidneys from wildtype littermates (wt) compared to Gli1KO (Gli1CreER$^{t2+/+}$;Gli2flox$^{-/-}$); Gli2KO (Gli1CreER$^{t2+/-}$;Gli2flox$^{+/+}$); Gli1/2KO (Gli1CreER$^{t2+/+}$;Gli2flox$^{+/+}$) and Gli3T (Gli1CreER$^{t2+/-}$;Gli3T$^{+/-}$) mice co-stained for BrdU, Ki67 and alpha-smooth muscle actin (αSMA). BrdU was given 3 hours before euthanasia. All used transgenic mice underwent surgery at 8-10 weeks of age and can be considered as mixed background with C57Bl/6J and 129S. Wildtype controls were littermates of the transgenic mice used in the experiments.

B: Quantification of cycling (Ki67+) interstitial myofibroblasts (αSMA+) in day 10 UUO and contralateral non-injured kidneys (CLK).

C: Quantification of cycling interstitial non-myofibroblast cells (αSMA-).

D: Cell cycle stages for interstial non-myofibroblast cells (αSMA-) were assessed by counting of all interstitial cells in high power fields (400x) that were negative for αSMA staining after costaining for BrDU (S-phase), phospho-Histone H3 (G2/M-phase; G0/G1-phase: all interstitial αSMA$^-$ cells - interstitial αSMA$^-$ BrDU$^+$ cells - interstitial αSMA$^-$/pH3$^+$ cells). ***p<0.001 versus wt, ###p<0.001 versus Gli1KO, by one way ANOVA with posthoc Bonferroni, data presented as mean±SEM. Scale bars 50µm.

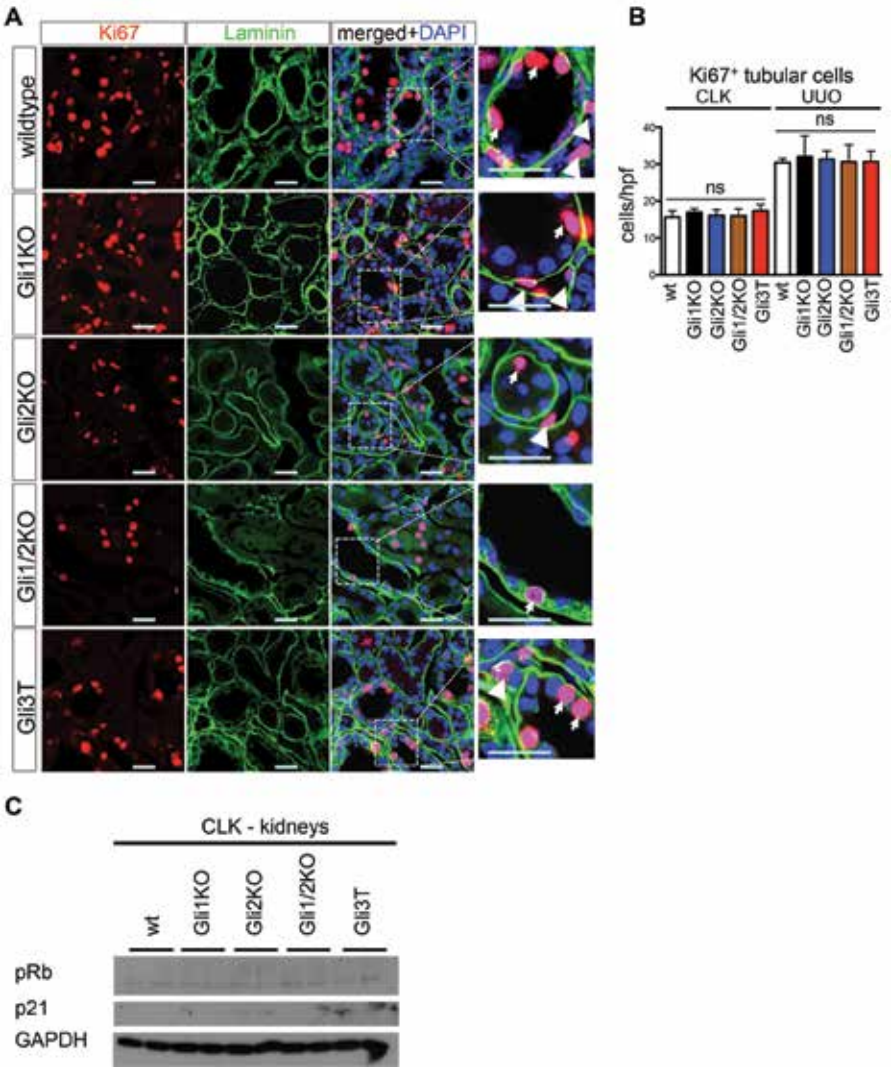

Figure S7: Proliferation of kidney tubular cells is not affected in the conditional knockout experiments.
A: Representative pictures of day 10 unilateral ureteral obstruction (UUO) kidneys from wildtype littermates (wt) compared to Gli1KO (Gli1CreER$^{t2+/+}$;Gli2flox$^{-/-}$); Gli2KO (Gli1CreER$^{t2+/-}$;Gli2flox$^{+/+}$); Gli1/2KO (Gli1CreER$^{t2+/+}$;Gli2flox$^{+/+}$) and Gli3T (Gli1CreER$^{t2+/-}$;Gli3T$^{+/-}$) mice co-stained for Ki67 and laminin to delineate tubular epithelial proliferation. Tubular epithelial cells (arrows) were easily detected as cells within the tubule surrounded by the laminin^{+} basement membrane. Whereas interstitial cells (arrowheads) were located in between two laminin^{+} layers of the basement membrane surrounding neighboring tubules. All used transgenic mice underwent surgery at 8-10 weeks of age and can be considered as mixed background with C57Bl/6J and 129S. Wildtype controls were littermates of the transgenic mice used in the experiments.
B: Tubular epithelial cells positive for the proliferation marker Ki67 were counted in 400x images (7 images / kidney in n=5 mice per group).
C: Representative western blots for phosphorylated retinoblastoma (pRb) and p21 in contralateral kidneys of Gli1KO, Gli2KO, Gli1/2KO, Gli3T mice and wiltype (wt) littermates. ns = non significant by one way ANOVA with posthoc Bonferroni , data presented as mean±SEM. Scale bars 25µm

.

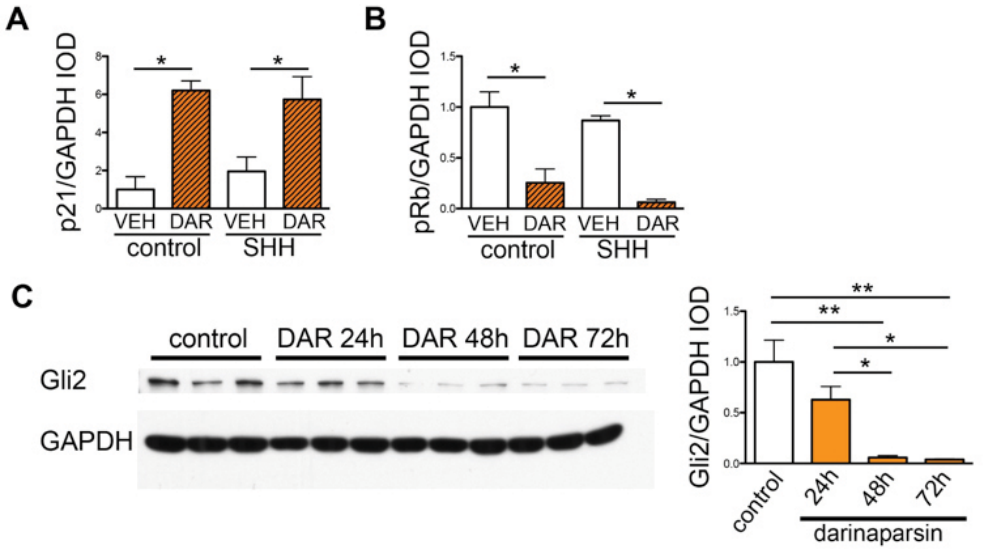

Figure S8: Darinaparsin treatment decreases Gli2 protein levels over time with upregulation of p21 and reduced phosphorylation of retinoblastoma.

A-B: Western blots from 2 experiments (total of n=3 biological replicates) of 10T1/2 cells treated with darinaparsin (DAR) or vehicle (VEH) with addition of sonic hedgehog (SHH) preconditioned medium (or control medium) were quantified by integrated optical density (IOD).

C: Representative western blot and quantification by integrated optical density (IOD) of human embryonic kidney cells (HEK293T) transfected with full-length Gli2 (pcDNA3.1-His-Gli2) and addition of normal saline (control) or darinaparsin (DAR, 0.5μM) over a time-course from 24 to 72 hours.

*p<0.05, **p<0.01, ***p<0.001, by t-test in A,B; by one way ANOVA with posthoc Bonferroni in C, data presented as mean±SEM.

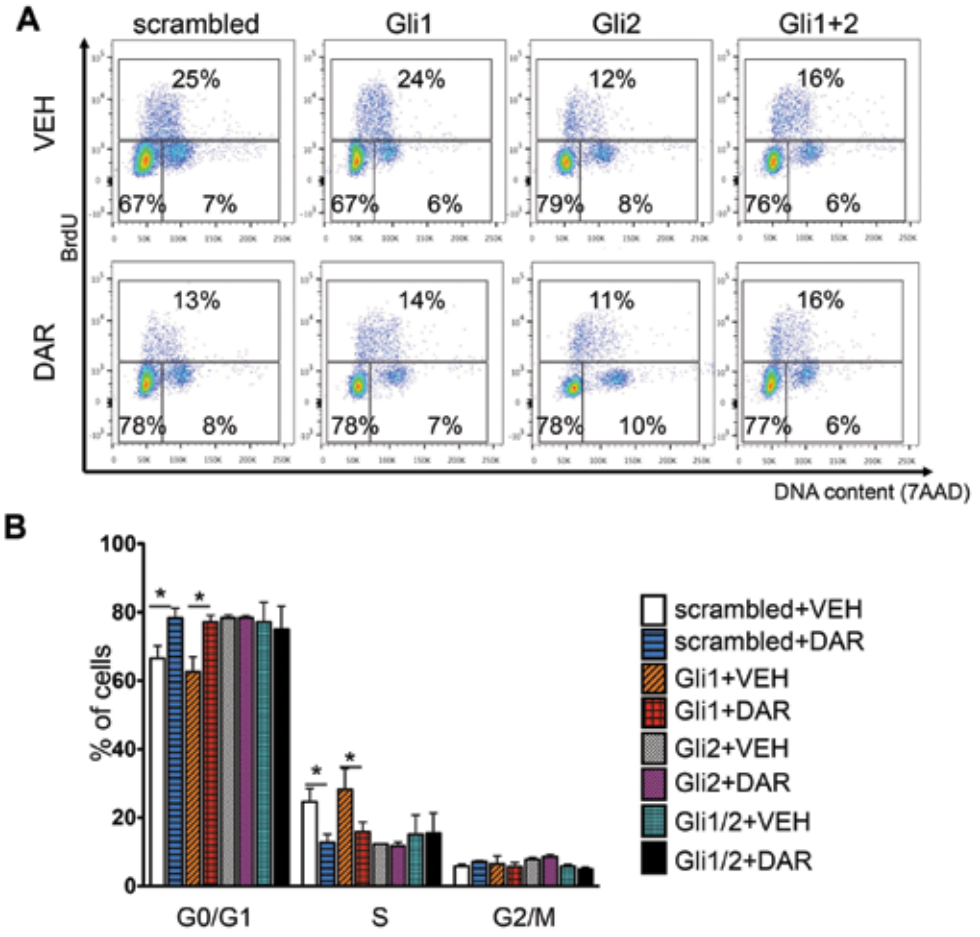

Figure S9: RNAi mediated knockdown of Gli2 abolishes the cell-cycle effect of darinaparsin.
A-B: Representative flow cytometric plots and quantification of 10T1/2 cells treated with siRNA against Gli1, Gli2, Gli1 and Gli2 or scrambled siRNA (control) with addition of darinaparsin (DAR, 0.5μM) or vehicle (VEH, normal saline). Note, darinaparsin treatment resulted in a G0/G1 cell cycle arrest of 10T1/2 cells treated with control siRNA and siRNA against Gli1 whereas siRNA against Gli2 or both Gli1+Gli2 decreased proliferation of cells with no further effect of darinaparsin treatment.
*p<0.05, by two way ANOVA with posthoc Bonferroni, data presented as mean±SEM.

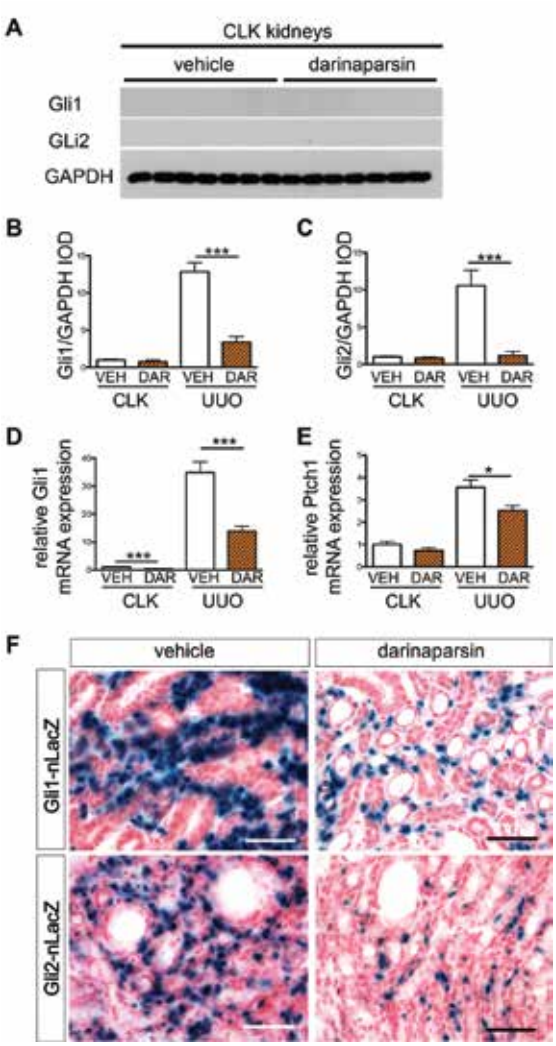

Figure S10: Darinaparsin treatment reduces the number of Gli1 and Gli2 expressing cells following UUO with decreased Gli1 and Gli2 protein levels and reduced hedgehog pathway activity

A: Representative western blots of contralateral (CLK) kidneys from wildtype (C57Bl/6J, 8-10 weeks old, all males) mice treated with darinaparsin (n=7) or vehicle (n=7) starting 2 days prior to UUO surgery until day 10 (blots from UUO kidneys in figure 5B).

B-C: Quantification of Gli1 and Gli2 protein levels in whole kidney lysates (UUO and CLK) of wiltype mice (C57Bl/6J) treated with darinaparsin (DAR, n=7) or vehicle (VEH, n=7) from 2 days prior to UUO surgery until day 10 (Experiment Figure 5 A-G).

D-E: Quantitative realtime PCR from whole kidney lysates of wildtype mice (C57Bl/6J) subjected to UUO (10days) and treated with darinaparsin (DAR, n=9) or vehicle (VEH, n=7) from 2 days prior to UUO surgery until day 10 indicates reduced mRNA expression of hedgehog readouts Gli1 and Ptch1 after darinaparsin treatment.

F: To determine whether darinparsin affects the expression of hedgehog effectors Gli1 and Gli2 darinaparsin was given daily (50mg/kg) to Gli1-nLacZ, Gli2-nLacZ reporter mice (mixed background of S129, Swiss Webster and C57Bl/6J; n=3 each, 2 males each, 8-10 week old,) starting 2 days prior to UUO. Mice were sacrificed at day 10 after surgery. 5-bromo-4-chloro-3-indolyl-β-D-galactopyranoside (X-gal) staining of these reporter mice shows a reduced number of Gli1 and Gli2 expressing cells. *p<0.05, ***p<0.001 vs vehicle treated mice by t-test, data is presented as mean±SEM, all scale bars 50µm

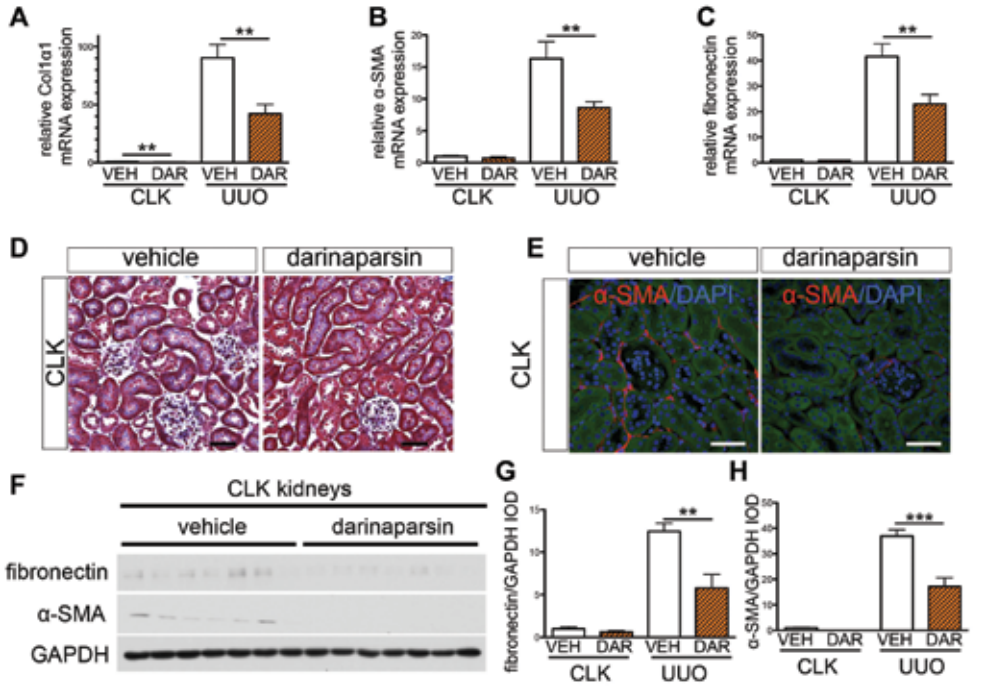

Figure S11: Darinaparsin treatment reduces mRNA expression of fibrotic readouts following unilateral ureteral obstruction (UUO)

Wildtype mice (C57Bl/6J, 8-10 weeks of age, all males) were subjected to UUO surgery and treated with darinaparsin (DAR, n=9) or vehicle (VEH, n=7) starting 2 days prior to UUO surgery until day 10. (Experiment of figure 5)

A-C: CollagenIαI, fibronectin and alpha smooth muscle actin (α-SMA) mRNA expression in whole unilateral ureteral obstruction (UUO) and contralateral (CLK) kidneys.

D-E: Representative images of trichrome stained or α-SMA immunostained contralateral non-injured kidneys (CLK).

F: Western blot for fibronectin and α-SMA from whole CLK kidneys.

G-H: Western blots for fibronectin and α-SMA were quantified by integrated optical density (IOD) indicating a significant reduced expression of both proteins in day 10 UUO kidneys from mice treated with darinaparsin (DAR) compared to the vehicle (VEH) group. (Representative western blot from UUO kidneys is shown in figure 5G).

**p<0.01, ***p<0.001 vs vehicle treated mice by t-test, data is presented as mean±SEM, all scale bars 50μm

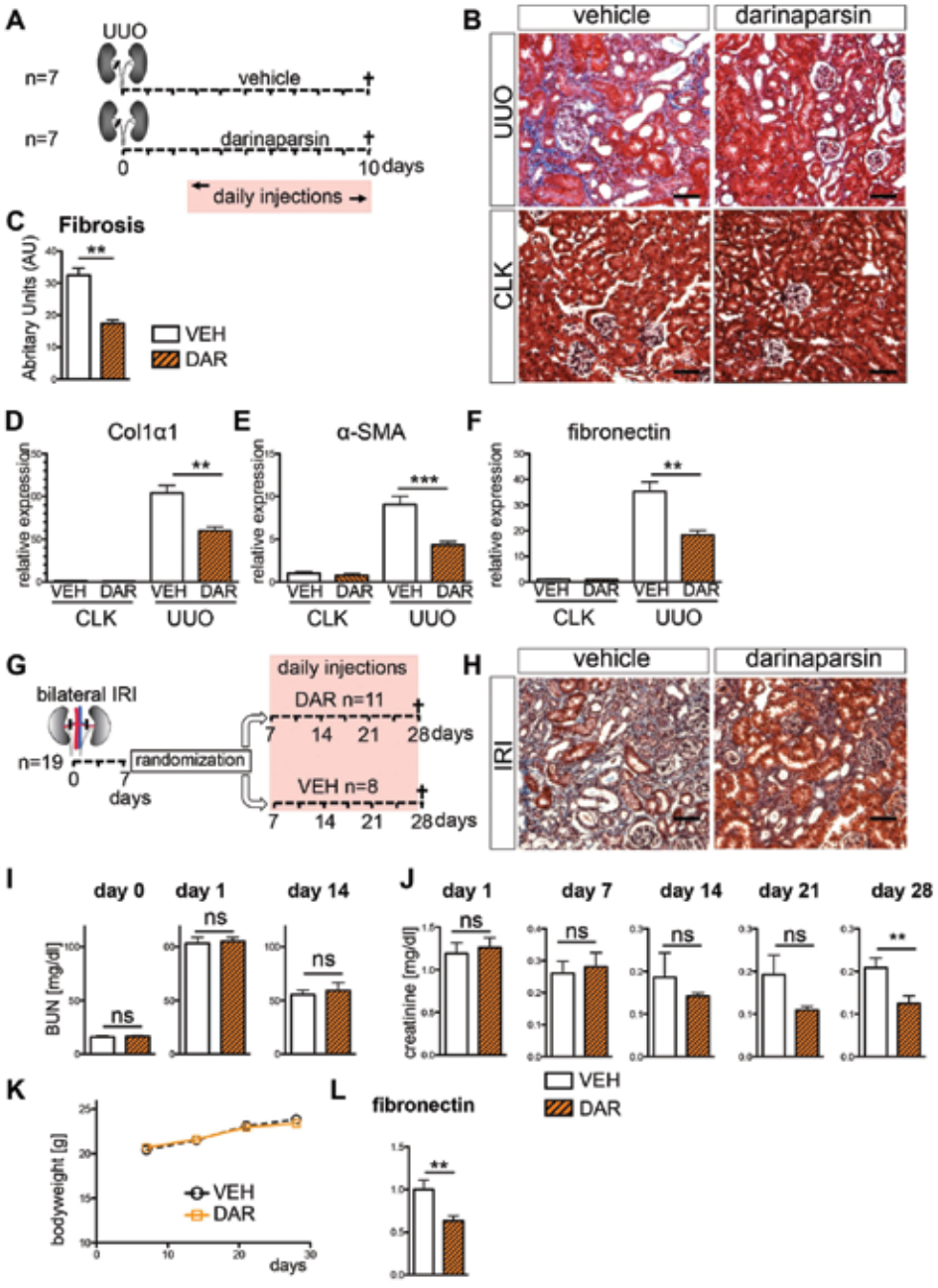
A
UUO
n=7
vehicle
n=7
darinaparsin
0
10 days
daily injections
B
vehicle
darinaparsin
UUO
CLK
C
Fibrosis
Abritary Units (AU)
VEH
DAR
D
Col1α1
relative expression
VEH DAR VEH DAR
CLK UUO
E
α-SMA
F
fibronectin
G
bilateral IRI
n=19
randomization
daily injections
DAR n=11
VEH n=8
7 14 21 28 days
H
IRI
I
day 0
day 1
day 14
BUN [mg/dl]
ns
J
day 1
day 7
day 14
day 21
day 28
creatinine [mg/dl]
K
bodyweight [g]
days
L
fibronectin

Figure S12: Therapeutic effect of darinaparsin after unilateral ureteral obstruction and bilateral ischemia re-perfusion injury.
A-F: A total of 14 mice (C57Bl/6J, 8-10 weeks old, all males) underwent unilateral ureteral obstruction (UUO), starting 2 days after surgery until sacrification 10 days after surgery n=7 mice were treated daily with darinaparsin (DAR, 50mg/kg i.p.) whereas n=7 mice served as a control group (daily injections of vehicle, VEH, i.p.) (A). Staining for Masson´s trichrome (B) and scoring revealed significant less interstitial fibrosis in the UUO kidneys of darinaparsin treated mice when compare to the UUO kidney of the control group (C). Determination of mRNA expression by quantitative realtime PCR demonstrated a significant lower expression of the fibrotic readouts collagen-1-alpha-1 (Col1α1, D), (alpha smooth muscle actin (α-SMA, E) and fibronectin (F) in the unilateral UUO kidneys of darinaparsin treated animals compared to vehicle treated animals.
G-H: Scheme of the bilateral ischemia re-perfusion injury experiment in n=19 wiltype mice (C57Bl/6J, 8-10 weeks old, all males) (G), representative Masson´s trichrome stained sections of IRI kidneys (H).
I: Measurement of blood urea nitrogen (BUN) revealed no significant difference between both groups at baseline and 7 days after ischemia reperfusion injury and at day 7 of treatment.
J: Measurement of serum creatinine indicated no significant difference between both groups at baseline and randomization with a significant lower creatinine in the darinaparsin treated group at 28 days after ischemia reperfusion injury.
K: Bodyweight data over time for vehicle (VEH) and darinaparsin (DAR) treated mice after ischemia reperfusion injury.
L: Quantitative realtime PCR analysis demonstrated significant lower mRNA expression of fibronectin in the IRI kidneys of darinaparsin treated mice. *p<0.05, **p<0.01, ***p<0.001, by t-test, data is presented as mean±SEM, all scale bars 50µm.

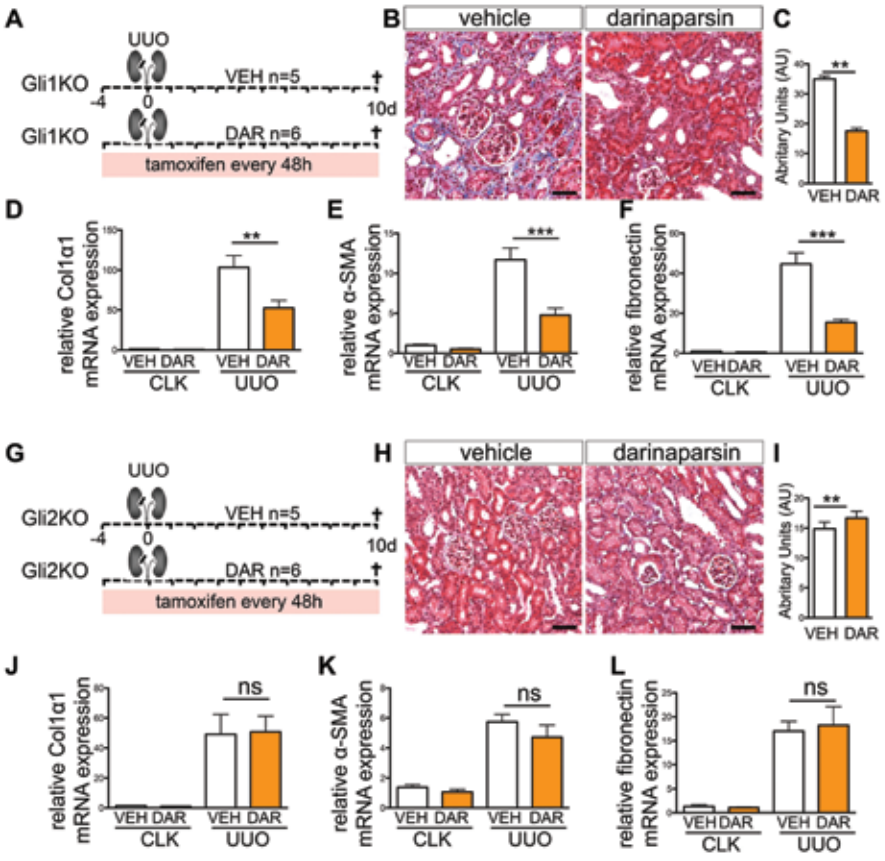

Figure S13: Darinaparsin treatment ameliorates fibrosis in Gli1KO mice but has not appreciable effect in conditional Gli2 knockout mice.

A: Gli1KO mice (Gli1LacZ$^{+/+}$; mixed background of 129S, Swiss Webster and C57Bl/6J, 8-10 weeks old) underwent unilateral ureteral obstruction (UUO) surgery and were treated with darinaparsin (DAR, n=6, 3 males, 50mg/kg bodyweight) or vehicle (normal saline, VEH n=5, 3 males) daily starting 2 days prior to surgery until euthanasia (day 10 after surgery). Mice of both groups received tamoxifen (10mg, p.o.) every 48h starting 2 days prior to UUO surgery.

B-C: Representative trichrome stained images and quantification of interstitial fibrosis indicating significantly decreased fibrosis in Gli1KO mice treated with darinaparsin compared to the vehicle treated group.

D-F: Quantitative realtime PCR for fibrotic readouts collagenIαI (CollαI), alpha smooth muscle actin (α-SMA) and fibronectin demonstrates reduced mRNA expression in the darinaparsin (DAR) treated group compared to the vehicle (VEH) treatment group of Gli1KO mice.

G: Gli2KO mice (Gli1CreER$^{+/-}$;Gli2flox$^{+/+}$; mixed background of 129S and C57Bl/6J, 8-10 weeks old) underwent UUO surgery and were treated with darinaparsin (DAR, n=6, 3 males) or vehicle (VEH, n=5, 3 males) starting 2 days prior to surgery until 10 days after surgery. Mice received tamoxifen (10mg, p.o.) every 48h starting 2 days prior to surgery until euthanasia.

H-I: Representative trichrome stained sections and quantification of interstitial fibrosis indicating no difference between the darinaparsin and vehicle treated group of Gli2KO mice.

J-L: Quantitative realtime PCR for fibrotic readouts collagenIαI (CollαI), alpha smooth muscle actin (α-SMA) and fibronectin from whole kidneys of Gli2KO mice treated with darinaparsin (DAR) or vehicle (VEH). **p<0.01, ***p<0.001, by t-test, data is presented as mean±SEM, all scale bars 50µm.

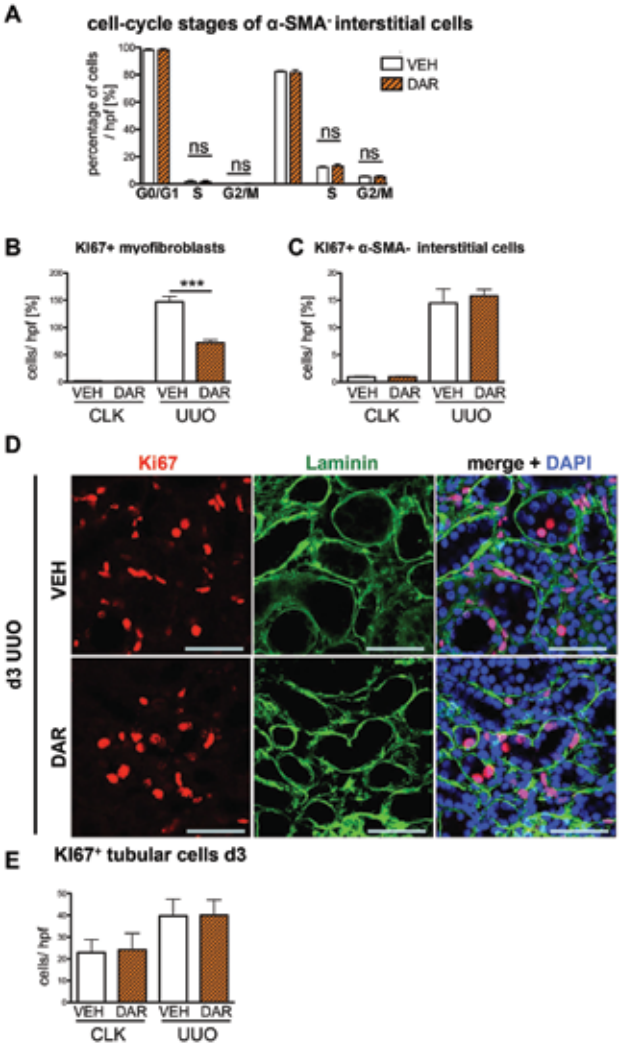

Figure S14: Darinaparsin treatment reduces proliferation of interstitial myofibroblasts but does not affect proliferation of other renal cell-types at day 3 following UUO.

Wildtype mice (C57Bl/6J, 8-10 weeks old, all males) were treated with darinaparsin (50mg/kg, n=6) or vehicle (n=6) starting 2 days prior to unilatereal ureteral obstruction (UUO) surgery and sacrified at day 3 after surgery. Bromdesoxyuridin (BrDU) was injected (100mg/kg) 3 hours prior to sacrification.

A: Cell cycle stages for interstitial non-myofibroblast cells (αSMA-) do not differ between darinaparsin (DAR) or vehicle (VEH) treated mice 3 days after UUO surgery.

B: Quantification of Ki67+ interstitial αSMA+ cells indicates reduced proliferation of myofibroblasts in the UUO kidneys of darinaparsin treated mice 3 days after surgery.

C: Quantification of Ki67+ interstitial αSMA- cells (non myofibroblasts) indicates no difference between darinaparsin and vehicle treated group.

D-E: Laminin staining was performed to delineate the tubules and cycling tubular epithelial cells were identified by staining for Ki67 and counting of Ki67+ cells within tubules (surrounded by laminin + basement membrane). ns=non-significant by one way ANOVA with posthoc Bonferroni; ***p<0.001, by t-test, data is presented as mean±SEM, all scale bars 50µm.

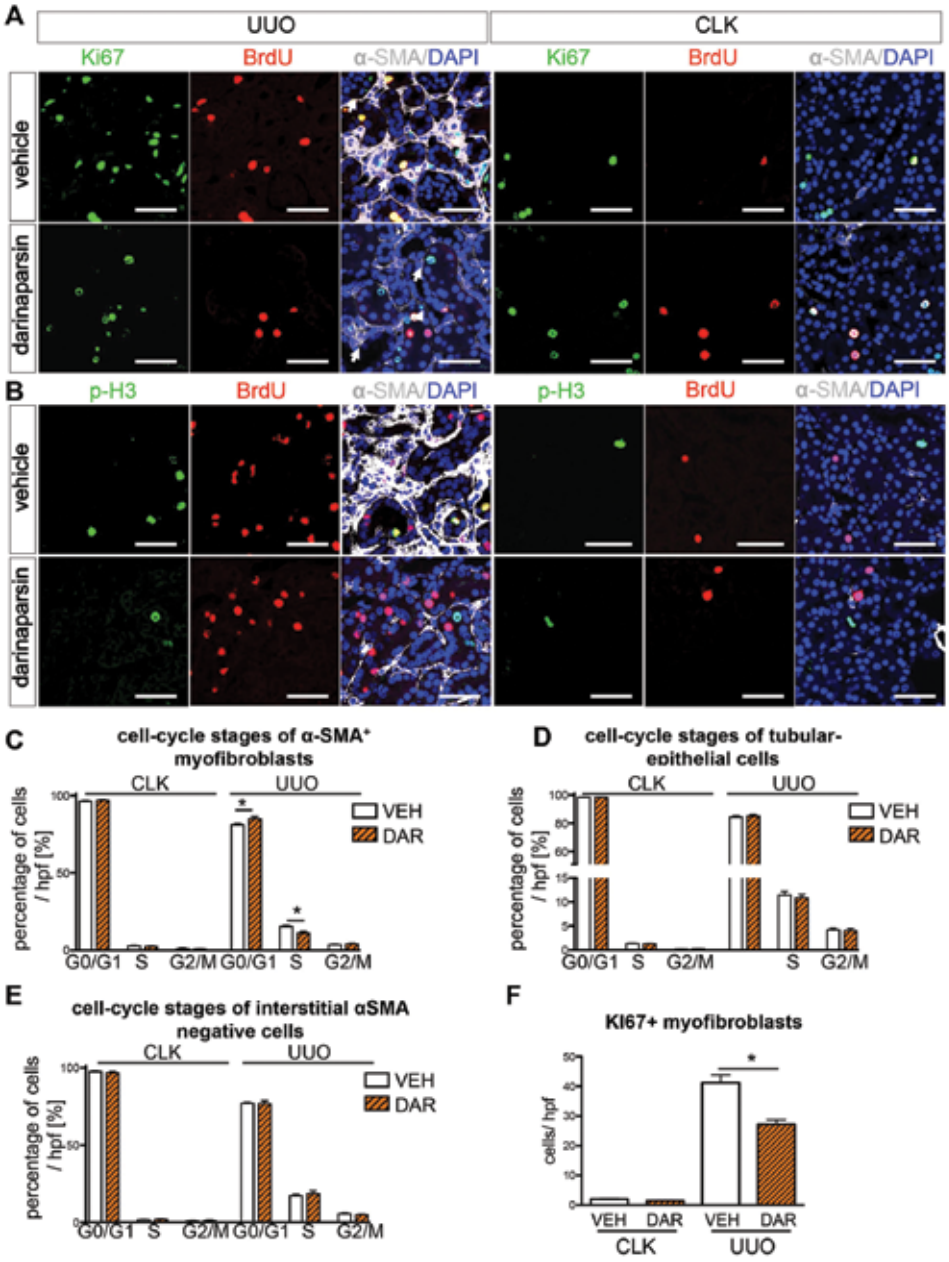

Figure S15: Darinaparsin treatment reduces proliferation of interstitial myofibroblasts 10 days after UUO surgery while tubular-epithelial cells and interstitial non-myofibroblasts were not affected.

Wildtype mice (C57Bl/6J, 8-10 weeks old, all males) underwent unilateral uretereal obstruction (UUO) surgery and received darinaparsin (DAR, n=7) or vehicle (VEH, n=7) daily starting 2 days after surgery until euthanasia at 10 days after surgery. Mice were injected with BrdU 3 hours prior to euthanasia.

A-B: Representative images of costained kidney sections from UUO and non-injured contralateral kidneys (CLK). Costaining for Ki67 + BrdU + alpha smooth muscle actin (αSMA) in A and phopspho-histone H3 (pH3) + BrdU + alpha smooth muscle actin (αSMA) in B.

C-E: Determination of cell-cycle stages indicated a G0/G1 cell-cycle arrest of interstitial myofibroblasts with no

effect on tubular-epithelial cells or interstitial αSMA- cells (non-myofibroblasts) at day 10 UUO. Cell cycle stages for interstitial myofibroblasts (αSMA+), for interstitial non-myofibroblasts (αSMA-) and tubular epithelial cells were calculated as follows: s-phase= BrdU+ cells; G2/M-phase= pH3+ cells; G0/G1-phase= all cells – BrdU+ - ph3+.
F: Ki67+ interstitial myofibroblasts were quantified by counting of Ki67/αSMA double positive interstitial cells.
*p<0.05 by one way ANOVA with posthoc Bonferroni, data is presented as mean±SEM, all scale bars 50µm.

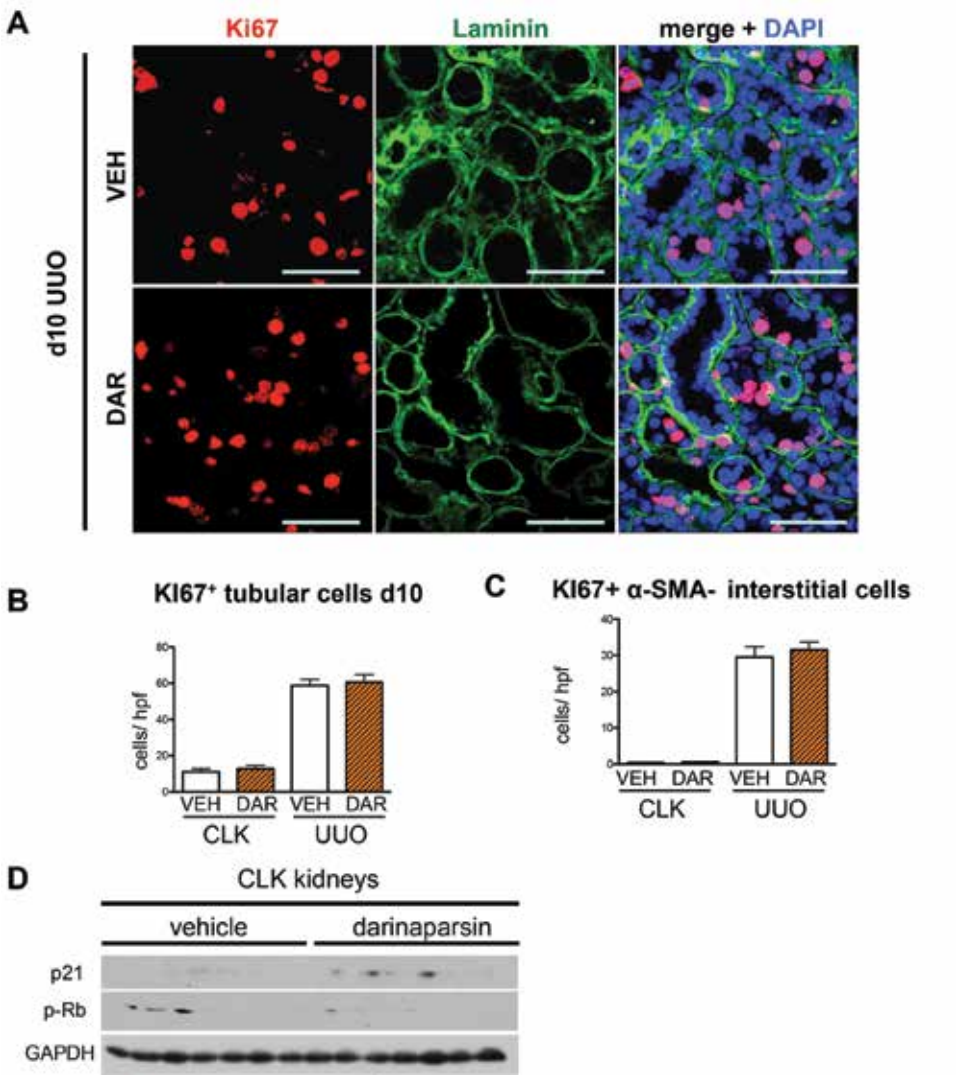

Figure S16: Darinaparsin treatment does not affect tubular epithelial proliferation at 10 days after UUO
A: Representative picture of kidney sections from day 10 UUO kidneys stained for Ki67 and laminin to determine tubular epithelial cell proliferation. Wildtype mice (C57Bl/6J, 8-10 weeks old, all males) received darinaparsin (DAR, n=7) or vehicle (VEH, n=7) daily from day 2-10 after UUO surgery.
B-C: We detected no difference in tubular epithelial Ki67+ cells (B) or cycling interstitial non-myofiroblasts (Ki67+/αSMA-) between the darinaparsin or the vehicle treated group-
D: Western blot analysis of whole CLK kidneys shows slightly increased levels of p21 with also a tendency to faintly reduction of phosphorylated retinoblastoma (p-Rb) in the darinaparsin treated mice. **(**UUO kidneys are shown in figure 6) Data is presented as mean±SEM, all scale bars 50µm.

Supplementary Table 1:

Primer pairs used for qt-RT-PCR in mouse:	
Gene	Sequence
GAPDH	Fw 5´-AGGTCGGTGTGAACGGATTTG -3´
	Rv 5`-TGTAGACCATGTAGTTGAGGTCA -3´
Gli1	Fw5´- ATCACCTGTTGGGGATGCTGGAT-3´
	Rv5´- CGTGAATAGGACTTCCGACAG -3´
Gli2	Fw5´-GTTCCAAGGCCTACTCTCGCCTG -3´
	Rv5´- CTTGAGCAGTGGAGCACGGACAT-3´
Ptch1	Fw5´- GCTGGAGGAGAACAAGCAAC-3´
	Rv5´- GAGCAAACATGTGCTCCAGA -3´
Col1α1	Fw5´- TGACTGGAAGAGCGGAGAGT-3´
	Rv5´-GTTCGGGCTGATGTACCAGT -3´
fibronectin	Fw5´-ATCTGGACCCCTCCTGATAGT -3´
	Rv5´-GCCCAGTGATTTCAGCAAAGG-3´
α-SMA	Fw5´-CTGACAGAGGCACCACTGAA -3´
	Rv5´- CATCTCCAGAGTCCAGCACA-3´

Supplementary Table 2:

Primer pairs used for qt-RT-PCR in human:	
Gene	Sequence
GAPDH	Fw 5´- GACAGTCAGCCGCATCTTCT-3´
	Rv 5`- GCGCCCAATACGACCAAATC-3´
Gli1	Fw5´- GAGCCAGAAGTTGGGACCTC-3´
	Rv5´- CCTCGCTCCATAAGGCTCAG -3´
Gli2	Fw5´- AAAGGCCTCTCCTTTGGTGG-3´
	Rv5´- CTTCCTTCCTGGTGTCGCAT -3´
Ptch1	Fw5´- CTTCTGGGAAGGGGCGAAAT -3´
	Rv5´- AGCATTTCCTCCCAGCTGTC -3´
Col1α1	Fw5´- CCCAGCCACAAAGAGTCTACA-3´
	Rv5´- ATTGGTGGGATGTCTTCGTCT -3´
fibronectin	Fw5´-AACAAACACTAATGTTAATTGCCCA-3´
	Rv5´-TCGGGAATCTTCTCTGTCAGC-3´
α-SMA	Fw5´- ACTGCCTTGGTGTGTGACAA-3´
	Rv5´- CACCATCACCCCCTGATGTC-3´

Supplementary Table 3: Basic characteristic of patients included

Subject	Age / sex / race	Surgery (nephrectomy)	Indication/ pathology	Pre-operative SCr, mg/dL*	Interstitial fibrosis	Risk factors for CKD
1	51 / M / C	Radical	Papillary urothelial carcinoma	1.18	>90%	unilateral severe hydronephrosis, HTN
2	64 / M / C	Partial	RCC	1.09	<10%	HTN
3	63 / M / C	Partial	RCC	0.98	80%	HTN, gout
4	69 / F / A	Radical	Papillary urothelial carcinoma; hydronephrosis	0.88	>90%	HTN, Hyperlipidemia, DM
5	59 / M / C	Radical	RCC	0.86	20%	Gout
6	60 / M / C	Radical	RCC	1.40 (eGFR 52)	<10%	none
7	72 / M / C	Radical	RCC	1.42 (eGFR 49)	40%	CAD, DM, HTN
8	52 / M / C	Radical	RCC	1.00	<10%	HTN, Hyperlipidemia
9	50 / M / C	Partial	RCC	0.65	<10%	none
10	56 / F /C	Radical	Metanephric adenoma	0.90	<10%	none

Abbreviations: A, Asian; C, Caucasian; eGFR, estimated glomerular filtration rate, ml/min/1.73m^2; M, male; RCC, renal cell carcinoma; SCr, serum creatinine; CKD, chronic kidney disease; HTN, hypertension; CAD, coronary artery disease; DM, diabetes mellitus

* All eGFR > 60 unless noted

REFERENCES

1. McCullough, K., et al., *Measuring the population burden of chronic kidney disease: a systematic literature review of the estimated prevalence of impaired kidney function.* Nephrol Dial Transplant, 2012. **27**(5): p. 1812-21.
2. McClellan, W.M. and L.C. Plantinga, *A public health perspective on CKD and obesity.* Nephrol Dial Transplant, 2013. **28 Suppl 4**: p. iv37-42.
3. 2013, U.A.D.R., *US Renal Data System: USRDS 2013 Annual Data Report: Atlas of Chronic Kidney Disease and End-Stage Renal Disease in the United States, Bethesda, MD, National Institutes of Health, National Institute of Diabetes and Digestive and Kidney Disease, 2013.*
4. Kramann, R., et al., *Matrix Producing Cells in Chronic Kidney Disease: Origin, Regulation, and Activation.* Curr Pathobiol Rep, 2013. **1**(4).
5. Kramann, R., D.P. DiRocco, and B.D. Humphreys, *Understanding the origin, activation and regulation of matrix-producing myofibroblasts for treatment of fibrotic disease.* J Pathol, 2013. **231**(3): p. 273-89.
6. Kramann, R., et al., *Perivascular Gli1+ progenitors are key contributors to injury-induced organ fibrosis.* Cell Stem Cell, 2015. **16**(1): p. 51-66.
7. Hui, C.C. and S. Angers, *Gli proteins in development and disease.* Annu Rev Cell Dev Biol, 2011. **27**: p. 513-37.
8. Briscoe, J. and P.P. Therond, *The mechanisms of Hedgehog signalling and its roles in development and disease.* Nat Rev Mol Cell Biol, 2013. **14**(7): p. 416-29.
9. Robbins, D.J., D.L. Fei, and N.A. Riobo, *The Hedgehog signal transduction network.* Sci Signal, 2012. **5**(246): p. re6.
10. Matise, M.P., et al., *Gli2 is required for induction of floor plate and adjacent cells, but not most ventral neurons in the mouse central nervous system.* Development, 1998. **125**(15): p. 2759-70.
11. Litingtung, Y. and C. Chiang, *Specification of ventral neuron types is mediated by an antagonistic interaction between Shh and Gli3.* Nat Neurosci, 2000. **3**(10): p. 979-85.
12. Park, H.L., et al., *Mouse Gli1 mutants are viable but have defects in SHH signaling in combination with a Gli2 mutation.* Development, 2000. **127**(8): p. 1593-605.
13. Humke, E.W., et al., *The output of Hedgehog signaling is controlled by the dynamic association between Suppressor of Fused and the Gli proteins.* Genes Dev, 2010. **24**(7): p. 670-82.
14. Bai, C.B., et al., *Gli2, but not Gli1, is required for initial Shh signaling and ectopic activation of the Shh pathway.* Development, 2002. **129**(20): p. 4753-61.
15. Ding, Q., et al., *Diminished Sonic hedgehog signaling and lack of floor plate differentiation in Gli2 mutant mice.* Development, 1998. **125**(14): p. 2533-43.
16. Mo, R., et al., *Specific and redundant functions of Gli2 and Gli3 zinc finger genes in skeletal patterning and development.* Development, 1997. **124**(1): p. 113-23.
17. Bai, C.B. and A.L. Joyner, *Gli1 can rescue the in vivo function of Gli2.* Development, 2001. **128**(24): p. 5161-72.
18. Yu, J., T.J. Carroll, and A.P. McMahon, *Sonic hedgehog regulates proliferation and differentiation of mesenchymal cells in the mouse metanephric kidney.* Development, 2002. **129**(22): p. 5301-12.
19. Aberger, F. and I.A.A. Ruiz, *Context-dependent signal integration by the GLI code: the oncogenic load, pathways, modifiers and implications for cancer therapy.* Semin Cell Dev Biol, 2014. **33**: p. 93-104.
20. Fabian, S.L., et al., *Hedgehog-Gli pathway activation during kidney fibrosis.* Am J Pathol, 2012. **180**(4): p. 1441-53.

21. Ding, H., et al., *Sonic hedgehog signaling mediates epithelial-mesenchymal communication and promotes renal fibrosis.* J Am Soc Nephrol, 2012. **23**(5): p. 801-13.
22. Zhou, D., et al., *Sonic hedgehog is a novel tubule-derived growth factor for interstitial fibroblasts after kidney injury.* J Am Soc Nephrol, 2014. **25**(10): p. 2187-200.
23. Dennler, S., et al., *Induction of sonic hedgehog mediators by transforming growth factor-beta: Smad3-dependent activation of Gli2 and Gli1 expression in vitro and in vivo.* Cancer Res, 2007. **67**(14): p. 6981-6.
24. Dennler, S., et al., *Cloning of the human GLI2 Promoter: transcriptional activation by transforming growth factor-beta via SMAD3/beta-catenin cooperation.* J Biol Chem, 2009. **284**(46): p. 31523-31.
25. Xie, J., et al., *A role of PDGFRalpha in basal cell carcinoma proliferation.* Proc Natl Acad Sci U S A, 2001. **98**(16): p. 9255-9.
26. Li, F., et al., *Sonic hedgehog signaling induces vascular smooth muscle cell proliferation via induction of the G1 cyclin-retinoblastoma axis.* Arterioscler Thromb Vasc Biol, 2010. **30**(9): p. 1787-94.
27. Bigelow, R.L., et al., *Sonic hedgehog induces epidermal growth factor dependent matrix infiltration in HaCaT keratinocytes.* J Invest Dermatol, 2005. **124**(2): p. 457-65.
28. Riobo, N.A., et al., *Phosphoinositide 3-kinase and Akt are essential for Sonic Hedgehog signaling.* Proc Natl Acad Sci U S A, 2006. **103**(12): p. 4505-10.
29. Ji, Z., et al., *Oncogenic KRAS activates hedgehog signaling pathway in pancreatic cancer cells.* J Biol Chem, 2007. **282**(19): p. 14048-55.
30. Schnidar, H., et al., *Epidermal growth factor receptor signaling synergizes with Hedgehog/GLI in oncogenic transformation via activation of the MEK/ERK/JUN pathway.* Cancer Res, 2009. **69**(4): p. 1284-92.
31. Stecca, B., et al., *Melanomas require HEDGEHOG-GLI signaling regulated by interactions between GLI1 and the RAS-MEK/AKT pathways.* Proc Natl Acad Sci U S A, 2007. **104**(14): p. 5895-900.
32. Pasca di Magliano, M., et al., *Hedgehog/Ras interactions regulate early stages of pancreatic cancer.* Genes Dev, 2006. **20**(22): p. 3161-73.
33. Wallace, V.A., *Purkinje-cell-derived Sonic hedgehog regulates granule neuron precursor cell proliferation in the developing mouse cerebellum.* Curr Biol, 1999. **9**(8): p. 445-8.
34. Dahmane, N. and A. Ruiz i Altaba, *Sonic hedgehog regulates the growth and patterning of the cerebellum.* Development, 1999. **126**(14): p. 3089-100.
35. Mann, K.K., et al., *Darinaparsin: a novel organic arsenical with promising anticancer activity.* Expert Opin Investig Drugs, 2009. **18**(11): p. 1727-34.
36. Tsimberidou, A.M., et al., *A phase I clinical trial of darinaparsin in patients with refractory solid tumors.* Clin Cancer Res, 2009. **15**(14): p. 4769-76.
37. Izzi, L., et al., *Boc and Gas1 each form distinct Shh receptor complexes with Ptch1 and are required for Shh-mediated cell proliferation.* Dev Cell, 2011. **20**(6): p. 788-801.
38. Mill, P., et al., *Sonic hedgehog-dependent activation of Gli2 is essential for embryonic hair follicle development.* Genes Dev, 2003. **17**(2): p. 282-94.
39. Li, Y., et al., *Sonic hedgehog signaling regulates Gli3 processing, mesenchymal proliferation, and differentiation during mouse lung organogenesis.* Dev Biol, 2004. **270**(1): p. 214-31.
40. Vokes, S.A., et al., *A genome-scale analysis of the cis-regulatory circuitry underlying sonic hedgehog-mediated patterning of the mammalian limb.* Genes Dev, 2008. **22**(19): p. 2651-63.
41. Kim, J., et al., *Arsenic antagonizes the Hedgehog pathway by preventing ciliary accumulation and reducing stability of the Gli2 transcriptional effector.* Proc Natl Acad Sci U S A, 2010. **107**(30): p. 13432-7.
42. Beauchamp, E.M., et al., *Arsenic trioxide inhibits human cancer cell growth and tumor development in mice by blocking Hedgehog/GLI pathway.* J Clin Invest, 2011. **121**(1): p. 148-60.

43. Tian, J., et al., *Darinaparsin: solid tumor hypoxic cytotoxin and radiosensitizer.* Clin Cancer Res, 2012. **18**(12): p. 3366-76.
44. Bansal, N., et al., *Darinaparsin inhibits prostate tumor initiating cells and Du 145 xenografts and is an inhibitor of hedgehog signaling.* Mol Cancer Ther, 2014.
45. Sasaki, H., et al., *Regulation of Gli2 and Gli3 activities by an amino-terminal repression domain: implication of Gli2 and Gli3 as primary mediators of Shh signaling.* Development, 1999. **126**(17): p. 3915-24.
46. Beauchamp, E.M. and A. Uren, *A new era for an ancient drug: arsenic trioxide and Hedgehog signaling.* Vitam Horm, 2012. **88**: p. 333-54.
47. Zhang, X.W., et al., *Arsenic trioxide controls the fate of the PML-RARalpha oncoprotein by directly binding PML.* Science, 2010. **328**(5975): p. 240-3.
48. Roessler, E., et al., *A previously unidentified amino-terminal domain regulates transcriptional activity of wild-type and disease-associated human GLI2.* Hum Mol Genet, 2005. **14**(15): p. 2181-8.
49. Kramann, R., M. Tanaka, and B.D. Humphreys, *Fluorescence microangiography for quantitative assessment of peritubular capillary changes after AKI in mice.* J Am Soc Nephrol, 2014. **25**(9): p. 1924-31.
50. Diaz, Z., et al., *A novel arsenical has antitumor activity toward As2O3-resistant and MRP1/ABCC1-overexpressing cell lines.* Leukemia, 2008. **22**(10): p. 1853-63.
51. Garnier, N., et al., *The novel arsenical darinaparsin is transported by cystine importing systems.* Mol Pharmacol, 2014. **85**(4): p. 576-85.
52. Garnier, N., et al., *The novel arsenical Darinaparsin circumvents BRG1-dependent, HO-1-mediated cytoprotection in leukemic cells.* Leukemia, 2013.
53. Machado, A.F., et al., *Teratogenic response to arsenite during neurulation: relative sensitivities of C57BL/6J and SWV/Fnn mice and impact of the splotch allele.* Toxicol Sci, 1999. **51**(1): p. 98-107.
54. DeSesso, J.M., et al., *An assessment of the developmental toxicity of inorganic arsenic.* Reprod Toxicol, 1998. **12**(4): p. 385-433.
55. Chaineau, E., et al., *Embryotoxic effects of sodium arsenite and sodium arsenate on mouse embryos in culture.* Teratology, 1990. **41**(1): p. 105-12.
56. Riobo, N.A. and D.R. Manning, *Pathways of signal transduction employed by vertebrate Hedgehogs.* Biochem J, 2007. **403**(3): p. 369-79.
57. Ribes, V., et al., *Early mouse caudal development relies on crosstalk between retinoic acid, Shh and Fgf signalling pathways.* Development, 2009. **136**(4): p. 665-76.
58. Hao, K., et al., *Hedgehog signaling pathway regulates human pancreatic cancer cell proliferation and metastasis.* Oncol Rep, 2013. **29**(3): p. 1124-32.
59. Sasai, K., et al., *Medulloblastomas derived from Cxcr6 mutant mice respond to treatment with a smoothened inhibitor.* Cancer Res, 2007. **67**(8): p. 3871-7.
60. Samarzija, I. and P. Beard, *Hedgehog pathway regulators influence cervical cancer cell proliferation, survival and migration.* Biochem Biophys Res Commun, 2012. **425**(1): p. 64-9.
61. Duman-Scheel, M., et al., *Hedgehog regulates cell growth and proliferation by inducing Cyclin D and Cyclin E.* Nature, 2002. **417**(6886): p. 299-304.
62. Nagao, H., et al., *Role of GLI2 in the growth of human osteosarcoma.* J Pathol, 2011. **224**(2): p. 169-79.
63. Zhang, D., et al., *shRNA-mediated silencing of Gli2 gene inhibits proliferation and sensitizes human hepatocellular carcinoma cells towards TRAIL-induced apoptosis.* J Cell Biochem, 2011. **112**(11): p. 3140-50.
64. Plaisant, M., et al., *Inhibition of hedgehog signaling decreases proliferation and clonogenicity of human mesenchymal stem cells.* PLoS One, 2011. **6**(2): p. e16798.
65. Lauth, M., et al., *Inhibition of GLI-mediated transcription and tumor cell growth by small-molecule antagonists.* Proc Natl Acad Sci U S A, 2007. **104**(20): p. 8455-60.

66. Shi, T., et al., *cDNA microarray gene expression profiling of hedgehog signaling pathway inhibition in human colon cancer cells.* PLoS One, 2010. **5**(10).

67. Moshai, E.F., et al., *Targeting the hedgehog-glioma-associated oncogene homolog pathway inhibits bleomycin-induced lung fibrosis in mice.* Am J Respir Cell Mol Biol, 2014. **51**(1): p. 11-25.

68. Humphreys, B.D., et al., *Intrinsic epithelial cells repair the kidney after injury.* Cell Stem Cell, 2008. **2**(3): p. 284-91.

69. Dunn, S.R., et al., *Utility of endogenous creatinine clearance as a measure of renal function in mice.* Kidney Int, 2004. **65**(5): p. 1959-67.

70. Lauth, M. and R. Toftgard, *Non-canonical activation of GLI transcription factors: implications for targeted anti-cancer therapy.* Cell Cycle, 2007. **6**(20): p. 2458-63.

71. Chiariello, M., E. Gomez, and J.S. Gutkind, *Regulation of cyclin-dependent kinase (Cdk) 2 Thr-160 phosphorylation and activity by mitogen-activated protein kinase in late G1 phase.* Biochem J, 2000. **349 Pt 3**: p. 869-76.

6

DISCUSSION

6.1 Gli1 as a novel marker of Mesenchymal Stem Cells (MSC)

Partly from: Role of Mesenchymal Stem Cells in kidney injury and fibrosis. By Christoph Kuppe and Rafael Kramann (Corresponding author: Rafael Kramann, MD; RWTH Aachen University; Division of Nephrology and Clinical Immunology; Email: rkramann@ukaachen.de)
In Curr Opinion Nephrol Hypertens 2016, 25:372-377

While studying hedgehog signaling in the kidney we observed that Gli1 expression in adult homeostasis specifically marks a perivascular cell population of MSC [3]. These $Gli1^+$ MSCs form a tremendous network from the adventitia of larger muscular arteries to the pericyte niche of microcapillaries across all major organs studied including, heart, liver, lung, kidney, muscle and bone marrow [3]. We generated a transgenic mouse model to genetically tag $Gli1^+$ MSC (Gli1CreER;R26tdTomato). $Gli1^+$ cells were isolated by fluorescence activated cell sorting (FACS) and in vitro studies revealed that $Gli1^+$ cells indeed fulfill all criteria for cells that have been termed MSC previously (surface marker pattern, increased colony forming unit fibroblast capacity – CFU – and three-lineage differentiation capacity into bone, cartilage and fat). However, as MSC are a solely in vitro characterized cell population and not much is known about their in vivo role, we termed $Gli1^+$ cells in vivo MSC-like. Others groups have shown in addition that Gli1marks MSC in the mouse incisor and craniofacial bones and that $Gli1^+$ cells play a role in bone and dental injury repair [4, 5].

6.2. The cellular origin of fibrosis

Partly from: Role of Mesenchymal Stem Cells in kidney injury and fibrosis. By Christoph Kuppe and Rafael Kramann (Corresponding author: Rafael Kramann, MD; RWTH Aachen University; Division of Nephrology and Clinical Immunology; Email: rkramann@ukaachen.de)
In Curr Opinion Nephrol Hypertens 2016, 25:372-377

As outlined in the introduction the cellular origin of myofibroblasts driving fibrosis in most organs has been very controversial for many years and the literature of the last decades has reported a variety of different progenitors including epithelium, endothelium, circulating cells and resident mesenchymal cells. Our data indicate that resident $Gli1^+$ MSCs are a major source of myofibroblasts in kidney, heart and bone marrow. Furthermore, they also contribute significantly to fibrosis in lung and liver. Importantly, our inducible genetic fate tracing experiments in kidney fibrosis indicate that proximal tubular epithelium does not contribute to the myofibroblast pool, whereas circulating monocytes show a limited contribution with approximatively 10% of renal myofibroblasts that are derived from monocytes. Importantly, these monocyte derived myofibroblasts primarily express proinflammatory cytokines and not much extracellular matrix suggesting that their contribution might be rather indirect by activation of resident mesenchymal cells such as Gli1+ pericytes and fibroblasts.

The in vivo role of MSC was quite unclear and based on the various studies that have used MSC as cellular therapy it was suggested that resident MSC become activated upon

organ injury, leave their pericyte niche and contribute to injury repair by secreting bioactive molecules that facilitate a regenerative microenvironment [6]. In order to study the role of Gli1$^+$ perivascular MSC in organ injury we performed genetic fate tracing of Gli1$^+$ cells in Gli1CreER;tdTomato mice subjected to injury of kidney, heart, liver, lung and bone-marrow [3, 7, 8]. To our surprise Gli1$^+$ cells acquired αSMA expression and contributed to the pool of myofibroblasts across all major organs studies.

We then genetically ablated Gli1$^+$ cells by using the heritable cell specific expression of the human diphtheria toxin receptor (Gli1CreER; iDTR) and injection of diphtheria toxin. Importantly, genetic ablation of Gli1$^+$ cells ameliorated fibrosis significantly and even stabilized organ function in the ascending aortic constriction model of heart failure. Furthermore, ablation of Gli1$^+$ cells in bone marrow fibrosis not only abolished fibrosis but also rescued bone marrow failure and stabilized hematopoiesis.[7]

Importantly, it has been controversially discussed if fibrosis per se has a degenerative effect after organ injury and thus questioned if anti-fibrotic strategies can restore organ function. The data of our study suggests that targeting Gli1$^+$ cells causing fibrosis stabilizes organ function pointing towards fibrosis as a disease entity itself. Using other models of organ injury (Ang-II for the heart, CCl4 for the liver, bleomycin for the lung) we showed that Gli1+ perivascular cells are an important source of myofibroblasts in heart, liver and lung fibrosis. Others have suggested that myofibroblasts in the kidney partially derive from the bone-marrow [9]. In order to decipher whether Gli1$^+$ cells are resident kidney cells or bone marrow derived cells bone marrow transplantation and parabiosis experiments were performed. The results clearly indicated that Gli1$^+$ resident perivascular cells are the major source of myofibroblasts in kidney injury and do not circulate from the bone marrow.

6.3 Targeting Hedgehog Gli to treat kidney fibrosis

Partly from: Hedgehog Gli Signaling in Kidney Fibrosis. By Rafael Kramann (Corresponding author: Rafael Kramann, MD; RWTH Aachen University; Division of Nephrology and Clinical Immunology; Email: rkramann@ukaachen.de)

In kidney development Shh expression in papillary collecting duct regulates mesenchymal cell proliferation and deletion of Shh leads to severe abnormalities in kidney development such as renal hypoplasia or aplasia [10, 11]. Ihh is expressed in nephrogenic tubules at the cortico-medullary boundary during later stages of kidney development [11]. However, Ihh knockout mice do not show a renal phenotype suggesting that Ihh is not required for kidney development [12].The Pallister-Hall Syndrome in humans is an autosomal dominant disorder with mutations in the Gli3 gene leading to multiple tissue malformations including polidactyly and renal dysplasia, renal hypoplasia and hydronephrosis [11].

Not much is known about the role of the Hh pathway in the adult kidney. Recent evidence suggests that in kidney injury the embryonically conserved Hh pathway is reactivated and epithelial derived Hh activates adjacent mesenchymal cells [13] [14-16].

Fabian et al. reported that after kidney injury two ligands Shh and Ihh were expressed by tubularepithelial cells while interstitial PDGFRb+ cells responded by upregulation of Gli1 and Gli2 [14]. The authors also reported that Shh treatment was able to increase proliferation in the pericyte / mesenchymal stem cell – like cell line 10T1/2 [17]. The smoothened antagonist IPI-926 abolished Gli1 expression following unilateral ureteral obstruction (UUO) but did not affect severity of kidney fibrosis [14]. Ding et al. also reported upregulation of Shh in renal tubular epithelial cells during kidney fibrosis [15]. The authors further showed that interstitial myofibroblasts express Gli1 and that recombinant Shh was able to induce aSMA expression in rat kidney fibroblasts. In contrast to Fabian et al. they reported that inhibition of Smo by cyclopamine reduced fibrosis severity [15]. The reasons for this discrepancy remain unclear and further studies are needed to clarify whether inhibition of Smo affects kidney fibrosis severity. Interestingly, it has been reported that conditional knockout of Smo in aSMA expressing cells significantly ameliorates liver fibrosis [18]. Zhou et al. reported increased tubular Shh expression in three mouse models of kidney injury and in human kidney biopsy specimen from CKD patients and increased proliferation of rat kidney fibroblasts when exposed to Shh [16]. Furthermore, Shh hydrodynamic gene transfer increased interstitial cell proliferation and fibrosis severity following ischemia reperfusion injury (IRI) [16]. In a recent study, Rauhauser et al. reported an effect of Hh signaling on macrophage infiltration, tubular proliferation and apoptosis [19]. The authors used NG2CreER;Smo-floxed mice to conditionally inactivate canonical Hh signaling in NG2+ pericytes and observed significantly reduced numbers of infiltrating F4/80+ macrophages following UUO, while they did not detect a difference on kidney fibrosis severity [19]. Glis2 is a repressor of Hh signaling, therefore mice carrying a heterozygous Glis2 loss of function mutation have increased Hh activity [19]. Interestingly, Rauhauser et al. demonstrated that Glis2 heterozygous mice showed increased Shh expression and more severe signs of tubular epithelial damage (dilatation, dedifferentiation of tubular epithelial cells) following UUO compared to their wildtype littermates [19]. Moreover, Glis2 heterozygous mice also showed increased collagen I expression following UUO in line with a pro-fibrotic role of increased Hh pathway activity [19].

In the kidney the relevant Gli1+ cell population also expresses Gli2. Interestingly, while Gli1 expression is specific for a perivascular cell population across major organs [3], and all cells that express Gli1 also express Gli2, we observed Gli2 expressing cells in some organs that do not express Gli1. One example are cardiomyocytes which clearly express Gli2 in Gli2nLacZ mice but do not express Gli1 (Kramann et al. unpublished). The reason for this remains elusive as it was assumed up to date that all three Gli transcriptional activators (Gli1-3) are expressed in Hh responsive cells.

We next sought to determine the difference of Gli1 versus Gli2 in Gli1^{+} myofibroblast precursors and evaluated Gli proteins as potential therapeutic targets in kidney fibrosis. We generated transgenic mouse models that either express the Gli3 repressor specifically

in Gli1+ cells to suppress all Gli proteins or conditional knockout of Gli2 in Gli1$^+$ cells. Mice were subjected to UUO surgery and compared to wildtype littermates, full Gli1 knockout (Gli1KO) mice and Gli1KO mice with additional conditional knockout of Gli2 in Gli1$^+$ cells [20]. Our data indicated that both inhibition of all Gli proteins by Gli3T expression or conditional knockout of Gli2 in Gli1$^+$ cells reduced kidney fibrosis following UUO, whereas knockout of solely Gli1 did not have any effect [20]. We identified a specific G0/G1 cell-cycle arrest in myofibroblasts, while other kidney cells were not affected, as the underlying mechanism in the reduction of kidney fibrosis. This finding might be due to the fact that Gli proteins are only expressed in renal myofibroblasts and their precursors but no other kidney cell-types. In vitro knockout of Gli2 in the mouse MSC-like cell line 10T1/2 also resulted in a G0/G1 cell cycle arrest while overexpression of Gli2 by retroviral delivery increased proliferation. We detected increased expression of p21 and subsequently reduced phosphorylation of retinoblastoma indicating that cells left the cell cycle at the G1 restriction point after knockout of Gli2.

The next question was whether this finding has therapeutic impact. Arsenic trioxide (ATO) is used to treat promyelocytic leukemia and it has been reported to antagonize both Gli1 and Gli2 [21]. Darinaparsin, a novel organic arsenic (S-dimethylarsino-glutathione) with decreased toxicity when compared to ATO, is currently undergoing clinical testing in hematologic malignancies and solid cancer [22, 23]. The mechanism of action of darinaparsin was unknown before and interestingly, ATO resistant myeloma cell lines are not resistant against darinaparsin treatment [24]. Our data indicated that darinaparsin directly binds Gli2 protein with subsequent reduction of Gli2 protein levels, presumably by directly affecting Gli2 protein stability [20]. Darinaparsin treatment induced a G0/G1 cell-cycle arrest in 10T1/2 cells while overexpression of Gli2 completely rescued this effect. We next asked whether lowering Gli2 protein levels in vivo by darinaparsin treatment might affect kidney fibrosis severity following UUO or IRI. Indeed, we observed significantly reduced kidney fibrosis severity in mice treated with darinaparsin when compared to vehicle treated mice. In line with our data on conditional Gli2 knockout, lowering Gli2 protein by darinaparsin treatment also induced a cell specific cell cycle arrest of myofibroblasts in vitro with upregulation of p21 and reduced pRb. Importantly, following IRI darinaparsin treatment not only reduced kidney fibrosis severity but also improved kidney function [20]. As darinaparsin is still an arsenic with potential side effects, we next investigated whether GANT61, a small molecule Gli inhibitor, also shows an anti-fibrotic effect in vivo. Indeed mice subjected to UUO and treated with GANT61 in a therapeutic regimen showed decreased kidney fibrosis severity when compared to vehicle treated mice.

Our data clearly suggests that targeting Gli2 is a promising therapeutic strategy in kidney fibrosis. Importantly, induction of a myofibroblast specific cell-cycle arrest did not only reduce kidney fibrosis severity but also improved kidney function. In our opinion targeting Gli proteins directly is a favorable strategy compared to an upstream inhibition of the Hh

pathway e.g. by inhibition of Smo. Emerging strong evidence in the cancer field suggests a direct activation of Gli proteins by pathways that are also known to drive kidney fibrosis such as TGFβ [25], PDGF [26, 27], EGFR , RAS and AKT/Pi3K signaling [28-32]. It is conceivable that the canonical Hh pathway is activated during kidney fibrosis as discussed above but the literature on whether Smo inhibition reduces kidney fibrosis is controversial [14, 15]. In line with this, inhibition of smoothened in lung fibrosis had no effect while direct inhibition of Gli proteins by GANT61 decreased fibrosis severity [33]. In conclusion, targeting Gli proteins directly downstream of the canonical Hh pathway might be a promising therapeutic strategy that blocks canonical and non-canonical activation of Hh transcriptional activators and therefore reduces myofibroblasts proliferation. However, further studies are needed to elucidate the role of non-canonical Gli activation in kidney injury and fibrosis.

Evidence for Hedgehog signaling and mesenchymal progenitor cells in human kidneys:

While the role of Hh signaling and $Gli1^{+}$ progenitor cells in mouse kidney fibrosis and CKD has been demonstrated it remains an open question whether the same mechanism also exists in human kidney fibrosis and whether these findings can be translated into novel therapeutics in human disease. We recently measured mRNA expression of Hh pathway members in kidney specimen from cancer nephrectomies. The specimen where blindly scored for fibrosis severity and our data suggests that specimen with a severe degree of interstitial fibrosis (>80%) showed significantly increased expression of Gli1, Gli2 and Ptch1 compared to specimen with a lower grade of interstitial fibrosis (<20%)[20]. This data points towards a role of Hh signaling in human kidney fibrosis. However, further studies are needed to evaluate the role of Hh signaling in human kidney homeostasis and disease.

While various progenitor populations have been described amongst human epithelial kidney cells [34-37] only one group has reported the isolation of MSC from human kidneys [38]. Bruno et al. studied human glomeruli cultures and reported a population of CD133−, CD146+ cells outgrowing from glomeruli with clonal long-term capacities, expression of MSC markers (CD29, CD44, CD166, CD73, CD90, CD105, CD146, vimentin, and nestin) and trilineage differentiation capacity towards chondrocytes, osteoblasts and adipocytes [38]. Possible links between MSC and pericytes have been suggested by various groups and it became evident that many, if not all, pericytes are MSC-like in all human tissues studied [39]. Beside the pericyte niche MSC also exist in the perivasculature (i.e. adventitia) of larg arteries [40]. While this clearly suggests that human kidney pericytes might also be MSC-like this has not been experimentally proven yet. Moreover, it remains an open question whether human kidney perivascular cells also express Gli1 and contribute to the myofibroblast pool after kidney injury.

6.4 Myelofibrosis and the bone marrow niche

From: The identification of fibrosis-driving myofibroblast precursors reveals new therapeutic avenues in myelofibrosis. By Rafael Kramann and Rebekka K Schneider (Corresponding authors: Rafael Kramann, MD; RWTH Aachen University; Division of Nephrology and Clinical Immunology; Email: rkramann@ukaachen.de and Rebekka K. Schneider, M.D., Ph.D.,Erasmus MC, Department of Hematology, Rotterdam)

Blood

Under normal conditions, the bone marrow provides a fine network of fibers, which provides support for the blood cells to grow. Bone marrow fibrosis or myelofibrosis (MF) is a disorder in which normal bone marrow tissue and blood-forming cells are gradually replaced with thick coarse fibers and scar-like tissue.[41] By definition, MF implies an increase in the bone marrow fiber content without explicit reference to quantity or quality. Over time, this leads to failure of the bone marrow to produce blood cells, to extramedullary hematopoiesis (typically in the spleen) resulting in (hepato)splenomegaly and ultimately to death. MF is a concomitant and non-specific feature due to a multitude of reactive as well as neoplastic disorders.

The myeloproliferative neoplasm (MPN) primary myelofibrosis (PMF), previously known as chronic idiopathic myelofibrosis or agnogenic myeloid metaplasia, is the prototypic example of progressive development of bone marrow fibrosis, has the worst prognosis of MPNs and is a complex disorder. Pathologically, MF is characterized by thickening and distortion of bony trabeculae, deposition of reticulin and collagen fibers, and megakaryocytic hyperplasia with atypical features.

William Dameshek speculated in an editorial in Blood already in 1951 that in MPNs the bone marrow proliferates excessively as a unit in response to a myelostimulatory factor.[42] This concept, he believed, could explain why the hyperplasia in MPNs includes all myeloid lineages and, as fibrosis is often present, the fibroblasts as well. It has become increasingly clear over the last couple of years that two distinct pathogenic processes contribute to the initiation and progression of PMF: 1. stem cell-derived clonal myeloproliferation and 2. a reactive cytokine-driven inflammatory fibrosis. This means in a very simplified description that in PMF (or in general in MPNs), hematopoietic stem cells acquire mutations – in most of the cases a JAK2(V617F) mutation – which leads to increased proliferation of the hematopoietic stem cell and replacement of normal blood formation (we refer to excellent reviews describing the mutational landscape in MPNs).[43-47] In the course of the disease, non-mutated, non-hematopoietic cells transform into fibrosis-driving cells. The biology of this cross-talk between malignant hematopoietic cells and a normal (non-hematopoietic) stromal cell which transforms into a fibrosis-driving cell remained completely elusive for decades, in particular as the cells driving fibrosis were just identified last year.[7, 48] The discovery of $Gli1^+$ and Leptin-receptor$^+$ ($LepR^+$) cells opened new avenues 1) to dissect pathomechanisms underlying the fibrotic transformation and 2) to identify novel therapeutic targets for

this so far incurable disease. Interestingly, these findings depicted striking similarities in the pathogenesis of solid organ fibrosis and MF. In particular, it became obvious that the common denominator of LepR$^+$ and Gli1$^+$ stromal cells is their progenitor state of fibrosis-causing myofibroblasts in the bone marrow. Myofibroblasts are fibrosis-driving cells and well characterized in solid organ fibrosis but their role and cellular origin in bone marrow fibrosis has remained obscure. Understanding the cellular and molecular mechanisms that govern the mesenchymal stromal cell (MSC)-to-myofibroblast transition and myofibroblast expansion in the bone marrow will be critical to understand the pathogenesis of bone marrow fibrosis and will guide the development of novel therapeutics. In this "*perspective article*", we will summarize the recent discoveries of MSCs as myofibroblast precursors and their implications for therapeutic options in the context of knowledge in the pathogenesis and therapy of solid organ fibrosis.

Stromal cells as the cellular origin of myofibroblasts: Chronic repetitive injury leads to fibrosis in virtually any organ. It has been estimated that fibrosis is involved in up to 45% of all deaths in the developed world.[49] The replacement of functional units of cells by myofibroblasts and extracellular matrix leading to progressive loss of organ function is the common feature of fibrosis across all organs. In solid organ fibrosis researchers across different disciplines have agreed on myofibroblasts as the fibrosis driving cells. Myofibroblasts are highly synthetically active and contractile cells that are characterized by dense rough endoplasmatic reticulum, collagen secretion granules and alpha-smooth muscle actin (α-SMA) expression.[50] α-SMA forms characteristic strong bundles of myofilaments, the so called stress fibers that promote strong contractile force generation and that have been widely used to identify myofibroblasts in fibrotic tissue. Multiple genetic fate tracing experiments have shed light on the cellular origin of myofibroblasts in heart, kidney, liver, lung and skin.[3, 8, 13] Over 25 years ago, investigators have observed myofibroblasts in electron microscopy studies of human bone marrow fibrosis.[51, 52] However, until recently, their functional role and contribution to bone marrow fibrosis remained unclear. Interestingly, and very different to the extensive literature of myofibroblasts in most organ systems, no other studies have followed up on this finding and have investigated the origin and role of myofibroblasts in bone marrow fibrosis.

We have recently identified that expression of the hedgehog transcriptional activator Gli1 specifically marks perivascular MSC-like cells.[3] Genetic fate tracing in heart, kidney, liver and lung injury demonstrated that these cells are a major source of myofibroblasts during solid organ fibrosis.[3] This prompted us to investigate the role of Gli1$^+$ MSC-like cells in MF. In the bone marrow Gli1$^+$ cells are located in the endosteal niche with direct contact to bone as well as perivascular around arterioles and marrow sinusoids.[7] Inducible genetic fate tracing experiments in two murine models of bone marrow fibrosis (thrombopoietin-ThPO or JAK2(V617F) overexpression in hematopoietic stem cells) indicated that Gli1$^+$

cells are fibrosis driving α-SMA$^+$ myofibroblasts of the bone marrow.[7] Importantly, using heritable expression of the human diphtheria toxin receptor in Gli1$^+$ cells, we demonstrated that ablation of Gli1$^+$ cells abolishes bone marrow fibrosis. This data indicated that Gli1$^+$ derived myofibroblasts are the cellular source of bone marrow fibrosis and a promising therapeutic target.

Interestingly, Decker et al. recently performed non-inducible genetic fate tracing in LepR-Cre;tdTomato;Col1a1-GFP mice that received ThPO overexpressing bone marrow and demonstrated that LepR$^+$ stromal cells tremendously expand and become collagen-producing myofibroblasts in bone marrow fibrosis.[48] They further demonstrated that LepR$^+$ cells express the mesenchymal markers platelet-derived growth factor receptor (PDGFR) α and β (also known as CD140a+b) and that PDGFRα is critical in development of bone marrow fibrosis as a LepR$^+$ cell specific knockout of PDGFRα resulted in tremendously reduced reticulin fibrosis.[48] Together, these two recent studies confirm for the first time the longstanding hypothesis that MSCs are indeed the cellular origin of bone marrow fibrosis. Importantly, beside the above mentioned work on Gli1$^+$ cells in solid organ fibrosis, seemingly equivalent tissue resident MSC populations have been reported as the cellular drivers of organ fibrosis in various organ systems.[53] It remains elusive whether in the bone marrow Gli1$^+$ and LepR$^+$ cells overlap or are distinct myofibroblast precursors. The role of monocyte-derived fibroblasts was recently discussed in MF.[54] Gli1$^+$ and LepR$^+$ cells are CD45$^-$ non-hematopoietic cells, indicating that their differentiation into myofibroblasts is a distinct process and independent of monocyte-derived fibrocytes. However, while fate tracing indicates that both stromal populations contribute to the myofibroblast pool, the data also suggest that not all myofibroblasts are derived from these stromal populations. Thus, a contribution of other cell types to the bone marrow myofibroblast pool remains an open question and monocyte-derived myofibroblasts might also contribute. The recently more widely available technologies of single cell analysis such as single cell RNA-Sequencing will shed light into the heterogeneity of the bone marrow stroma in homeostasis and disease.

Importantly, recent data indicate that besides elimination of the malignant hematopoietic clone, targeting the mesenchymal stroma might be a novel therapeutic strategy in MF. To explore whether pharmacologically targeting the Hedgehog-Gli signaling pathway might affect expansion of Gli1$^+$ stromal cells and fibrosis severity, we combined genetic fate tracing of Gli1$^+$ cells in the JAK(V617F) induced MF model with a pharmacologic therapeutic regimen using the small molecule direct Gli-inhibitor “Gli antagonist 61 (GANT61)”. Treatment with GANT61 or vehicle was initiated 8 weeks after bone marrow transplantation and importantly pharmacologic Gli inhibition resulted in tremendously decreased Gli1$^+$ cell expansion and virtually abolished bone marrow fibrosis.[7] Furthermore, GANT61 treatment reduced splenomegaly and also the Jak2(V617F) induced hematopoietic phenotype with increased long-term HSCs and multipotent progenitor cells, suggesting an effect of both the malignant clone and fibrosis-driving stromal cells.[7]

Others and we have already reported that targeting Hedgehog-Gli signaling is a therapeutic strategy in solid organ fibrosis. Indeed, the data indicate that targeting Gli proteins directly inhibits $Gli1^+$ cell proliferation and myofibroblast differentiation resulting in reduced fibrosis severity and improved organ function.[20] While inhibition of Hedgehog-Gli signaling upstream (e.g. by Smo inhibition) failed to improve pulmonary fibrosis[33] and kidney fibrosis[14], the direct inhibition of Gli proteins by GANT61 ameliorated fibrosis in both organs.[20, 33] Therefore, targeting Gli proteins directly might be an interesting and novel therapeutic approach in MF.

The treatment of MF can be divided into two broad categories: 1) eradication of the malignant hematopoietic clone and 2) targeting of various signaling pathways and mediators implicated in MF. In MF, allogeneic hematopoietic stem cell transplantation (HSCT) is the only therapeutic intervention with curative potential, effectively eradicating the malignant hematopoietic clone as well as leading to reversal of fibrosis and MPN-associated histomorphological features of the bone marrow.[55] Importantly, regression of bone marrow fibrosis at day +100 after HSCT in patients with MF is associated with improved survival, independently of IPSS score at the time of transplantation, as demonstrated by Kroger *et al*.[56] **This study highlights the prognostic significance of bone marrow fibrosis which is now accounted for in the Mutation-Enhanced International Prognostic Score System (MIPSS) for transplantation age patients with MF.**[57] It also raises the potential of improving outcomes of HSCT by combining anti-fibrogenic strategies prior to or even after the transplant.

Development of therapeutic strategies in MF: Apart from HSCT, none of the conventional therapies applied in the treatment of MF are considered curative. With the introduction of selective JAK inhibitors over the last 10 years, initial expectation of clonal suppression was dampened by the observations of persistent clonal hematopoiesis and mostly unaltered MPN morphological features in the bone marrow.[58-60] One publication and several abstracts on more detailed histopathological analyses of the bone marrow indicate that ruxolitinib treatment in MF modulates the microenvironment as the number of macrophages and mast cells, microvascular density, microvessel area and the inflammatory reaction are reduced. Long-term therapy with ruxolitinib thus may provide a clinically meaningful delay of bone marrow fibrosis progression as the observed alterations in the microenvironment seem to be associated with more favorable outcome.[61-64] Further, JAK inhibitors have been shown to improve patient constitutional symptoms and reduce splenomegaly, but the monotherapy does not significantly reduce mutant allele burden in the majority of MPN patients.[60, 65, 66] The therapeutic window for JAK inhibitors is limited due to the essential role of the JAK-STAT signaling pathway in normal hematopoiesis, which has been observed in the clinic where these inhibitors have been associated with dose limiting toxicities. Therefore, there is a need to identify additional pathways that might be involved in the development and

maintenance of MPN mutant clones, which could be targeted in combination with JAK2 for improved therapeutic benefit.[67-69]

Identifying novel and effective anti-fibrotic therapeutics with minor side effects in both solid organ fibrosis and MF is the Holy Grail in fibrosis research. Various anti-fibrotic strategies in solid organs and also MF aim in particular at targeting inflammation and fibrogenic cytokines such as PDGF and transforming growth factor (TGF) b (among various others).[13, 49]. Targeting fibrogenic cytokines alone or in combination with ruxolitinib is an active area of investigation in the treatment of MF. Pirfenidone, the first anti-fibrotic compound on the market (approved in Japan for idiopathic pulmonary fibrosis in 2008, in Europe 2011 and FDA approved in 2014) has anti-inflammatory properties and inhibits TGFb and p38 signaling.[70] The results of a phase II trial of pirfenidone treatment in 28 MF patients were already published in 2001.[71] However, although TGFb and inflammation are thought to play a central role in the disease pathogenesis of MF, none of the patients had improvement in bone marrow fibrosis, anemia or a reduction in spleen weight. Other strategies focus on the resolution of the excessive formation of extracellular matrix in fibrosis. Lysyl oxidase (LOX) Lysyl oxidase-like are amine oxidases involved in crosslinking of collagen and elastin fibers and were described to be up-regulated in the serum of patients with MF.[72] Simtuzumab, a humanized antibody against LOX-like 2 was tested in monotherapy and in combination with ruxolitinib. Simtuzumab alone or with ruxolitinib was well tolerated but did not produce clinical benefit nor consistently reduce bone marrow fibrosis by 24 weeks.[73] PTX2 is a soluble pattern recognition receptor of the innate immune system that may aid in the removal of damaged tissue and regulate monocyte differentiation states.[74] PRM-151, a recombinant form of human pentraxin 2 (PTX2) is investigated in the treatment of various fibrotic disease[74] and also MF, alone and in combination with ruxolitinib. A phase II study in combination with ruxolitinib (13 patients completed at least 72 weeks) showed that the combination was well tolerated and the authors reported an infrequent improvement in fibrosis grade at week 48.[75] However, long-term results need to be awaited before final conclusions can be drawn.

In summary, results from these studies suggest that targeting single inflammatory cytokines or extracellular matrix proteins alone might not be sufficient to inhibit the fibrotic transformation, but that multiple pathways that drive cellular processes in the fibrotic transformation need to be inhibited in parallel in order to block the complex interaction between malignant hematopoietic cells, inflammatory cytokines, dysplastic megakaryocytes and fibrosis-driving cells.

Targeting Hedgehog-Gli signaling as a novel therapeutic option: A 20-100 fold increase in the expression of hedgehog target genes, including Gli1 and Ptch1, has been observed in granulocytes isolated from MPN patients[76] as well as an increased expression in the spleen of GATA1^{low} myelofibrotic mice.[77] Preclinical and clinical data suggest that

hedgehog pathway inhibitors have therapeutic activity in MF. Sonidegib (LDE-225), saridegib (IPI-926) and PF-04449913, all smoothened (SMO)-inhibitors, are currently under clinical investigation, alone or in combination with other agents, in MF. The essential function and druggability render SMO well suited for pharmacological inhibition. Sonidegib in combination with ruxolitinib was tested in a multicenter, phase Ib/II study: the maximum tolerated dose was not reached during the dose escalation phase, but improvements in leukocytosis, thrombocytosis, bone marrow fibrosis and mutant allele burden were noticed, indicating synergistic effects of sonidegib and ruxolitinib (ASH abstract). A total of 27 MF patients were treated at the recommended phase II dose with ruxolitinib. Although the combination was relatively well tolerated and resulted in approximately 50% of patients achieving a ≥35% decrease in spleen volume, only two treated patients had at least a one grade reduction in bone marrow fibrosis. A clinical study analyzing saridegib monotherapy had negative results.[78] The reduction in splenomegaly was modest, symptoms as evaluated by MPN-SAF scores did not improve significantly and only four out of ten evaluated patients had minimal to modest decreases in bone marrow fibrosis after three months. Importantly, exploratory studies evaluating markers of Hh signaling in this study did not show a reduction of Gli1 mRNA and protein levels, indicating that Gli1 might be activated by non-canonical, SMO-independent (oncogenic) pathways in MF (**Figure 1**)Accumulating data indicate that Gli proteins can also be activated in a SMO-independent fashion by TGF-β[25, 79], platelet PDGF signaling[26, 27], and AKT/PI3K pathways[28-32, 80], all of which have also been reported to play an important role in JAK2(V617F) mutated MPN. In light of these studies, it is obvious that the regulation of Gli activity is not only subject to canonical Hh/PTCH/SMO-dependent signaling, but also controlled by integration of multiple, oncogenic, non-HH signals. This concept has led in the cancer field to the hypothesis that Gli proteins are an information nexus in the regulation of cell fate, stemness and oncogenesis. We found that Gli1-expression is significantly increased in stromal cells from MPN patients and in murine $Gli1^{+}$ stromal cells in response to JAK2(V617F) mutant cells. As outlined above, our data in a murine model demonstrate that pharmacologic targeting of Gli proteins with a small molecule Gli inhibitor ameliorates bone marrow fibrosis in JAK2(V617F) MPN. We thus propose that Gli proteins in hematopoietic and stromal cells in MF can be activated independent of canonical Hh signaling, potentially explaining the poor response of SMO-inhibitors in patients with PMF. Targeting abnormal Gli activation in fibrosis-causing cells and in the mutant hematopoietic clone might be an optimal strategy for treating MF as Gli and Hh-signaling were shown to be dispensable for normal hematopoiesis in two back-to-back seminal papers published in 2009,[81-83] potentially allowing to spare normal hematopoiesis while eliminating both malignant hematopoietic cells and activated fibrosis-driving cells. Clearly, future studies are needed to dissect the complex role of canonical and non-canonical Hh-signaling in MF and to understand the altered gene expression patterns in fibrosis-driving cells during the fibrotic transformation.

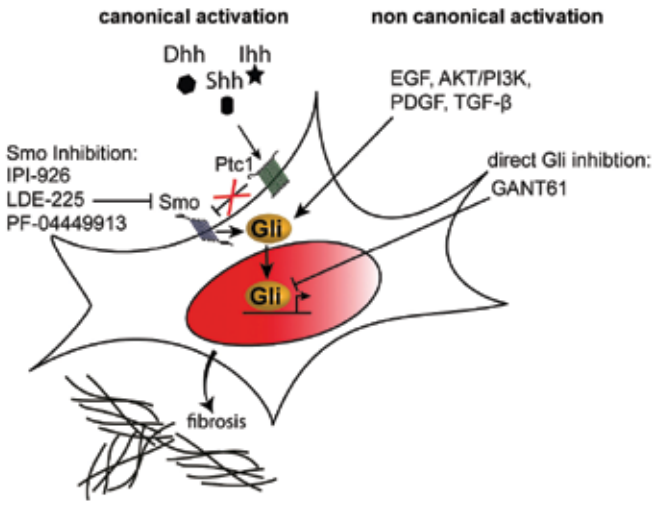

Figure 1: Targeting Hedgehog Gli signaling in myelofibrosis
In canonical Hedgehog-Gli signaling one of the three ligands Indian (Ihh), Sonic (Shh) or Desert Hedgehog (Dhh) binds to the receptor patched 1 (Ptc1) which subsequently releases its tonic inhibition on the transmembrane protein smoothened (Smo). Smo then activates the Gli family zink finger transcription factors which translocate into the nucleus and activate expression of Hedgehog target genes. Canonical Hedgehog activation can be inhibited by various Smo inhibitiors such as IPI-926 (Saridegib), LDE-225 (Sonidegib) and PF-0444991 among others. Recent evidence indicates that Gli proteins can also be activated non canonically and directly, thus independent of Ptc1 and Smo. Various pathways such as EGF, AKT/PI3K, Platelet Derived Growth Factor (PDGF) signaling and Transforming Growth Factor beta (TGF-β) signaling have been reported to directly activate Gli proteins. A direct inhibition of Gli proteins by small molecule compounds such as Gli Antagonist 61 (GANT61) will have the advantage to block Gli proteins independent of their mechanism of activation.

Functionally reprogrammed hematopoietic niche in MPN and implications for graft function after allogenic stem cell transplantation: It was already noted more than 30 years ago that MF is associated with delayed hematopoietic reconstitution after allogeneic stem cell transplantation. Using intensity-reduced conditioning regimens (RIC-HSCT), HSCT has become a well-established curative treatment for high-risk MF patients with acceptable post-transplant non-relapse mortality, but one of the complications is still poor graft function. It has been hypothesized that the relatively high incidence of poor graft function observed in patients with MF after allogeneic stem cell transplantation may be caused by splenomegaly before and after transplantation, which may result in sequestration of transplanted $CD34^+$ cells and sequestration of peripheral blood cells.[84] There is also growing evidence that molecular genetics influence outcome for patients with MF. Kröger et al. demonstrated in a study screening 169 patients with MF that ASXL1 and IDH2 are independent risk factors for lower progression-free survival.[85] In a cohort of 1514 patients with myelodysplastic syndrome (MDS) before transplant, Lindsley et al. showed that JAK2 mutations were associated with a higher rate of death without relapse but not a higher risk of relapse, regardless of conditioning intensity.[86] The mechanism of these effects of *JAK2* mutations is unknown, but might be associated with an influence of JAK2 mutations on altering the bone microenvironment (**Figure 2**). In general, significant bone marrow fibrosis is reported in 10-20% of patients with MDS and, interestingly, is not necessarily linked to mutations in CALR or JAK2. These data suggest that mutations can influence the bone marrow niche and graft function independent of fibrosis. However, once fibrosis is established and the stem cell niche is significantly remodeled, and this is true for MDS and MPN, the overall survival is significantly reduced even in patients who underwent allogeneic stem cell transplantation, suggesting that the effect on the microenvironment/stem cell niche is not completely reversible after allogeneic HSCT (**Figure 2**).[87-89] In summary, these data on the influence of fibrosis and mutations on outcome after allogeneic HSCT indicate that the hematopoiesis-supporting HSC niche (bone marrow microenvironment) might be altered in the presence of mutated HSCs and that these changes even persist after HSCT, in terms of a functionally reprogrammed stroma (**Figure 2**).

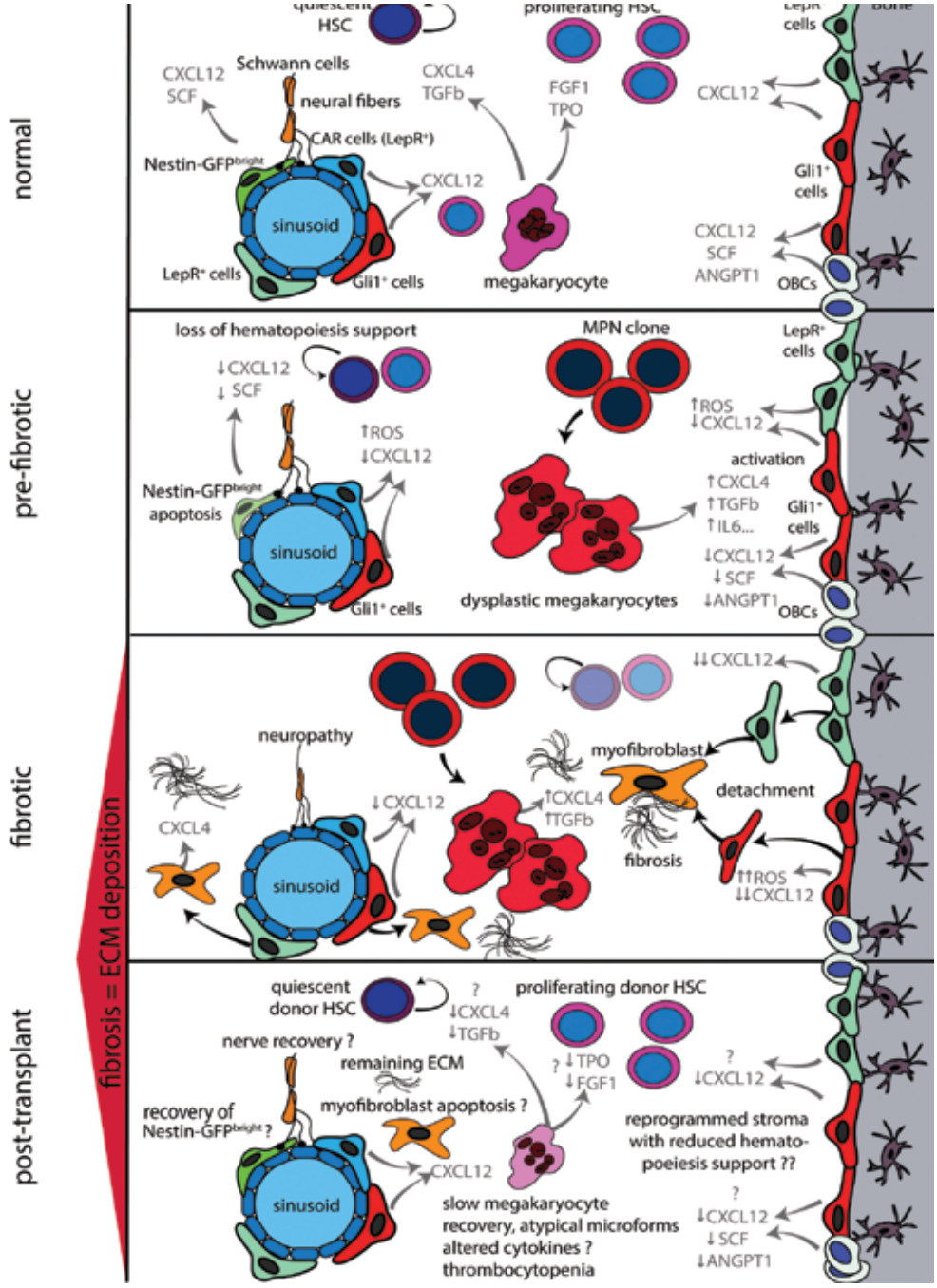
normal
pre-fibrotic
fibrotic
post-transplant
fibrosis = ECM deposition
HSC
proliferating HSC
Schwann cells
CXCL12
SCF
neural fibers
CXCL4
TGFb
FGF1
TPO
CAR cells (LepR+)
Nestin-GFPbright
CXCL12
sinusoid
LepR+ cells
Gli1+ cells
megakaryocyte
CXCL12
Gli1+ cells
CXCL12
SCF
ANGPT1
OBCs
loss of hematopoiesis support
↓CXCL12
↓ SCF
↑ROS
↓CXCL12
Nestin-GFPbright
apoptosis
sinusoid
Gli1+ cells
MPN clone
dysplastic megakaryocytes
LepR+
cells
↑ROS
↓CXCL12
activation
↑CXCL4
↑TGFb
↑IL6...
Gli1+
cells
↓CXCL12
↓SCF
↓ANGPT1
OBCs
neuropathy
CXCL4
↓CXCL12
sinusoid
↑CXCL4
↑TGFb
myofibroblast
fibrosis
↓↓CXCL12
detachment
↑↑ROS
↓↓CXCL12
quiescent
donor HSC
?
↓CXCL4
↓TGFb
proliferating donor HSC
nerve recovery ?
remaining ECM
recovery of
Nestin-GFPbright ?
myofibroblast apoptosis ?
sinusoid
CXCL12
? ↓TPO
↓FGF1
?
↓CXCL12
reprogrammed stroma
with reduced hemato-
poeiesis support ??
slow megakaryocyte
recovery, atypical microforms
altered cytokines ?
thrombocytopenia
?
↓CXCL12
↓SCF
↓ANGPT1

Continued figure legend fo figure 2: The MPN clone gives rise to mutant, dysplastic megakaryocytes which contribute to a proinflammatory environment that damages sensitive elements of the microenvironment, such as Nes^+ MSCs, Schwann cells and their associated nerve terminals and thus contributes to the loss of normal hematopoiesis. Megakaryocytes derived from the malignant MPN clone further significantly contribute to reprogramming of stromal cells. Stromal cell subsets loose their hematopoiesis-support (e.g. loss of CXCL12, increased cellular stress through accumulation of reactive oxygen species (ROS) and maintain a pro-fibrotic environment that favors the malignant hematopoietic clone and leads to a vicious cycle which leads to a bone marrow fibrosis and continuous production of extracellular matrix proteins, inflammation, loss of normal hematopoiesis and expansion of the MPN clone. In the fibrotic phase, stromal cell subsets acquire an abnormal phenotype, start proliferating, detaching and migrating from their normal niches and can be found abundantly in the marrow cavity where they differentiate into myofibroblasts under the influence of CXCL4 secreted by megakaryocytes. They also start expressing CXCL4, which further negatively affects normal hematopoiesis and induces myofibroblast differentiation. The inflammatory environment created by the MPN clone, mutant megakaryocytes and functionally and transcriptionally reprogrammed stromal cells (myofibroblasts) leads to a self-reinforcing niche. It remains unclear how this self-reinforcing niche is interrupted through hematopoietic stem cell transplantation (HSCT). The post-transplant phase raises numerous open questions as indicated by the question marks. Detailed histopathological studies on bone marrow biopsies post-transplant indicates resolution of bone marrow fibrosis but it remains an open question if the reprogrammed stroma in bone marrow fibrosis regains its function and if the stromal reprogramming is a reversible process after HSCT. Megakaryocytes in post-transplant bone marrows, show atypical microforms exhibiting a dysplastic aspect which might be due to an altered interaction between functionally not completely recovered stromal cells (recipient bone marrow) and donor megakaryocytes. This disturbed interaction can in turn negatively affect regenerating hematopoiesis, in line with delayed hematopoiesis recovery in patients with bone marrow fibrosis after HSCT. Another open question is if nerve fibers and $Nestin^+$ stromal cell subsets are able to recover after HSCT. Future studies will shed light on regenerative processes in the bone marrow microenvironment after HSCT and answer the question if the reprogrammed self-reinforcing niche in bone marrow fibrosis is reversible. Cytokines and growth factors are highlighted in grey. CXCL12=C-X-C motif chemokine 12; SCF=stem cell factor/steel factor; TGFb=transforming growth factor b; ANGPT1=angiopoietin; FGF1=fibroblast growth factor 1; TPO=thrompoietin; ROS= reactive oxygen species; CXCL4= C-X-C motif chemokine 4 (or platelet factor 4).

Recent studies using different models of hematopoietic malignancies associated with bone marrow fibrosis were able to mechanistically elucidate how malignant, mutated hematopoietic cells and also pro-inflammatory cytokines activate distinct subsets of stromal cells in the bone marrow, support their fibrotic and secretory activity and influence their reduced hematopoiesis-supporting capacity.[7, 90, 91]

Two recent studies show that malignant hematopoietic cells in murine models of MPN[90] and acute myeloid leukemia (AML)[92] can damage $Nestin^+$ (Nes^+)-MSCs and adjacent nerve cells. In these models, the hematological malignancy created neuropathic changes in the bone marrow niche, which affected the activity of MSCs and altered the function of the HSC niche. Importantly, in the presence of malignant hematopoietic cells, an abnormal population of Nes-MSCs expanded with skewed osteoblastic differentiation and down-regulated expression of many HSC retention factors, including CXCL12 and SCF, indicating loss of hematopoiesis-support of the HSC niche in MDS. Thus, these studies indicate that the MPN- and AML-induced neuropathy promotes the development of a self-reinforcing malignant niche, which favors disease development and progression at the expense of normal HSC maintenance. Schepers et al. demonstrated that osteoblastic lineage cells (OBCs), derived from multipotent stromal cells, expand in the presence of malignant hematopoietic cells resulting in matrix production and trabecular thickening.[91] They demonstrated that *BCR-ABL*$^+$ malignant hematopoietic cells stimulate MSCs to proliferate

and to adopt an abnormal differentiation program resulting in the overproduction of functionally altered OBCs, which accumulate in the bone marrow cavity as inflammatory myelofibrotic cells. The authors investigated the molecular basis of this observation and found that leukemia-conditioned OBCs aberrantly expressed several key molecules known to coordinate niche function and HSC retention, including the chemokine CXCL12, n-cadherin, stem cell factor (SCF), angiopoietin-1 (ANGPT1), and TGFb-1 and -2. The data indicate that malignant hematopoietic cells diminish hematopoietic-supportive capacity of bone marrow stromal and niche cells indirectly through changes in the physical and cytokine environment. In line with these studies, our own study on Gli1$^+$ cells and also the analysis of LepR$^+$ cells demonstrated altered expression of many HSC-regulatory genes and cytokines, including a broad down-regulation of HSC retention factors, in particular CXCL12, in MF, indicating transcriptional reprogramming from hematopoiesis-support to inflammatory, pro-fibrotic programs.

One of the common denominators in solid organ fibrosis and MF seems to be inflammation, which is either induced by tissue injury (e.g. also in the bone marrow through radiation, certain drugs or infections) or the presence of a malignant hematopoietic clone. In contrast to acute inflammatory reactions, which are characterized by rapidly resolving vascular changes, edema, and neutrophilic infiltration, pathogenic fibrosis typically results from chronic inflammatory reactions — defined as responses that persist for several weeks or months and in which inflammation and repair processes occur simultaneously. Despite having obvious etiological and clinical distinctions, most chronic fibrotic disorders have in common a persistent irritant that sustains the production of growth factors, proteolytic enzymes, angiogenic factors, and fibrogenic cytokines, which together stimulate the deposition of connective tissue elements that progressively remodel and destroy normal tissue architecture.[7, 91, 93] In particular oxidative stress and the antioxidant system appear to be crucial modulators of processes such as TGFb signaling and metabolic homeostasis, which play a critical role in fibrosis development and persistence. Reactive oxygen species (ROS) levels contribute to the fibrotic process either directly or indirectly via enhanced inflammation. Vice versa, fibrosis and the inflammation might further increase ROS formation or stimulate the production of cytokines and growth factors, in terms of a vicious cycle.[94, 95] In MF, ROS expression is significantly increased in fibrosis-driving stromal cells (**Figure 2**).[7] Our data indicate that the inhibition of Gli/Hh signaling might also influence the inflammatory reaction in Gli1$^+$ cells. Endothelin 1, a potent vasoconstrictor, plays a role in solid organ fibrosis through the stimulation of ROS production. Treatment with the Gli inhibitor GANT61 in MF, significantly reduced the expression of endothelin 1, CXCL4 and MMP9 in Gli1$^+$ fibrosis-driving cells, all important mediators of tissue repair, inflammation and fibrosis and reduced the increased PI3K and STAT5 expression in JAK2(V617F) mutant hematopoietic cells, indicating that Gli/Hedgehog inhibition can modulate the inflammatory reaction in bone marrow fibrosis and interrupt the vicious

cycle of inflammation and myofibroblast differentiation. Future studies will dissect the role of Gli/Hedghehog inhibition on the inflammatory, pro-fibrotic program in MF.

The systematic dissection of events that convert the bone marrow from a nurturing environment to a hostile, fibrotic niche may hold important translational value for the treatment of hematopoietic neoplasms. The dynamic between malignant hematopoietic cells and stromal cells describes an active process in which reprogramming of niche components by neoplastic cells favors MF and leukemic proliferation while compromising normal hematopoiesis. Microenvironmental contributions to leukemic drug resistance have long been appreciated, and the current work suggests that, similarly, MPN-associated bone marrow dysfunction is an elegantly orchestrated component of the disease progression and fibrotic transformation rather than a simple case of physical competition for available space and resources within the bone marrow. The mechanisms by which the neoplastic cells sustain this microenvironment that favors malignant hematopoiesis at the expense of normal hematopoiesis remain enigmatic but studies accumulate which show a central role of both inflammation and megakaryocytes/platelets in this process.

Mechanisms in the transcriptional and functional reprogramming of stromal cells in MPN: A large amount of experimental evidence in solid organ fibrosis implies that platelets play a central role in the fibrotic process, mainly by releasing profibrotic mediators. Platelets tend to accumulate and activate at sites of tissue injury, the initiating event in most cases of solid fibrosis. Platelets are the major cellular source for TGF-β and PDGFs, two of the most powerful pro-fibrotic mediators in the human body. In the bone marrow, a central role has been attributed to megakaryocytes. In all MPNs, megakaryocytes proliferate, have pathognomonic multilobulated nuclei and exhibit clustering in the marrow. These megakaryocytes have abnormal location of p-selectin on their intracytoplasmic vacuoles and demarcation membrane system (DMS) that leads to the increased emperipolesis (the passage of a cell into the cytoplasm of another cell) of neutrophils. The neutrophils release their enzymes in the megakaryocytes leading to the release of cytokines such as TGF-β; PDGFs and fibroblast growth factor (FGF) from their alpha granules. Over years, the standing hypothesis was that these growth factors then stimulate a stromal cell population to cause fibrosis and endothelial cells to cause neoangiogenesis. The significant breakthrough of identifying $Gli1^+$ and $LepR^+$ cells as fibrosis-driving cells in the bone marrow confirmed the central role of megakaryocytes in transcriptionally reprogramming hematopoiesis-supporting cells to fibrosis-driving cells. As mentioned above, in $LepR^+$ cells PDGFRα is critical in development of bone marrow fibrosis as a $LepR^+$ cell specific knockout of PDGFRa resulted in tremendously reduced reticulin fibrosis and vice versa the activation of the PDGFR± pathway in bone marrow $LepR^+$ cells led to expansion of these cells and extramedullary haematopoiesis as features of PMF. Differential gene expression analysis in $Gli1^+$ cells in bone marrow fibrosis demonstrated that megakaryocyte-associated genes

were significantly up-regulated, in particular the chemokine CXC motif ligand 4 (CXCL4) and the arachidonate lipoxygenase enzyme ALOX12, which have been implicated to play a role in fibrosis [96-99], HSC regulation[1] and are linked to megakaryocyte, platelet and stromal cell biology. [100, 101]

Future studies will focus on dissecting the interaction between megakaryocytes derived from the MPN clone with fibrosis-driving cells. An important question to be answered is if the interaction between dysplastic megakaryocytes and fibrosis-driving stromal cells mainly functions via cytokines and growth factors or if there is heterocellular transfer of material, e.g. through mitochondrial transfer or microvesicles.[102, 103] The interaction between dysplastic megakaryocytes and stromal cells is a promising therapeutic target and previous studies demonstrated that targeting activated pathways in fibrosis-driving cells or also the impaired differentiation of megakaryocytes in MPN through e.g. Aurora kinase inhibition can ameliorate bone marrow fibrosis. This concept was proven in murine model by treatment with MLN8237, a selective AURKA inhibitor.[104] MLN8237 promoted polyploidization and differentiation of megakaryocytes with PMF-associated mutations and had potent anti-fibrotic and antitumor activity *in vivo* in mouse models of PMF.

Conclusions and future directions

The recent discovery of MSC populations as the cellular origin of fibrosis-driving myofibroblasts is an important step forward towards better understanding of the bone marrow niche in MF and development of novel targeted therapeutics. Novel emerging techniques that allow single cell characterization will help to understand the heterogeneity of MSCs in homeostasis and disease. It remains an open question whether the reported $LepR^+$ and $Gli1^+$ cells overlap or whether multiple distinct myofibroblast precursors exist in the bone marrow. While recent studies shed light on some mechanisms of MSC activation and expansion, further studies are needed to elucidate the exact mechanisms of how the malignant hematopoietic cells recruit and reprogram MSCs towards fibrosis-driving myofibroblasts. Targeting Gli proteins directly or through pharmacological intervention in the PDGFRα signaling-pathway might be interesting novel therapeutic options. However, further studies are needed to identify novel and specific Gli inhibitors and to test these as stand-alone therapy or in a combinatory regime with existing JAK inhibitors.

6.4 Future questions

Several open questions remaind to be answered in future experiments. Our data indicate that Gli1 marks perivascular MSC in all major organ systems studied. However, it remainds elusive whether all Gli1$^+$ cells are MSC and whether all MSC express Gli1.

Approximatively half of all myofibroblasts were derived from the Gli1 lineage with circulating monocytes contributing 10% and thus the cellular source of the remaining 30-50% of myofibroblasts remains unclear. To be speculative most likely the remaining myofibroblasts are from resident fibroblasts and pericytes that differ from Gli1 lineage. Anothher important question is the heterogeneity among pericytes and also Gli1$^+$ cells. The most commonly used pericytes maker NG2/CSPG4 is only expressed by a small fraction of Gli1+ cells and interestingly fate tracing studies have shown that NG2$^+$ cells do not contribute to fibrosis. Our data indicate that Gli1$^+$ cells can also be pro-regenerative and might play a role in angiogenesis. Furthermore our studies that are not included in this thesis have shown that adventitial Gli1$^+$ cells serve as a progenitor pool for vascular smooth muscle cells and also play a role as osteoblast progenitors in vascular calcifciation during athero- and arteriosclerosis. It remains unclear whether all Gli1$^+$ cells have this capacity or whether rather various subpopulations exists among pericytes and Gli1$^+$ cells including myofibroblast precusors, osteoblasts precursors and vascular smooth muscle cell progenitors. New advances in single cell resolution high trouhgput genomics will certainly help to unrable these important questions.

REFERENCES

1. Bruns, I., et al., *Megakaryocytes regulate hematopoietic stem cell quiescence through CXCL4 secretion.* Nat Med, 2014. **20**(11): p. 1315-20.
2. Zhao, M., et al., *Megakaryocytes maintain homeostatic quiescence and promote post-injury regeneration of hematopoietic stem cells.* Nat Med, 2014. **20**(11): p. 1321-6.
3. Kramann, R., et al., *Perivascular Gli1+ progenitors are key contributors to injury-induced organ fibrosis.* Cell Stem Cell, 2015. **16**(1): p. 51-66.
4. Zhao, H., et al., *The suture provides a niche for mesenchymal stem cells of craniofacial bones.* Nat Cell Biol, 2015. **17**(4): p. 386-96.
5. Zhao, H., et al., *Secretion of shh by a neurovascular bundle niche supports mesenchymal stem cell homeostasis in the adult mouse incisor.* Cell Stem Cell, 2014. **14**(2): p. 160-73.
6. Caplan, A.I. and D. Correa, *The MSC: an injury drugstore.* Cell Stem Cell, 2011. **9**(1): p. 11-5.
7. Schneider, R.K., et al., *Gli1+ Mesenchymal Stromal Cells Are a Key Driver of Bone Marrow Fibrosis and an Important Cellular Therapeutic Target.* Cell Stem Cell, 2017. **20**(6): p. 785-800 e8.
8. El Agha, E., et al., *Mesenchymal Stem Cells in Fibrotic Disease.* Cell Stem Cell, 2017. **21**(2): p. 166-177.
9. LeBleu, V.S., et al., *Origin and function of myofibroblasts in kidney fibrosis.* Nat Med, 2013. **19**(8): p. 1047-53.
10. Yu, J., T.J. Carroll, and A.P. McMahon, *Sonic hedgehog regulates proliferation and differentiation of mesenchymal cells in the mouse metanephric kidney.* Development, 2002. **129**(22): p. 5301-12.
11. Cain, J.E. and N.D. Rosenblum, *Control of mammalian kidney development by the Hedgehog signaling pathway.* Pediatr Nephrol, 2011. **26**(9): p. 1365-71.
12. St-Jacques, B., M. Hammerschmidt, and A.P. McMahon, *Indian hedgehog signaling regulates proliferation and differentiation of chondrocytes and is essential for bone formation.* Genes Dev, 1999. **13**(16): p. 2072-86.
13. Kramann, R., D.P. DiRocco, and B.D. Humphreys, *Understanding the origin, activation and regulation of matrix-producing myofibroblasts for treatment of fibrotic disease.* J Pathol, 2013. **231**(3): p. 273-89.
14. Fabian, S.L., et al., *Hedgehog-Gli pathway activation during kidney fibrosis.* Am J Pathol, 2012. **180**(4): p. 1441-53.
15. Ding, H., et al., *Sonic hedgehog signaling mediates epithelial-mesenchymal communication and promotes renal fibrosis.* J Am Soc Nephrol, 2012. **23**(5): p. 801-13.
16. Zhou, D., et al., *Sonic hedgehog is a novel tubule-derived growth factor for interstitial fibroblasts after kidney injury.* J Am Soc Nephrol, 2014. **25**(10): p. 2187-200.
17. Fabian, S.L. and B.D. Humphreys, *What's past is prologue: developmental pathways and chronic allograft dysfunction.* Am J Transplant, 2012. **12**(1): p. 5-6.
18. Michelotti, G.A., et al., *Smoothened is a master regulator of adult liver repair.* J Clin Invest, 2013. **123**(6): p. 2380-94.
19. Rauhauser, A.A., et al., *Hedgehog signaling indirectly affects tubular cell survival after obstructive kidney injury.* Am J Physiol Renal Physiol, 2015. **309**(9): p. F770-8.
20. Kramann, R., et al., *Pharmacological GLI2 inhibition prevents myofibroblast cell-cycle progression and reduces kidney fibrosis.* J Clin Invest, 2015. **125**(8): p. 2935-51.
21. Kim, J., et al., *Arsenic antagonizes the Hedgehog pathway by preventing ciliary accumulation and reducing stability of the Gli2 transcriptional effector.* Proc Natl Acad Sci U S A, 2010. **107**(30): p. 13432-7.
22. Mann, K.K., et al., *Darinaparsin: a novel organic arsenical with promising anticancer activity.* Expert Opin Investig Drugs, 2009. **18**(11): p. 1727-34.

23. Tsimberidou, A.M., et al., *A phase I clinical trial of darinaparsin in patients with refractory solid tumors.* Clin Cancer Res, 2009. **15**(14): p. 4769-76.
24. Tian, J., et al., *Darinaparsin: solid tumor hypoxic cytotoxin and radiosensitizer.* Clin Cancer Res, 2012. **18**(12): p. 3366-76.
25. Dennler, S., et al., *Induction of sonic hedgehog mediators by transforming growth factor-beta: Smad3-dependent activation of Gli2 and Gli1 expression in vitro and in vivo.* Cancer Res, 2007. **67**(14): p. 6981-6.
26. Xie, J., et al., *A role of PDGFRalpha in basal cell carcinoma proliferation.* Proc Natl Acad Sci U S A, 2001. **98**(16): p. 9255-9.
27. Li, F., et al., *Sonic hedgehog signaling induces vascular smooth muscle cell proliferation via induction of the G1 cyclin-retinoblastoma axis.* Arterioscler Thromb Vasc Biol, 2010. **30**(9): p. 1787-94.
28. Bigelow, R.L., et al., *Sonic hedgehog induces epidermal growth factor dependent matrix infiltration in HaCaT keratinocytes.* J Invest Dermatol, 2005. **124**(2): p. 457-65.
29. Riobo, N.A., et al., *Phosphoinositide 3-kinase and Akt are essential for Sonic Hedgehog signaling.* Proc Natl Acad Sci U S A, 2006. **103**(12): p. 4505-10.
30. Ji, Z., et al., *Oncogenic KRAS activates hedgehog signaling pathway in pancreatic cancer cells.* J Biol Chem, 2007. **282**(19): p. 14048-55.
31. Schnidar, H., et al., *Epidermal growth factor receptor signaling synergizes with Hedgehog/GLI in oncogenic transformation via activation of the MEK/ERK/JUN pathway.* Cancer Res, 2009. **69**(4): p. 1284-92.
32. Stecca, B., et al., *Melanomas require HEDGEHOG-GLI signaling regulated by interactions between GLI1 and the RAS-MEK/AKT pathways.* Proc Natl Acad Sci U S A, 2007. **104**(14): p. 5895-900.
33. Moshai, E.F., et al., *Targeting the hedgehog-glioma-associated oncogene homolog pathway inhibits bleomycin-induced lung fibrosis in mice.* Am J Respir Cell Mol Biol, 2014. **51**(1): p. 11-25.
34. Kramann, R., T. Kusaba, and B.D. Humphreys, *Who regenerates the kidney tubule?* Nephrol Dial Transplant, 2015. **30**(6): p. 903-10.
35. Harari-Steinberg, O., et al., *Identification of human nephron progenitors capable of generation of kidney structures and functional repair of chronic renal disease.* EMBO Mol Med, 2013. **5**(10): p. 1556-68.
36. Buzhor, E., et al., *Reactivation of NCAM1 defines a subpopulation of human adult kidney epithelial cells with clonogenic and stem/progenitor properties.* Am J Pathol, 2013. **183**(5): p. 1621-33.
37. Lombardi, D., F. Becherucci, and P. Romagnani, *How much can the tubule regenerate and who does it? An open question.* Nephrol Dial Transplant, 2015.
38. Bruno, S., et al., *Isolation and characterization of resident mesenchymal stem cells in human glomeruli.* Stem Cells Dev, 2009. **18**(6): p. 867-80.
39. Crisan, M., et al., *A perivascular origin for mesenchymal stem cells in multiple human organs.* Cell Stem Cell, 2008. **3**(3): p. 301-13.
40. Murray, I.R., et al., *Natural history of mesenchymal stem cells, from vessel walls to culture vessels.* Cell Mol Life Sci, 2014. **71**(8): p. 1353-74.
41. Kuter, D.J., et al., *Bone marrow fibrosis: pathophysiology and clinical significance of increased bone marrow stromal fibres.* Br J Haematol, 2007. **139**(3): p. 351-62.
42. Dameshek, W., *Some speculations on the myeloproliferative syndromes.* Blood, 1951. **6**(4): p. 372-5.
43. Klampfl, T., et al., *Somatic mutations of calreticulin in myeloproliferative neoplasms.* N Engl J Med, 2013. **369**(25): p. 2379-90.

44. Levine, R.L., *JAK-mutant myeloproliferative neoplasms.* Curr Top Microbiol Immunol, 2012. **355**: p. 119-33.
45. Nangalia, J., et al., *Somatic CALR mutations in myeloproliferative neoplasms with nonmutated JAK2.* N Engl J Med, 2013. **369**(25): p. 2391-405.
46. Tefferi, A., et al., *The prognostic advantage of calreticulin mutations in myelofibrosis might be confined to type 1 or type 1-like CALR variants.* Blood, 2014. **124**(15): p. 2465-6.
47. Levine, R.L. and D.G. Gilliland, *Myeloproliferative disorders.* Blood, 2008. **112**(6): p. 2190-8.
48. Decker, M., et al., *Leptin-receptor-expressing bone marrow stromal cells are myofibroblasts in primary myelofibrosis.* Nat Cell Biol, 2017. **19**(6): p. 677-688.
49. Friedman, S.L., et al., *Therapy for fibrotic diseases: nearing the starting line.* Sci Transl Med, 2013. **5**(167): p. 167sr1.
50. Eyden, B., *The myofibroblast: a study of normal, reactive and neoplastic tissues, with an emphasis on ultrastructure. part 2 - tumours and tumour-like lesions.* J Submicrosc Cytol Pathol, 2005. **37**(3-4): p. 231-96.
51. Biagini, G., et al., *Stromal cells in primary myelofibrosis: ultrastructural observations.* Virchows Arch B Cell Pathol Incl Mol Pathol, 1985. **48**(1): p. 1-8.
52. Thiele, J., et al., *Ultrastructure of bone marrow tissue in so-called primary (idiopathic) myelofibrosis-osteomyelosclerosis (agnogenic myeloid metaplasia). I. Abnormalities of megakaryopoiesis and thrombocytes.* J Submicrosc Cytol Pathol, 1991. **23**(1): p. 93-107.
53. Lemos, D.R. and J.S. Duffield, *Tissue-resident mesenchymal stromal cells: Implications for tissue-specific antifibrotic therapies.* Sci Transl Med, 2018. **10**(426).
54. Verstovsek, S., et al., *Role of neoplastic monocyte-derived fibrocytes in primary myelofibrosis.* J Exp Med, 2016. **213**(9): p. 1723-40.
55. Rondelli, D., et al., *Allogeneic hematopoietic stem-cell transplantation with reduced-intensity conditioning in intermediate- or high-risk patients with myelofibrosis with myeloid metaplasia.* Blood, 2005. **105**(10): p. 4115-9.
56. Kroger, N., et al., *Dynamic of bone marrow fibrosis regression predicts survival after allogeneic stem cell transplantation for myelofibrosis.* Biol Blood Marrow Transplant, 2014. **20**(6): p. 812-5.
57. Guglielmelli, P., et al., *MIPSS70: Mutation-Enhanced International Prognostic Score System for Transplantation-Age Patients With Primary Myelofibrosis.* J Clin Oncol, 2018. **36**(4): p. 310-318.
58. Wilkins, B.S., et al., *Resolution of bone marrow fibrosis in a patient receiving JAK1/JAK2 inhibitor treatment with ruxolitinib.* Haematologica, 2013. **98**(12): p. 1872-6.
59. Deininger, M., et al., *The effect of long-term ruxolitinib treatment on JAK2p.V617F allele burden in patients with myelofibrosis.* Blood, 2015. **126**(13): p. 1551-4.
60. Harrison, C., et al., *JAK inhibition with ruxolitinib versus best available therapy for myelofibrosis.* N Engl J Med, 2012. **366**(9): p. 787-98.
61. Caocci, G., et al., *Modulation of bone marrow microenvironment following ruxolitinib therapy in myelofibrosis.* Leuk Lymphoma, 2016. **57**(5): p. 1215-8.
62. Kvasnicka, H.M., et al., *Ruxolitinib-Induced Modulation of Bone Marrow Microenvironment in Patients with Myelofibrosis Is Associated with Inflammatory Cytokine Levels.* Blood, 2014. **124**(21): p. abstract 3182.
63 .Kvasnicka, H.M., et al., *Ruxolitinib Therapy Effectively Modulates CD34+ Hematopoietic Progenitors and Bone Marrow Angiogenesis in Patients with Myelofibrosis.* Blood, 2014. **124**(21): p. abstract 4578.
64. Kvasnicka, H.M., et al., *Changes in Activated Bone Marrow Macrophages and Mast Cells in Patients with Myelofibrosis Following Ruxolitinib Therapy.* Blood, 2014. **124**(21): p. abstract 3184.
65. Verstovsek, S., et al., *A double-blind, placebo-controlled trial of ruxolitinib for myelofibrosis.* N Engl J Med, 2012. **366**(9): p. 799-807.

66. Harrison, C.N., et al., *Long-term findings from COMFORT-II, a phase 3 study of ruxolitinib vs best available therapy for myelofibrosis.* Leukemia, 2016.

67. Harrison, C.N. and D.P. McLornan, *Current treatment algorithm for the management of patients with myelofibrosis, JAK inhibitors, and beyond.* Hematology Am Soc Hematol Educ Program, 2017. **2017**(1): p. 489-497.

68. Vannucchi, A.M. and C.N. Harrison, *Emerging treatments for classical myeloproliferative neoplasms.* Blood, 2017. **129**(6): p. 693-703.

69. Nangalia, J. and A.R. Green, *Myeloproliferative neoplasms: from origins to outcomes.* Hematology Am Soc Hematol Educ Program, 2017. **2017**(1): p. 470-479.

70. King, T.E., Jr., et al., *A phase 3 trial of pirfenidone in patients with idiopathic pulmonary fibrosis.* N Engl J Med, 2014. **370**(22): p. 2083-92.

71. Mesa, R.A., et al., *A phase II trial of pirfenidone (5-methyl-1-phenyl-2-[1H]-pyridone), a novel anti-fibrosing agent, in myelofibrosis with myeloid metaplasia.* Br J Haematol, 2001. **114**(1): p. 111-3.

72. Tadmor, T., et al., *The expression of lysyl-oxidase gene family members in myeloproliferative neoplasms.* Am J Hematol, 2013. **88**(5): p. 355-8.

73. Verstovsek, S., et al., *A phase 2 study of simtuzumab in patients with primary, post-polycythaemia vera or post-essential thrombocythaemia myelofibrosis.* Br J Haematol, 2017. **176**(6): p. 939-949.

74. Duffield, J.S. and M.L. Lupher, Jr., *PRM-151 (recombinant human serum amyloid P/pentraxin 2) for the treatment of fibrosis.* Drug News Perspect, 2010. **23**(5): p. 305-15.

75. Bose, P. and S. Verstovsek, *Developmental Therapeutics in Myeloproliferative Neoplasms.* Clin Lymphoma Myeloma Leuk, 2017. **17S**: p. S43-S52.

76. Bhagwat, N., et al., *Improved Efficacy Of Comibnation Of JAK2 and Hedgehog Inhibitors in Myelofibrosis.* Blood, 2013. **122**(21).

77. Zingariello, M., et al., *Characterization of the TGF-beta1 signaling abnormalities in the Gata1low mouse model of myelofibrosis.* Blood, 2013. **121**(17): p. 3345-63.

78. Sasaki, K., et al., *Phase II evaluation of IPI-926, an oral Hedgehog inhibitor, in patients with myelofibrosis.* Leuk Lymphoma, 2015. **56**(7): p. 2092-7.

79. Dennler, S., et al., *Cloning of the human GLI2 Promoter: transcriptional activation by transforming growth factor-beta via SMAD3/beta-catenin cooperation.* J Biol Chem, 2009. **284**(46): p. 31523-31.

80. Pasca di Magliano, M., et al., *Hedgehog/Ras interactions regulate early stages of pancreatic cancer.* Genes Dev, 2006. **20**(22): p. 3161-73.

81. Gao, J. and I. Aifantis, *Hedgehog and hematopoietic stem cell differentiation: don't believe the hype!* Cell Cycle, 2009. **8**(23): p. 3789-90.

82. Gao, J., et al., *Hedgehog signaling is dispensable for adult hematopoietic stem cell function.* Cell Stem Cell, 2009. **4**(6): p. 548-58.

83. Hofmann, I., et al., *Hedgehog signaling is dispensable for adult murine hematopoietic stem cell function and hematopoiesis.* Cell Stem Cell, 2009. **4**(6): p. 559-67.

84. Alchalby, H., et al., *Incidence and risk factors of poor graft function after allogeneic stem cell transplantation for myelofibrosis.* Bone Marrow Transplant, 2016. **51**(9): p. 1223-7.

85. Kroger, N., et al., *Impact of Molecular Genetics on Outcome in Myelofibrosis Patients after Allogeneic Stem Cell Transplantation.* Biol Blood Marrow Transplant, 2017. **23**(7): p. 1095-1101.

86. Lindsley, R.C., et al., *Prognostic Mutations in Myelodysplastic Syndrome after Stem-Cell Transplantation.* N Engl J Med, 2017. **376**(6): p. 536-547.

87. Della Porta, M.G., et al., *Clinical relevance of bone marrow fibrosis and CD34-positive cell clusters in primary myelodysplastic syndromes.* J Clin Oncol, 2009. **27**(5): p. 754-62.

88. Fu, B., et al., *Bone marrow fibrosis in patients with primary myelodysplastic syndromes has prognostic value using current therapies and new risk stratification systems.* Mod Pathol, 2014. **27**(5): p. 681-9.
89. Kroger, N., et al., *Allogeneic stem cell transplantation for myelodysplastic syndromes with bone marrow fibrosis.* Haematologica, 2011. **96**(2): p. 291-7.
90 .Arranz, L., et al., *Neuropathy of haematopoietic stem cell niche is essential for myeloproliferative neoplasms.* Nature, 2014. **512**(7512): p. 78-81.
91. Schepers, K., et al., *Myeloproliferative neoplasia remodels the endosteal bone marrow niche into a self-reinforcing leukemic niche.* Cell Stem Cell, 2013. **13**(3): p. 285-99.
92. Hanoun, M., et al., *Acute myelogenous leukemia-induced sympathetic neuropathy promotes malignancy in an altered hematopoietic stem cell niche.* Cell Stem Cell, 2014. **15**(3): p. 365-75.
93. Iredale, J.P., *Models of liver fibrosis: exploring the dynamic nature of inflammation and repair in a solid organ.* J Clin Invest, 2007. **117**(3): p. 539-48.
94. Morry, J., W. Ngamcherdtrakul, and W. Yantasee, *Oxidative stress in cancer and fibrosis: Opportunity for therapeutic intervention with antioxidant compounds, enzymes, and nanoparticles.* Redox Biol, 2017. **11**: p. 240-253.
95. Wynn, T.A., *Common and unique mechanisms regulate fibrosis in various fibroproliferative diseases.* J Clin Invest, 2007. **117**(3): p. 524-9.
96. Zaldivar, M.M., et al., *CXC chemokine ligand 4 (Cxcl4) is a platelet-derived mediator of experimental liver fibrosis.* Hepatology, 2010. **51**(4): p. 1345-53.
97. van Bon, L., et al., *Proteome-wide analysis and CXCL4 as a biomarker in systemic sclerosis.* N Engl J Med, 2014. **370**(5): p. 433-43.
98. Burstein, S.A., et al., *Platelet factor-4 excretion in myeloproliferative disease: implications for the aetiology of myelofibrosis.* Br J Haematol, 1984. **57**(3): p. 383-92.
99. Leoni, P., et al., *Platelet abnormalities in idiopathic myelofibrosis: functional, biochemical and immunomorphological correlations.* Haematologica, 1994. **79**(1): p. 29-39.
100. Desplat, V., et al., *Effects of lipoxygenase metabolites of arachidonic acid on the growth of human blood CD34(+) progenitors.* Blood Cells Mol Dis, 2000. **26**(5): p. 427-36.
101. Abraham, N.G., et al., *Modulation of erythropoiesis by novel human bone marrow cytochrome P450-dependent metabolites of arachidonic acid.* Blood, 1991. **78**(6): p. 1461-6.
102. Moschoi, R., et al., *Protective mitochondrial transfer from bone marrow stromal cells to acute myeloid leukemic cells during chemotherapy.* Blood, 2016. **128**(2): p. 253-64.
103. Lemoinne, S., et al., *The emerging roles of microvesicles in liver diseases.* Nat Rev Gastroenterol Hepatol, 2014. **11**(6): p. 350-61.
104. Wen, Q.J., et al., *Targeting megakaryocytic-induced fibrosis in myeloproliferative neoplasms by AURKA inhibition.* Nat Med, 2015. **21**(12): p. 1473-80.

A

ADDENDUM

ENGLISH SUMMARY

The studies presented in this thesis focused on the identification of myofibroblast precursors and their regulation in fibrotic disease (**chapter 2-5**). The overall goal of the project was to dissect the origin and regulation of myofibroblast for the development of novel therapeutics in fibrosis.

Tissue fibrosis, or scar formation, is the common final pathway of virtually all chronic diseases and affects nearly every organ, including kidney, heart, lung, bone marrow and liver, among others. Myofibroblasts are the cells that cause fibrosis but their cellular origin has been controversial and partly unknown for many years. Over hundred years ago researchers have already noticed that fibrosis always emanates from the perivasculature. While studying Hedgehog (Hh) signaling in the kidney we observed a new perivascular cell population defined by expression of the Hedgehog transcriptional activator Gli1 (**chapter 2**). We have generated a genetic model to label these cells, by crossing Gli1CreERt2 mice with the Rosa26-tdTomato reporter line, and thus were able to specifically genetically tag $Gli1^+$ cells and descending cells. $Gli1^+$ cells were either intimately associated with microvasculature and in direct contact with $CD31^+$ endothelial cells or localized in the adventitia of arteries distant from endothelial cells. This perivascular niche comprising adventitia and pericyte niche is the reported niche of mesenchymal stem cells (MSC). To characterize Gli^+ cells by accepted criteria defined for MSC, we cultured FACS purified $Gli1^+$ cells and demonstrated their trilineage differentiation capacity toward chondrocytes, adipocytes and osteoblasts regardless of their origin. Whole organ flow-cytometry confirmed the expression of typical MSC markers of the $Gli1^+$ cell-population in situ.

We next performed fate tracing studies of $Gli1^+$ MSC following heart, kidney, liver, lung and bone marrow injury (**chapter 2-3**) and our studies indicated that $Gli1^+$ MSC are a major source of myofibroblasts in all major organ systems studied. Perivascular Gli1+ MSC dramatically expanded and gained α-smooth muscle actin expression, indicating a transdifferentiation into myofibroblasts driving organ fibrosis. Our data indicate that 40-65% of all myofibroblasts in these organs were derived from resident $Gli1^+$ perivascular cells. A contribution of bone-marrow derived circulating $Gli1^+$ cells to the myofibroblast pool was excluded using parabiosis and bone-marrow transplantation experiments indicating that resident Gli1+ MSC are the source of most myofibroblasts (**chapter 2**). In order to assess the functional contribution of Gli1+ MSC to fibrosis and loss of organ function, we generated mice expressing the human diphtheria toxin receptor (iDTR) in $Gli1^+$ MSC (Gli1CreERt2, iDTR). This strategy enabled us to ablate $Gli1^+$ MSC following injury by administration of diphtheria toxin (DTX). Gli1CreERt2; iDTR mice were injected with tamoxifen and subjected to ascending aortic constriction (AAC) or UUO surgery followed by injection of DTX or vehicle. Ablation of $Gli1^+$ MSC and their descendant myofibroblasts dramatically reduced renal and cardiac fibrosis. Remarkably, echocardiographic analysis of the left ventricular

function demonstrated that ablation of MSC rescued chronic heart failure by preserving left ventricular ejection fraction. Similary, genetic ablation of Gli1$^+$ MSC in myelofibrosis rescued bone marrow failure and stabilized hemoglobin lebels (**chapter 3**). In the bone marrow fibrosis is mostly a result of mutations in hematopoietic stem cells such as Jak2(V617F) (disscussed in **chapter 3 and 6**) importantly, it was entirely unclear how hematopoietic cells that acquire a mutation than communicate with mesenchymal cells and induce fibrosis, mainly because the cellular source of myofibrolblast precursors in the bone marrow was unclear. Our data indicates that the malignant hematopoietic clone produces the chemokine CXCL4 which activates resident Gli1+ cells to leave their perivascular and endosteal bone marrow niche and then differentiate towards myofibroblasts (**chapter 3**). Our data indicate that resident perivascular Gli1+ cells are MSC and a major source of fibrosis driving myofibroblasts in heart, kidney, lung and liver.

However, while our data indicated that approximatively 40-65% of myofibroblast where derived from the Gli1 lineage the source of other myofibroblasts remained elusive. As epithelium is one major suggeste source to the myofibroblast lineage by a process called epithelial mesenchymal transition (EMT) we performed genetic fate tracing using SLC34a1CreER;tdTomato mice that allow proximal tubule specific fate tracing. Importantly, we demonstrated that proximal tubular epithelium does not contribute to the pool of myofibroblasts in kidney fibrosis (**chapter 4**). Circulating hematopoietic cells such as fibrocytes and macrophages as well as bone marrow MSC are discussed as other possible precursors for myofibroblasts. We perform parabiosis with genetic fate tracing of all cells in one mouse and induction of kidney fibrosis in the other parabiont and observed that indeed a small percentage of circulating cells (10%) transdifferentiates into aSMA expressing myofibroblasts in kidney fibrosis. Single cell-RNA-Sequencing confirmed this finding in an unbiased approach and indicated that monocytes are the source of circulating myofibroblast precursors. However, these circulating cells did not express much extracellular matrix components and primarily contributed to kidney fibrosis via indirect mechanisms by secretion of proinflammatory cytokines presumably activating resident kidney pericytes (**chapter 4**).

As we reported Gli1$^+$ MSC like cells as a major source of myofibroblasts in fibrotic disease we aimed to elucidate the role of Gli preoteins in these cells. In vitro RNAi and lentiviral overexpression experiments suggested that Gli2 drives pericyte proliferation and a knockdown of Gli2 resulted in a G0/G1 cell cycle arrest by upregulation of p21 with subsequently reduced retinoblastoma phosphorylation (**chapter 5**). However, Gli1 knockdown did not show any effect as Gli2 protein can compensate for Gli1 loss. Similarly in vivo conditional knockout of Gli2 in Gli1$^+$ cells or inhibition of all Gli proteins in Gli1$^+$ cells by transgenic overexpression of dominant negative Gli3T resulted in a cell-cycle arrest of Gli1+ cells with subsequently reduced kidney fibrosis severity whereas a full Gli1 knockout did not affect cell-cycle of pericytes or kidney fibrosis severity. Importantly, we then showed

that pharmacologically targeting Gli2 protein with the novel organic arsenic darinaparsin or the small molecule Gli antagonist GANT61 also reduced kidney fibrosis severity by induction of a cell specific cell-cycle arrest in Gli1$^+$ pericytes and descending myofibroblasts. This pharmacologic approach not only ameliorated fibrosis but also stabilized kidney function following acute kidney injury in mice. Similarly, we also demonstrated that pharmacologically targeting Gli proteins inhibits expansion of Gli1$^+$ cells in myelofibrosis (**chapter 3**).

In conclusion, our data indicate that the transcription factor Gli1 specifically marks mesenchymal stem cells in the perivasculature of various major organ systems and that these Gli1$^+$ MSCs are a critical source of fibrosis driving myofibroblasts after organ injury. As cell specific genetic ablation of Gli1$^+$ cells or inhibition of their cell-cycle progression by pharmacologically targeting Gli proteins resulted in reduced fibrosis and stabilized organ function Gli1$^+$ cells are a promising novel therapeutic target in fibrotic disease. While we do not find evidence for epithelial cells as myofibroblast precursors our data indicate that criculating monocytes contribute a minor fraction of myofibroblasts in the kidney. However, these circulating myofibroblast precursors do not secrete much extracellular matrix and primarily affect fibrosis through indirect mechanisms by secretion of proinflammatory cytokines.

DUTCH SUMMARY (NEDERLANDSE SAMENVATTING)

De studies gepresenteerd in deze thesis hadden als focus om myofibroblast precursors te identificeren en hun rol in fibrose regulatie te bestuderen (**hoofdstuk 2-5**). Het hoofddoel van het project was om de oorsprong en regulatie van myofibroblasten te onderzoeken voor de ontwikkeling van nieuwe behandel methodes voor fibrose.

Weefselfibrose, of littekenvorming, is het eindstadia van de meeste chronische ziekten en tast vrijwel elk orgaan aan zoals de nieren, hart, longen, beenmerg en de lever. Myofibroblasten zijn de cellen die fibrose veroorzaken, maar hun cellulaire oorsprong is een onderwerp van controverse en nog vrijwel onbekend. Meer dan honderd jaar geleden merkten wetenschappers al op dat fibrose altijd ontstaat vanuit de perivasculaire laag. Bij het bestuderen van de Hedgehog (Hh) signalering in de nieren, hebben wij een nieuwe perivasculaire cel populatie onderzocht, die gekenmerkt wordt door expressie van de Hedgehog transcriptie activator Gli1 (**hoofdstuk 2**). Om deze cellen te kunnen labelen hebben we een genetisch muismodel gegenereerd. Door Gli1CreERt2 muizen te kruisen met Rosa26-tdTomato reporter muizen, waren we in staat om specifiek Gli1+ cellen en afstammelingen hiervan genetisch te labelen. Met behulp van dit model hebben wij geconstateerd dat de Gli1+ cellen nauw verbonden waren aan de microvasculatuur in direct contact met CD31+ endotheelcellen, of echter juist gelokaliseerd waren in de adventitia ver afgelegen van endotheelcellen. Deze perivasculaire niche van adventitia en pericyte niche is de gerapporteerde niche van mesenchymale stamcellen (MSC). Om Gli1+ cellen te karakteriseren met de geaccepteerde criteria voor MSC, hebben we in celkweek de capaciteit van FACS gesorteerde Gli1+ cellen, ongeacht hun oorsprong, om te kunnen differentiëren in chondrocyten, adipocyten en osteoblasten aangetoond. Flowcytometrische analyse van volledige organen bevestigde *in situ* dat de Gli1+ cel populatie typische MSC-markers tot expressie bracht.

Vervolgens hebben wij middels fate tracing studies van Gli1+ MSC na inductie van letsel in hart, nieren, lever, longen en beenmerg (**hoofdstuk 2-3**) aangetoond dat Gli1+ MSC een belangrijke bron van myofibroblasten zijn in deze orgaansystemen. Perivasculaire Gli1+ MSC expandeerden sterk en vertoonden α-smooth muscle actin expressie, wat aangeeft dat er een transdifferentiatie in myofibroblasten plaatsgevonden heeft die orgaan fibrose stimuleert. Uit onze data blijkt dat 40-65% van alle myofibroblasten in bovengenoemde organen afkomstig waren van Gli1+ cellen uit de perivasculaire laag. Een mogelijke bijdrage van circulerende Gli1+ afkomstige uit het beenmerg werd uitgesloten aan de hand van resultaten uit parabiose en beenmergtransplantatie experimenten. Dit geeft aan dat de GL1+ MSC in de perivasculaire laag de primaire bron zijn van myofibroblasten (**hoofdstuk 2**). Om vervolgens de functionele bijdrage te bepalen van Gli1+ MSC in fibrose en bij het verlies van orgaanfunctie, hebben we muizen gegenereerd die de humane difterie toxine receptor (iDTR) tot expressie brengen in Gli1+ MSC (Gli1CreERt2, iDTR). Deze strategie staat ons toe

om na geïnduceerd letsel specifiek GLi1+ MSC te verwijderen middels difterie toxine (DTX) injecties. Gli1CreERt2; iDTR muizen werden geïnjecteerd met tamoxifen en onderworpen aan ascending aortic constriction (AAC) of unilateral ureteral obstruction UUO operatie gevolgd door injectie van DTX of vehicle. Verwijdering van Gli1+ MSC en hun respectievelijke myofibroblast afstammelingen resulteerde in drastisch verminderde nier- en hartfibrose. Opmerkelijk was dat na echocardiografische analyse van de linker ventriculaire functie, bleek dat verwijdering van MSC resulteerde in herstel stabilizerrs chronisch hartfalen door behoud van linkerventrikelejectiefractie. Bovendien, genetische verwijdering van Gli1+ MSC in myelofibrose herstelde beenmerg falen en stabiliseerde hemoglobine levels (**hoofdstuk 3**). In het beenmerg is fibrose vooral het resultaat van mutaties in hematopoietische stamcellen zoals Jak2(V617F) (besproken in **hoofdstuk 3 en 6**). Bovendien was het nog volkomen onduidelijk hoe hematopoietische stamcellen met een mutatie kunnen communiceren met mesenchymcellen om vervolgens fibrose te induceren. Dit komt vooral door het feit dat de cellulaire oorsprong van myofibroblast precursors in het beenmerg nog niet ontrafeld was. Uit onze data blijkt dat de kwaadaardige hematopoietische kloon het chemokine CXCL4 produceert. CXCL4 kan vervolgens Gli1+ cellen induceren te migreren vanuit hun perivasculaire en endosteal beenmerg niche en differentiatie in myofibroblasten (**hoofdstuk 3**). Onze resultaten tonen aan dat perivasculaire Gli1+ cellen MSC zijn en een belangrijke bron van myofibroblasten die fibrose in hart, nieren, longen en lever aansturen.

Alhoewel uit onze data blijkt dat circa 40-65% van de myofibroblasten afstammelingen waren van de Gli1, is nog altijd onduidelijk wat de bron is van de overige myofibroblasten. Het endotheel werd in literatuur voorgesteld als een belangrijke bron voor de myofibroblast lijn gezien de aanwezigheid hier van het proces epithelial mesenchymal transition (EMT). Wij hebben genetische fate tracing gedaan met SLC34a1CreER;tdTomato muizen specifiek in de proximale tubulus. In dit model hebben wij aangetoond dat proximaal tubulair endotheel niet bijdraagt aan de pool van myofibroblasten in nierfibrose (**hoofdstuk 4**). Circulerende hematopoietische cellen zoals fibrocyten en macrofagen evenals beenmerg MSC, werden besproken als andere mogelijke precursors voor myofibroblasten. Middels parabiose met fate tracing van alle cellen in de ene muis en inductie van nierfibrose in de andere parabiont, hebben wij geobserveerd dat inderdaad een klein percentage van circulerende cellen (10%) differentiëren in myofibroblasten die αSMA tot expressie brengen. Single-cell RNA sequencing bevestigde deze bevinding objectief en indiceerde dat monocyten de bron zijn van circulerende myofibroblast precursors. Echter, deze circulerende cellen brachten minimale extracellulaire matrixelementen tot expressie en leverden primair een bijdrage aan nierfibrose via indirecte mechanismen zoals secretie van pro-inflammatoire cytokines die vermoedelijk pericyten van de nieren activeerden (**hoofdstuk 4**).

Gezien we hebben aangetoond dat Gli1+ MSC-cellen een belangrijke bron zijn voor myofibroblasten in fibrose, waren we vervolgens geïnteresseerd om de rol van Gli1 eiwitten te verklaren in deze cellen. *In vitro* RNAi en lentivirale overexpressie experimenten suggereerden dat Gli2 de pericyte proliferatie drijft. Een knockdown van Gli2 resulteerde in een G0/G1 celcyclus stop door opregulatie van p21 met daaropvolgend verminderde retinoblastoma-fosforylering (**hoofdstuk 5**). Echter, Gli1 knockdown liet geen enkel van de bovengenoemde effecten zien aangezien Gli2 eiwit kan compenseren voor het verlies van Gli1 functie. Een vergelijkbare *in vivo* conditionele knock-out van Gli2 of inhibitie van alle Gli eiwitten in Gli1+ cellen door middel van transgene overexpressie van dominante negatieve Gli3T, resulteerde in een celcyclus stop met als gevolg verminderde nierfibrose. Terwijl een volledige Gli1 knock-out geen effect had op de celcyclus van pericyten of op de mate van nierfibrose. Vervolgens toonden we aan dat farmacologisch beïnvloeden van het Gli2 eiwit, met het recent ontdekte organisch arseen darinaparsine of de Gli antagonist GANT61, zorgde voor verminderde mate van nierfibrose middels inductie van een cel specifieke celcyclus stop in Gli1+ pericyten en respectievelijke myofibroblast afstammelingen. Deze farmacologische aanpak deed niet alleen de fibrose status verbeteren maar stabiliseerde ook de nierfunctie na acuut nierletsel bij muizen. Evenals observeerden we dat farmacologisch beïnvloeden van Gli1 eiwitten de expansie van Gli1+ cellen in myelofibrose inhibeerde (**hoofdstuk 3**).

Concluderend, onze data toont aan de transcriptie factor Gli1 specifiek de mesenchymale stamcellen labelt in de perivasculaire laag van verschillende orgaansystemen. Bovendien, hebben deze Gli1+ MSC een essentiële rol als fibrose drijvende myofibroblasten na orgaan letsel. Aangezien cel specifieke verwijdering van Gli1+ cellen, of inhibitie van hun celcyclus door farmacologisch beïnvloeden van Gli eiwitten, resulteerde in verminderde fibrose en gestabiliseerde orgaanfunctie, zijn Gli1+ cellen veelbelovend als kandidaat voor nieuwe therapeutische behandelingen in fibrose. Alhoewel, we geen bewijs gevonden hebben voor endotheelcellen als myofibroblast precursors, blijkt dat uit onze data dat de circulerende monocyten een kleiner aandeel hebben in de bijdrage aan myofibroblasten in de nieren. Echter, deze circulerende myofibroblast precursors secreten minimale extracellulaire matrix en beïnvloeden primair fibrose door indirecte mechanismen via secretie van pro-inflammatoire cytokines.

CURRICULUM VITAE

Rafael Kramann was born in Euskirchen, Germany on November 19th, 1981. After receiving his high school diploma in Euskirchen, he went to Medical School in Aachen and graduated in 2007. He performed his MD thesis in the Department of Cardiology at RWTH Aachen (Supervisor Prof. Rainer Hoffmann) on „Two-dimensional strain echocardiography to analyse regional left-ventricular function before and after aortic valve replacement in different aortic valve pathologies." He defended his MD thesis in June 2018 with *magna cum laude*. He started his clinical training (residency and fellowship) in the department of Nephrology, Hypertensiology, Rheumatology and Immunology (Medical Clinic 2) at RWTH Aachen, Germany in January 2008 and performed research on the role of MSC in vascular disease in collaboration with the Department of Pathology in parallel. In this time he was awarded his first indipendent research grants and supervised technicians and MD students in the laboratory. From 2012 to 2015 he performed his PhD training mainly in the laborator of Benjamin Humphreys, MD, PhD at the Bigham and Women´s Hospital and the Harvard Medical School, Boston, MA, USA. He studied the role of pericytes and MSC in organ fibrosis and vascular disease. He is recipient of various prestigous awards including the Stanley Shaldon Award of the European Renal Association (ERA-EDTA), the Nils Alwall and Carl Ludwig Awards of the German Society of Nephrology, the Tersteegen Award of the German Dialysis association (DN e.V.) and the Grand Prize in the Harvard Innovation Lab Dean´s Health and Lifescience Challenge for founding the early biotech venture company MatriTarg Laboratories.

EDUCATION AND PROFESSIONAL EXPERIENCE

09/2017 - present	Full Professor (W2) and Chair of Nephro-Cardiology, Department of Medicine 2 – Nephrology, Hypertensiology, Rheumatology and Immunology, RWTH Aachen University, Aachen, Germany
09/2017	Board Certification for Internal Medicine and Nephrology (Board of Physicians, Northrhine – Ärztekammer Nordrhein)
02/2017	Offer for Full Professor of Medicine position (W2), Division of Nephrology, RWTH Aachen University, Aachen Germany
06/2015-present	Principal Investigator, Laboratory of Translational Cardiovascular and Kidney Research (www.kramannlab.com), Associate Physician, Division of Nephrology and Clinical Immunology, RWTH Aachen University, Aachen Germany
01/2012-06/2015	Postdoctoral Research Fellow Brigham and Women´s Hospital, Research Fellow Harvard Medical School, Renal Division, Harvard Medial School, Boston, MA, USA (Laboratory of Benjamin Humphreys, MD, PhD)
09-12/2011	Principal investigator license for clinical trials and Good clinical practice (GCP) training (Centrial GmbH, Tübingen, Germany)
01/2008-12/ 2011	Residency and Renal Fellowship, Division of Nephrology, University Hospital RWTH Aachen, Germany
2005-2008	Medical Thesis, Department of Cardiology, RWTH Aachen University. Disputation with *magna cum laude*.
12/2007	Medical State Examination and License to Practice Medicine (Grade 1.0; top 1%)
08/2004-04/2006	Student Research Assistant Institute of Pathology, RWTH Aachen University, Germany
02-04/2004	Student Assistant, Grünenthal Pharmaceuticals, Aachen, Germany
2001-2007	Medical School, RWTH Aachen University, Germany

FELLOWSHIPS

01/2012-12/2014	Postdoctoral research fellowship, German Research Foundation (DFG)
01/2013-12/2013	Research Fellowship RWTH Aachen University, Germany
01/2008-12/2012	Internal Medicine and Nephrology, RWTH Aachen, Germany

FOUNDER:

Co-Founder and Chief Executive Officer (CEO) of MatriTarg Laboratories (Harvard Innovation lab, early stage venture dedicated to develop novel antifibrotic therapeutics) March 2013-Mai 2015, Boston, MA, USA; idea patented and licensed to Chugai Pharmaceuticals (Japan) and a consortium of Bayer AG and Evotec AG (Germany).

TEACHING ACTIVITIES

2017-present	Lectures and Practical Courses in Molecular Biology, H2020 INTRICARE Program
2016-present	Introduction into hemodialysis, Biomedical Engineering, RWTH Aachen University
2015-present	Lectures and Practical Course in medical history taking for medical students AIXTRA clinical skills lab, RWTH Aachen University
2015-present	Lectures and Seminars in Immunology & Rheumatology, RWTH Aachen University
2015-present	Bedside teaching in internal medicine for medical students, RWTH Aachen University Medical School, Aachen, Germany
2015-present	Lectures in Nephrology and Internal Medicine, RWTH Aachen University Medical School, Aachen, Germany
2012-2015	Lectures and Practical Courses in Molecular Biology, Brigham and Women´s Hospital, Boston, MA, USA
2010-2011	Instructing medical students in Intensive Care Medicine April 2010- April 2011, RWTH Aachen University Medical School, Aachen, Germany
2008	Instructing medical students in electrocardiogram analysis, July 2008 (AIXTRA clinical skills lab Aachen) RWTH Aachen University, Medical School, Aachen, Germany
2008-2011	Instructor in physical examination January 2008 – December 2011 RWTH Aachen University, Medical School, Aachen, Germany

LABORATORY SUPERVISION

09/2009-08/2010	Simone Couson, graduate student, MD thesis, RWTH Aachen
10/2009-12/2011	Johanna Erpenbeck, graduate student, MD thesis, RWTH Aachen
02/2012-02/2014	Mari Tanaka, Bachelor in Human Developmental and Regenerative Biology,Harvard University, Cambridge, USA
01/2013-05/2015	Flavia Machado, PhD and Janewit Wongboonsin,MD Renal Division, Brigham and Women´s Hospital and Harvard Medical School Boston, MA, USA
03/2013-03/2014	Sukanya K Moudgalya, Bachelor in Biotechnology, Harvard Medical School, Boston, MA
05/2015-	Nadine Kaesler, PhD, postdoc, RWTH Aachen, Germany
01/2016	Sylvia Menzel, BSc, graduate Student, RWTH Aachen, Germany
09/2016-	Nazanin Kabgani, PhD, postdoc, RWTH Aachen, Germany
01/2017-	Suresh Kaushik, PhD, postdoc, RWTH Aachen, Germany
01/2018	Yaoxian Xu,MSc graduate student, RWTH Aachen, Germany
03/2017-	Konrad Hoeft, graduate student, RWTH Aachen, Germany
05/2017-	Christoph Kuppe, MD postdoc, RWTH Aachen, Germany
05/2017	Susanne Ziegler, PhD postdoc, RWTH Aachen, Germany
08/2017	Anne Babbler, PhD postdoc, RWTH Aachen, Germany
10/2017	Judith Schimpf, MD postdoc, RWTH Aachen, Germany
10/2017	Maurice Halder,MSc graduate student, RWTH Aachen, Germany

PATENTS AND INVENTIONS

- Uses of Gli1 in detecting tissue fibrosis, *PCT/US2015/014796 **
- Uses of Gli1, Provisional Patent US 62/011,259
- Invention of Gli1 Progenitor Cell Line from Heart and Kidney Partners Healthcare, Boston, MA USA #ID23147

REVIEWER

JOURNALS:

Cell Stem Cell, Circulation, Journal of the American Society of Nephrology, Clinical Journal of the American Society of Nephrology, Kidney International, Biomaterials, Heart, American Heart Journal, The Journal of Pathology, American Journal of Pathology, Nephrology Dialysis and Transplantation, BMC Nephrology, Plos One, Histology and Histopathology, Pediatric Nephrology, Molecular Therapy, Cell & Tissue Research, Scientific Reports, Kidney and Blood Pressure Research

ABSTRACTS AND GRANTS:

- International Society of Nephrology – Abstracts World Congress of Nephrology (WCN) 2015
- American Society of Nephrology (ASN) Abstracts Renal Week 2014, 2015, 2016, 2017
- European Renal Association, European Dialysis and Transplant Association (ERA-EDTA) Abstracts 2016, 2017
- Dutch Kidney Foundation Grant Reviewer 2016 -
- German Research Foundation (DFG) Grant Reviewer 2016-
- Agence Nationale De La Recherche (France) Grant Reviewer 2017-

MEMBERSHIPS OF SCIENTIFIC SOCIETIES

2015- German Society of Nephrology
2012- European Renal Association European Dialysis and Transplantation Association (ERA-EDTA)
2012- CKD-MBD working group of the European Renal Association (ERA-EDTA)
2011- American Society of Nephrology (ASN)
2011 International Society of Nephrology (ISN)
2008- German Society of Internal Medicine (DGIM)
2008- Stem Cell Network North Rhine Westphalia

PRIZES, AWARDS AND HONORS

11/2016 Best Abstract Award, American Society of Nephrology, Kidney Week 2016, Chicago, IL, USA

10/2015 Bernd Tersteegen Award of the Verband Deutsche Nierenzentren (German Dialysis Association DNeV; 8000€)

09/2015 Carl Ludwig Award of the German Society of Nephrology (DGFN), DGFN meeting Berlin, Germany (2500€)

12/2014 Kramann et al. Cell Stem Cell (Epub Nov 20, 2014) selected as #1 Nephrology Story in 2014 by the Renal Fellow Network of the USA, featured by National Kidney Foundation and American Society of Nephrology

12/2014 Fellow of the American Society of Nephrology (FASN) for Contribution to the Society and Excellence in Research

11/2014 Advances in Research Award, American Society of Nephrology, Kidney Week 2014, Philadelphia, PA, November 2014 ($800)

09/2014 Nils Alwall Award for Clinical Research of the German Society of Nephrology (DGFN), DGFN meeting Berlin, Germany (3000€)

05/2014 Stanley Shaldon Award, European Renal Association, European Dialysis and Transplant Association (ERA-EDTA) meeting Amsterdam, The Netherlands (10 000€)

09/2013 Career Development Award, American Society of Nephrology, Renal Week, Atlanta, GA ($800)

05/2013 Winner of the inaugural Harvard Innovation Lab´s Deans Health and Life Sciences Challenge “MatriTarg Laboratories: Targeting resident multipotent stem cells to develop new treatments for solid organ fibrotic disease” Boston, MA, ($45 000)

03/2013 Winner of the Harvard Stem Cell Institute Imaging Contest, Boston, MA, ($900)

09/2011 German Society of Nephrology Award for Young Investigators, Berlin, Germany, (25000€)

09/2011 Best Abstract Award, European Renal Association - European Dialysis and Transplant Association (ERA-EDTA) meeting, Prague, Czech Republic (1000€)

11/2011 Travel Grant, GlaxoSmithKline Foundation, American Society of Nephrology, Renal Week 2011, Philadelphia (900€)

09/2011 Travel Grant, German Society of Nephrology Annual Meeting September 2011, Berlin, Germany (200€)

06/2010 Travel Grant, *8th ISSCR meeting, San Francisco, June 16-19, 2010,* German Academic Exchange Service (1800€)

LIST OF PUBLICATIONS

Published articles: 61
H-Index: 33
citations: 2822
first and last authorship: 30

Research articles (peer reviewed):

1. **Kramann R**, Machado F, Wu H, Kusaba T, Hoeft K, Schneider RK, Humphreys BD Parabiosis and single-cell RNA-Sequencing reveal a limited contribution of monocytes to myofibroblasts in kidney fibrosis. JCI insight 2018 3(9) [IF: N/A]
2. Höhne M, Frese CK, Grahammer F, Dafinger C, Ciarimboli G, Butt L, Binz J, Hackl MJ, Rahmatollahi M, Kann M, Schneider S, Altintas MM, Schermer B, Reinheckel T, Göbel H, Reiser J, Huber TB, **Kramann R**, Seeger-Nukpezah T, Liebau MC, Beck BB, Benzing T, Beyer A, Rinschen MM. Single nephron proteomes connect morphology and function in proteinuric kidney disease. Kidney Int. 2018 Mar 9. [Epub ahead of print]
3. Kaesler N, Verhulst A, De Mare A, Deck A, Behets A, Behets GJ, Hyusein A, Evenepoel P, Floege J, Marx N, Babler A, Kramer I, Kneissel M, **Kramann R**, Weis D, D´Haese PC, Brandenburg VM Sclerostin deficiency modifies the development of CKD-MBD in mice. *Bone* 2018 107:115-123 [IF: 4.1]
4. Kaesler N, Verhulst A, De Maré A, Deck A, Behets GJ, Hyusein A, Evenepoel P, Floege J, Marx N, Babler A, Kramer I, Kneissel M, **Kramann R**, Weis D, D'Haese PC, Brandenburg VM. Sclerostin deficiency modifies the development of CKD-MBD in mice. Bone 2017 Nov 21; 10:115-123 [IF:4.1]
5. Brandenburg VM, Reinartz S, Kaesler N, Krüger T, Dirrichs T, **Kramann R**, Peeters F, Floege J, Keszei A, Marx N, Schurgers LJ, Koos R. Slower Progress of Aortic Valve Calcification with Vitamin K Supplementation. *Circulation* 2017; 135:2081-2083 [IF: 19.3]
6. Mukherjee E, Maringer K, Bushnell D, Schaefer C, **Kramann R**, Ho J, Humphreys BD, Bates C and Sims-Lucas S. Endothelial markers expressing stromal cells are critical for kidney formation. *Am J Physiol Renal Physiol* 2017 in press [IF: 3.4]
7. Schneider RK, Mullaly A, Dugourd A, Peisker F, Hoogenboezem R, Van Strien PMH, Bindels EM, Heckl D, Büsche G, Fleck D, Müller-Newen G, Wongboonsin J, Ventura-Ferreira M, Puelles VG, Saez-Rodriguez J, Ebert BL, Humphreys BD and **Kramann R.**[#] Gli1^{+} mesenchymal stromal cells are key drivers of bone marrow fibrosis and important cellular therapeutic targets. *Cell Stem Cell* 2017 20(6):785-800 [#]**corresponding author,** highlighted by editorials in Cell Stem Cell, Science Translational medicine and Experimental Hematology [IF: 23.4]
8. **Kramann R,**[#] Wongboonsin J, Chang-Panesso M, Machado FG, Humphreys BD Gli1 pericyte loss induces capillary rarefaction and proximal tubular injury. *J Am Soc Nephrol* 2017 28(2):776-784 [#]**Corresponding author,** highlighted by and editorial in JASN [IF 9.5]
9. **Kramann R,** [#] Goettsch C, Wongboonsin J, Iwata H, Schneider RK, Kuppe C, Kaesler N, Chang-Panesso M, Machado FG, Gratwohl S, Madhurima K, Hutcheson JD, Jain S, Aikawa E, Humphreys BD. Adventitial MSC-like cells are progenitors of vascular smooth muscle cells and drive vascular calcification in chronic kidney disease. *Cell Stem Cell* 2016 19(5):628-642 [#]**Corresponding author**, highlighted by editorials in Cell Stem Cell, Nature Reviews Nephrology , Kidney International and a special article in Stem Cell Investigation [IF 23.4]
10. Brandenburg V, **Kramann R**, Kaesler N, Korbiel J; Schmitz S, Krueger T, Floege J, Ketteler M. Calcific Uremic Arteriolopathy (Calciphylaxis): Data from a Large Nation-wide Registry - *Nephrol Dial Transplant* 2016 Jan 29 Epub ahead of print [IF 4.1]

11. Schneider RK, Schenone M, Ventura Ferreira M, **Kramann R**, Joyce CE, Hartigan C, Beier F, Brümmendorf TH, Germing U, Platzbecker U, Buesche G, Knuechel R, Chen MC, Waters CS, Chen E, Chu LP, Novina C, Lindsley RC, Carr SA, Ebert BL Rps14 haploinsufficiency causes a block in erythroid differentiation mediated by S100A8/S100A9 - *Nature medicine* 2016 Mar;22(3):288-97 [IF 30.3]
12. Goettsch C, Hutcheson JD, Aikawa M, Iwata H, Pham T, Nykjaer A,; Kjolby M, Rogers M, Michel T, Shibasaki M, Hagita S, **Kramann R**, Rader J, Libby P, Singh SA, Aikawa E Sortilin mediates vascular calcification via its recruitment into extracellular vesicles. *J Clin Invest* 2016 Apr 1;126(4):1323-36 [IF 13.7]
13. Ventura Ferreira MS, Bergmann C, Bodensiek I, Peukert K, Abert J, **Kramann R**, Kachel P, Rath B, Rütten S, Knuchel R, Ebert BL, Fischer H, Brümmendorf TH, Schneider RK. An engineered multicomponent bone marrow niche for the recapitulation of hematopoiesis at ectopic transplantation sites. *J Hematol Oncol* 2016 Jan 25;9(1):4 [IF 6.2]
14. Barros X, Dirrichs T, Koos R, Reinartz S, Kaesler N, **Kramann R**, Gladziwa U, Ketteler M, Floege J, Marx N, Torregrosa JV, Keszei A, Brandenburg VM Epicardial adipose tissue in long-term hemodialysis patients: its association with vascular calcification and long-term development. *J Nephrol* 2016, Apr;29(2):241-50 [IF: 2.2]
15. **Kramann R**, Fleig SV, Schneider RK, Fabian SL, DiRocco DP, Maarouf M, Wongboonsin J, Ikeda Y, Heckl D, Chang SL, Rennke HG, Waikar SS, Humphreys BD Pharmacological Gli2 Inhibition prevents myofibroblast cell-cycle progression and reduces kidney fibrosis. *J Clin Invest* 2015 Aug 3;125(8):2935-51; highlighted by Nature Reviews Nephrology [IF: 13.7]
16. Maarouf, OH, Aravamudhan A, Rangarajan D, Kusaba T, Zhang V, Welborn J, Gauvin D, Hou X, **Kramann R**, Humphreys BD Paracrine Wnt1 Drives Interstitial Fibrosis without Inflammation by Tubulointerstitial Crosstalk. *J Am Soc Nephrol* 2015 Mar;27(3):781-90 [IF: 9.5]
17. **Kramann R#**, Schneider RK, DiRocco DP, Machado F, Fleig S, Bondzie FP, Henderson JM, Ebert BL, Humphreys BD Perivascular Gli1+ Progenitors Are Key Contributors to Injury-Induced Organ Fibrosis. *Cell Stem Cell* 2015 Jan 8;16(1):51-66 **#Corresponding author** (highlighted by an editorial in Cell Stem Cell and Kidney International, selected as #1 Nephrology Story in 2014 by the Renal Fellow Network of the USA, featured by National Kidney Foundation and American Society of Nephrology, December 2014) [IF: 23.4]
18. Schneider RK, Ademà V, Heckl D, Järås M, Mallo M, Lord AM, Chu LP, McConkey ME, **Kramann R**, Mullally A, Bejar R, Solé F, Ebert BL. Role of Casein Kinase 1A1 in the Biology and Targeted Therapy of del(5q) MDS. *Cancer Cell* 2014 Oct 13;26(4):509-20 [IF: 23.9]
19. **Kramann R#**, Erpenbeck J, Schneider RK, Röhl A, Hein M, Brandenburg V, van Diepen M, Dekker F, Marx N, Floege J, Becker M, Schlieper G. Speckle tracking echocardiography detects uremic cardiomyopathy early and predicts cardiovascular mortality in end-stage renal disease. *J Am Soc Nephrol* 2014; 25(10):2351-65 **#Corresponding Author** [IF: 9.5]
20. **Kramann R,** Tanaka M, Humphreys BD. Fluorescence Microangiography for Quantitative Assessment of Peritubular Capillary Changes after Acute Kidney Injury. *J Am Soc Nephrol* 2014; 25(9):1924-31 (featured with cover art on September issue 2014) [IF: 9.5]
21. Klinkhammer B*, **Kramann R***, Mallau M, Makowska A, van Roeyen C, Rong Song, Buecher E, Boor P, Kovacova K, Zok S, Denecke B, Stuettgen E, Otten S, Floege J, Kunter U Mesenchymal stem cells from rats with chronic kidney disease exhibit premature senescence and loss of regenerative potential. *Plos One* 2014;9(3):e92115. *both authors contributed equally [IF: 3.5]
22. Kusaba T, Lalli M, **Kramann R**, Kobayashi A, Humphreys BD. Differentiated kidney epithelial cells repair injured proximal tubule. *Proc Natl Acad Sci USA* 2014 Jan;111(4):1527-32 [IF: 9.8]
23. **Kramann R#,** Kunter U, Brandenburg VM, Leisten I, Ehling J, Klinkhammer B, Bovi M, Knüchel R, Floege J and Schneider RK. Osteogenesis of heterotopically transplanted mesenchymal stromal cells in rat models of chronic kidney disease. *J Bone Miner Res* 2013 Dec;28(12):2523-34 **#corresponding author** [IF: 6.6]

24. Brandenburg VM*, **Kramann R*** Koos R, Krüger T, Schurgers L, Mühlenbruch G, Hübner S, Gladziwa U, Drechsler C, Ketteler M. Relationship between Sclerostin and Cardiovascular Calcification in Hemodialysis Patients: A cross-sectional study**.** *BMC Nephrol* 2013 Oct 10;14:219 * both authors contribute equally [IF: 2.3]

25. Koos R, Brandenburg V, Mahnken AH, Schneider RK, Dohmen G, Marx N, **Kramann R.** Sclerostin as potential novel biomarker for aortic valve calcification: an in vivo and ex vivo study. *J Heart Valve Dis 2013 May*; 22:317-325 [IF: 1.0]

26. **Kramann R#**, Brandenburg V, Ketteler M, Jahnen-Dechent W, Knüchel R, Floege J, Schneider RK. Novel insights into osteogenesis and matrix remodelling associated with calcific uremic arteriolopathy *Nephrol Dial Transplant* 2013 Apr;28(4):856-68 **#corresponding author** [IF: 4.1]

27. **Kramann R#**, Frank D, Brandenburg VM Takahama J, Kürger T, Riehl J, Floege J. Prognostic impact of renal arterial resistance index upon renal allograft survival: The time point matters. *Nephrol Dial Transplant* 2012 Oct;27(10):3958-63. **#corresponding author** [IF: 4.1]

28. **Kramann R**, Couson S, Henkel C, Neuss S, Floege J, Knuechel R, Schneider RK. Uremia disrupts the vascular niche in a three-dimensional co-culture system of human mesenchymal stem cells and endothelial cells. *Nephrol Dial Transplant* 2012 Jul;27(7):2693-702. [IF: 4.1]

29. van de Kamp J, **Kramann R,** Anraths J, Schöler HR, Ko K, Knüchel R, Zenke M, Neuss S, Schneider RK. Epithelial morphogenesis of germline-derived pluripotent stem cells on organotypic skin equivalents in vitro. *Differentiation* 2012 Mar;83(3):138-47. [IF: 2.9]

30. Leisten I*, **Kramann R***, Ventura Ferreira MS, Ziegler P, Wagner W, Neuss S, Knüchel R, Schneider RK. 3D co-culture of hematopoietic stem and progenitor cells and mesenchymal stem cells in collagen scaffolds as a model of the hematopoietic niche. *Biomaterials* 2012 Feb;33(6):1736-47. * Both authors contributed equally [IF: 8.3]

31. Yagmur E, Koch A, Haumann M, **Kramann R**, Trautwein C, Tacke F. Hyaluronan serum concentrations are elevated in critically ill patients and associated with disease severity. *Clin Biochem* 2012 Jan;45(1-2):82-7. [IF: 2.2]

32. **Kramann R,** Couson S, Neuss S, Bornemann J, Bovi M, Kunter U, Floege J, Knuechel R, Schneider RK. Exposure to uremic serum induces a pro-calcific phenotype in human mesenchymal stem cells. *Arterioscler Thromb Vasc Biol* 2011 Sep;31(9):e45-54. [IF: 6.3]

33. Schneider RK, Anraths J, **Kramann R**, Bornemann J, Bovi M, Knüchel R, Neuss S. The role of biomaterials in the direction of mesenchymal stem cell properties and extracellular matrix remodelling in dermal tissue engineering. *Biomaterials* 2010; 31:7948-59 [IF: 8.3]

34. Schneider RK, Püllen A, **Kramann R**, Bornemann J, Knüchel R, Neuss S, Perez-Bouza A. Long-term survival and characterisation of human umbilical cord-derived mesenchymal stem cells on dermal equivalents. *Differentiation* 2010; 79(3):182-93 [IF: 2.9]

35. Schneider RK, Püllen A, **Kramann R**, Raupach K, Bornemann J, Knuechel R, Pérez-Bouza A, Neuss S. The osteogenic differentiation of adult bone marrow and perinatal umbilical mesenchymal stem cells and matrix remodelling in three-dimensional collagen scaffolds. *Biomaterials* 2010; 31(3):467-80 [IF: 8.3]

36. Becker M, Lenzen A, Ocklenburg C, Stempel K, Kühl H, Neizel M, Katoh M, **Kramann R**, Wildberger J, Kelm M, Hoffmann R. Myocardial deformation imaging based on ultrasonic pixel tracking to identify reversible myocardial dysfunction. **J** *Am Coll Cardiol* 2008; 51(15):1473-81 [IF: 15.3]

37. Becker M, Franke A, Breithardt OA, Ocklenburg C, Kaminski T, **Kramann R**, Knackstedt C, Stellbrink C, Hanrath P, Schauerte P, Hoffmann R. Impact of left ventricular lead position on the efficacy of cardiac resynchronisation therapy: a two-dimensional strain echocardiography study. *Heart* 2007; 93(10):1197-203 [IF: 6.0]

38. Becker M, **Kramann R**, Dohmen G, Lückhoff A, Autschbach R, Kelm M, Hoffmann R. Impact of left ventricular loading conditions on myocardial deformation parameters: analysis of early and late changes of myocardial deformation parameters after aortic valve replacement. *J Am Soc Echocardiogr* 2007; 20(6):681-9 [IF: 4]
39. Becker M, **Kramann R**, Franke A, Breithardt OA, Heussen N, Knackstedt C, Stellbrink C, Schauerte P, Kelm M, Hoffmann R. Impact of left ventricular lead position in cardiac resynchronization therapy on left ventricular remodelling. A circumferential strain analysis based on 2D echocardiography. *Eur Heart J* 2007; 28(10):1211-20 [IF: 14.7]
40. Becker M, Hoffmann R, Kühl HP, Grawe H, Katoh M, **Kramann R**, Bücker A, Hanrath P, Heussen N. Analysis of myocardial deformation based on ultrasonic pixeltracking to determine transmurality in chronic myocardial infarction. *Eur Heart J* 2006; 27(21):2560-6 [IF: 14.7]
41. Becker M, Bilke E, Kühl H, Katoh M, **Kramann R**, Franke A, Bücker A, Hanrath P, Hoffmann R. Analysis of myocardial deformation based on pixel tracking in two-dimensional echocardiographic images enables quantitative assessment of regional left ventricular function. *Heart* 2006; 92(8):1102-8 [IF: 6]

Reviews and Editorials (*peer reviewed*):

1. **Kramann R**, Schneider RK. The identification of fibrosis-driving myofibroblast precursors reveals new therapeutic avenues in myelofibrosis. Blood. 2018 Mar 23. pii: blood-2018-02-834820. doi: 10.1182/blood-2018-02-834820. [Epub ahead of print] [IF: 13.164]
2. Schurgers LJ, Akbulut AC, Kaczor DM, Halder M, Koenen RR and **Kramann R.** Initiation and Propagation of Vascular Calcification Is Regulated by a Concert of Platelet- and Smooth Muscle Cell-Derived Extracellular Vesicles. Front. Cardiovasc. Med., 06 April 2018 epub ahead of print [IF: N/A]
2. Noels H, Boor P, Goettsch C, Hohl M, Jahnen-Dechent W, Jankowski V, Kindermann I, **Kramann R,** Lehrke M, Linz D, Maack C, Niemeyer B, Roma LP, Schuett K, Speer T, Wagenpfeil S, Werner C, Zewinger S, Böhm M, Marx N, Floege J, Fliser D, Jankowski J. The new SFB/TRR219 Research Centre. Eur Heart J. 2018 Mar 21;39(12):975-977. doi: 10.1093/eurheartj/ehy083. [IF: 20.212]
4. Gleitz HFE, **Kramann R*** Schneider RK* Understanding deregulated cellular and molecular dynamics in the hematopoietic stem cell niche to develop novel therapeutics in bone marrow fibrosis. J Pathol. 2018 Mar 23. doi: 10.1002/path.5078. [Epub ahead of print] *shared senior author [IF: 6.894]
5. El Agha A, **Kramann R**, Schneider RK, Li X, Seeger S, Humphreys BD, Bellusci S. Mesenchymal Stem Cells in Fibrotic Disease *Cell Stem Cell* 2017 Aug 3;21(2):166-177 [IF: 23.4]
6. Hoeft K and **Kramann R**. Developmental Signaling and Organ Fibrosis. *Current Pathobiol Rep 2017* in press [IF: not listed]
7. Brandenburg V.M., **Kramann R**., Göttsch C., Kaesler N. Update kardiovaskuläre Kalzifikation. *Der Nephrologe* 2017 in press
8. Brandenburg VM, Kaesler N, **Kramann R**, Floege J, Marx N Magnesium: a kardio-renal viewpoint *Dtsch Med Wochenschr*. 2016 Oct 141(21):1537-1542 [IF: 0.7]
9. Brandenburg VM, Kaesler N, Göttsch C, **Kramann R.** Vaskuläre Kalzifikation – Entstehung und prognostische Bedeutung. *Kardio up* 2016; 12(03): 259-271 [IF: n.a.]
10. **Kramann R.** Hedgehog Gli signalling in kidney fibrosis. *Nephrol Dial Transplant* 2016 Dec; 31(12):1989-1995 [IF: 4.1]
11. Kuppe C, **Kramann R.** Role of mesenchymal stem cells in kidney injury and fibrosis. *Curr Opin Nephrol Hypertens* 2016 Jul;25(4):372-7. [IF: 3.2]
12. Brandenburg VM, Evenepoel P, Floege J, Goldsmith D, **Kramann R**, Massy Z,Mazzaferro S, Schurgers LJ, Sinha S, Torregrosa V, Ureña-Torres P, Vervloet M,Cozzolino M; ERA-EDTA Working Group on CKD-MBD and EUCALNET. Lack of evidencedoes not justify neglect: how can we address unmet medical needs incalciphylaxis? *Nephrol Dial Transplant* 2016 Aug; 31(8):1211-9 [IF: 4.1]

13. **Kramann R**, Kusaba T, Humphreys BD Who regenerates the kidney tubule? *Nephrol Dial Transplant* 2015 Jun;30(6):903-910 [IF: 4.1]
14. **Kramann R**, Humphreys BD Kidney Pericytes: Balancing Regeneration and Fibrosis *Sem Nephrol* 2014 2014 Jul;34(4):374-383 [IF: 3.8]
15. **Kramann R,** DiRocco DP, Maarouf O, Humphreys BD Matrix-Producing Cells in Chronic Kidney Disease: Origin, Regulation, and Activation. *Current Pathobiol Rep* 2013, Dec;1(4) [IF: not listed]
16. **Kramann R**, DiRocco DP, Humphreys BD Understanding the origin, activation and regulation of matrix-producing myofibroblasts for treatment of fibrotic disease. *J Pathol* 2013 Nov;231(3):273-89 [IF: 7.3]
17. **Kramann R**, Schneider RK. Parathyroid hormone related protein and cell survival regulation in the kidney. *Kidney Int* 2013 May;83(5):777-9 IF: 8.5]
18. **Kramann R**, Floege J, Ketteler M, Marx N, Brandenburg VM. Medical options to fight mortality in end-stage renal disease: a review of the literature. *Nephrol Dial Transplant* 2012 2 Dec;27(12):4298-307. [IF: 4.1]
19. Brandenburg VM, **Kramann R**, Specht P, Ketteler M. Calciphylaxis in CKD and beyond. *Nephrol Dial Transplant* 2012 Apr;27(4):1314-8. [IF: 3.6]
20. **Kramann R,** Moeller MJ. The next level of complexity: Post-transcriptional regulation by microRNAs. *Kidney Int* 2011 Oct;80(7):692-3. [IF: 8.5]

SUMMARY OF PHD TRAINING AND TEACHING ACTIVITIES

Name PhD student: Rafael Kramann	PhD period: June 2014- October 2018
Erasmus MC Department: Internal Medicine	Promotor(s): Prof. Dr. R. Zietse, Prof. E. Hoorn
Research School: Molecular Medicine (Mol Med)	Supervisor: Prof. Dr. R. Zietse, Prof. E. Hoorn

1. PhD training

	Year	Workload (Hours/ECTS)
General academic skills/Research skills		
• Biomedical English Writing and Communication	2015	1
• Research Management for PhDs and Postdocs	2015	1
• Laboratory animal science	2015	3
• Basic introduction course SPSS	2015	0.6
• Photoshop and Illustrator CS5 workshop	2015	0.3
• Flow cytometry introduction/FlowJo	2015	1
In-depth courses and workshops		
• Nephrology clinical conference	2015-2018	4
• Analysis of microarray and RNA seq data	2015	1
• Genome engineering course Broad Institute, Cambridge,	2015	1
• Fibrosis work discussion Brigham and Women´s Hospital and RWTH Aachen University (weekly, Tuesdays)	2015-2018	3
• Work in progress meeting Department of Nephrology, Brigham and Women's hospital, Boston, USA and RWTH Aachen, Germany	2015-2018	2
• Nephrology lunch meeting, BWH and RWTH Nephrology	2015-2018	2
• Journal Club	2015-2018	2
Presentations		
• American Society of Nephrology Kidney Week (oral)	2014	1
• American Society of Nephrology Kidney Week (oral)	2015	1
• American Society of Nephrology Kidney Week (oral)	2016	1
• American Society of Nephrology Kidney Week (invited lecture)	2017	1
• European Renal Associaton, European Dialysis and Transplant Association (ERA-EDTA) Meeting (invited lecture)	2014	1
• European Renal Associaton, European Dialysis and Transplant Association (ERA-EDTA) Meeting (oral)	2015	1

Presentations		
• European Renal Associaton, European Dialysis and Transplant Association (ERA-EDTA) Meeting (invited lecture)	2016	1
• European Renal Associaton, European Dialysis and Transplant Association (ERA-EDTA) Meeting (invited lecture)	2017	1
• Budapest Nephrology Summer School (invited lecture)	2017	1
• Harvard Innovation Lab (invited lecture)	2014	1
• Brigham and Women´s Hospital, Nephrology Lunch Seminar	2014	1
• Brigham and Women´s Hospital, Nephrology Lunch Seminar	2015	1
• Brigham and Women´s Hospital, Next Leaders in Regenerative Medicine Lecture Series	2015	1
	2015	1
• Harvard Stem Cell Institute	2015	1
International conferences		
• ERA-EDTA Meeting 2014	2014	1
• ERA-EDTA Meeting 2015	2015	1
• ERA-EDTA Meeting 2016	2016	1
• ERA-EDTA Meeting 2017	2017	1
• American Society of Nephrology Meeting 2013	2013	1
• American Society of Nephrology Meeting 2014	2014	1
• American Society of Nephrology Meeting 2015	2015	1
• American Society of Nephrology Meeting 2016	2016	1
• American Society of Nephrology Meeting 2017	2017	1
• Budapest Nephrology Summer School 2017	2017	1
2. Teaching activities		
• Lecturing		
• Internal Medicine	2014-2018	4
Teaching activities		
• Supervising master students	2014-2018	4
• Supervising international summer students	2014-2018	4
• Supervising PhD Students	2014-2018	4
total		**62.9**

ACKNOWLEDGEMENTS

I owe a great amount of gratitude to many people who have accompanied, guided, supported, motivated, entertained and inspired me through the tumultuous roads of science and lab life over the last years.

Dear Professor Floege, you have been extremely supportive since I started my residency in your division in 2008 and you phenomenal support and mentorship is ongoing since then. You made it possible to combine both clinical work in internal medicine and nephrology and start a career in basic and translational research. You tought me how to write a paper and even more important how to apply for funding and how to present your science to a broader audience. Your suggestions for writing papers and scientific grants were and still are immensily helpful and incredible fast. Emailing you a grant at 3AM in the morning sometines resulted in receiving your complete and always very helpful corrections at 5AM. I still remember getting the first corrections of my very first written first-author paper back from you and the entire text was red. All this was incredible helpful for me and I am sure that I would not where I am currently without your help and support. All my paper and grant writing skills have been tremendously improved by your support and always when I am preparing a talk I have your presentation on “how to ruin your presentation” in mind which helps me to keep my story telling straight and include not too much information on every slide. I am deeply grateful for all our meetings and discussions and your guidance in my clinical and scientific career.

Dear Professor Humphreys, Dear Ben: I still remember how nervous I was before interviewing with you in May 2011 in Boston. From the first minutes talking to you, I knew that being in your lab and being mentored by you would be the best thing that could happen in my scientific career. Your mentorship throughout the 3.5 years in your lab and now being back in Europe, has been and is phenomenal. Your support is ongoing since you became chief of nephrology at Washington University in St Louis and I am grateful that I can always come to your lab to perform some cutting edge experiments that are not possible in Europe due to various reasons. I am deeply grateful for all our scientific discussions and your guidance in my scientific career. You gave me so much strength in science and confidence in designing experiments and testing hypotheses. I feel more confident about what I want and how I get there. Your lab is perfectly balanced – scientifically as well as with various personalities; everyone collaborates, there is no back stabbing, there is constant laughter, a little bit of drama and wonderful extracurricular activities – at your place, the Yard house or of course at Bertucci’s and now after transition to Washington University in St Louis at one of the great bars and restaurants in the Central Westend. I thank you from the bottom of my heart for having offered me the opportunity to work in your lab and for guiding me to where I am today.

Dear Dr. Kunter, dear Uta, I have started to do research in your group beside clinical residency and I am very thankful for everything I have learned from you, all the time we have worked together and some wonderful discussions about research, clinical work and life.

Dear Professor Zietse, dear Bob, since the first time we have talked, you have been an incredible and thoughtful mentor for me. Thank you for all the amazing conversations about science and career choices and for creating an academic home for me in Rotterdam. I am so incredibly grateful for your support to make this possible and for thinking through all the details. Thank you also for getting the ball rolling on my thesis and the defense. I am very happy to work at Erasmus MC and to interact with you. You are an exceptional mentor and I am looking forward to many collaborations, discussions and conversations about science, life and the world.

Dear Professor Hoorn, dear Ewout, thanks for being incredible helpful for my start in Rotterdam and for integrating me into collaborative research grants and the nephrology community in Rotterdam and the netherlands. I am much looking forward to various fascinating collaborative projects together with you.

Dear Professor Gribnau, dear Joost, I still remember our first conversation at a dinner with the board of directors. Within just a few minutes, we were in the middle of an inspiring conversation about organoids and autosomal dominant polycystic kidney disease and retrospective fate tracing based on promotor methylation. Since then we had multiple great disscussions and I am very happy that you offered me labspace in your department and that we can start various collaborations on organoids and kidney disease. I am very much looking forward to this in the upcoming years.

Dear Professor Goldschmeding, dear Roel, thanks for being incredible helpful and collaborative and for guiding my research interest towards senescence. You made my start in the Netherlands very enjoyable and I am very much looking forward to our collaboration in TASKFORCE and beyond.

Dear Professor Duncker, dear Dirk Jan, I still remember when I visited you the first time and saw you incredible coronary angiography set-up and pig models. I am very much hoping that our collaboration on adventitial cells in atherosclerosis and the translation from mouse work to pigs and later humans will be a success. I am looking forward to many projects and fruitful discussions.

To my family, particularly my parents and brothers, thank you for your love and constant support throughout all the years of education and academic career. I would have been certainly not where I am now without your tremendous support. You always have a helping hand an open door and an open ear for me and I am incredible thankful for this!

To Rebekka, my beloved, beautiful, amazing, smart, supportive, loving, caring, patient and passionate wife. Everything I am and I have reached was only possible because of you. We met in the first days of medical school and went through an amazing journey of studying, traveling, working on different continents, research & science, grant applications, interviews, publishing and so much more together. Words cannot express how grateful I am for every minute we spend together and I am very much looking forward to the exciting times to come with four of us.

To Clara and Jakob our wonderful children. You rocked our life since your birth and is has been the most wonderful time of your life being with you. I am very much looking forward to the coming years with all of us together.